

AD-A159 147

AN EXPERIMENTAL STUDY OF AN ULTRA-MOBILE VEHICLE FOR
OFF-ROAD TRANSPORTAT. (U) OHIO STATE UNIV RESEARCH
FOUNDATION COLUMBUS R B MCGHEE ET AL. MAY 85

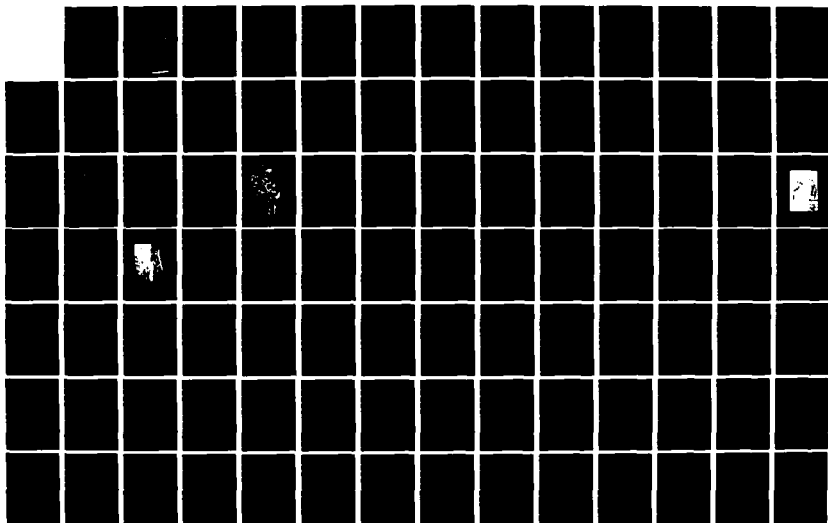
173

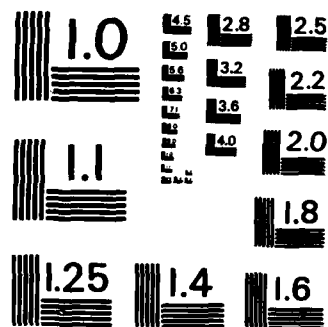
UNCLASSIFIED

ADA903-82-K-0058

F/G 13/6

NL





MICROCOPY RESOLUTION TEST CHART
NATIONAL BUREAU OF STANDARDS-1963-A

2

AD-A159 147

RF Project 762945/714250
Final Report
Appendix 2 (Dissertation)

Project Title:
AN EXPERIMENTAL STUDY OF AN ULTRA-MOBILE
VEHICLE FOR OFF-ROAD TRANSPORTATION

Principal Investigators:
Robert B. McGhee and Kenneth J. Waldron
College of Engineering

Appendix 2 - Dissertation:
KINEMATIC OPTIMAL DESIGN OF A
SIX-LEGGED WALKING MACHINE

Shin-Min Song, B.S.M.E., M.S.M.E.

DTIC
ELECTED
SEP 13 1985
S
1

CLEARED
FOR PUBLICATION

Project for the Period
October 1, 1981 - September 30, 1984

AUG 05 1985 4

DIRECTORATE FOR THE JOURNAL OF INFORMATION
AND SECURITY REVIEW (DASIS-PA)
DEPARTMENT OF DEFENSE

DEFENSE ADVANCED RESEARCH PROJECTS AGENCY
Arlington, Virginia 22209

Contract No. MDA903-82-K-0058

APPROVED FOR PUBLIC RELEASE;
DISTRIBUTION IS UNLIMITED (A)

REVIEW OF THIS MATERIAL DOES NOT IMPLY
DEPARTMENT OF DEFENSE INDOORSEMENT OF
FACTUAL ACCURACY OR OPINION.

May 1985

OSU

The Ohio State University
Research Foundation

1314 Kinnear Road
Columbus, Ohio 43212-3063

DTIC FILE COPY

85 09 12 003

KINEMATIC OPTIMAL DESIGN OF A
SIX-LEGGED WALKING MACHINE

Dissertation

Presented in Partial Fulfillment of the Requirements for
the Degree Doctor of Philosophy in the Graduate School of
The Ohio State University

by

Shin-Min Song, B.S.M.E., M.S.M.E.

* * * * *

The Ohio State University

1984

Reading Committee:

Professor N. Berme

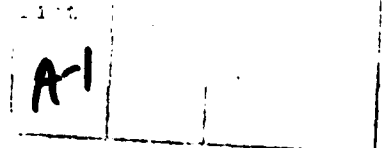
Professor G.L. Kinzel

Professor H.R. Velkoff

Professor K.J. Waldron

Approved by

K.J. Waldron
Advisor
Department of Mechanical Engineering



ACKNOWLEDGEMENTS

I wish to acknowledge the encouragement and advice that I have received throughout my graduate program from my advisor, Professor Kenneth J. Waldron. Many of the results of this work were developed under his timely guidance. His patience and care in reviewing this manuscript is also greatly appreciated. I am also grateful to Professor Gary L. Kinzel for his many helpful suggestions regarding my detailed research work, and to Professor Necip Berme for his helpful attitude throughout my program. I am very much indebted to Professor Robert B. McGhee from whom I received much help and many creative ideas in the area of gait study.

I would like to thank all of my fellow workers on the Walking Machine Project. I enjoyed the experience of working with them, and appreciate the help I have received from them. Among them, I am especially grateful to Mr. Vincent J. Vohnout for his constant discussion with me regarding various aspects of the leg design. I also appreciate Mr. Blaine W. Lilly and Mr. Walter D. Blake for their help and suggestions in proofreading my manuscript. Thanks also go to Mrs. Mary Trufant for her careful and efficient typing of this manuscript.

Finally, I thank my parents and all members of my family for their continuing support and encouragement in my studies.

This work was supported by the Defense Advanced Research Projects Agency under Contracts MDA 903-81-C-0138 and MDA 903-82-K-0058.

VITA

August 12, 1951 Born - Taipei, Taiwan, R.O.C.

June 1973 B.S., Mechanical Engineering, Tatung
Institute of Technology, Taipei,
Taiwan, R.O.C.

March 1981 M.S., Mechanical Engineering, The
Ohio State University, Columbus, Ohio.

1980 - 1982 Graduate Teaching Associate, Department
of Mechanical Engineering, The Ohio
State University, Columbus, Ohio.

1980 - 1984 Graduate Research Associate,
Department of Mechanical Engineering,
The Ohio State University, Columbus,
Ohio.

PUBLICATIONS

Song, S.M., Waldron, K.J., Kinzel, G.L., "Computer-Aided Geometric Design of Legs for a Walking Vehicle," Proceedings of the 8th Oklahoma State University Applied Mechanisms Conference, St. Louis, Missouri, September 1983.

Waldron, K.J., Ficke, J.A., Song, S.M., "RECSYN II: A Powerful Application of Interactive Graphics in Mechanical Engineering," Design Engineering Conference, Chicago, March 1982, To appear in Engineering Design Graphics Journal.

Song, S.M., Waldron, K.J., "Theoretical and Numerical Improvements to an Interactive Linkage Design Program - RECSYN," Proceedings of the 7th Oklahoma State University Applied Mechanisms Conference, Kansas City, Missouri, December 1981.

Song, S.M., Vohnout, V.J., Waldron, K.J., Kinzel, G.L., "Computer-Aided Design of a Leg for an Energy Efficient Walking Machine," Proceedings of the 7th Oklahoma State University Applied Mechanisms Conference, Kansas City, Missouri, December 1981, also in Mechanism and Machine Theory, Vol. 19, No. 1, pp. 17-24, 1984.

Waldron, K.J., Song, S.M., Wang, S.L. and Vohnout, V.J., "Mechanical and Geometric Design of the Adaptive Suspension Vehicle," Proceedings of Symposium on Theory and Practice of Robots and Manipulators, Udine, Italy, June 1984.

FIELDS OF STUDY

Major Field: Mechanical Engineering

Studies in Kinematics and Robotics	Professors K.J. Waldron and G.L. Kinzel
Studies in System Dynamics and Control:	Professors E.O. Doebelin and K. Srinivasan
Studies in Mechanical Design:	Professors J.A. Collins and G.L. Kinzel
Studies in Dynamics and Vibration:	Professors W.E. Clausen and D.R. Houser
Studies in Computer Engineering:	Professors K.J. Breeding and K. Srinivasan
Studies in Mathematics:	Professor H.D. Colson

TABLE OF CONTENTS

	Page
ACKNOWLEDGEMENTS	iii
VITA	v
LIST OF FIGURES	xv
LIST OF TABLES	xxiii

Chapter

1	INTRODUCTION	1
	1.1 Reasons for Development of Multi-Legged Walking Machines	1
	1.2 The ASV and Objectives of this Dissertation . .	3
	1.3 Organization of this Dissertation	9
2	SURVEY OF PREVIOUS WORK	12
	2.1 Introduction	12
	2.2 Survey of Legged Vehicles	14
	2.3 Survey of Gait Study	22
	2.4 Summary	25
3	GAIT ANALYSIS PART I -- BACKGROUND FOR GAIT ANALYSIS AND GAITS FOR LEVEL WALKING	27
	3.1 Introduction	27
	3.1.1 Control Modes of the ASV	28

TABLE OF CONTENTS - continued

Chapter		Page
	3.1.2 Contents of Sections	32
3.2	Mathematical Background and Graphical Methods for Gait Analysis	33
	3.2.1 Basic Definitions and Theorems for Gait Analysis	33
	3.2.2 Graphical Methods for Gait Analysis . .	41
3.3	Gait Selection for a Walking Machine	48
3.4	Gaits for Level Walking	52
	3.4.1 Wave Gaits	55
	3.4.2 Equal Phase Gaits (EPH Gaits)	80
	3.4.3 Backward Periodic Gaits	94
	3.4.4 Discontinuous Follow-The-Leader (FTL) Gait	104
	3.4.4.1 Introduction	104
	3.4.4.2 A General Approach of Discontinuous FTL Gaits	109
	3.4.4.3 The Schedule of Body Motions .	114
	3.4.4.4 Modification of the General Approach for Two Dimensional Body Motion	118
	3.4.5 Continuous FTL Gait	120
	3.4.5.1 Periodic Gaits with the Stepping Characteristic of FTL Gaits . .	120
	3.4.5.2 Strategies to Avoid Forbidden Regions	127
	3.4.5.3 Special Methods for Large Leg Adjustments	135

TABLE OF CONTENTS - continued

Chapter	Page
3.4.5.4 Dexterous Periodic Gaits	137
3.5 Summary	139
4 GAIT ANALYSIS PART II -- GAITS FOR IRREGULAR TERRAIN .	142
4.1 Introduction	142
4.2 Gaits for Walking on a Slope	145
4.2.1 Walking on a Slope by Adjusting the Walking Height and/or the Body Attitude	146
4.2.1.1 Walking Along a Line of Maximum Gradient	146
4.2.1.2 Walking Along a Zero Gradient Line	153
4.2.1.3 Relationship to Walking Volume .	160
4.2.1.4 Walking in an Arbitrary Direction	162
4.2.2 Walking on a Slope by Adjusting the Beginning and the End of the Stroke . . .	166
4.3 Ditch Crossing	170
4.3.1 Ditch Crossing with a Periodic Gait . . .	170
4.3.2 Introduction to Large Obstacle Gait (LOG)	172
4.3.2.1 Programmable Features of LOGs .	172
4.3.2.2 General Approach to Formulize a LOG	175
4.3.3 Ditch Crossing with a LOG	177
4.3.4 Relationship to Walking Volume	181
4.4 Vertical Step Crossing	182
4.4.1 Vertical Ranges	182

TABLE OF CONTENTS - continued

Chapter		Page
4.4.2	Leg and Body Motion	190
4.4.2.1	Tetrapod Walking Mode	195
4.4.2.2	Tetrapod Walking Mode with Lateral Body Motion	197
4.4.3	Stepping Down	199
4.4.3.1	Stepping Down by Gravity	203
4.4.4	Relationship to Walking Volume	204
4.5	Isolated Wall Crossing	207
4.5.1	General Approach	207
4.5.2	Narrow Wall Crossing	210
4.5.3	Relationship to Walking Volume and Body Structure	212
4.6	Overall Walking Volume of the ASV	212
4.7	Summary	215
5	LEG DESIGN BY FOUR-BAR LINKAGE SYNTHESIS	217
5.1	Introduction	217
5.1.1	Energy Efficiency in Robots and Walking Machines	221
5.1.2	Contents of Sections	224
5.2	An Introduction to RECSYN	225
5.2.1	Functions of the Program	225
5.2.2	Operation of the Program	229
5.3	Design of a Four-Bar Leg	235
5.3.1	Design Specification	235

TABLE OF CONTENTS - continued

Chapter		Page
5.3.2	Basic Geometric Design	238
5.3.2.1	Calculation of Design Positions	240
5.3.2.2	Design Procedure	246
5.3.3	Optimization of Leg Linkages	250
5.3.3.1	Crank Selections	253
5.3.3.2	Varying a, b and h	259
5.3.3.3	Varying Spacing Angles	264
5.3.3.4	Varying the Beginning and the End of a Full Step	266
5.3.3.5	Using Foot Design Positions	266
5.3.3.6	Vertical Leg Stroke	268
5.3.4	Bearing Loads, Actuating Torque and Mounting Positions of the Main Actuator	275
5.3.5	Interference	280
5.3.6	Abduction and Adduction	280
5.4	Design of a Seven-Bar Leg	283
5.4.1	Calculation of Design Positions	284
5.4.2	Shank Linkage Design	287
5.5	Summary	295
6	DESIGN OF A PANTOGRAPH LEG	297
6.1	Introduction	297
6.2	Motion Characteristics of Pantographs	300
6.2.1	Nomenclature of Pantographs	300

TABLE OF CONTENTS - continued

Chapter		Page
6.2.2	Two Dimensional (2D) Pantographs	303
6.2.2.1	Basic Theorems	303
6.2.2.2	Principal Axes and Actuator Arrangements	308
6.2.2.3	Singularities of 2D Pantographs	311
6.2.3	Three Dimensional (3D) Pantographs . . .	311
6.2.3.1	Basic Theorems	311
6.2.3.2	Principal Axes and Actuator Arrangements for 3D Pantographs	317
6.2.3.3	Singularities of 3D Simple Pantographs	318
6.3	Design of a Pantograph Leg	320
6.3.1	Design Specifications	320
6.3.2	Design Procedure	320
6.3.2.1	Skew Angles and Actuator Arrangements	323
6.3.2.2	Offset of Walking Envelope . .	324
6.3.2.3	Ratio of Upper Link to Lower Link	327
6.3.3	Bearing Loads, Interference Study and Stress Analysis	327
6.4	Analytical Study of Walking Envelope of Planar Pantograph Leg	331
6.4.1	Formulation of Equations of Motion Limits	332
6.4.1.1	Equations of Motion Limits 1 and 2	332

TABLE OF CONTENTS - continued

Chapter		Page
	6.4.1.2 Equation of Motion Limit 3 . .	339
	6.4.1.3 Equation of Motion Limit 4 . .	342
	6.4.2 Optimization of Walking Envelope	344
6.5	Comparison of the Seven-Bar Leg and the Pantograph Leg	349
6.6	Summary	352
7	ANKLE DESIGN	353
7.1	Introduction	353
7.2	Rigid Foot and Foot with an Ankle Joint	354
7.3	Active Ankle System	358
7.4	Passive Ankle System	358
	7.4.1 Parallel Linkage System	361
	7.4.2 Hydraulic Master-Slave Ankle System . .	365
	7.4.2.1 Rotary Actuator System	365
	7.4.2.2 Some Alternatives	367
7.5	Summary	375
8	CONCLUSION	
8.1	Research Summarization and Evaluation	377
	8.1.1 Gait Analysis	377
	8.1.2 Leg Design	379
8.2	Research Extension	380
	8.2.1 Gait Analysis	381
	8.2.2 Leg Design	382

TABLE OF CONTENTS - continued

Chapter	Page
APPENDIX A. A GRAPHICAL METHOD TO FORMULATE THE GAIT STABILITY MARGIN OF 2N-LEGGED WAVE GAIT	383
APPENDIX B. EFFECTS ON GAIT STABILITY MARGINS OF VARYING THE STROKE OBTAINED BY THE STATIONARY GAIT PATTERN METHOD	389
APPENDIX C. STRESS ANALYSIS OF FOUR-BAR LEG BY FINITE ELEMENT METHODS	394
REFERENCES	404

LIST OF FIGURES

Figure	Page
1.1 Patent drawing of a mechanical horse in 1893	4
1.2 Patent drawing of a walking vehicle in 1913	5
1.3 Artist's conception of the ASV	7
2.1 The G.E. Quadruped	16
2.2 The OSU Hexapod	19
3.1 Simplified dimensions of the ASV	34
3.2 Stability margin SM of a support pattern	39
3.3 Longitudinal stability margin SL of a support pattern	39
3.4 A footfall formula of a quadruped gait	43
3.5 A gait diagram of quadruped gait	43
3.6 An event sequence of a quadruped	44
3.7 A successive gait pattern	45
3.8 A stationary gait pattern of a quadruped gait	46
3.9 A lateral motion sequence of a hexapod	47
3.10 Classification of gaits	54
3.11 Gait diagrams of wave gaits	57
3.12 Symmetric characteristic of a periodic, constant phase increment gait	65
3.13 Gait stability margin of wave gaits and backward wave gaits	72

LIST OF FIGURES - continued

Figure		Page
3.14	Effects on gait stability margin of wave gaits by varying stroke (obtained from graphical methods). . .	78
3.15	Schematic configuration of a leg for walking machines	82
3.16	Gait diagrams of EPH gaits	85
3.17	Gait stability margin of EPH gaits	86
3.18	Gait diagrams of backward wave gaits	96
3.19	Gait diagrams of backward EPH gaits	98
3.20	Gait stability margin of backward periodic gaits . .	99
3.21	Gait stability margin of major periodic gaits	101
3.22	Possible event sequences with backward stepping sequence	106
3.23	Successive gait pattern of an FTL gait with event sequence 1-3-5-2-4-6	110
3.24	A pair of successive stable segments and central segments	112
3.25	Stable segments and central segments of a step of an FTL gait	115
3.26	A truncated stable area (shaded area)	119
3.27	Gait stability margin of continuous FTL gaits	125
3.28	Gait diagrams of continuous FTL gaits	126
3.29	Stationary gait pattern of a continuous FTL gait with $P/R = 1.2$ and $\beta = 2/3$	128
3.30	A hexapod crossing a ditch by front or rear foot adjustments in a continuous FTL gait	131
3.31	A hexapod crossing forbidden regions by lateral foot adjustments in a continuous FTL gait	134

LIST OF FIGURES - continued

Figure		Page
3.32	A hexapod crossing large forbidden regions by lateral foot adjustments corporated with (a) lateral body motion, and (b) symmetric rear foot adjustments	136
4.1	Major irregularities of a rough terrain, (a) a slope (b) a ditch (c) a vertical step (d) an isolated wall	143
4.2	Support pattern of a hexapod walking on a slope by lowering the body height	148
4.3	The maximum slope angle with level body attitude . .	150
4.4	Walking on a slope of a hexapod with reduced body inclination, $\theta > \phi_0$	152
4.5	Walking on a slope of a hexapod by combining body inclination reduction and lowering of the body . . .	152
4.6	Walking on a slope along a zero gradient line by lowering the body height	154
4.7	Walking on a slope along a zero gradient line by leveling the body attitude	157
4.8	Walking on a slope in an arbitrary direction	163
4.9	Relationship of angles for walking on a slope	165
4.10	Walking on a slope by shifting the centers of strokes to the downhill side	169
4.11	Footprints of a dexterous wave gait	172
4.12	Lateral motion sequence of a complete ditch crossing	174
4.13	Ranges of a hexapod in ditch crossing, (a) front foot and rear foot (b) middle foot	178
4.14	Ditch crossing by tilting the body attitude	180
4.15	Front-foot vertical range, $\theta > \gamma$	183

LIST OF FIGURES - continued

Figure		Page
4.16	Front-foot vertical range, $\theta \leq \gamma$	183
4.17	Middle-foot vertical range	186
4.18	Rear-foot vertical range	187
4.19	Lateral motion sequence of a stepping up	192
4.20	A criterion of tetrapod walking mode at the second phase	193
4.21	Tetrapod walking mode	196
4.22	Tetrapod walking mode with lateral body motion . . .	198
4.23	Lateral motion sequence of stepping down with varying body angle	201
4.24	To step down a large step	203
4.25	A wall crossing	208
4.26	A narrow wall crossing	211
4.27	Overall walking volume of the ASV	213
5.1	Back-drive in one-joint actuator system	222
5.2	A "mammal" type leg with a two-joint actuator . . .	226
5.3	Linkage types designed by RECSYN	227
5.4	The display for the selection of driven-crank--before selection	230
5.5	The display for the selection of driven-crank--after selection	232
5.6	The display for the selection of driving-crank . . .	232
5.7	Solution linkage generated by RECSYN	234
5.8	Structure of a walking machine leg	239
5.9	Trajectories of three and four position synthesis .	241

LIST OF FIGURES - continued

Figure		Page
5.10	Symbols to define a position of the foot point P . .	241
5.11	A full step used for the calculation of design positions	244
5.12	Foot trajectory of a four-bar leg	248
5.13	Consecutive footpaths of the four-bar leg, the vertical variation is exaggerated	249
5.14	Design procedure of a four-bar leg	251
5.15	Crank selections in RECSYN	255
5.16	Foot trajectory of leg linkage with $h = 1.8$, $a = 1$, $b = 1$, and crank selection case 1	257
5.17	Foot trajectory of leg linkage with $h = 1.8$, $a = 1$, $b = 1$, and crank selection case 3	258
5.18	Foot trajectory of leg with $h = 1.6$	260
5.19	Foot trajectory of leg with $h = 1.7$	261
5.20	Foot trajectory of leg with $h = 1.9$	262
5.21	Foot trajectory of the leg linkage generated from design positions with spacing angles of 0° and 50° .	265
5.22	Foot trajectory of a leg linkage designed by foot design positions	267
5.23	Foot trajectory obtained from the modified foot design positions	269
5.24	Foot trajectories of a four-bar leg with variable driving-crank	271
5.25	Foot trajectories of a four-bar leg with variable driven-crank	272
5.26	Foot trajectories of a four-bar leg with variable shank	274

LIST OF FIGURES - continued

Figure		Page
5.27	Free body diagrams of a four-bar leg	276
5.28	Free body diagrams of the driving-crank with linear actuator	277
5.29	Actuating torque of a four-bar leg in one step . . .	279
5.30	Interference study of a pair of four-bar legs, the three foot stroke of the shank is strengthened by a slide mechanism	281
5.31	The ASV with four-bar legs	285
5.32	Design positions of shank linkage	287
5.33	A shank linkage generated by RECSYN	288
5.34	Foot trajectories of a shank linkage	289
5.35	A seven-bar leg generated by FORBAR	291
5.36	Foot trajectories of a seven-bar leg	292
5.37	Interference study of seven-bar legs	293
5.38	A design of the seven-bar leg	294
6.1	The three dimensional pantograph mechanisms used in PV II	299
6.2	A general configuration of a pantograph manipulator	301
6.3	A skew pantograph	304
6.4	Simple pantographs	304
6.5	Principal axes and actuator arrangements of 2D pantographs	310
6.6	An example of a 2D singular position	312
6.7	A 3D work space of pantographs	312
6.8	The impossibility of a 3D fully decoupled skew pantograph	314

LIST OF FIGURES - continued

Figure		Page
6.9	3D simple pantograph	316
6.10	Analytical study of the work space for a 2D simple pantograph	319
6.11	Walking envelopes of pantograph leg with 90° skew angle and (a) T type or (b) inverse T type actuator arrangement	325
6.12	Walking envelopes of pantograph leg with 180° skew angle and (a) T type or (b) inverse T type actuator arrangement	326
6.13	Comparison of walking envelopes of two pantograph legs	328
6.14	Overall walking volume of the ASV with simple pantograph legs	329
6.15	A design of the leg driving system	330
6.16	Analytical study of motion limit 1 and 2 of a skew pantograph leg with case 3 actuator arrangement . .	335
6.17	Analytical study of motion limit 1 and 2 of a skew pantograph leg with case 4 actuator arrangement . .	338
6.18	A skew pantograph leg at position of motion limit 3	341
6.19	An example of the walking envelope obtained by analytical method	345
6.20	Ellipses of motion limit 1 with different skew angles, $\phi = 160^\circ$, $R = 4$, $AB = 0.8$, case 3 actuator arrangement	347
6.21	The breadboard leg	351
7.1	Soil deformation of a rigid round foot and a flat foot with an ankle joint	356
7.2	A weak support of a foot with a free angle joint . .	359
7.3	Two conceptual designs of active ankle system . . .	360

LIST OF FIGURES - continued

Figure		Page
7.4	Two sets of double, parallel linkages	362
7.5	A parallel linkage passive ankle system	363
7.6	Hydraulic master-slave ankle system made by rotary actuators	366
7.7	Angular displacement of the shank relative to the foot of the pantograph leg in one step	368
7.8	Hydraulic master-slave ankle system composed of two double-ended actuators	369
7.9	Hydraulic master-slave ankle system composed of two single-ended actuators and special mechanism	371
7.10	Hydraulic master-slave ankle system composed of two single-ended actuators and two dummy actuators . . .	372
7.11	Hydraulic master-slave ankle system composed of two single-ended actuators	373
7.12	A schematic configuration of the master-slave passive ankle system used in the ASV breadboard leg.	374
B.1	Gait diagram and stationary gait pattern of a four-legged wave gait with $\beta = 5/6$	390
C.1	A finite element model of the four-bar leg with space beam elements	395

LIST OF TABLES

Table	Page
1.1 Design Specifications of the ASV	8
3.1 Summary of gait selection	53
3.2 Effects on stability margin of wave gait by varying stroke R (obtained from analytical methods)	77
3.3 Gait stability margin S of backward periodic gaits .	102
4.1 Gradability of the ASV	160
4.2 Maximal ditch width can be crossed by a periodic gait in normal walking mode	171
4.3 Vertical ranges and corner distances of all three phases in vertical step crossing	189
4.4 Rear-foot vertical range of a hexapod with additional strokes in rear legs (unit : inch)	206
4.5 Mobility of the ASV	215
5.1 Knee design positions with $a = 1$, $b = 1$ and $h = 1.8$, the leg height is 6.5 feet	245
5.2 Foot design positions with $a = 1$, $b = 1$ and $h = 1.8$, the leg height is 6.5 feet	246
5.3 Characteristics of legs obtained by different crank selections	256
5.4 Characteristics of legs with different values of h .	263
5.5 Design positions with $a = 1$, $b = 1$, $h = 1$, and spacing angles of 0° and 50°	264

LIST OF TABLES - continued

Table		Page
5.6	Foot design positions according to Table 5.5, the two central design positions are moved down by .07 feet	268
6.1	Characteristics of ellipses of motion limit 1 with case 3 actuator arrangement, $AB = 0.8$, $R = 4$ and $\phi = 160^\circ$	348
A.1	Stability margins of six-legged wave gait	385
A.2	Different combinations of terms	385
A.3	Gait stability margins of eight-legged wave gaits .	387
C.1	The input data file of the four-bar leg for SUBERB	398
C.2	The displacements of nodes	400
C.3	The end forces for beams	401
C.4	The generalized forces transmitted to element nodes in nodal coordinate directions	402
C.5	The stress results for beam elements	403

Chapter 1

INTRODUCTION

1.1 Reasons for Development of Multi-Legged Walking Machines

The history of the land transportation of human beings is marked by the following great events. In the earliest days, man depended on his own legs for transportation. Almost at the same time, animals were trained by man to carry people or cargo. Animals then became the most important means of human transportation for centuries to follow. Later, the invention of the wheel, which may be regarded as the greatest invention in the history of human transportation, greatly improved the efficiency of transportation. Vehicles built on wheels and pulled by man or animal became the most effective means of transportation on land for many centuries. A road system was constructed to enhance the effectiveness of wheeled vehicles. About two centuries ago, another great invention, the heat engine, was developed and initiated the Industrial Revolution. Animal or human powered vehicles were then replaced by engine powered vehicles. The road systems were also developed into well paved road and railroad systems. Today in the Twentieth Century, the application of the wheel seems to have reached its climax, and man's original means of transportation, his legs, has assumed a very secondary role for long distance transportation.

Today, nearly all terrestrial vehicles are based on a wheeled system. (A tracked vehicle can be considered as a wheeled vehicle which carries and lays its own road.). Through the centuries, wheeled vehicles, operating on paved roads, have proven to be the most efficient means for long distance land transportation. Moreover, wheeled and tracked vehicles also serve as off-road vehicles on relatively smooth natural terrain with acceptable performance. Therefore, wheels are so entrenched in our culture that it is easy to think that men and animals have been forced to adopt an inferior legged locomotion scheme due to the inability of nature to create a rotating joint.

However, recent research reveals that the real situation contradicts this view of locomotion. In his book [1], Bekker showed that the average speed on rough, hard terrain is 5-10 mph for tracked vehicles and 3-5 mph for wheeled vehicles while animals can reach a maximum speed on the order of 35 mph. Also, for a terrain with a 10 inch layer of plastic soil, the power required for propulsion is 10 hp/ton for a tracked vehicle and 15 hp/ton for a wheeled vehicle, but only 7 hp/ton for a legged, walking machine.

In another book [2], Bekker applied soil mechanics to explain the superior mobility of legged locomotion exhibited by animals in comparison to wheeled or tracked vehicles. That is, a wheel or track sinks into soft soil and produces a depression out of which it is continuously trying to climb, while legs create only discrete footprints in which any back slip pushes up soil behind the foot which increases traction.

Moreover, comfort in transportation in irregular terrain is also in favor of legged locomotion. According to our own experience and observation, in a certain degree of rough terrain it is more comfortable to ride on horseback than to sit in a vibrating wheeled or tracked vehicle while both are traveling at the same speed.

Hence, at least four potential advantages of legged vehicles over wheeled or tracked vehicles can be concluded from the above discussion. These advantages are:

1. Higher speed.
2. Better fuel economy.
3. Greater mobility.
4. Better comfort.

In addition to these potential advantages as incentives to develop a legged walking machine, one investigation shows that roughly fifty percent of the land on Earth is not accessible to conventional wheeled or tracked vehicles [3]. A walking machine which can travel where terrain difficulties make wheeled or tracked vehicles ineffective will be very useful in applications in many areas such as commerce, science, agriculture, military ... etc.

1.2 The ASV and Objectives of this Dissertation

Even before men became aware of these potential advantages, they were inspired to dream about walking machines. Two examples of many incidents related to this inspiration are given below. In 1893, Rygg obtained a patent for the design of a mechanical horse (see Figure 1.1). There is no evidence to prove that he actually built this machine.

(no Model.)

L. A. RYGG.
MECHANICAL HORSE.

No. 491,927.

Patented Feb. 14, 1893.

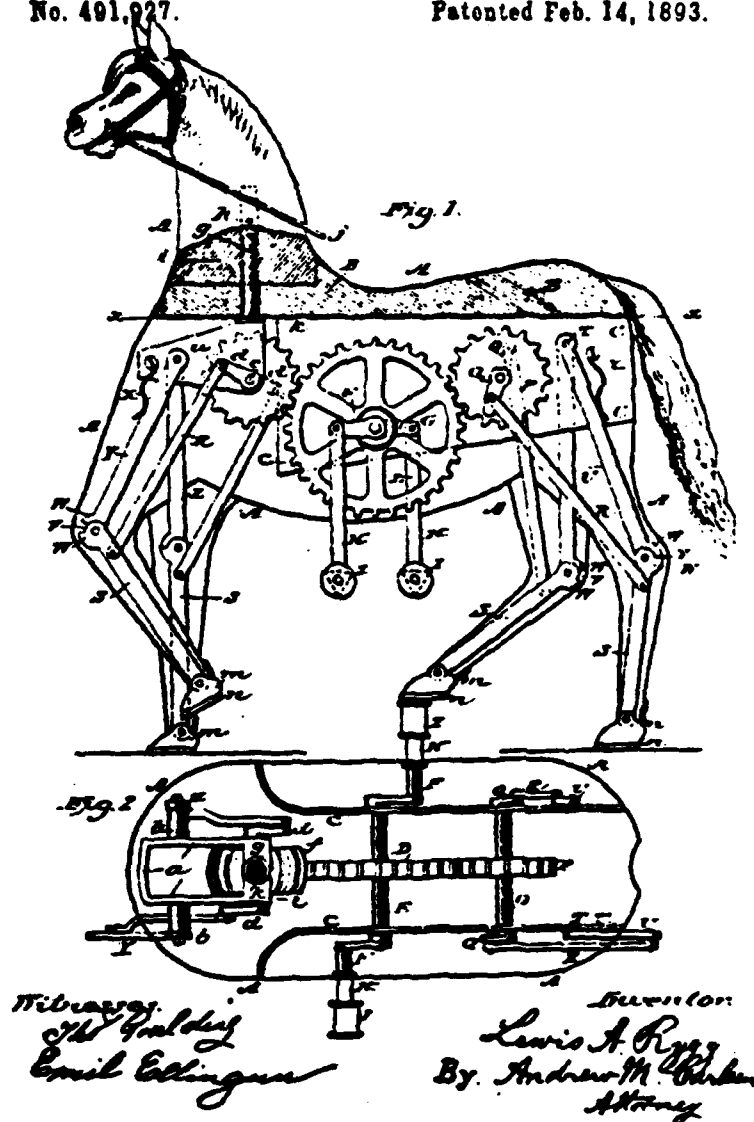


Figure 1.1: Patent drawing of a mechanical horse in 1893.

In 1913, Bechtolsheim obtained a patent for his design of a four-legged machine (see Figure 1.2). Again, there is no report of his success in building this machine.

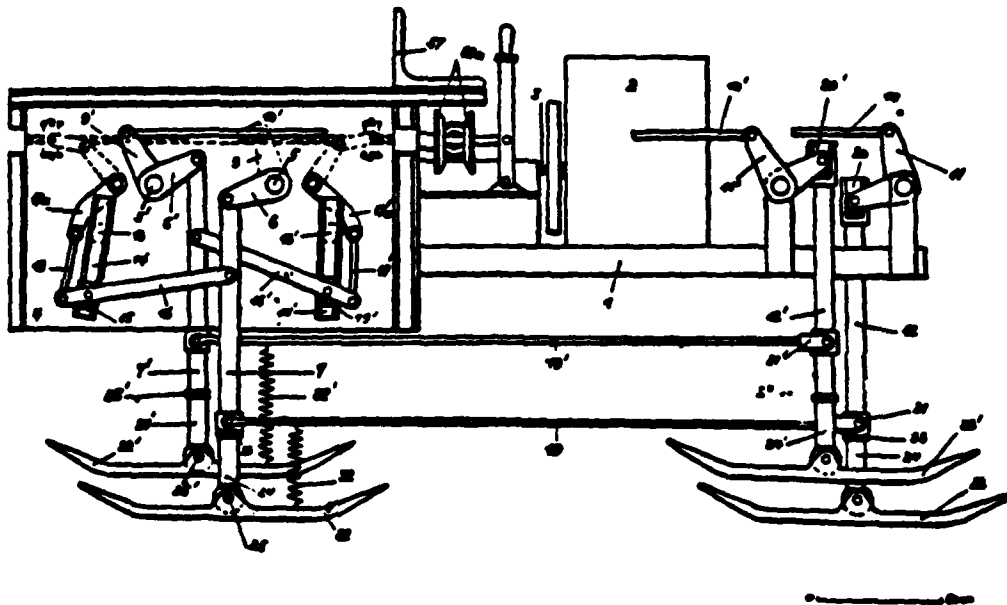


Bild. 2. — Der Schreitwagen des Freiherrn v. Bechtolsheim.
DEP 554354 aus dem Jahre 1913.

Figure 1.2: Patent drawing of a walking vehicle in 1913.

In the mid 1950's, a number of research groups started to study and develop walking machines in a systematic way. About a decade later, walking machines began to be designed and built by different groups in laboratories. Up to the present time, according to the

author's knowledge, about a dozen of these walking machines have been built [4 through 21]. Although some of these machines were able to walk in laboratories and demonstrate some mobility on certain occasions, all of these walking machines are still in their infancy and do not exhibit any of the advantages mentioned above in a practical sense.

The reasons for this slow progress mainly arise from the complexity of leg coordination control, the limited understanding of walking gaits and the lack of the development of practical machine legs. However, based on these previous research efforts and modern technologies in robotics and in microcomputers, a major improvement in legged walking machines is expected in the near future.

Currently, a research program at the Ohio State University, with the aid of some other research groups¹ is developing a fully self-contained, automatically terrain-adaptive, six-legged walking machine. This walking machine, known as the Adaptive Suspension Vehicle (ASV), has one human operator, can carry 500 pounds payload and is expected to demonstrate fuel economy and mobility which are superior to that of conventional wheeled and tracked vehicles in rough terrain. Figure 1.3 shows an artist's conception of the latest version of the ASV.

¹ University of Wisconsin, which is in charge of the flywheel power supply system, and Environmental Research in Michigan (ERIM), which is in charge of the video terrain-scanning system, are the two major support groups.

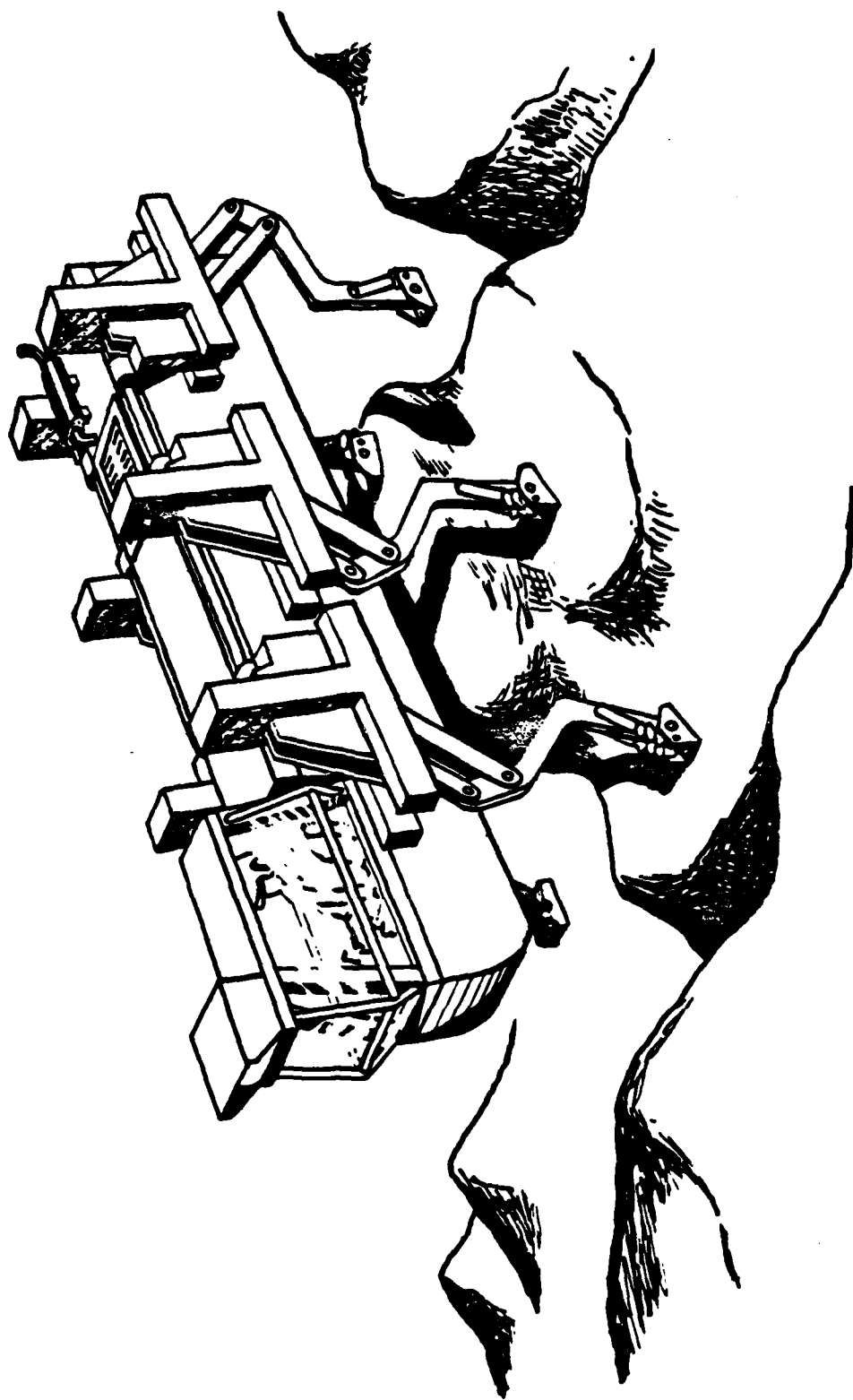


Figure 1.3: Artist's conception of the ASV.

In order to provide a more complete understanding of the ASV, the design specifications² are given in Table 1.1.

Table 1.1
Design Specifications of the ASV.

-Dimensions:	16 feet in length. 10 feet in height. 7 feet in track width.
-Weight:	6000 pound dry weight.
-Payload:	500 pound.
-Speed:	5 mph cruise speed. 8 mph sprint speed.
-Endurance:	10 hours.
-Grade climb ability:	> 60% slope. 70% for cross slope.
-Mobility:	
	* Ditch crossing: 6 feet.
	* Vertical step crossing: 5.5 feet.
	* Isolated wall crossing: 4.5 feet.
	* Fording depth: 4 feet.
-Fuel economy:	better than conventional vehicles in rough terrain.

² The design specifications fo the ASV has been revised along with the new development in the project.

In order to achieve this goal, research in the area of control, gait study, leg geometry, and power transmission and actuation are in progress to lay a proper theoretical foundation for the design of the ASV. Other research including development of a terrain scanning system, man-machine interface engineering, and different sensing techniques are also in progress to support this design.

The research described in this dissertation is part of the ASV project. The main objective of this dissertation is to kinematically design the leg mechanisms as well as the overall geometry of the ASV. As will be explained in the later chapters, both energy efficiency and mobility are closely related to leg geometry. In order to support the design of leg geometry, a sufficient analysis of walking gaits and mobility should be carried out. Hence, this dissertation can be divided into two major parts:

1. Gait analysis: To study the gaits used in level walking and obstacle crossing and the relationship of vehicle mobility to leg walking volumes.
2. Design of leg geometry: To design an optimal leg geometry which provides the required walking volume according to gait analysis, good energy efficiency, and simplicity in structure for good mechanical reliability.

1.3 Organization of this Dissertation

^A Chapter 2 is a review of previous work in the following two areas: The mechanical structure of walking machines and walking gaits. This review is given by way of historical surveys which highlight the important events in both areas.

In Chapter 3, the mathematical and graphical background for gait analysis is presented. The gait selection problem in different types of terrain is also discussed. Detailed studies of the major gaits used in level walking are presented. These major gaits include wave gaits, equal phase gaits, backward periodic gaits, discontinuous follow-the-leader gaits, and continuous follow-the-leader gaits. The relationship between gait stability and leg walking volume is also discussed.

In Chapter 4, gaits for walking on gradients and methods to improve stability are studied. Also, gaits which may be used in crossing three major obstacle types are studied. The three major obstacle types are ditches, vertical steps and isolated walls. In each case, the relationship between vehicle mobility and leg walking volume is studied.

In Chapter 5, the design of leg geometries based on four-bar linkages is discussed. Major techniques to optimize leg linkages for optimal walking volume are introduced. Other design aspects, including bearing loads, actuating force, mounting positions of the actuators, interference problems and stress analysis, are also considered. This design results in a four-bar leg and a seven-bar leg.

In Chapter 6, the design of a different leg geometry, based on a pantograph mechanism, is presented. A theoretical background of the motion characteristics of pantographs is given first. Then a design derived mainly by computer-aided graphical methods is shown. An analytical study of the walking volume of pantograph legs is also developed.

In Chapter 7, some other related items of the leg design are discussed. One of these is the foot-ankle system. A few conceptual

passive foot-ankle systems are introduced. The second is a numerical method to find the shortest crank for a four-finitely-separated-position-synthesis problem. The shortest crank usually results in a crank rocker, which is the most desirable linkage type in many applications.

Finally, in Chapter 8, the research work presented in this dissertation is evaluated and the future development of walking machines is discussed.

Chapter 2

SURVEY OF PREVIOUS WORK

2.1 Introduction

This chapter is a review of the previous work related to walking machines. Two surveys which highlight the important events are given below. One survey covers the hardware built in the past with emphasis on leg structures. The other survey covers the research in gaits. These surveys are given according to the chronological sequence of the reports or papers so that the trend of development can be understood.

Before we come to these surveys, it is helpful to point out the lack of the success in the design of a practical walking machine in the previous work, although the accomplishment has been significant. According to the author's observation, this results mainly from deficiencies of knowledge in three areas: control, gaits and actuation and leg design. If any of these three areas is not developed to fully satisfy the need of a practical walking machine, success will be limited.

The control of a legged vehicle, in the past, has been regarded as the most crucial aspect and has received considerable attention. Nearly all the walking machines constructed so far were built for

control study. However, many aspects of control require more study. This is particularly true of control of statically unstable locomotion.

Gait was originally studied by zoologists attempting to understand animal locomotion. It was not studied in a systematic way by engineers prior to the past twenty years. Before the ASV project began, the development of gait study included the study of animal locomotion, the study of periodic gaits, some computer simulation of the hexapod walk in irregular terrain, and the implementation of a few gaits for the walk in smooth terrain. As far as the need of an all-terrain practical walking machine, more study is required to enhance the vehicle's mobility in rough terrain and in obstacle crossing.

Research on power transmission, actuation and leg geometry is the newest topic of research among the three. In the following survey, only a few machines prior to the ASV project have shown a well considered leg design (the Space General Machine, the G.E. Quadruped and the PV II). It has been recognized gradually that a functional and efficient leg can not depend on control alone. More research on these issues is required for a practical walking machine.

Knowledge in these three areas has been made up gradually by researchers in the ASV project and in other groups. This dissertation contributes to the second and the third areas. The following are the two surveys which provide a proper understanding of the starting point of this dissertation

2.2 Survey of Legged Vehicles

In 1960, an extensive study of linkage mechanisms for legged locomotion undertaken by Shigley was reported in reference [4]. In that paper, he proposed several mechanisms which may be used as a leg for a walking machine. These mechanisms included four-bar linkages, linkages with a slide in a cam-groove, pantograph mechanisms...etc. He also built a vehicle with four rectangular frames. Each frame served as a leg and was nearly as long as the body. The legs were moved in pairs and the stroke was short enough to ensure static stability. The motion of the legs was controlled by a set of double-rocker linkages. Although it did function, it required non-circular gears for uniform velocity of foot motion and was found to be not practical.

In the early 1960's, Space General Corporation developed two walking machines in order to explore the concept of legged locomotion for a lunar rover. One of these was an externally powered, six-legged machine [5] while the other was a self-contained, eight-legged machine [6]. The leg motions of both machines were coordinated by cams and transmitted by linkages. These vehicles were quite effective within their design goals. The eight-legged machine could turn in its own length using a form of skid steering. The terrain adaptability was poor, however, due to a lack of the necessary degrees of freedom.

In 1966 and 1968, a four-legged machine dubbed the "Phoney Pony" built by Frank and McGhee at the University of Southern California was reported in references [7] and [8], respectively. This was the first legged vehicle to walk autonomously under full computer control.

Each leg possessed two degrees of freedom, and the joint coordination was performed by a computer instead of by cams or linkages. The leg was composed by two links and two single-degree-of-freedom joints. Both joints were actuated by electric motors via a worm gear speed reducer. The machine was powered externally through a cable and walked with two different gaits: the quadruped walk and the quadruped trot.

In 1968, a 3000 pound quadruped built by General Electric Corporation was reported [9, 10] (see Figure 2.1). Each leg possessed three degrees of freedom. The knee joint had one degree of freedom and the hip joint had two degrees of freedom. Each degree of freedom was actuated through a crank by a linear hydraulic cylinder. The operator controlled the four legs by his hands and feet through a master-slave type hydraulic servo system. Control of this 12-degree-of-freedom system was very demanding and difficult. Only a few people learned how to master it and they found operation for extended periods to be tiring. Although the G.E. quadruped did demonstrate impressive obstacle climbing ability and good mobility in difficult terrain, it became clear that a computer controlled system is necessary for a multi-degree-of-freedom vehicle.

In 1969, the largest off-road vehicle in the world, a coal-mining dragline called "Big Muskie," built by the Bucyrus-Erie Company was reported in reference [11]. The vehicle weighs twenty-seven million pounds and has four hydraulically powered legs. When it moves, the four legs raise the body and move forward or backward one stride and then lower the body to the ground. While the body

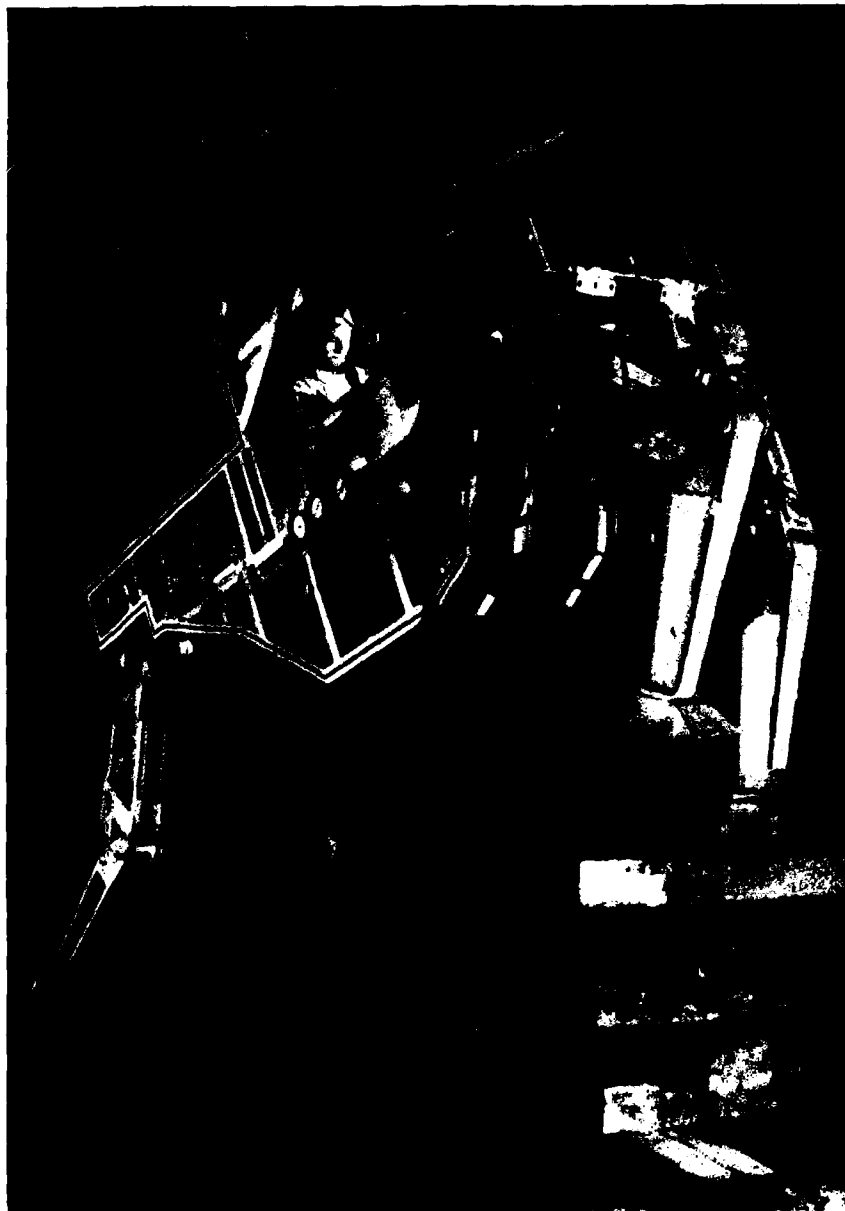


Figure 2.1: The G.E. Quadruped.

remains on the ground, the legs lift and move to the next position. This motion is cycled by an electronic sequencer.

In 1972, a group at the Institute Mihailo Pupin in Belgrade, Yugoslavia, built a biped exoskeleton to help paraplegics [12]. This biped was pneumatically powered and coordinated by an analog computer. It was successfully operated with or without a patient.

In 1972, an electrically powered, six-legged walking machine built by Petternella and his associates at the University of Rome was reported in reference [13]. This machine was similar to the Phoney Pony except that interaction between the human operator and the machine was attempted.

Since 1972 Kato, at Waseda University in Tokyo, Japan, has developed a series of computer controlled bipeds [14]. These bipeds could climb stairs under the control of an operator. The major flaw of these bipeds is a lack of speed. They required up to 90 seconds to complete one step.

In 1974, in Russia, a six-legged vehicle built at Moscow Physio-Technical Institute was first reported by Schneider et al [15]. Later, in 1978, the development of two six-legged walking machines was described by Okhotsimski and his colleagues [16]. One was operated under control of an analog computer and the other was equipped with a scanning distance-measuring system. Pictures of these machines were displayed in another of Okhotsimski's papers in 1978 [17]. Both machines were powered externally and one of them could turn in its body length. From the pictures, the leg structure is an "insect" type

leg composed of one upper link and one lower link. Each leg has three degrees of freedom. The joint is actuated by motors and gears. The foot pad is attached on the lower link with a gimbal joint.

In 1977, a six-legged walking machine, the OSU Hexapod, built by McGhee and his associates at the Ohio State University first walked in the laboratory [18]. This vehicle has been continuously improved since then by adding force sensors, gyroscopes, proximity sensors and a camera system [19,20]. This vehicle is fully controlled by a PDP 11/70 computer via an umbilical and is powered externally through a cable. The weight of this machine is 300 pounds. This machine was built primarily to study control algorithms for a walking machine. Each leg has three degrees of freedom and is made of two links connected by joints. Each joint is composed of an electric motor and a worm gear. Figure 2.2 shows the Hexapod is climbing down a step via a remote joy stick control.

In 1980, a four-legged walking machine called the PV II, built by Hirose and Umetani of the Tokyo Institute of Technology was reported in reference [21]. It only weighs 22 pounds and walks at an average speed of 0.8 in/sec with a power consumption of 10 Watts. Although this low power consumption is mainly due to its light weight and slow speed, a sophisticated leg design should also partially contribute to this relatively high efficiency. The leg geometry is a three dimensional pantograph mechanism. Each direction of motion is powered by a DC motor via a power screw speed reduction system. A passive ankle system is also included in the leg design. The PV II can maintain a



Figure 2.2: The OSU Hexapod.

horizontal body orientation and has contact sensors on each foot to detect contact with obstacles in its path or with the ground. It is powered externally and is controlled by an external computer via an umbilical cable.

In 1982, a one-legged walking machine, the Monopod,¹ was built by Vohnout at the Ohio State University [47]. The Monopod is a 20 inch high four-bar leg which is mounted on the inner frame of a three-wheeled cart. The inner frame is allowed to move vertically relative to the cart along ball bushings. During walking, the leg pushes the cart forward to gain speed in contact phase. The foot is then lifted by shortening the driven crank of the four-bar via a DC motor and ball screw system. The cart keeps on moving after the foot is lifted because of the inertial momentum. The machine was initially controlled externally by a PDP 11/70 computer. Later, the computer was replaced by an on-board microcomputer (Intel 8086). The Monopod was built to test the energy efficiency of the four-bar leg. The tested data was compared to the data of the OSU Hexapod and an improvement in specific resistance² by a factor of 20 was obtained.

Also in 1982, a six-legged passive walking machine, the DUWE, was built by Brown at the Ohio State University [48]. The DUWE was moved by a towing cart in front of the vehicle. A load cell was installed in

¹ Both the Monopod and the DUWE are part of the ASV project.

² The specific resistance is a dimensionless coefficient used to compare the efficiency of different biological and mechanical locomotion systems regardless of their weight [45].

the towing cable to measure the towing force. The DUWE walked in an alternating tripod gait. Each of the three legs (the front leg, the rear leg and the middle leg on the opposite side) were synchronized by a pulley and cable system. The vehicle was controlled by an Apple II microcomputer which was placed on the cart. The leg structure was similar to that of the Monopod except that the foot was lifted by shortening the driven crank via a toggle mechanisms actuated by a solenoid. The specific resistance of this vehicle also showed an even larger improvement over that of the OSU Hexapod. If the solenoid had been replaced by the same DC motor and ball screw system used in the Monopod, the improvement over the Hexapod was projected to be two orders of magnitude.

In 1983, a hopping machine was built by Raibert at Carnegie-Mellon University [50,58]. This hopping machine has only one leg and must hop continually in order to maintain balance. The leg has three degrees of freedom. The vertical motion is provided by a pneumatic cylinder which is mounted on the body frame via a gimbal joint. Two hydraulic actuators control the lateral motion of the leg. This machine is powered and controlled externally.

Also in 1983, a six-legged vehicle was built by Sutherland [50]. This machine was the first self-contained walking machine controlled by an on-board microcomputer. This machine could walk on smooth terrain and carry a human operator. Each leg had three degrees of freedom actuated by three hydraulic actuators. The leg structure was composed of two links and two joints. The hip joint was a universal

joint. The foot was moved by the coordination of three actuators. The on-board power supply was a gasoline engine which drove a set of hydraulic pumps.

In 1983, a six-legged "Functionoid," the ODEX I, built by Odetics Inc. demonstrated its strength and agility and was reported in reference [51]. The ODEX I can walk into a small truck under remote control only using leg movements pre-programmed with knowledge of the height of the truck bed. This is very different from step climbing by the OSU Hexapod or ASV. The ODEX I only weighs 370 pounds, yet it can lift a 900 pound weight. This machine is powered by an on-board aircraft battery and is controlled by on-board computers which receive commands from a joystick via radio telemetry. The six legs are mounted axisymmetrically around the body. Each leg has three degrees of freedom. The leg mechanism is a planar linkage mounted to the body via a vertical joint. The two degrees of motion of the planar leg linkage are actuated by motor and ball screw systems. The vertical rotating joints are moved by motors and gears.

2.3 Survey of Gait Study

As early as 1899, Muybridge used successive photographs to study the locomotion of animals [22]. In 1901, he applied the same techniques to the study of human locomotion [23]. His works are regarded as classics in the study of walking gaits.

In 1961, Tomovic and Kurplus of Yugoslavia were the first to use mathematical methods to analyze legged locomotion [24]. They applied the theory of finite states to legged locomotion systems. That is,

a leg is considered to be in either one of two states: on the ground or in the air.

In 1965, Hildebrand developed the concept of a gait formula³ to describe symmetric gaits in a complete and accurate way. He first defined the stride as the distance the body moves in one locomotion cycle. He then defined two independent variables used in the gait formula. One is the ratio of the time each foot is on the ground to each stride interval. The second is the ratio of the time the footfall of a fore foot lags behind the footfall of a hind foot on the same side to the stride interval. He also introduced the gait diagram to describe the gaits of horses [25].

In 1968, McGhee extended the work of Hildebrand and gave a strong mathematical base for the analysis of walking gaits. He defined the basic terminologies⁴ such as stride length, duty factor, phase...etc. He also adopted Tomovic's concept and defined a gait matrix [26].

In 1968, McGhee and Frank used longitudinal stability margins to study statically stable walking gaits of a quadruped. They proved mathematically that there is a unique optimum gait which maximizes the longitudinal stability margin of a quadruped [27]. The resultant gait stability margin is $\beta - 3/4$ where β is the duty factor, or ratio of the contact phase time to the stride period.

³ The gait formula defined by Hildebrand is slightly different from the definition given in Section 3.2.1.

⁴ The definitions of the terminologies used in this section are given in Section 3.2.1.

In 1972, McGhee and Jain defined another mathematical description of a gait, the "event sequence." They also categorized the 5,040 theoretically possible connected quadruped gaits into 492 column compatible classes. Then by the methods of column permutation and complementation they further reduced column compatible classes into 45 equivalence classes [28].

In 1973, Bessonov and Umnov showed by numerical experimentation that a regular and symmetric hexapod gait with the following phase relationships maximizes the longitudinal stability margin of all periodic gaits of a hexapod [29]:

$$\phi_3 = \beta, \quad \phi_5 = 2\beta - 1, \quad \beta \geq 0.5 \quad (2.1)$$

where ϕ_n is the phase of leg n and β is the duty factor. Phase is measured as the ratio of the time footfall of leg n lags behind that of leg 1 to the stride period.

In 1974, Sun further reduced the 45 equivalence classes of McGhee and Jain into 14 equivalence classes by the methods of wider class transformation. He also developed a computer program to calculate the longitudinal stability margins of six-legged regular and symmetric gaits. From the results of his program, he also found that the gait defined by Equation (2.1) maximizes the gait stability margin of hexapod gaits. His work was carried out independently of the work done by Bessonov and Umnov [30].

In 1979, a non-periodic gait, known as "free gait," was introduced by McGhee and Iswandhi [40]. A free gait is suitable for locomotion

over terrain which includes regions not suitable for weight bearing. These regions must be avoided by the control computer in deciding when and where to successively place the feet of the vehicle. Algorithms of free gait have been implemented into simulated coordination programs and vehicle motion displayed on graphical terminals. This preliminary study has shown the practicality of this algorithm for a walking vehicle. Free gaits depend on a terrain analysis system which can specify those regions which are not suitable for weight bearing.

In 1983, Tsai successfully implemented a follow-the-leader gait into a computer program on the OSU Hexapod [36]. In a follow-the-leader mode on each side of the body, the front leg steps on a selected foothold. The middle leg steps in the footprints of the front leg. The rear leg steps in the footprints of the middle leg. The selection of a foothold for the front leg was made by the human operator using a laser beam. In this way, the vehicle can avoid those regions which are not suitable for weight bearing while the operator is only concerned about the footholds for the two front legs.

2.4 Summary

From experience with walking machines built in the past, three aspects which are crucial for the design of a practical walking machine were found to require further study: control of legged vehicles, gaits and actuation and leg design. The vehicle control was regarded as the most crucial aspect of walking machine design because of its complexity. Intensive study in this area was done and is being

carried out by many researchers.

Efficient machine legs and actuation systems were not seriously studied until very recently. The legs of many previously built walking machines were made by directly connecting two links with actuated joints and resulted in poor efficiency. Only one recently built walking machine showed sophisticated leg design and had been shown to be more efficient than previously built machines. This machine used a pantograph as the basic leg mechanism. Among all the walking machines mentioned in this chapter, the Space General Machine, the Phoney Pony, the G.E. Quadruped, the Monopod and the DUWE had a vertical leg structure, or a "mammal" type leg, while most of the other machines had a horizontal leg structure, or an "insect" type leg.

The gait study in the past was concentrated on straight line locomotion in smooth terrain. Only very recently, algorithms such as free gaits and follow-the-leader gaits for walk in rough terrain were studied. Gait for obstacle crossing was very scarce in literature.

Chapter 3

GAIT ANALYSIS PART I - BACKGROUND FOR GAIT ANALYSIS AND GAITS FOR LEVEL WALKING

3.1 Introduction

A gait of an articulated living creature or a walking machine is the corporate motion of the legs, which motion can be defined as the time and the location of the placing and lifting of each foot, coordinated with the motion of the body in its six degrees of freedom, in order to move the body from one place to another. Therefore, for a certain motion of an animal or a walking machine, a gait can be defined. On the other hand, for a given well-defined gait, the motion of the animal or walking machine can also be precisely defined. Consequently, gaits describe and determine the speed, the direction of motion and the mobility of an animal or a walking machine. To a designer of a walking machine, a good understanding of gaits is essential. For instance, the number of legs, the leg geometry and the mobility performance are very much related to the selected gait.

The following example should explain the importance of gait analysis in the design of a walking machine. It has been noted that animals use similar gaits for certain motions. For example, horses have one gait for walking, another gait for trotting, and another gait for galloping. This similarity is also found in many other kinds

of animals. It appears that under certain conditions, e.g., a given speed, all members of a species adopt a similar gait. Moreover, very often, different species may use similar gaits under the same conditions of motion. For instance, the gaits for slow speed walking of tigers, lions, dogs, deer and many other animals are very similar.

A possible conclusion is that, under some conditions of motion, a certain gait is optimal. Thus different species adopt it spontaneously. The reasons for this optimality may be related to stability, leg structure, speed, mobility... etc. It is of great interest to determine the optimal gaits for various conditions and the reasons of their optimality. This understanding would help to choose proper gaits for a walking machine under various conditions. Leg performance and coordination should be compatible with all of the gaits which may be used. The most crucial aspect of the design of a walking machine is leg design and coordination. This design should be based on the results of gait analysis.

Due to the complexity of gait analysis, many aspects are still poorly understood. However, a few researchers in the past two decades have worked on this subject and a mathematically systematized foundation has been laid. Based on this foundation, many useful definitions and theorems for gait analysis have been developed. At the present time, it is possible to carry out further research in an efficient way.

3.1.1 Control Modes of the ASV

In order to obtain an overall understanding of the gaits for a walking machine, it is helpful to understand the control organization

of the machine. The proposed control scheme for the ASV is a kind of supervisory control instead of individual limb control. That is, the human operator only controls the general motion of the body, a problem of from two to six degrees of freedom, and leaves the other details, such as the control of individual limbs and the coordination of leg motion, to a computer.

The operator's cab is equipped with aircraft-style controls and displays; the operator steers and controls the speed through a three-axis joystick. An optical radar mounted on top of the cap provides terrain information which is used for foothold selection and body orientation in some control modes.

There are six control modes in total [37]. The first mode is the utility mode. This mode is used to check all major vehicle subsystems and for reprogramming the control computer.

The second, third and fourth modes are in so called "top-down" mode, in which the operator steers the vehicle along a good pathway in which every point can bear the load of a foot. In this mode, there is no capability for avoiding a hole immediately ahead of the vehicle. Hence, these modes are only suitable for the walking in relatively smooth terrain.

The second mode is the close maneuvering mode. It is a three-axis control mode in which the turning center for body rotation can be placed anywhere along the vehicle longitudinal axis. The operator gives a command of an arbitrary combination of yaw rotational rate, forward velocity, and lateral velocity through the three-axis joystick. Proximity sensors are used to keep a specified ground

clearance automatically for the legs in transfer phase¹. The optical radar is not used in this mode.

The third mode is the cruise mode. This mode is designed so that the vehicle has the most efficient fuel economy in cruise speed. Body crab angle is limited to a relatively small value. A crab angle is the angle between the longitudinal direction of the body and the direction of the motion. The minimum turning radius is held to several body lengths. Since an even power consumption is desirable, an equal phase gait² is expected to be used.

The fourth mode is the dash mode. In this mode, all aspects of vehicle performance are sacrificed for speed. Specifically, maneuverability is limited, ride characteristics are expected to be rough and fuel economy is expected to be poor. A wave gait with a low duty factor is expected to be used.

The last two modes are in so called "bottom-up" mode, in which the terrain condition is brought into consideration. In this case, the terrain immediately ahead of and around the vehicle is divided into discrete cells. Each cell is about the size of a footprint and is designated as either a permitted cell (suitable for weight bearing) or a forbidden cell.

The fifth mode is the terrain following mode. In this mode, all vehicle sensors are used. The optical radar provides terrain

¹ For definitions, please refer to Section 3.2.1.

² For gaits, please refer to Section 3.3.

information for the selection of the footholds. An algorithm making use of the free gait is implemented and is described as follows. The decision of placing and lifting of legs and their locations is made by a computer program. This program is written according to the reachability of each leg and the suitability of the land. The reachability is the kinematically reachable region of each leg. The suitability depends on the permitted cells of the ground. During locomotion, the operator gives the direction of body motion only. The computer selects some permitted cells in the reachable region of each leg, and generates the commands to place and lift the legs to accomplish the body motion. At any instant, the legs on the ground should ensure that the vehicle will be statically stable. If the percentage of forbidden cells is high, the vehicle may come to a position where no permitted cells are accessible for the placing of the legs to accomplish a desired body motion. The vehicle is said to be deadlocked and has to move back and change its direction of motion. A computer simulation of this approach has been successfully developed [38,39,40].

The sixth mode is the precision footing mode. In a general sense, a precision footing mode is a mode in which the operator selects a foothold and gives the commands controlling leg motion for each leg. This is the most basic control mode for rough terrain locomotion and was used by the G.E. Quadruped in the 1960's. At that time, the selection of footholds and the control of leg motion and coordination was all done by the operator through a master-slave hydraulic system. This resulted in rapid fatigue and marginal

stability due to high demands placed on the operator's motion coordination skills.

However, for the ASV, the operator is greatly aided by the help of computer-aided control and sensing technology. In this mode, the operator is able to control individual legs by means of joystick or keyboard. A CRT display shows the vehicle stability margin at any instance. Body motion control can be either automatic [41] or manual. In the manual mode. Joystick axes can be assigned either to translational or rotational body velocity control.

3.1.2 Contents of Sections

In Section 3.2, an introduction to the mathematical background and the graphical methods used for gait analysis is given. Both analytical methods and graphical methods are used interchangeably or simultaneously in the later sections and chapters.

In Section 3.3, a general guideline for the selection of a proper gait according to the conditions of terrain, the stability requirements, the power requirements, and the speed is given. A general description of the major gaits and their applications is also introduced. These gaits are periodic gaits, non-periodic gaits, wave gaits, equal phase gaits, backward periodic gaits, discontinuous follow-the-leader gaits, continuous follow-the-leader gaits, dexterous periodic gaits and large obstacle gaits.

In Section 3.4, a detailed study of the major gaits for level walking in different terrain is given. These major gaits include all the gaits mentioned in the last section except the large obstacle

gaits. In the next chapter, gaits for slope walking and obstacle crossing are studied.

3.2 Mathematical Background and Graphical Methods for Gait Analysis

Both analytical and graphical methods are necessary for gait analysis. The application of each method depends on the problem. Generally speaking, the analytical method serves as the main tool for gait analysis. With it, one can analyze numerous gaits in an efficient way. The graphical method provides a clear understanding of the gait geometry and is easy to relate to practical needs. In many instances, both methods are necessary to solve a problem.

3.2.1 Basic Definitions and Theorems for Gait Analysis

The basic definitions and theorems for gait analysis used in this dissertation are introduced in this section. Most of this work was established by McGhee and his co-workers and can be found in [31]. A few definitions in this section are modified from those of McGhee or defined by the author for the convenience of the discussion. In the later sections, many more definitions and theorems are given by the author along with the discussion. All the definitions and theorems are independently assigned a serial number. In order to help the understanding of the definitions, a hexapod with simplified dimensions is shown in Figure 3.1. These dimensions are used to calculate the performance of the ASV in the following chapters. In the following discussion, if not specified, the leg number of a $2n$ -legged animal is assigned as 1, 3, 5, ..., $2n-1$ on the left side and 2, 4, 6, ..., $2n$ on the right side from the front to the rear.

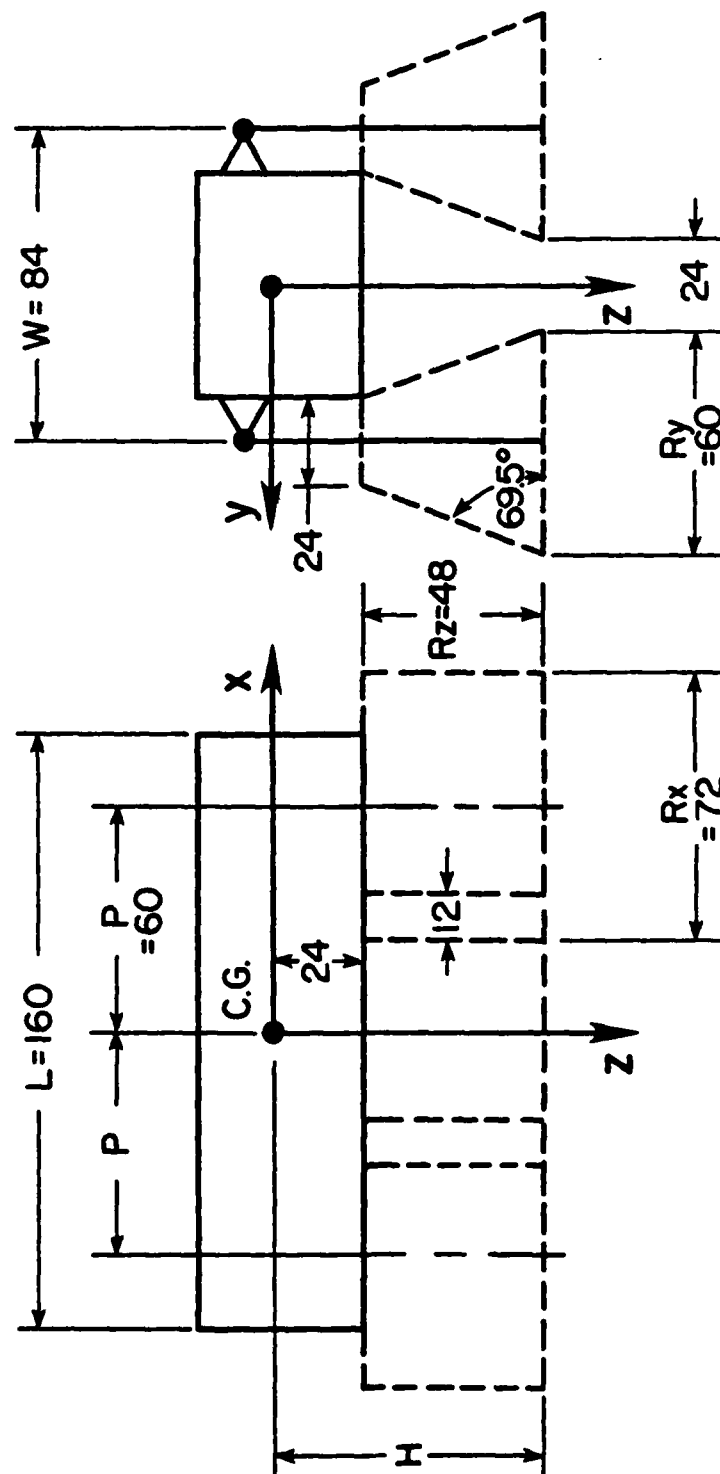


Figure 3.1: Simplified dimensions of the ASV.

Definition 1: The transfer phase of a leg is the period in which the foot is not on the ground. The leg state of a leg in transfer phase is 1.

Definition 2: The support phase of a leg is the period in which the foot is on the ground. The leg state of a leg in support phase is 0.

Definition 3: The cycle time, T , is the time for a complete cycle of a leg locomotion of a periodic gait.

Definition 4: The duty factor, β_i , is the time fraction of a cycle time in which leg i is in the support phase.

$$\beta_i = \frac{\text{time of support phase of leg } i}{\text{cycle time of leg } i}$$

Definition 5: The leg phase, ϕ_i , is the fraction of a cycle period by which the contact of leg i on the ground lags behind the contact of leg 1.

Definition 6: The leg stride, λ , is the distance the center of gravity translates during one complete locomotion cycle.

Definition 7: The leg stroke, R , is the distance through which the foot is translated relative to the body during the support phase.

Definition 8: The stroke pitch P , is the distance between the centers of strokes of the adjacent legs on one side.

Definition 9: The effective body length L_b , of a $2n$ -legged animal or walking machine is the distance between the centers of strokes of the front and the rear pair of legs. If all the stroke pitches are the same, the body length is

$$L_b = (n-1) \cdot P \quad (3.1)$$

Definition 10: A gait matrix, G , is a n -column matrix whose successive rows are n binary numbers (0 or 1) corresponding to the successive leg states of a gait of a n -legged animal or machine, and the total number of rows is equal to the number of states of the legs in one cycle of locomotion.

Definition 11: A gait formula, g , for a n -legged animal or machine is defined as

$$g = (\beta_1, \beta_2, \dots, \beta_n, \phi_2, \phi_3, \dots, \phi_n)$$

Definition 12: The dimensionless foot position, (X_i, Y_i) , is a pair of coordinate values which specifies the position of contact point of leg i . The X - Y coordinate system is chosen so that the origin is at the center of gravity, the X axis is aligned with the direction of motion and directed forward and the Y axis is normal to X and directed toward the right side of the X axis. The scale of the X and Y axes is chosen so that $\lambda = 1$.

Definition 13: The dimensionless initial foot position, (γ_i, δ_i) , is the value of the pair of coordinates (X_i, Y_i) of the initial contact position of leg i during any locomotion cycle.

Definition 14: The kinematic gait formula, K , for an n -legged locomotion system is defined as

$$K = (\beta_1, \beta_2, \dots, \beta_n, \gamma_1, \gamma_2, \dots, \gamma_n, \delta_1, \delta_2, \dots, \delta_n, \phi_2, \phi_3, \dots, \phi_n)$$

Definition 15: An event of a gait is the placing or lifting of a foot during locomotion. Each event is assigned a number. For a n-legged animal or machine, event i and $i+n$ are assigned to the placing and lifting events of leg i respectively.

Definition 16: A gait is singular if any two or more events occur simultaneously during a locomotion cycle.

Definition 17: A regular gait with the same duty for all legs.

$$\beta_i = \beta_j = \beta \quad \begin{array}{l} i, j=1, 2, \dots, n \\ n \text{ is the leg number} \end{array}$$

Definition 18: A gait is symmetric if the motion of the legs of any right-left pair is exactly half a cycle out of phase.

Definition 19: A support pattern of a animal or a walking machine is a two dimensional point set in a horizontal plane consisting of the convex hull of the vertical projection of all foot points in support phase.

Definition 20: A gait is periodic if similar states of the same leg during successive strokes occur at the same interval for all legs, that interval being the cycle time. Otherwise, it is a non-periodic gait.

Definition 21: The stability margin, SM, is the shortest distance of the vertical projection of center of gravity to the boundaries of the support pattern in the horizontal plane (see Figure 3.2).

Definition 22: The front stability margin and the rear stability margin are the distances from the vertical projection of the center of gravity to the front and rear boundaries of the support pattern,

respectively, as measured in the direction of motion. The longitudinal stability margin, SL , is the shorter of these two (see Figure 3.3).

Definition 23: The longitudinal gait stability margin, S , or the gait stability margin in brief, for a periodic gait, G , is the minimum of SL over an entire cycle of locomotion. A gait is statically stable if $S \geq 0$. Otherwise, it is statically unstable.

Definition 24: The dimensionless longitudinal gait stability margin normalized to stride, S^* , for a periodic gait, G , implied by a kinematic gait, K , is defined as

$$S^*(K) = S(K)/\lambda \quad (3.2)$$

The dimensionless longitudinal gait stability margin normalized to stroke pitch, S_p , for the same gait is defined as

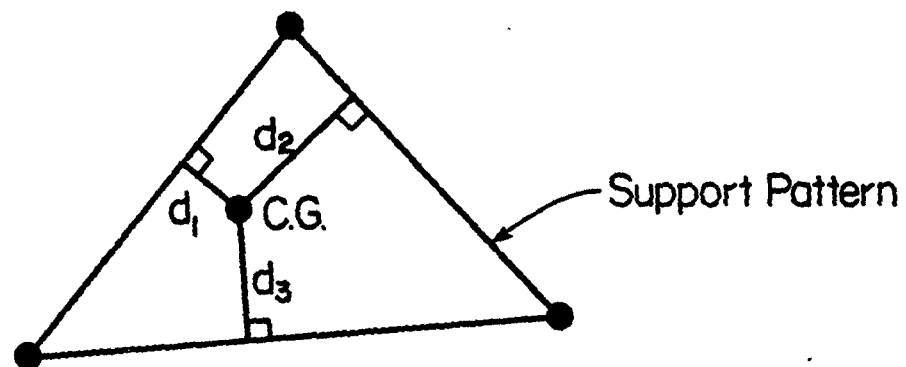
$$S_p(K) = S(K)/P \quad (3.3)$$

The dimensionless longitudinal gait stability margin normalized to stroke, S_r , for the same gait is defined as

$$S_r(K) = S(K)/R \quad (3.4)$$

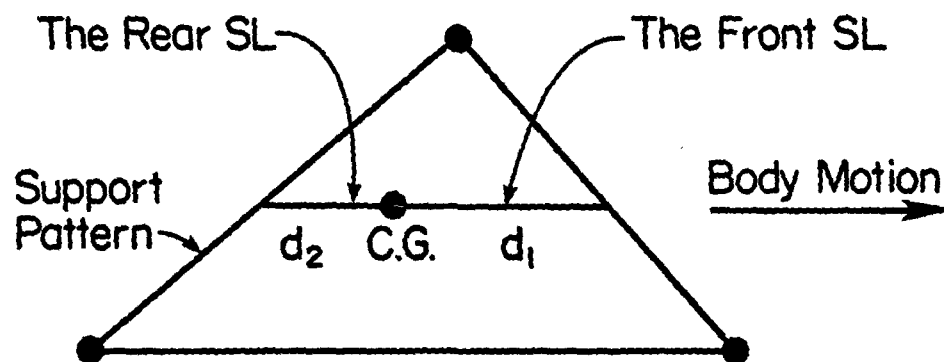
S^* , S_p and S_r can be called dimensionless gait stability margin or gait stability margins if there is no ambiguity.

Based on the definitions given above, several important theorems and results of gait analysis have been developed. These theorems and results are described as follows.



$SM = \text{Minimum of } d_1, d_2 \text{ and } d_3$

Figure 3.2: Stability margin SM of a support pattern.



$SL = \text{Minimum of } d_1 \text{ and } d_2$

Figure 3.3: Longitudinal stability margin SL of a support pattern.

Theorem 1: McGhee and Frank [27] have proved mathematically that there is a unique optimal gait which maximizes the static stability of a four-legged animal. The resultant gait stability margin S^* is

$$S^* = \beta - 3/4 \quad \text{for } R \leq P \text{ and } 3/4 < \beta < 1 \quad (3.5)$$

Bessonov and Umnov [29] made an extensive study by numerical experimentation to examine the gait stability margin of all possible six legged regular gaits. They discovered that, for a six legged gait, the gait stability margin is maximized by a regular symmetric gait defined as

$$\phi_3 = \beta, \quad \phi_5 = 2\beta - 1, \quad 1/2 \leq \beta < 1 \quad (3.6)$$

From Theorem 1 and Bessonov's discovery, an interesting fact was observed, normally that both gaits with optimal stability for four and six legs are the gaits used by many animals. It seems that animals automatically optimize their gait for locomotion. Moreover, there is a similarity between these two gaits: the placing of each foot runs from the rear leg to the front leg along either side as a wave and further, each pair of legs is 180° out of phase. That is, it is a symmetric gait. It is also a regular gait. This kind of gait is called the wave gait. Due to the nature of optimal stability, wave gaits have been proposed for use in walking machines by many people [29,32,33,34,35].

Sun [30] discovered by numerical experimentation that the gait stability margin of a $2n$ -legged regular symmetric gait is maximized by a wave gait. The general form of wave gait can be described as

$$\phi_{2m+1} = F(m\beta), m = 1, 2, \dots, n-1, \quad 3/n \leq \beta < 1 \quad (3.7)$$

where $F(X)$ is the fractional part of real number X , that is, it is X modula 1, and m denotes successive legs on the left side numbered from front to back.

The formula for the gait stability margins of wave gaits for 6-legged animals was not previously found. Sun has developed a computer program, HSM, to compute the gait stability margin for regular symmetric gaits [30]. Hence the gait stability margin of 6-legged wave gaits can be calculated by that program. This program has been modified by the author and further developed into a new program, HSM2, which stands for Hexapod Stability Margin Version 2. HSM2 is used as a powerful tool to interactively analyze many different gaits in the later sections of this thesis. Several useful results are obtained and a general formula for the gait stability margin of wave gaits for $2n$ -legged locomotion system will be derived.

3.2.2 Graphical Methods for Gait Analysis

Several useful graphical methods for gait analysis are presented in this section. The degree of complexity and the functions of the methods vary widely. Some of these techniques can only partially represent a gait, some can fully represent a gait, some can be used to study the stability margin of a periodic gait and some can be used to study gaits for obstacle crossing. A designer can choose the proper method according to his need. One common characteristic of the graphical methods is that they give a quick understanding and a

geometric representation of a gait. This characteristic is not found in mathematical formulae or computational algorithms. Therefore graphical methods are helpful in gait analysis and are important on many occasions such as the optimization of gaits or the study of the changing of gaits during locomotion.

Motion picture camaras were used by Muybridge [22] to study the animal locomotion in the 1880's. He conducted a series of experiments to take sequential photographs of the motion of 25 kinds of animals by triggering a battery of still cameras. Later, he used the same technique to study human locomotion. His work is very comprehensive and useful and is still considered a classical work in the area of locomotion study.

Footfall formulas were devised by students of legged locomotion for representing gaits a long time ago [25]. The animal is viewed from above as it moves from left to right. Black circles indicate that the corresponding legs are in the support phase, and the arrows indicate the direction of motion of the body during the corresponding foot patterns. Figure 3.4 shows an example of a footfall formula.

The gait diagram was first used by Hildebrand to record the gaits according to the films of motion pictures [25]. Each horizontal line is assigned to a leg, and the darkened lines indicate the period of the support phase. The beginning and end of a darkened line correspond respectively to the placing and lifting of a foot. This method not only records the sequence of placing and lifting of different feet, it also records the duration of the support and transfer phases of each leg. Hence, it leads to a mathematical analysis of walking gaits.

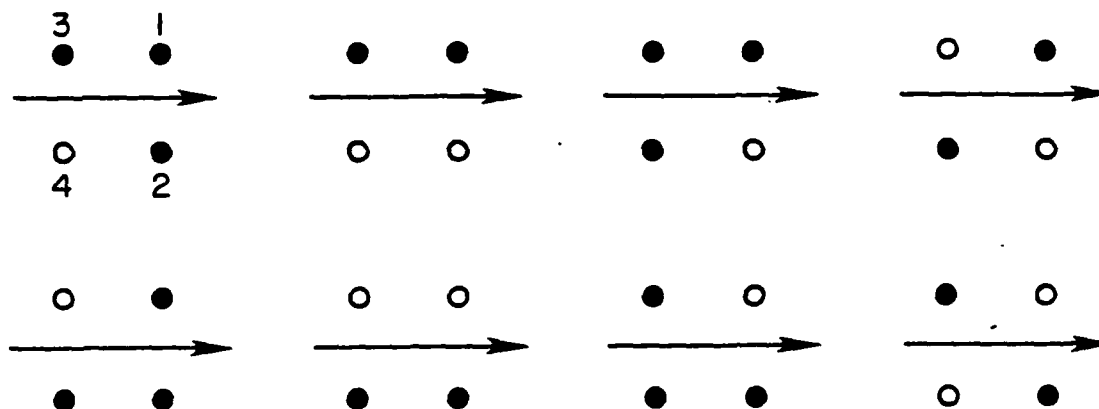


Figure 3.4: A footfall formula of a quadruped gait.

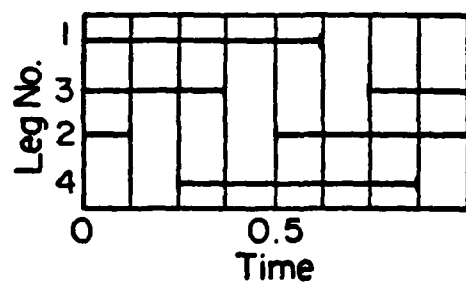
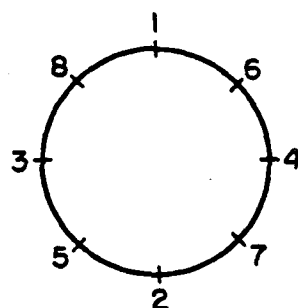


Figure 3.5: A gait diagram of quadruped gait.

Figure 3.5 shows an example of a gait diagram.

An event sequence is the placing and lifting sequence of a gait. For a periodic gait, it is convenient to record the sequence on a circle. The circumference of the circle represents the cycle time and is generally normalized to be 1. Figure 3.6 shows the event sequence of a quadruped gait. Events 1,2,3,4 are the placing events and events 5,6,7,8 are the lifting events of legs 1,2,3 and 4, respectively. The sequence is read in a clockwise sense.



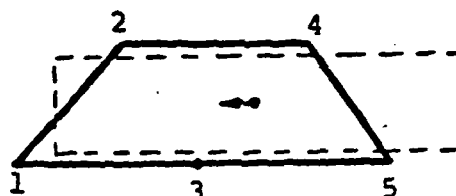
E=16472538

Figure 3.6: An event sequence of a quadruped.

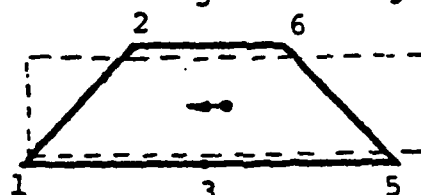
A successive gait pattern is a series of successive support patterns of a gait. The dashed rectangles and the darkened dot are the body of the machine and the vertical projection of the center of gravity, respectively, at the beginning of the support pattern. The arrow indicates the position of the projection at the end of that pattern. Figure 3.7 shows an example of a successive gait pattern

Time Sequence

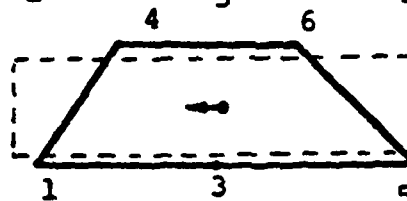
t1



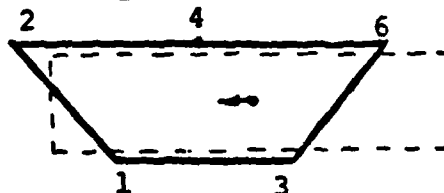
t2



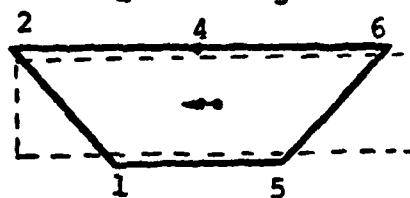
t3



t4



t5



t6

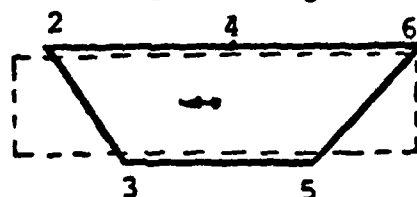


Figure 3.7: A successive gait pattern.

The stationary gait pattern was first used by the author to study the gait stability margin of periodic gaits. It is drawn according to the gait diagram. This method is very useful because it shows the support patterns at different times and the corresponding body motion for each support pattern in one single diagram. The stability margin of a gait can be calculated directly from the diagram. Figure 3.8 is an example of a stationary gait pattern.

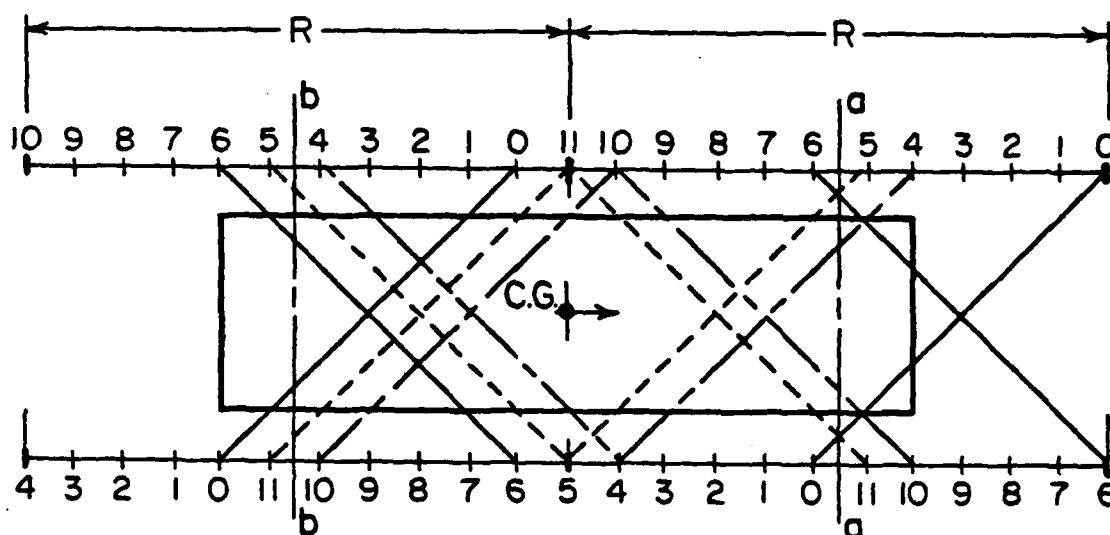


Figure 3.8: A stationary gait pattern of a quadruped gait.

The lateral motion sequence is the successive lateral views of a walking machine during motion (see Figure 3.9). The dashed rectangles indicate the walking envelopes of the legs. That is, any point in a rectangle is accessible to the foot of the corresponding leg. The darkened dot is the center of gravity. The arrow points to

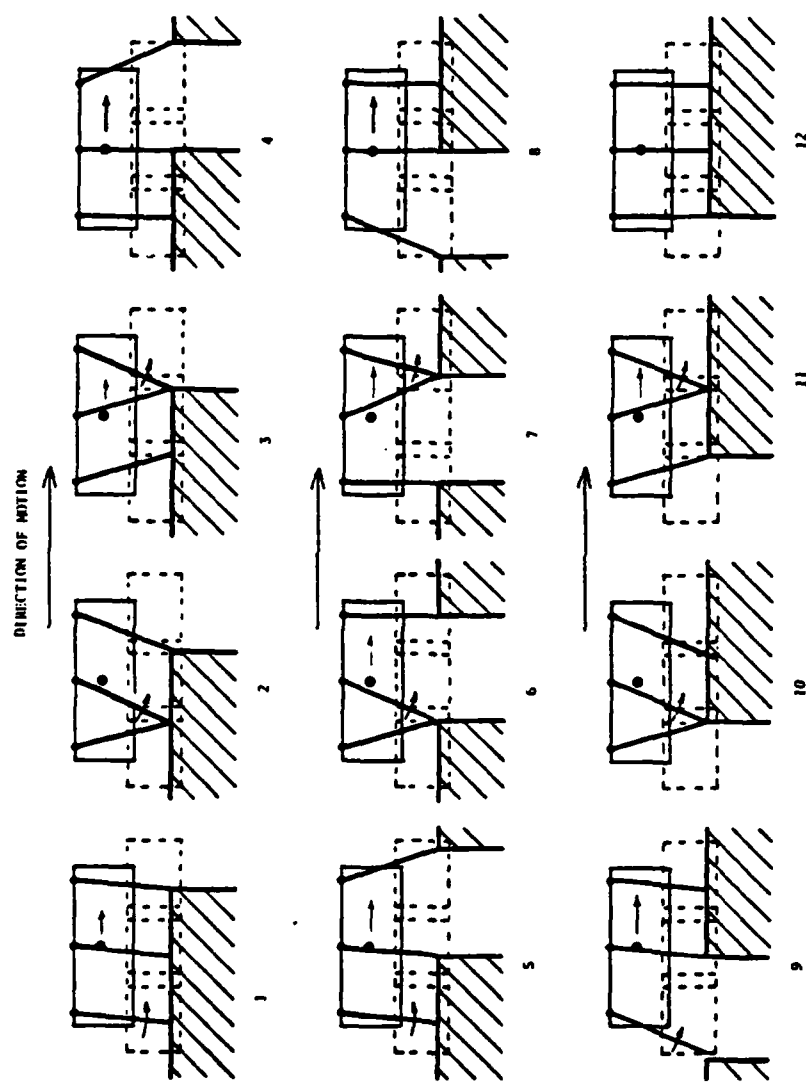


Figure 3.9: A lateral motion sequence of a hexapod.

the end position of the center of gravity in the current leg pattern. This method is very useful in studying obstacle crossing. If the corresponding support patterns are also shown, the stability at each instant can be visualized.

Computer-aided graphical methods have been used to simulate the locomotion of a walking machine during the last decade. Both two and three dimensional pictures can be generated on the screen. A corresponding support pattern with the projection of the center of gravity is shown on the top of the machine to indicate the stability at each instant. The machine can be animated to aid in understanding of the gait.

3.3 Gait Selection for a Walking Machine

The gait selection problem depends on the following factors: condition of the terrain, stability requirements, ease of control, smoothness of body motion, speed requirements, mobility requirements and power requirements. Although this is a very complicated problem and needs further research and more practical experiments for a fuller understanding, a general guideline can be developed and is described below.

Since the gait selection is very dependent on the condition of the terrain, it is helpful to define the terrain conditions before the gait selection is studied. As mentioned in Section 3.1.1, level ground can be divided into many discrete cells. Each cell is about the size of a footprint, and can be classified into either a permitted cell if it is suitable for foot bearing or a forbidden cell if it is not. This

concept can be extended to a three dimensional terrain as follows:
A forbidden cell is a place on the terrain which is not suitable for the placing of a foot due to weak soil structure, steep slope, interference between terrain and legs or any other reasons.

Based on this concept, any terrain can be roughly categorized into one of the following three types. One is called perfect terrain, in which no forbidden cell exists in the planned pathway. The second is called fair terrain, in which a few forbidden cells exist in the pathway; the human operator can avoid them by simple maneuvering of the machine or the machine can negotiate the terrain automatically using the terrain scanner and a free gait algorithm. The third is called rough terrain, in which many forbidden cells exist in the pathway. The human operator has to carefully select a few permitted cells for the placement of the feet.

According to Definition 20, gaits are of two types: periodic and non-periodic. In general, periodic gaits are preferable because they are easy to be implemented into a computer program.

If the terrain is a perfect terrain, a periodic gait should be used. Among the many periodic gaits, wave gaits give the optimal gait stability. The wave gait is also the gait used by many animals. Equal phase (EPH) gaits can equally distribute the placing and lifting events in a locomotion cycle. Hence, fluctuations in power consumption are minimized. When the power system of a walking machine is sensitive to peaks of instantaneous power consumption, EPH gaits should be applied. For both wave gaits and EPH gaits, the sequence of placing events of the legs on each side runs from the rear leg and proceeds forward to

the front leg. Therefore, they are in the category of forward periodic gaits. If the sequence of placing events is reversed, they become backward periodic gaits. For a backward gait, the front leg is placed first, the middle leg follows, and finally the rear leg. This kind of placing sequence is recommended for a discontinuous follow-the-leader gait which will be discussed shortly. Backward periodic gaits can also be used in perfect terrain. However, the main interest in the backward periodic gait is the possibility that it can be modified into a follow-the-leader gait.

If the terrain is a rough terrain, a periodic gait can not be used because it lacks the ability to locate the feet exactly on the few permitted cells. Therefore, a non-periodic gait has to be used. Among the many non-periodic gaits, the most basic is the precision footing gait in which the human operator controls the body motion and individual leg motion through a precision footing mode. However, due to the heavy demands on the human operator, precision footing gaits should be used only when no other gaits are suitable for the terrain condition. If there are some large obstacles in the path way, a large obstacle gait (LOG) should be used. LOGs are specifically designed for different large obstacles. For some obstacles such as a typical ditch, LOG may be fully automated. For the other obstacles, LOG may be generated through a precision footing mode. If there are no large obstacles in the way, a follow-the-leader (FTL) gait should be used. In an FTL gait, the human operator selects only the locations for the two front legs, the computer program then automatically places the middle legs on the exact place where the front legs

were, then the rear legs on the exact place where the middle legs were. Thus, FTL gaits can guarantee all the legs are placed on the permitted cells during locomotion. An FTL gait can be either non-periodic or periodic. A non-periodic FTL gait generates discontinuous body motion and is also called a discontinuous FTL gait. On the contrary, a periodic FTL gait generates continuous body motion and can reach higher speed, and is called continuous FTL gait. If the rough terrain has only a few permitted cells, a discontinuous FTL gait is suitable. If more permitted cells exist, a continuous FTL gait or a free gait should be applied.

If the terrain is a fair terrain, that is, only a few forbidden cells exist in the pathway, the continuous FTL gaits should be used because it can avoid these forbidden cells and maintain smooth body motion. Other periodic gaits, such as wave gaits, EPH gaits and backward periodic gaits, can also be used if they are subject to adjustment by the system in response to data from the terrain scanner. This adjustment mainly consists of placing the feet ahead, behind, to the right of or to the left of the original footholds. If a forbidden region is detected by the system, the computer would adjust the legs according to a pre-programmed implemented strategy to avoid the forbidden region while maintaining the periodic feature of the gait. This is called the dexterous periodic gait. The strategy used by a dexterous periodic gait to avoid a forbidden region is very similar to the strategy used by the continuous FTL gait. Another option for fair terrain is the free gait.

A chart to summarize the principle of gait selection is shown in Table 3.1. The relationship among all the gaits discussed above is shown in Figure 3.10.

The speed of a walking machine usually affects gait stability. If the speed is increased, the cycle time of the gait is decreased, thus, leg speed in the support phase and return phase is increased. When the return speed of the legs reaches the maximum speed of the actuating system, the duty factor is decreased in order to maintain speed. Hence, gait stability is decreased.

3.4 Gaits for Level Walking

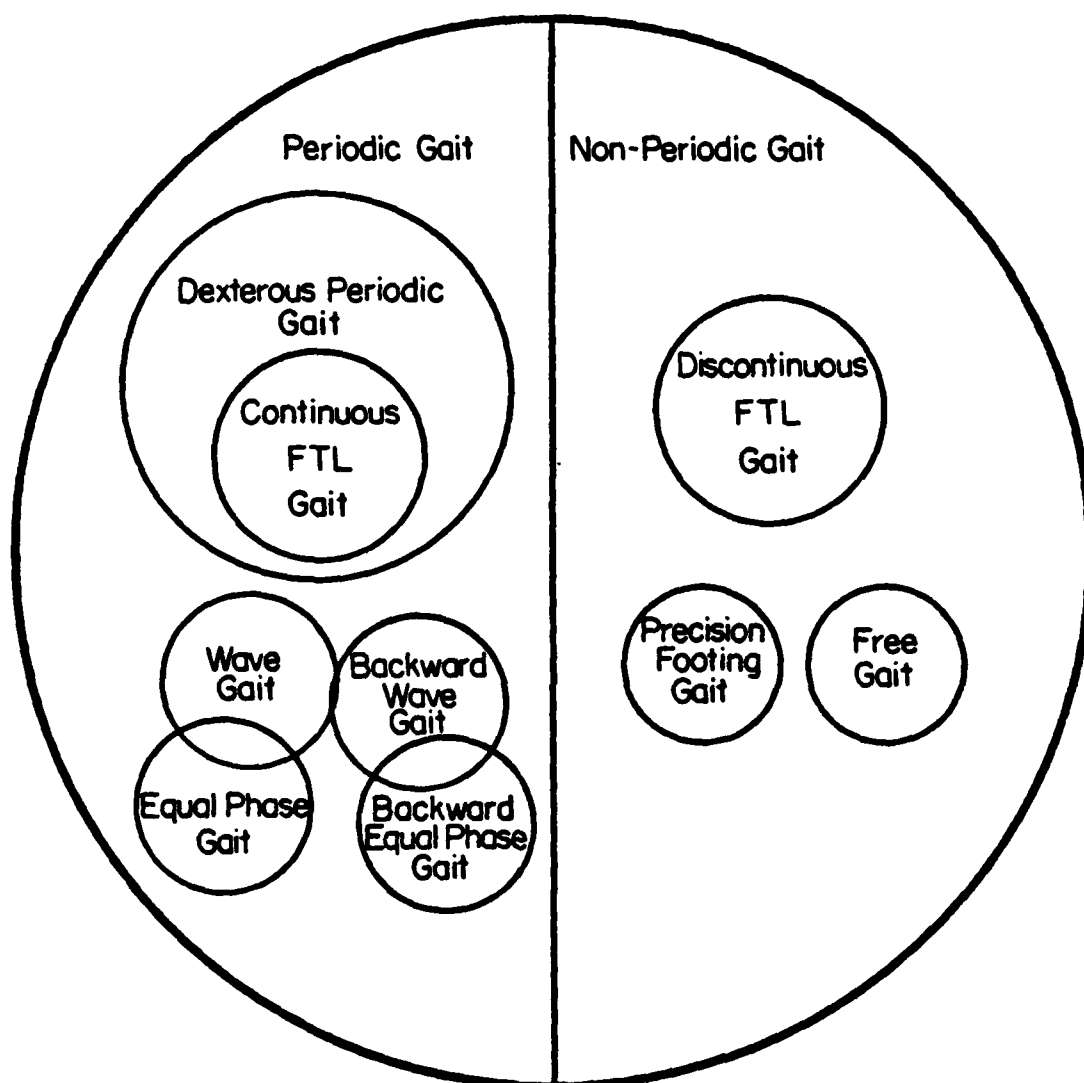
In this section gaits for level walking in perfect terrain, fair terrain and rough terrain are studied in detail. Wave gaits, equal phase gaits and backward periodic gaits are covered in Sections 3.4.1, 3.4.2 and 3.4.3 respectively. All of these three gaits can be used for the walking in a perfect terrain. Wave gaits are important for the ASV because of their optimal gait stability. A complete analysis of the gait stability margin and of various effects on the gait stability margin by varying the stroke and the stroke pitch is given. In the study of equal phase gaits and backward periodic gaits emphasis is placed on the matter of equally distributing events and on the backward stepping sequence respectively. On many occasions, program HSM2 is applied to study the relationship of gait stability margin and the duty factor.

Discontinuous FTL gait is discussed in Section 3.4.4. A general approach to generation of a discontinuous FTL gait is developed. This

Table 3.1

Summary of Gait Selection

gaits	gait stability	suitable terrain	computer implemen- tation	power consump- tion	smoothness of body motion
wave gait	good	perfect	easy	not even	good
EPH gait	good	perfect	easy	even	good
backward wave gait	fair	perfect	easy	not even	good
backward EPH gait	fair	perfect	easy	even	good
dexterous periodic gait	good or fair	fair	fair	even or not even	good
continuous FTL gait	fair	fair or rough	fair	not even	good
discontinuous FTL gait	very good	rough	hard	not even	poor
LOG gait	fair	obstacle	fair	not even	poor
precision footing gait	very good	rough with obstacles	very hard	not even	poor
free gait	good	rough	hard	not even	fair



Classification of Gaits

Figure 3.10: Classification of gaits.

gait is suitable for rough terrain.

Continuous FTL gait is studied in Section 3.4.5. A periodic gait with the nature of FTL gait is discussed first, methods to modify it into a continuous FTL gait are then introduced. Strategies for a continuous FTL gait to pass over different forbidden regions are also introduced. The methods used to modify a periodic gait into a dexterous gait are discussed in principle. The continuous FTL gait is suitable for rough terrain with many permitted cells and for fair terrain, while the dexterous periodic gait is only good for fair terrain.

3.4.1 Wave Gaits

In Section 3.2, the mathematical expression of a wave gait for a $2n$ -legged animal or machine is quoted as:

$$\phi_{2m+1} = F(m\beta), \quad m = 1, 2, \dots, n-1 \quad \text{and} \quad 1 > \beta \geq 3/n$$

where $F(X)$ is the fractional part of real number X , and m denotes successive legs after leg 1 on the left side number from front to back. From this definition, wave gaits for four, six, and eight legged animals and machines are shown as follows:

$$2n = 4, \quad \phi_3 = \beta, \quad \beta \geq 3/4 \quad (3.8)$$

$$2n = 6, \quad \phi_3 = \beta, \quad \phi_5 = 2\beta - 1, \quad \beta \geq 1/2 \quad (3.9)$$

$$2n = 8, \quad \phi_3 = \beta, \quad \phi_5 = 2\beta - 1, \quad \phi_7 = F(3\beta), \quad \beta \geq 3/8 \quad (3.10)$$

From Theorem 1, the gait stability margin of four legged gait is maximized by a wave gait. The formula for the gait stability margin is

$$S^* = \beta - 3/4, \quad \beta \geq 3/4 \text{ and } R \leq P \quad (3.11)$$

Unlike the case of a four legged wave gait, the equation for the gait stability margin of a 6-legged wave gait was not previously derived. Since the equation for a 4-legged wave gait is very simple, and since wave gaits are very important for the ASV because of their optimal stability margin, it is desirable to find a formula to calculate the gait stability margin of 6-legged wave gaits or, more generally, for $2n$ -legged wave gaits.

Both graphical methods and analytical methods can be applied to derive such an equation. The results of these two methods are consistent. Since the analytical method provides a good foundation in mathematics, and the equations derived from it are more general, a complete analytical derivation is given below. The graphical approach is also noteworthy and can be applied to other gaits for which the analytical method is not available. This approach is detailed in Appendix A. Figure 3.11 shows the gait diagrams of wave gaits for several duty factors.

Definition 25: A fractional function $F(X)$ of a real number X is defined as follows

If $X \geq 0$, $Y =$ the fractional part of X

If $X < 0$, $Y = 1 -$ the fractional part of $-X$

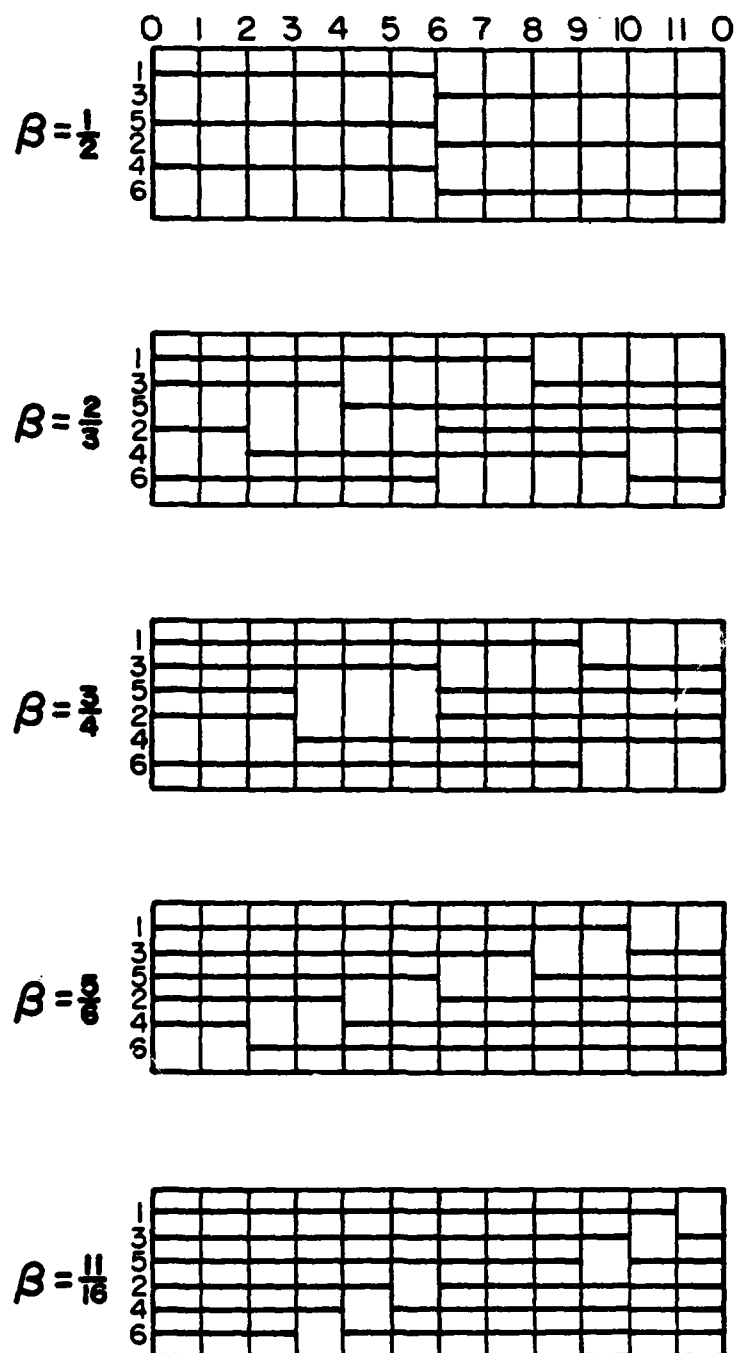


Figure 3.11: Gait diagrams of wave gaits.

According to the definition of $F(X)$, the following rules of $F(X)$ can be established.

$$F(F(X)) = F(X) \quad (3.12)$$

$$F(-X) = 1 - F(X) \quad (3.13)$$

$$F(N + X) = F(M + X), \quad N \text{ and } M \text{ are integer} \quad (3.14)$$

$$F(A + F(B)) = E(A + B) \quad (3.15)$$

Definition 26: The phase of leg i relative to leg j , ϕ_{i-j} , is the time phase of the placing of leg i after the placing of leg j . When leg j is the left rear leg, the phase of leg i relative to the left rear leg is called the negative phase and is denoted as ϕ_i' .

$$\phi_{i-j} = 1 - \phi_{j-i} \quad (3.16)$$

Definition 27: A local phase, $L\phi_i$, of leg i is the time phase of the current leg position after the placing of the leg. If the time phase after the placing of leg j is t , the local phase of leg i can be calculated as

$$L\phi_i = F(t - \phi_{i-j}) \quad (3.17)$$

Definition 28: A constant phase increment gait is a gait which has the same phase difference for successive legs on the same side.

Theorem 2: For a periodic, regular and symmetric gait of a $2n$ -legged walking machine, any support pattern has a mirror symmetric support pattern about the longitudinal axis of the body in one

locomotion cycle. The time phase between each pair of symmetric support patterns is $1/2$.

Proof: Let the gait have arbitrary phases X_n , where n denotes the leg number of the legs on the left side as

$$\phi_1 = 0$$

$$\phi_3 = X_3$$

$$\vdots$$

$$\phi_{2n-1} = X_{2n-1}$$

From the definition of the symmetric gait, the phases of the legs on the right side are

$$\phi_2 = 1/2$$

$$\phi_4 = F[1/2 + X_3]$$

$$\vdots$$

$$\phi_{2n} = F[1/2 + X_{2n-1}]$$

At any time phase t_1 , $0 \leq t_1 \leq \beta$, the local phases of all legs become

$$L\phi_1 = t_1$$

$$L\phi_3 = F[t_1 - X_3]$$

$$\vdots$$

$$L\phi_{2n-1} = F[t_1 - X_{2n-1}]$$

$$L\phi_2 = F[t_1 - 1/2]$$

$$L\phi_4 = F[t_1 - 1/2 - x_3]$$

: :

$$L\phi_{2n} = F[t_1 - 1/2 - x_{2n-1}]$$

Since the velocity of the vehicle is R/β , the leg is moving with speed $-R/\beta$ relative to the body. The position of each leg, P_n , relative to the center of the stroke becomes

$$P_1 = R/2 - t_1 \cdot R/\beta$$

$$P_3 = R/2 - F[t_1 - x_3] \cdot R/\beta$$

: :

$$P_{2n-1} = R/2 - F[t_1 - x_{2n-1}] \cdot R/\beta$$

$$P_2 = R/2 - F[t_1 - 1/2] \cdot R/\beta$$

$$P_4 = R/2 - F[t_1 - 1/2 - x_3] \cdot R/\beta$$

: :

$$P_{2n} = R/2 - F[t_1 - 1/2 - x_{2n-1}] \cdot R/\beta$$

After a half cycle of locomotion, the time phase t_1' becomes $t_1 + 1/2$. Substitute t_1' into t_1 in the above equations to find the new positions of each leg P_n' relative to the center of the stroke.

$$P_1' = R/2 - F[t_1 + 1/2] \cdot R/\beta$$

$$P'_3 = R/2 - F[t_1 - 1/2 - X_3] \cdot R/\beta$$

: :

$$P'_{2n-1} = R/2 - F[t_1 - 1/2 - X_{2n-1}] \cdot R/\beta$$

$$P'_2 = R/2 - t_1 \cdot R/\beta$$

$$P'_4 = R/2 - F[t_1 - 1 - X_3] \cdot R/\beta$$

: :

$$P'_{2n} = R/2 - F[t_1 - X_{2n-1}] \cdot R/\beta$$

Comparing the new positions P'_n to the old positions P_n and applying the rules of fractional function shows

$$P'_1 = P_2$$

$$P'_3 = P_4$$

: :

$$P'_{2n-1} = P_{2n}$$

$$P'_2 = P_1$$

$$P'_4 = P_3$$

: :

$$P'_{2n} = P_{2n-1}$$

This means that, after half a cycle, the foot positions of the left side become the foot positions of the right and vice versa. Thus, the support patterns of the second half cycle are symmetric to the support patterns of the first half cycle along the longitudinal axis of the body. In other words, after a half cycle, the support patterns are the mirror images of those of the first half cycle along the longitudinal axis. This completes the proof.

Theorem 3: For a periodic, regular and constant phase increment gait of a $2n$ -legged walking machine, any support pattern has a symmetric support pattern along the lateral axis of the body, which goes through the center of the body and is perpendicular to the longitudinal axis, in one locomotion cycle. The time phase from a support pattern to its mirror image is

$$\Delta t = \beta - F[2t - (n-1) \cdot (1-X)] \quad (3.18)$$

where t is the time phase of the support pattern and X is the constant phase increment.

Proof: Let the phases of successive legs on either side be incremented by a constant X , $0 < X < 1$, and the leg on the right side have an arbitrary phase difference Y relative to the corresponding leg on the left side. At any time phase t , $0 \leq t \leq \beta$, the local phases of each leg become

$$L\phi_1 = t$$

$$L\phi_3 = F[t-X]$$

$$\vdots \quad \quad \vdots$$

$$L\phi_{2n-3} = F[t - (n-2) \cdot X]$$

$$L\phi_{2n-1} = F[t - (n-1) \cdot X]$$

$$L\phi_2 = t - Y$$

$$L\phi_4 = F[t - Y - X]$$

$$: \quad :$$

$$L\phi_{2n-2} = F[t - Y - (n-2) \cdot X]$$

$$L\phi_{2n} = F[t - Y - (n-1) \cdot X]$$

Let the direction of the body motion be the positive direction. If the stroke is 1, the velocity of the vehicle is $1/\beta$ and the legs on the ground are moving at speed $-1/\beta$ relative to the body. The position of each leg P_n relative to the center of the stroke is

$$P_1 = 1/2 - t/\beta$$

$$P_3 = 1/2 - F[t - X]/\beta$$

$$: \quad :$$

$$P_{2n-3} = 1/2 - F[t - (n-2) \cdot X]/\beta$$

$$P_{2n-1} = 1/2 - F[t - (n-1) \cdot X]/\beta$$

$$P_2 = 1/2 - F[t - Y]/\beta$$

$$P_4 = 1/2 - F[t - Y - X]/\beta$$

: :

$$P_{2n-2} = 1/2 - F[t - Y - (n-2) \cdot X]/\beta$$

$$P_{2n} = 1/2 - F[t - Y - (n-1) \cdot X]/\beta$$

Referring to Figure 3.12, the time phase for leg 1 and leg $2n-1$ to move to the corresponding center of the stroke are t_a and t_b respectively.

$$t_a = P_1 \cdot \beta = \beta/2 - t$$

$$t_b = P_{2n-1} \cdot \beta = \beta/2 - F[t - (n-1) \cdot X]$$

The time phase for leg 1 to move to a position which is the mirror image of the position of leg $2n-1$ along the lateral axis is

$$\begin{aligned} t_a + t_b &= \beta - t - F[t - (n-1) \cdot X] \\ &= \beta - F[2t - (n-1) \cdot X] \end{aligned}$$

The local phase of leg 1 at this position is

$$t' = t + t_a + t_b = \beta - F[t - (n-1) \cdot X]$$

By substituting t' for t , the new foot positions of each leg P'_n at time phase t' become

$$\begin{aligned} P'_1 &= 1/2 - 1 + F[t - (n-1) \cdot X]/\beta \\ &= -1/2 + F[t - (n-1) \cdot X]/\beta \end{aligned}$$

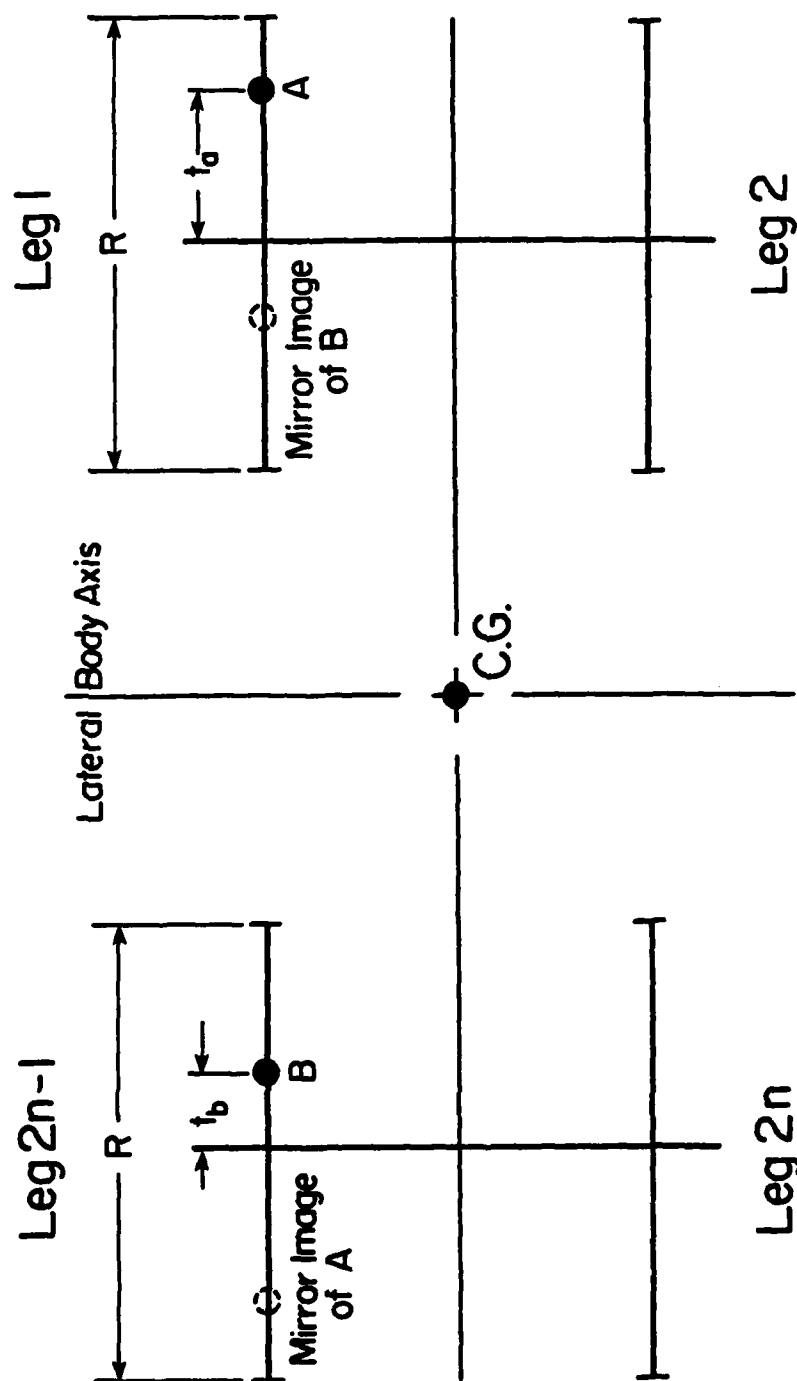


Figure 3.12: Symmetric characteristic of a periodic, constant phase increment gait.

$$P'_3 = 1/2 - F\{\beta - F[t - (n-1) \cdot X] - X\}/\beta$$

$$= 1/2 - 1 + F[t - (n-2) \cdot X]/\beta$$

$$= -1/2 + F[t - (n-2) \cdot X]/\beta$$

: :

$$P'_{2n-3} = 1/2 - F\{\beta - F[t - (n-1) \cdot X] - (n-2) \cdot X\}/\beta$$

$$= 1/2 - 1 + F[t - X]/\beta$$

$$= -1/2 + F[t - X]/\beta$$

$$P'_{2n-1} = 1/2 - F\{\beta - F[t - (n-1) \cdot X] - (n-1) \cdot X\}/\beta$$

$$= 1/2 - 1 + t/\beta$$

$$= -1/2 + t/\beta$$

$$P'_2 = 1/2 - 1 + F[t - Y - (n-1) \cdot X]/\beta$$

$$= -1/2 + F[t - Y - (n-1) \cdot X]/\beta$$

$$P'_4 = 1/2 - F\{\beta - F[t - (n-1) \cdot X] - Y - X\}/\beta$$

$$= 1/2 - 1 + F[t - Y - (n-2) \cdot X]/\beta$$

$$= -1/2 + F[t - Y - (n-2) \cdot X]/\beta$$

: :

$$\begin{aligned}
 P'_{2n-2} &= 1/2 - F\{\beta - F[t - (n-1) \cdot X] - Y - (n-2) \cdot X\}/\beta \\
 &= 1/2 - 1 + F[t - Y - X]/\beta \\
 &= -1/2 + F[t - Y - X]/\beta
 \end{aligned}$$

$$\begin{aligned}
 P'_{2n} &= 1/2 - F\{\beta - F[t - (n-1) \cdot X] - Y - (n-1) \cdot X\}/\beta \\
 &= 1/2 - 1 + F[t - Y]/\beta \\
 &= -1/2 + F[t - Y]/\beta
 \end{aligned}$$

Comparing these positions P'_n to the original positions P_n gives

$$P'_1 = -P_{2n-1}$$

$$P'_3 = -P_{2n-3}$$

: :

$$P'_{2n-3} = -P_3$$

$$P'_{2n-1} = -P_1$$

$$P'_2 = -P_{2n}$$

$$P'_4 = -P_{2n-2}$$

: :

$$P'_{2n-2} = -P_4$$

$$P'_{2n} = -P_2$$

This indicates that the support pattern at time phase t' is symmetrically related to the support pattern at time phase t about the lateral body axis, and the time interval between these two symmetric support patterns is $t_a + t_b$. This completes the proof.

Theorem 4: If a $2n$ -legged animal or walking machine walks in a wave gait and $1/2 \leq \beta$, during the transfer phase of a rear leg, the two legs nearest to this rear leg are always on the ground.

Proof: The phase difference of successive legs of a wave gait is β . The negative phase difference of successive legs is $1 - \beta$. At the time of lifting of a rear leg, the local phase of this leg is β . The local phase of the leg ahead of it is $\beta - (1 - \beta) = 2\beta - 1$. The local phase of the leg on the other side is $\beta - 1/2$. Since $1 > \beta \geq 1/2$, this gives

$$1 + \beta > 2\beta \text{ and } \beta > 2\beta - 1$$

which indicates the leg ahead of it is on the ground and

$$1/2 > \beta - 1/2 \text{ and } \beta > \beta - 1/2$$

which indicates the corresponding leg on the opposite side of the vehicle is on the ground.

At the time of placing of the same leg, the local phase of the leg ahead of it becomes $2\beta - 1 + (1 - \beta) = \beta$. This indicates that this leg is on the ground and is being lifted. The leg on the opposite side has a local phase of $\beta - 1/2 + (1 - \beta) = 1/2$. Since $\beta \geq 1/2$, this leg is on the ground. Therefore, at the time of lifting and placing of a rear leg, the legs ahead of it and on the opposite side of the vehicle are on the ground. Since the length of the transfer phase is $1 - \beta \leq 1/2$, no

other leg can be both lifted and placed during the transfer phase. This indicates that these two nearest legs are always on the ground during the transfer phase of a rear leg. This completes the proof.

Theorem 5: For a $2n$ -legged animal or walking machine, the longitudinal gait stability margin of a wave gait is

$$S = (n/2 - 1) \cdot P + (1 - 3/(4\beta)) \cdot R \quad R \leq P, 1/2 \leq \beta < 1 \quad (3.19)$$

where P is the stroke pitch and R is the stroke. If $R = P$, the dimensionless longitudinal gait stability margin normalized to the stride becomes

$$S^* = (n/2) \cdot \beta - 3/4 \quad R = P, 1/2 \leq \beta < 1 \quad (3.20)$$

Proof: A wave gait is a periodic regular symmetric gait. From Theorem 2, the support patterns of the first half cycle and of the second half cycle are symmetric about the longitudinal body axis. It is sufficient to study the longitudinal stability margin for a half cycle. A wave gait is also constant phase incremented. From Theorem 3, the support patterns are symmetric along the lateral body axis. The minimal longitudinal stability margin in the forward direction, the minimal front SL, is the same as that in the backward direction, the minimal rear SL. Hence, it is sufficient to study the minimal rear SL in a half cycle.

From Theorem 4, during the time of one rear leg is lifted, the leg ahead of it and the leg opposite it are always on the ground. Therefore, the rear boundary of the support pattern always is defined by either these two legs on the ground or the two rear legs. Since $R \leq P$, the footprint of the rear leg on the ground is always behind the footprint

of the leg ahead of it. Hence, the minimal rear SL is determined by the first kind of boundary, that is, the rear boundary during the transfer phase of the rear leg. The minimal rear SL happens at the moment of the lifting of the rear leg since the center of gravity is moving forward away from the rear boundary of the support pattern. At the moment rear leg $2n-1$ is lifted, the local phase of the leg ahead of it, leg $2n-3$, is $\beta - (1-\beta) = 2\beta - 1$. The local phase of the opposite leg, $2n$, is $\beta - 1/2$. At the moment a leg is placed, the rear leg is at a distance $((n-1)/2) \cdot P - R/2$ behind the center of gravity, and the leg ahead of the leg is at $((n-3)/2) \cdot P - R/2$ behind the center of gravity.

Since the velocity of the body is R/β , the leg is moving at velocity $-R/\beta$ relative to the body during its contact phase. Taking the direction of motion of the body to be positive, the positions of legs $2n-3$ and $2n$ at the time leg $2n-1$ is lifted can be computed as

$$P_{2n-3} = -((n-3)/2) \cdot P + R/2 - (R/\beta) \cdot (2\beta-1)$$

$$P_{2n} = -((n-1)/2) \cdot P + R/2 - (R/\beta) \cdot (\beta - 1/2)$$

The minimal longitudinal stability margin is defined as

$$S = -(P_{2n-3} + P_{2n})/2$$

Hence,

$$S = (n/2 - 1) \cdot P + (1 - 3/(4\beta)) \cdot R$$

If $P = R$, the dimensionless longitudinal stability margin normalized to the stride can be obtained by dividing Equation (3.19) by R/β

$$S^* = (n/2 - 1) \cdot \beta + (1 - 3/(4\beta)) \cdot \beta$$

$$= (n/2) \cdot \beta - 3/4$$

This completes the proof.

The program HSM2 is used to study the gait stability margin of hexapod wave gaits. The result is shown in Figure 3.13. This result is consistent with Equation (3.20). The direct effect of varying R can be observed from Equation (3.19). The second term is negative for $\beta < 3/4$ and is positive for $\beta > 3/4$. Hence, for $\beta < 3/4$, reducing R increases stability. For $\beta > 3/4$, reducing R decreases stability. Thus, for $\beta < 3/4$, the maximal gait stability margin is

$$S_{\max} = (n/2 - 1) \cdot P \quad \text{for } \beta > 3/4 \quad (3.21)$$

For $\beta > 3/4$, the maximal gait stability margin is

$$S_{\max} = (n/2 - 1) \cdot P + (1 - 3/(4\beta)) \cdot R_0 \quad \text{for } \beta > 3/4 \quad (3.22)$$

where R_0 is the maximal possible value of R and $R_0 \leq P$. In the first of these two cases, the maximal stability situation is a singular one in which $R = 0$ and the vehicle cannot, in fact move. For any $R > 0$, no matter how small, the vehicle can move at a speed determined by the stepping frequency. It is a similar type of singular situation to that encountered when maximizing stability by varying β . When $\beta = 1$, stability is maximized but the vehicle can no longer move.

Theorem 5 only covers the case in which $R \leq P$. For the case in which $R > P$, the situation is more complicated because the moment of lifting of a rear leg is not always the moment of minimal stability

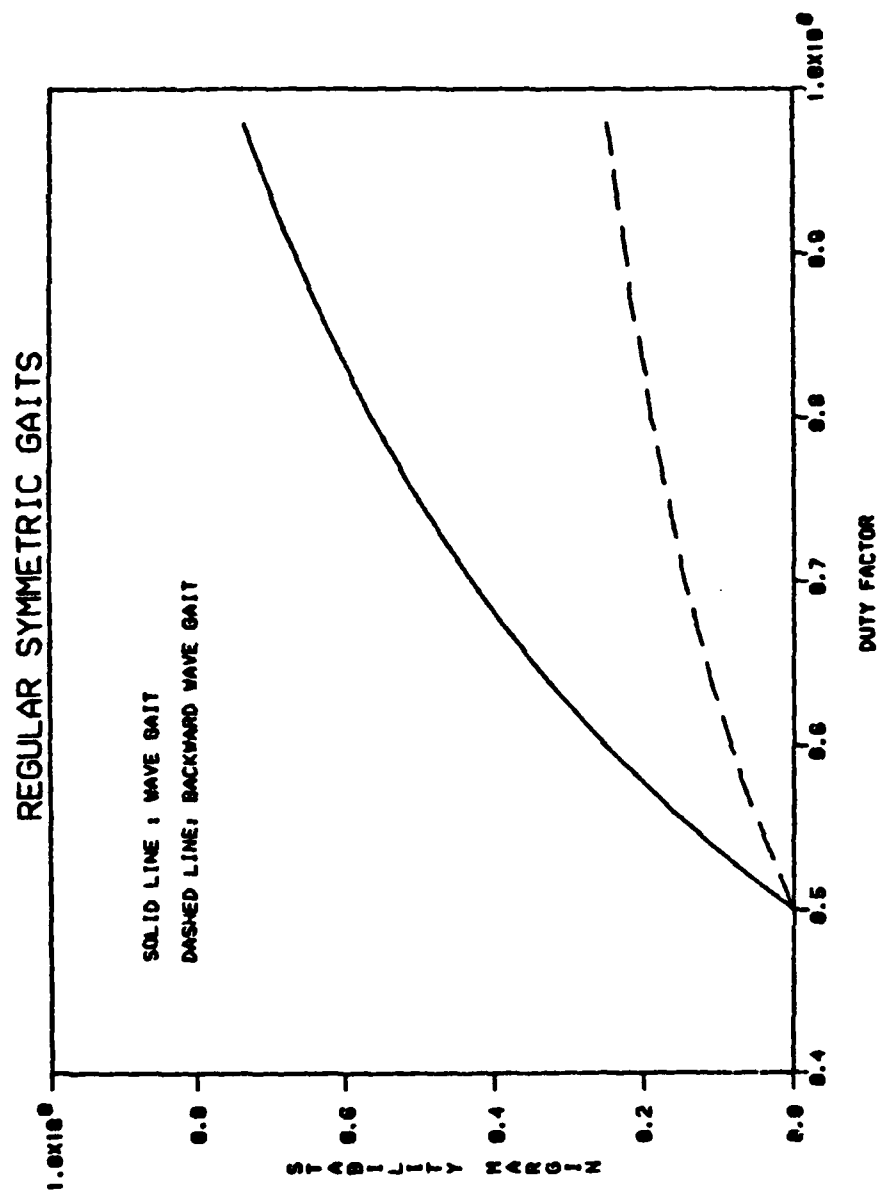


Figure 3.13: Gait stability margin of wave gaits and backward wave gaits.

AD-A159 147

AN EXPERIMENTAL STUDY OF AN ULTRA-MOBILE VEHICLE FOR
OFF-ROAD TRANSPORTAT. (U) OHIO STATE UNIV RESEARCH
FOUNDATION COLUMBUS R B MCGHEE ET AL. MAY 85

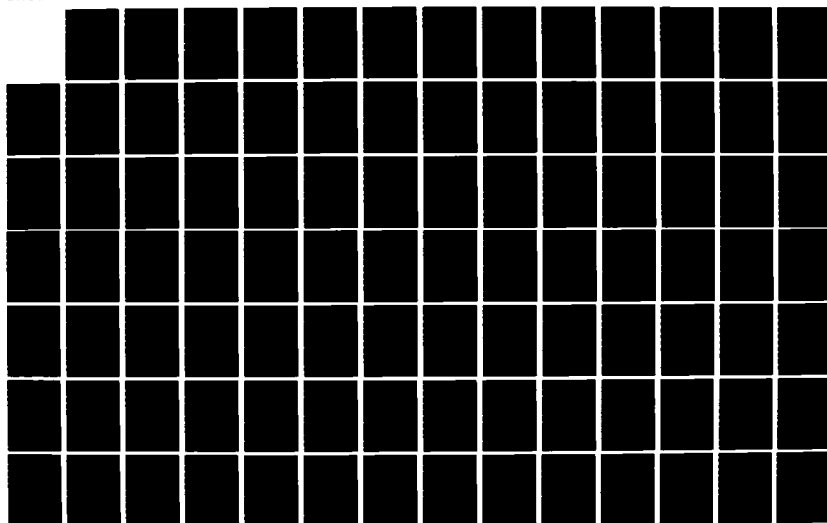
2/3

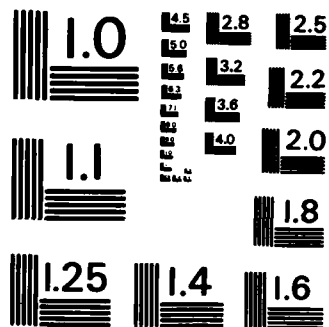
UNCLASSIFIED

MDA903-82-K-0058

F/G 13/6

NL





MICROCOPY RESOLUTION TEST CHART
NATIONAL BUREAU OF STANDARDS-1963-A

margin. The following theorem deals with the case of overstride ($R > P$).

Theorem 6: For a $2n$ -legged animal or walking machine with $R > P$, the longitudinal gait stability margin of a wave gait with $1/2 \leq \beta < 1$ is the lesser of S_1 and S_2 , where

$$S_1 = (n/2 - 1) \cdot P + (1 - 3/(4\beta)) \cdot R \quad (3.23)$$

$$S_2 = (n/2 - 1/2) \cdot P + (1/(4\beta) - 1/2) \cdot R \quad (3.24)$$

Proof: Since a wave gait is a periodic regular symmetric and constant phase increment gait, it is sufficient to study the rear minimal SL in half a cycle. A half cycle can be considered from the lifting of one rear leg $2n-1$ to the lifting of the other rear leg $2n$. According to Theorem 3, when leg $2n-1$ is in transfer phase, the two nearest legs $2n-3$ and $2n$ are always on the ground. During this period the rear boundary is composed of legs $2n-3$ and $2n$, and the case of worst stability is at the moment of lifting of leg $2n-1$ since the center of gravity is always moving away from the rear boundary.

At the moment leg $2n-1$ is placed, the local phases of legs $2n-3$ and $2n$ are $2\beta - 1 + 1 - \beta = \beta$ and $\beta - 1/2 + 1 - \beta = 1/2$ respectively. Hence leg $2n-3$ is being lifted and leg $2n$ is on the ground. Therefore, between the placing of leg $2n-1$ and the lifting of leg $2n$, the rear boundary is composed of legs $2n-1$ and $2n$, and the case of worst stability occurs at the moment the leg $2n-1$ is placed.

Hence, the lesser of the rear SL at these two instants of worst stability is the minimal rear SL during a half cycle, and it is also the

longitudinal gait stability margin in one cycle. The minimal rear SL at the first instant of worst stability, S_1 can be calculated as in Theorem 5.

$$S_1 = (n/2 - 1) \cdot P + (1 - 3/(4\beta)) \cdot R$$

The positions of leg $2n-1$ and $2n$ at the second instant of worst stability are

$$P_{2n-1} = -(n/2 - 1/2) \cdot p + R/2$$

$$P_{2n} = -(n/2 - 1/2) \cdot p - R/(2\beta) + R/2$$

The minimal rear SL at this time becomes

$$\begin{aligned} S_2 &= -(P_{2n-1} + P_{2n})/2 \\ &= (n/2 - 1/2) \cdot P + (1/(4\beta) - 1/2) \cdot R \end{aligned}$$

Therefore, the longitudinal gait stability margin is the lesser of S_1 and S_2 . This completes the proof.

As a matter of face, Theorem 6 also covers the case of $R \leq P$. In which case, S_1 is always less than S_2 . This can be seen as follows. Subtracting S_1 from S_2 gives

$$\Delta S = S_2 - S_1 = P/2 + (1/\beta - 3/2) \cdot R \quad (3.25)$$

Since $1/2 \leq \beta \leq 1$, $-1/2 \leq 1/\beta - 3/2 \leq 1/2$. If $R \leq P$, $\Delta S \geq 0$ always.

Therefore, the gait stability margin is determined by S_1 always, which is Theorem 6.

The effects on gait stability margin by reducing the stroke R has been discussed before. For $\beta < 3/4$, increasing R would increase S_1 . For $\beta > 3/4$, increasing R would decrease S_1 .

For the case of S_2 , since the second term is always less than zero in the range of $1/2 < \beta < 1$, increasing R always decreases S_2 . With these facts in mind, many other effects on gait stability margin of varying R can be observed from Equation (3.25).

For $\beta \leq 2/3$, $\Delta S = P/2 > 0$. The gait stability is determined by S_1 always. Therefore, increasing R would decrease gait stability.

For $2/3 < \beta < 3/4$, the condition of $\Delta S \geq 0$ is $(1/\beta - 3/2) \cdot R \geq -P/2$. Since $1/\beta - 2/3$ is negative in the assigned range of β , dividing both sides by $1/\beta - 2/3$ would change the direction of the inequality and give

$$R/P < \beta/(3\beta - 2) \quad \text{for } \Delta S \geq 0 \quad (3.26)$$

Therefore, the gait stability margin is determined by S_1 . Increasing R would decrease the gait stability. If $R/P > \beta/(3\beta - 2)$, the gait stability is determined by S_2 and increasing R would decrease gait stability.

For $\beta = 3/4$, the gait stability margin is determined by S_1 if $R/P \leq 3$. That is, the gait stability margin is constant for varying R . If $R/P > 3$, the gait stability margin is determined by S_2 , and increasing R would decrease the gait stability.

For $\beta > 3/4$, the gait stability margin is determined by S_1 if $R/P \leq \beta/(3\beta - 2)$, and increasing R would increase the gait stability. If $R/P > \beta/(3\beta - 2)$, the gait stability margin is determined by S_2 , and

increasing R would decrease the gait stability. Table 3.2 is a summary of all the cases discussed above.

A different approach to study of the effects on gait stability margin of varying R for four and six legged wave gaits using graphical methods is also worked out independently, and the results are shown in Figure 3.14. By comparing Figure 3.14 to the results in Table 3.2, it is found that both results are consistent and the results obtained from the graphical approach are a subset of the analytical results. The graphical method is described in Appendix B.

Up to this point, P is regarded as fixed. However, if $R < R_0$, it is possible to shift the center of the stroke, effectively changing stability. The following theorem states this fact.

Theorem 7: For a $2n$ -legged animal or walking machine and $1/2 \leq \beta < 1$, the maximal longitudinal gait stability margin of a wave gait obtained by shifting the centers of the strokes is

$$S_{\max} = (n/2 - 1) \cdot P + (1 - 3/(4\beta)) \cdot R + K(n) \cdot (R_0 - R)/4$$

$$\text{where } K(n) = 0 \text{ for } n = 2$$

$$= 1 \text{ for } n = 3$$

$$= 2 \text{ for } n \geq 4$$

(3.27)

and R_0 is the maximal possible value of R , P is the original stroke pitch and $R \leq P$.

Proof: Since $R \leq P$, the gait stability margin before any shifting of the center of stroke is defined by Equation (3.19). It has been shown in the proof of Theorem 5 that the case of minimal stability margin

Table 3.2

Effects on Stability Margin of Wave Gait by Varying Stroke R
(obtained from analytical methods)

Range of β	R \uparrow	Equa- tion of S	R/P	R \uparrow	Equa- tion of S	Break Point	R_{\max}
$\beta \leq 2/3$	S \uparrow	S1	all	S \uparrow	S1	None	Infinitive
$2/3 < \beta < 3/4$	S \uparrow	S1	$> \beta/(3\beta-2)$	S \uparrow	S2	$\frac{\beta \cdot P}{3\beta-2}$	$\frac{(n/2-1/2) \cdot P}{(2\beta-1)/(4\beta)}$
			$\leq \beta/(3\beta-2)$	S \uparrow	S1		
$\beta = 3/4$	S \rightarrow	S1	> 3	S \uparrow	S2	3P	$\frac{(n/2-1/2) \cdot P}{(2\beta-1)/(4\beta)}$
			≤ 3	S \rightarrow	S1		
$\beta > 3/4$	S \uparrow	S1	$> \beta/(3\beta-2)$	S \uparrow	S2	$\frac{(n/2-1/2) \cdot P}{(1-3/(4\beta))}$	$\frac{(n/2-1/2) \cdot P}{(2\beta-1)/(4\beta)}$
			$\leq \beta/(3\beta-2)$	S \uparrow	S1		

\uparrow : Decreasing

\uparrow : Increasing

\rightarrow : Constant

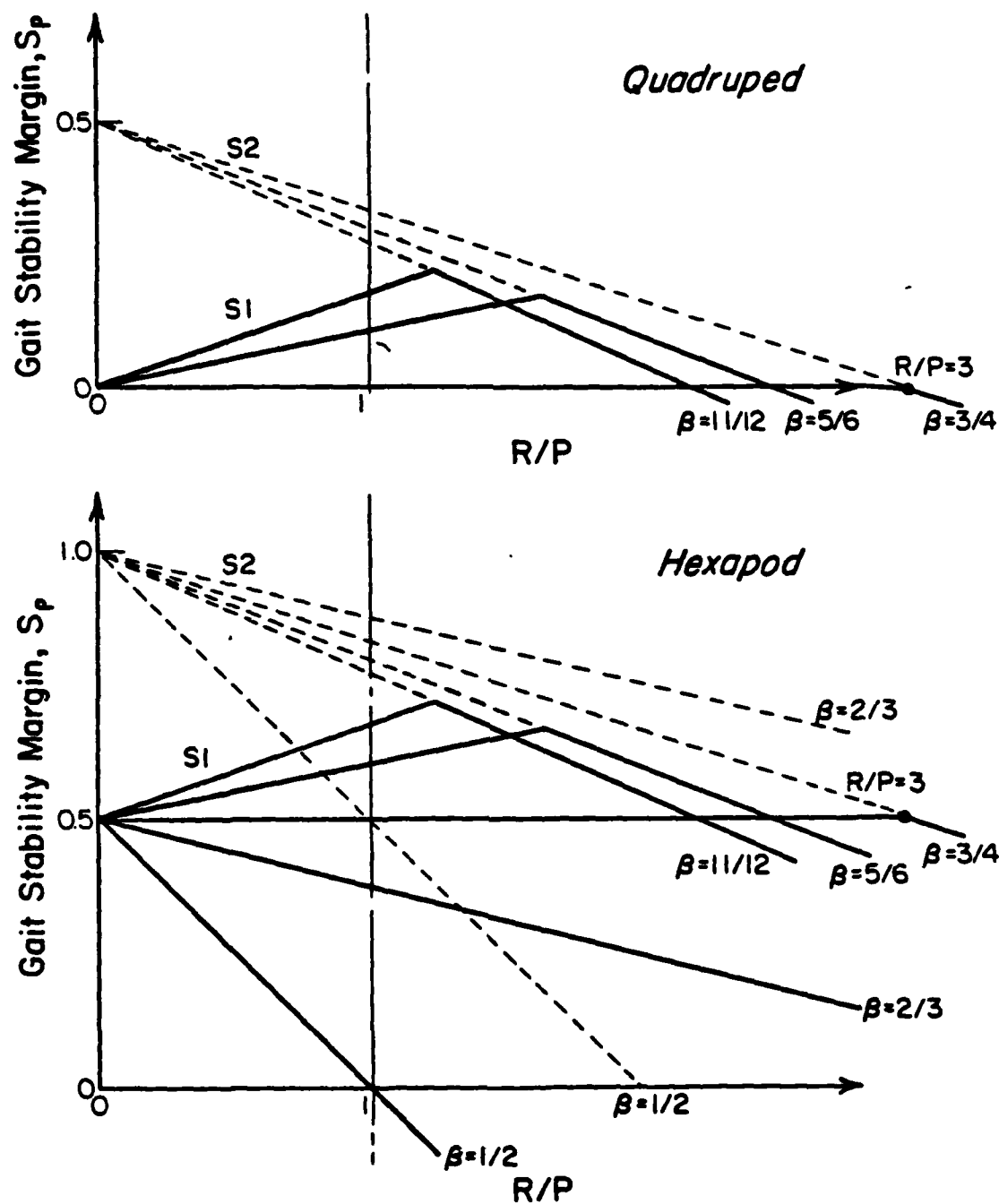


Figure 3.14: Effects on gait stability margin of wave gaits by varying stroke (obtained from graphical methods).

is at the moment of lifting of a rear leg. From Theorem 4, the rear boundary is composed of the two nearest legs to the lifting leg, that is, one leg ahead of it and the other rear leg. If the positions of these two legs are changed, the gait stability margin is also changed. The change of gait stability margin is the average of the changes of these two leg positions.

The center of stroke of each leg pair can be shifted outward (away from the center of gravity) except for those of any pair aligned with the center of gravity. Since the boundary of minimal stability margin depends on only the last two leg pairs (also the two leg pairs nearest the front by symmetry), only shifting of these legs affects the gait stability. Therefore, the maximal gain of stability margin by shifting the centers of stroke is to shift those leg pairs with the maximal value. The maximal possible value of this shift is $(R_0 - R)/2$.

For the case of a four legged wave gait, both leg pairs have to be shifted simultaneously in opposite directions because of symmetry. Thus the two legs which define the rear boundary are also shifted in opposite directions through the same distance. The stability margin remains the same. Hence $K(2) = 0$.

For the case of a six legged wave gait, the middle leg pair can not be shifted because it is aligned with the center of gravity. Thus only the rear leg is shifted back by $(R_0 - R)/2$, and the stability margin is increased by $(R_0 - R)/4$. Hence $K(3) = 1$.

For the case of eight and more legged wave gait, the last two leg pairs and the front two leg pairs can be shifted away from the

center of gravity by the maximal amount. After shifting, the stroke pitches in between the four extreme leg pairs may change, they do not affect the gait stability. Therefore, the stability is increased by the distance of $(R_0 - R)/2$. Hence, $K(n) = 2$ for $n \geq 4$. Addition of the increased stability margin to Equation (3.19) results in Equation (3.27). This completes the proof.

This effect strengthens the stabilizing effect of shortening the stroke for $\beta < 3/4$ and $n > 2$ provided the center of stroke is, at the same time, appropriately displaced. It also masks the destabilizing effect of shortening stroke when $\beta > 3/4$ since $1/4 \geq (1 - 3/(4\beta))$. Hence, stability can be increased by shortening stroke for all duty factors for $n \geq 3$. In the four legged case, however, stability is always decreased by shortening stroke for $\beta > 3/4$. The maximal gait stability margin for the singular case $R = 0$ is

$$S_{\max} = (n/2 - 1) \cdot P + K(n) \cdot R_0/4 \quad (3.28)$$

3.4.2 Equal Phase Gaits (EPH Gaits)

Equal phase gaits are useful when it is vital to distribute power consumption as evenly as possible over a cycle. A possible arrangement of a hydraulic system for the ASV is described as follows. There are three central hydraulic pumps to supply all eighteen actuators on the six legs. The first is for the all six main drive actuators (main actuators in brief). The second is for the all six lifting actuators. The third is for the all six abduction and adduction,

or lateral leg swing, actuators (lateral actuators in brief). The functions of these actuators are shown schematically in Figure 3.15. The main actuator and the lifting actuator move the feet in a horizontal direction and in a vertical direction independently. The lateral actuator moves the feet inward and outward on a circular arc.

In a straight line locomotion, the main actuator moves the feet backward (relative to the direction of the body motion) when the leg is in the support phase, and it moves the feet forward when the leg is in the transfer phase. The maximal foot velocity in the transfer phase should be greater than that in the support phase since it takes some time to decelerate and accelerate the feet in the reverse direction after lifting, and then to move the feet to their forward positions and hold them there for a short time before placing them. At this short time, the foot is still moving relative to the body since foot velocity should be zero relative to the ground. Hence, the main actuator is always moving during locomotion. The sum of the flow rates of all six main actuators depends on the numbers of leg in support phase and in transfer phase. In a wave gait, these numbers are constant for some duty factors and vary reciprocally with one leg shifts from support phase to transfer phase and back to support phase for the other duty factors. Hence, the sum of flow rate in main drive system is approximately constant.

However, this is not true of the sum of flow rates in the lifting system. In transfer phase, the foot has to be lifted up quickly to move back to the front in a raised position in order to

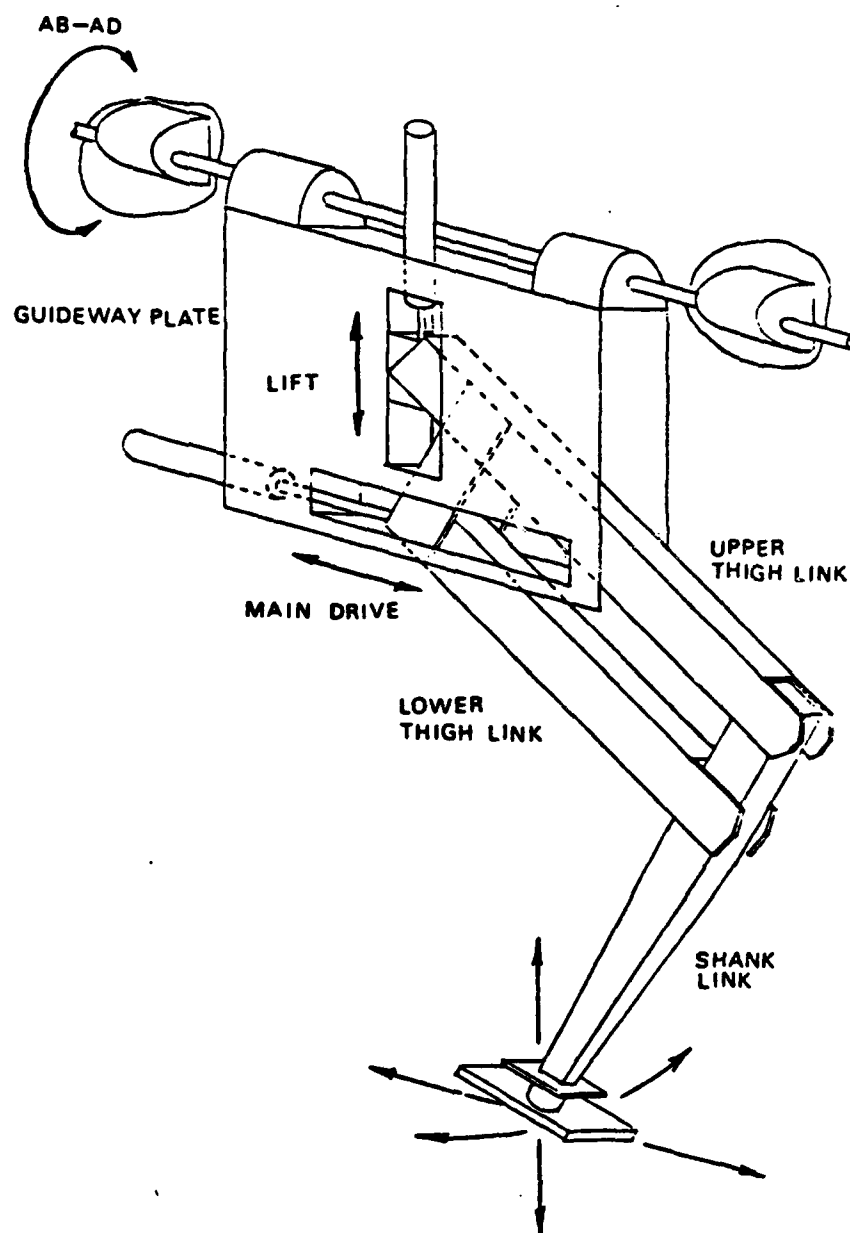


Figure 3.15: Schematic configuration of a leg for walking machines.

avoid any obstacles, then is put down quickly to complete the transfer phase. Thus, there are two peak of flow rate for each leg in one locomotion cycle. If a wave gait with $\beta = 0.5$ is used for locomotion, all the three placing events and the three lifting events happen at the same time. An extremely high peak flow rate is required in the lifting system. As a result, either a very large pump or a very large hydraulic accumulator is needed to supply this high instantaneous flow. Either strategy will increase the weight of the system significantly. A way to avoid the problem is to use an equal phase gait allowing use of a hydraulic system with a smaller instantaneous flow capacity. An equal phase gait will equally distribute the placing events and the lifting events in a locomotion cycle. Hence, the extreme high peak of system flow is diminished.

The third actuator, the lateral actuator, is usually locked during straight line locomotion and only needs limited flow for turning. It does not create high peaks of flow in its supply system.

Since an EPH gait is both regular and symmetric, if the placing events are equally distributed in one locomotion cycle, the lifting events are also equally distributed, and if the placing events of the legs on one side is equally distributed, the placing events of the legs on the other side are also equally distributed. Therefore, it is sufficient to study the placing events on the left side only.

There are two methods to equally distribute the placing events in a locomotion cycle. The first is to equally distribute the placing events of the legs on one side in a half cycle. Due to the symmetry of the gait, the placing events of the legs on the other side would

be equally distributed in the other half cycle. Thus, all the placing events are equally distributed in a full cycle. This is a half cycle EPH gait. The second is to equally distribute the placing events on one side over a full cycle. The placing events of all legs would be equally distributed in a full cycle only if the number of leg pairs is odd. This is a full cycle EPH gait. These two kinds of EPH gaits of a $2n$ -legged walking machine can be described mathematically as follows.

For a half cycle EPH gait

$$\phi_{2m+1} = 1 - m/(2n) \quad m = 1, 2, \dots, n-1 \quad (3.29)$$

For a fully cycle EPH gait

$$\phi_{2m+1} = 1 - m/n \quad m = 1, 2, \dots, n-1 \text{ and } n \text{ is odd} \quad (3.30)$$

where m denotes successive legs after leg 1 on the left side numbered from front to rear.

For a hexapod, the phase difference is $1/6$ or 60° for a half cycle EPH gait and $1/3$ or 120° for a full cycle EPH gait. Figure 3.16 shows the gait diagrams of EPH gaits of both kinds for various duty factors. Several important features of EPH gait can be observed from the diagrams. The full cycle EPH gait at $\beta = 2/3$ and the half cycle EPH gait at $\beta = 5/6$ are identical to the wave gait with the same duty factor. At $\beta = 3/4$, both placing events and lifting events together are equally distributed in a cycle. The phase difference between any two events is $1/12$ or 30° . An EPH gait of this nature is called a complete EPH gait.

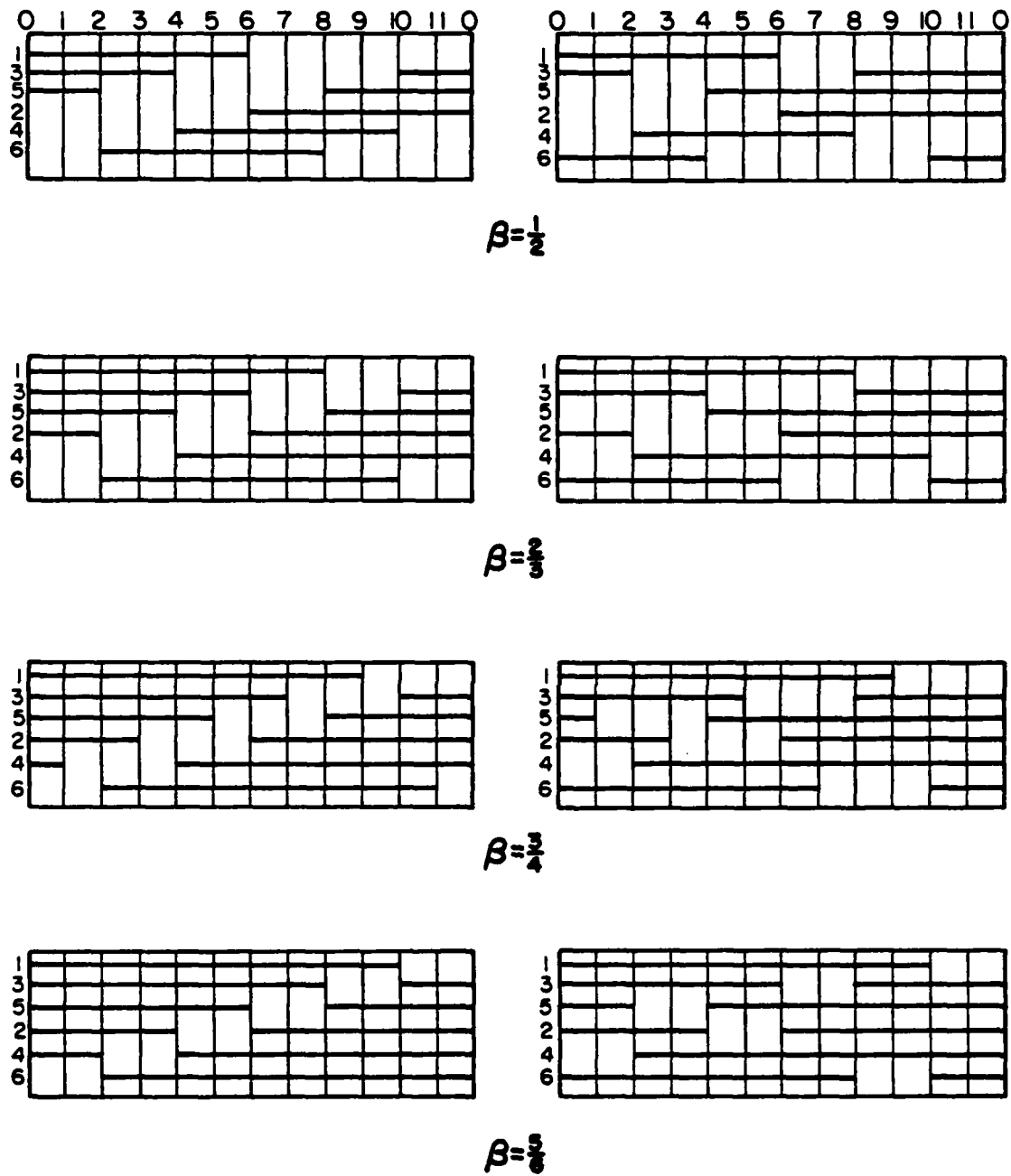


Figure 3.16: Gait diagrams of EPH gaits.

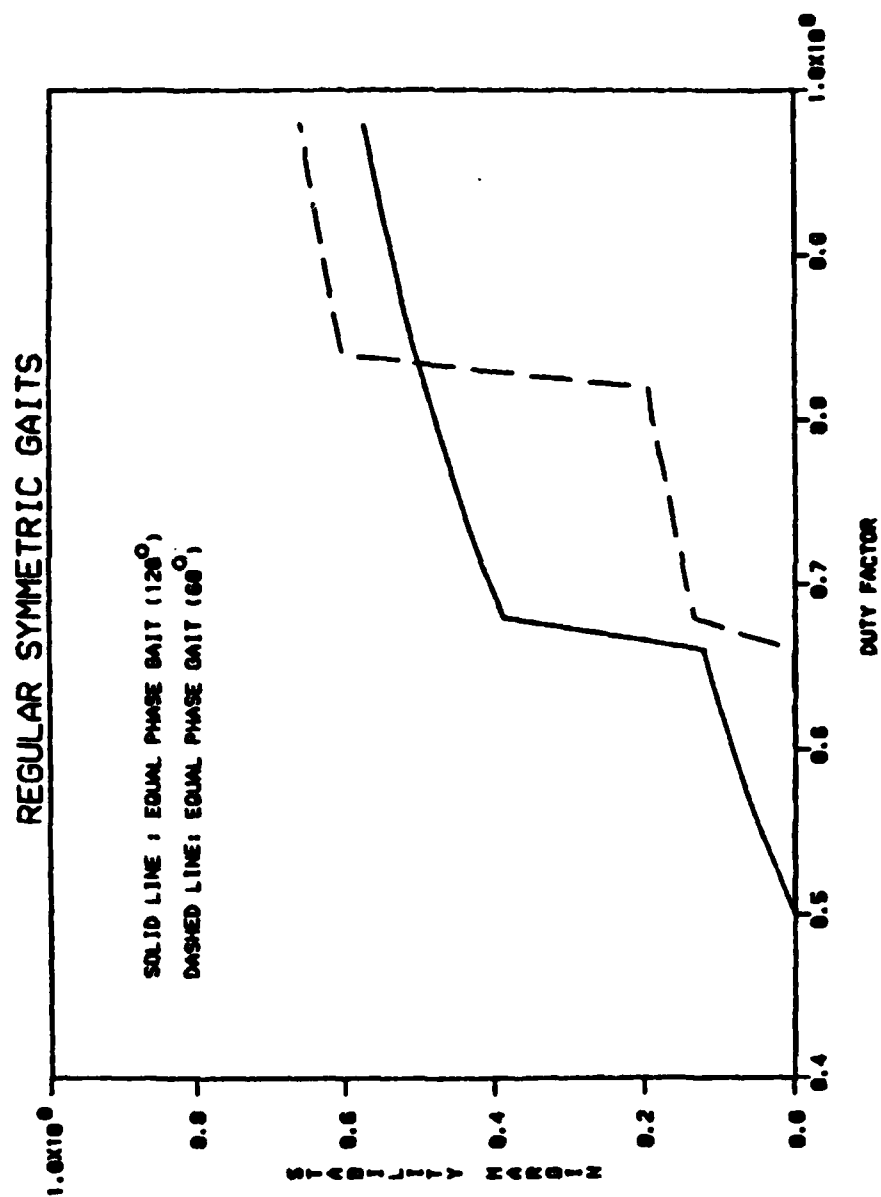


Figure 3.17: Gait stability margin of EPH gaits.

Figure 3.17 shows the computer result of the relationship between the gait stability margin of both kinds of EPH gait and the duty factor. For the full cycle EPH gait, there is a discontinuity at $\beta = 2/3$ where the gait stability margin jumps up to that of a wave gait. The reason for this jump can be seen in the following theorem, or by observing the stationary gait patterns. When $\beta < 2/3$, the minimal SL occurs at the moment of the lifting of a middle leg. When $2/3 \leq \beta < 1$, the minimal SL occurs at the moment of the lifting of a rear leg.

For the half cycle EPH gait, there are two discontinuities at $\beta = 2/3$ and $\beta = 5/6$ respectively. At $\beta = 2/3$, the stability margin jumps from an unstable value to $S_T = 1/8$. At $\beta = 5/6$, the stability jumps to that of wave gait. From the gait diagram of $\beta = 1/2$ in Figure 3.16, in the period between the lifting of leg 1 and the placing of leg 5, there is no leg on left side is on the ground. This instability does not diminish until the duty factor is increased to $2/3$. The second discontinuity at $\beta = 5/6$ occurs for the same reason of that of a full cycle EPH gait. That is, when $2/3 \leq \beta < 5/6$, the minimal SL occurs at the moment a middle leg is lifted. When $5/6 \leq \beta < 1$, it occurs at the moment a rear leg is lifted.

According to Theorem 3, for any periodic, constant phase increment gait, the support pattern is symmetric about the lateral body axis. Therefore, it is sufficient to study the minimal rear SL for gait stability margin. In the case of a wave gait, the minimal rear SL always occurs at the moment a rear leg is lifted. In the case of other gaits, such as EPH gaits, the calculation of the minimal SL

is not that simple. A rule for the calculation of the minimal rear SL is described as follows.

Rule for the calculation of the gait stability margin: Any lifting and/or placing of the legs which are inside, rather than on the two boundaries of, the current support pattern do not change the support pattern. Therefore, they do not affect the SL. Any placing of the leg which is behind the rear boundary would increase the rear SL. Any lifting of the leg which is on the rear boundary would reduce the rear SL. In other words, such a leg is being lifted at a time when there is no leg on the same side behind it on the ground. The moment of lifting of such a leg is called a critical time of the gait. Therefore, the gait stability of a periodic and constant phase increment gait is the minimum of all the rear SL at the critical times in one locomotion cycle. If the gait is symmetric, a calculation in half a cycle will be sufficient.

Theorem 8: For a six-legged full cycle EPH gait, the gait stability margin is

$$S = (1/2 - 1/(4\beta)) \cdot R \quad \text{for } 1/2 \leq \beta < 2/3 \quad (3.31)$$

$$S = P/2 + (1/2 - 5/(12\beta)) \cdot R \quad \text{for } 2/3 \leq \beta < 1 \quad (3.32)$$

Proof: A full cycle EPH gait is a constant phase increment gait an increment $1 - 1/n$, which is $2/3$ for a hexapod. It is also a symmetric gait. According to the rule mentioned above, the gait stability is the minimum of the rear SL at all the critical times. At the time leg 1 is lifted, the local phases of leg 3 and leg 5 are

$$L\phi_3 = \beta - 2/3$$

$$L\phi_5 = \beta - 1/3$$

Since $\beta - 1/3$ is always less than β , leg 5 is on the ground. Therefore, this is not a critical time.

At the time leg 3 is lifted, since the negative phase difference is $1 - 2/3 = 1/3$, the local phases of legs 1 and 5 can be calculated as follows.

$$L\phi_1 = \beta - 1/3$$

$$L\phi_5 = \beta - 2/3$$

Therefore, leg 1 is always on the ground. Leg 5 is in the transfer phase when

$$F(\beta - 2/3) > \beta$$

The only opportunity for this to be true is $\beta - 2/3 < 0$. Therefore,

$$F(\beta - 2/3) = F(1 + \beta - 2/3) = F(\beta + 1/3) > \beta$$

This is always true for all $\beta < 2/3$. For $1/2 \leq \beta < 2/3$, leg 5 is always in transfer phase. Thus, this is a critical time. The phase of leg 6 relative to leg 3 is $-1/2 + 2/3 = 1/6$. The positions of leg 1 and leg 6 at this time are

$$P_1 = P + R/2 - (\beta - 1/3) \cdot R/\beta$$

$$P_6 = -P + R/2 - (\beta - 1/6) \cdot R/\beta$$

The rear SL_3 is

$$\begin{aligned} SL_3 &= -(P_1 + P_6)/2 \\ &= (1/2 - 1/(4\beta)) \cdot R \end{aligned}$$

Another critical time is when leg 5 is being lifted. The local phases of legs 3 and 6 at this time is

$$L\phi_3 = \beta - 1/3$$

$$L\phi_6 = \beta - 1/2$$

Obviously both legs are on the ground for all β . Hence,

$$P_3 = R/2 - (\beta - 1/3) \cdot R/\beta$$

$$P_6 = -P + R/2 - (\beta - 1/2) \cdot R/\beta$$

The rear SL at this moment is

$$\begin{aligned} SL_5 &= -(P_3 + P_6)/2 \\ &= P/2 + (1/2 - 5/(12\beta)) \cdot R \end{aligned}$$

Comparing SL_3 to SL_5 by subtraction

$$SL_3 - SL_5 = -P/2 + R/(6\beta)$$

Since $1/2 \leq \beta < 2/3$ and $R < P$ for no overstroke, $SL_3 < SL_5$. Therefore,

$$S = (1/2 - 1/(4\beta)) \cdot R$$

For the case of $2/3 \leq \beta < 1$, the only critical time is when leg 5 is being lifted. Thus, the gait stability margin is

$$S = SL_5 = P/2 + (1/2 - 5/(12\beta)) \cdot R$$

This completes the proof.

Theorem 9: For a six-legged half cycle EPH gait, the gait stability margin is:

$$\text{Gait is unstable} \quad \text{for } 1/2 \leq \beta < 2/3$$

$$S = (1/2 - 1/(4\beta)) \cdot R \quad \text{for } 2/3 \leq \beta < 5/6$$

$$S = P/2 + (1/2 - 1/(3\beta)) \cdot R \quad \text{for } 5/6 \leq \beta < 1 \quad (3.34)$$

Proof: Similar to the proof of Theorem 8, the moments of the lifting of the three legs on the left side are checked as potential critical times. The phase increment for a half cycle EPH gait is $1 - 1/(2n)$, which is $5/6$ for a hexapod. Therefore, at the time leg 1 is lifted, the local phases of leg 3 and leg 5 are

$$L\phi_3 = F(\beta - 5/6)$$

$$L\phi_5 = F(\beta - 2/3)$$

For $1/2 \leq \beta < 2/3$, both $L\phi_3$ and $L\phi_5$ are greater than β .

Therefore, both legs 3 and 5 are in transfer phase, and this is a critical time. Since all three legs on the left side are in transfer phase at this moment, the gait is unstable.

At the time leg 3 is lifted, since the negative phase difference is $1 - 5/6 = 1/6$, the local phases of legs 1 and 6 can be calculated as follows.

$$L\phi_1 = \beta - 1/6$$

$$L\phi_5 = F(\beta - 5/6)$$

Leg 1 is always on the ground since $\beta - 1/6 < \beta$ for all $\beta > 1/2$.

Leg 5 is in transfer phase when $F(\beta - 5/6) > \beta$. The only possibility is $\beta - 5/6 < 0$, which leads to $\beta < 5/6$. Since $\beta < 2/3$ has been covered in the first critical time, only $2/3 \leq \beta < 5/6$ is considered for this second critical time. The phase of leg 6 relative to leg 3 is $-1/2 + 5/6 = 1/3$ and the local phase of leg 6 is

$$L\phi_6 = \beta - 1/3$$

This is less than β always. Therefore, leg 6 is on the ground. The rear boundary is composed of legs 1 and 6.

$$P_1 = P + R/2 - (\beta - 1/6) \cdot R/\beta$$

$$P_6 = -P + R/2 - (\beta - 1/3) \cdot R/\beta$$

The rear SL at this time is

$$\begin{aligned} SL_3 &= -(P_1 + P_6)/2 \\ &= (1/2 - 1/(4\beta)) \cdot R \end{aligned}$$

The moment of leg 5 being lifted is also a critical time. The local phases of legs 3 and 6 are

$$L\phi_3 = \beta - 1/6$$

$$L\phi_6 = \beta - 1/2$$

Both are less than β for all $1/2 \leq \beta < 1$. Therefore, both legs 3 and 6 are on the ground. The leg positions are

$$P_3 = R/2 - (\beta - 1/6) \cdot R/\beta$$

$$P_6 = -P + R/2 - (\beta - 1/2) \cdot R/\beta$$

The rear SL at this time is

$$\begin{aligned} SL_5 &= -(P_3 + P_6)/2 \\ &= P/2 + (1/2 - 1/(3\beta)) \cdot R \end{aligned}$$

and

$$SL_3 - SL_5 = -P/2 + R/(12\beta)$$

Since $P > R$ and $\beta \leq 2/3$, SL_3 is less than SL_5 always. Therefore, the gait stability margin is SL_3 for $2/3 \leq \beta < 5/6$.

For the case of $5/6 \leq \beta < 1$, leg 5 is on the ground when leg 3 is being lifted. The moment leg 3 is lifted is no longer a critical time. Hence, the only critical time for this range of β is at the moment leg 5 is lifted and the gait stability margin is SL_5 . This completes the proof.

In order to have better gait stability, a full cycle EPH gait should be used when β is less than $5/6$. For β greater than or equal to $5/6$, the half cycle EPH gait should be used. This can be seen clearly from Figure 3.17 or by comparing Equation (3.34) to Equation (3.32).

3.4.3 Backward Periodic Gaits

Both wave gaits and EPH gaits have the same stepping sequence. That is, the placing events of the legs on the same side run from the rear and proceed forward to the front of the vehicle. Any gait with such a stepping sequence is called a forward gait. For a hexapod forward gait, the placing event sequence of the left side and the right side are 1-5-3 and 2-6-4 respectively since the placing of a front leg is considered to be the beginning of a cycle. If the stepping sequence is reversed, the gait is called a backward gait. For a hexapod backward gait, the stepping sequences become 1-3-5 and 2-4-6. This stepping sequence is particularly interesting because it is suitable to a follow-the-leader (FTL) gait which has only one leg movement at a time.

A forward gait can also be an FTL gait. One example is the continuous FTL gait described in Section 3.4.5. However, an FTL gait with forward stepping sequence requires that two legs move simultaneously. This can be seen as follows. After leg 1 is placed, leg 5 is lifted and moved to the ready position for the placement. At this time, leg 3 has to be lifted to release its foot print for leg 5. Therefore, there is a short time that both leg 3 and leg 5 are in

transfer phase. Since only leg 1 is on the ground on the left side at this time, the stability margin is less than that of an FTL gait with a backward stepping sequence which maintains at lease five legs on the ground. A backward periodic gait has the potential to be modified into an FTL gait with maximum stability.

If a periodic constant phase increment gait with phase increment X is a forward gait, it can be modified into a backward periodic gait by replacing the phase increment X with $1-X$. Therefore, both wave gaits and EPH gaits can be modified into backward wave gaits and backward EPH gaits respectively. For a $2n$ -legged vehicle, a backward wave gait is described as

$$\phi_{2m+1} = F(1 - m\beta), \quad \begin{array}{l} m = 1, 2, \dots, n-1 \\ \text{and } 1 > \beta \geq 3/n \end{array} \quad (3.35)$$

where m denotes successive legs on the left side after leg 1 numbered from front to rear. For a hexapod, the backward wave gait becomes

$$\phi_3 = 1 - \beta, \quad \phi_5 = 2 - 2\beta, \quad 1 > \beta \geq 1/2 \quad (3.36)$$

Figure 3.18 shows the gait diagrams of backward wave gait with different duty factors. For a $2n$ -legged vehicle, a half cycle backward EPH gait is described as

$$\phi_{2m+1} = m/2n, \quad m = 1, 2, \dots, n-1 \quad (3.37)$$

A full cycle backward EPH gait is described as

$$\phi_{2m+1} = m/n, \quad m = 1, 2, \dots, n-1 \text{ and } n \text{ is odd} \quad (3.38)$$

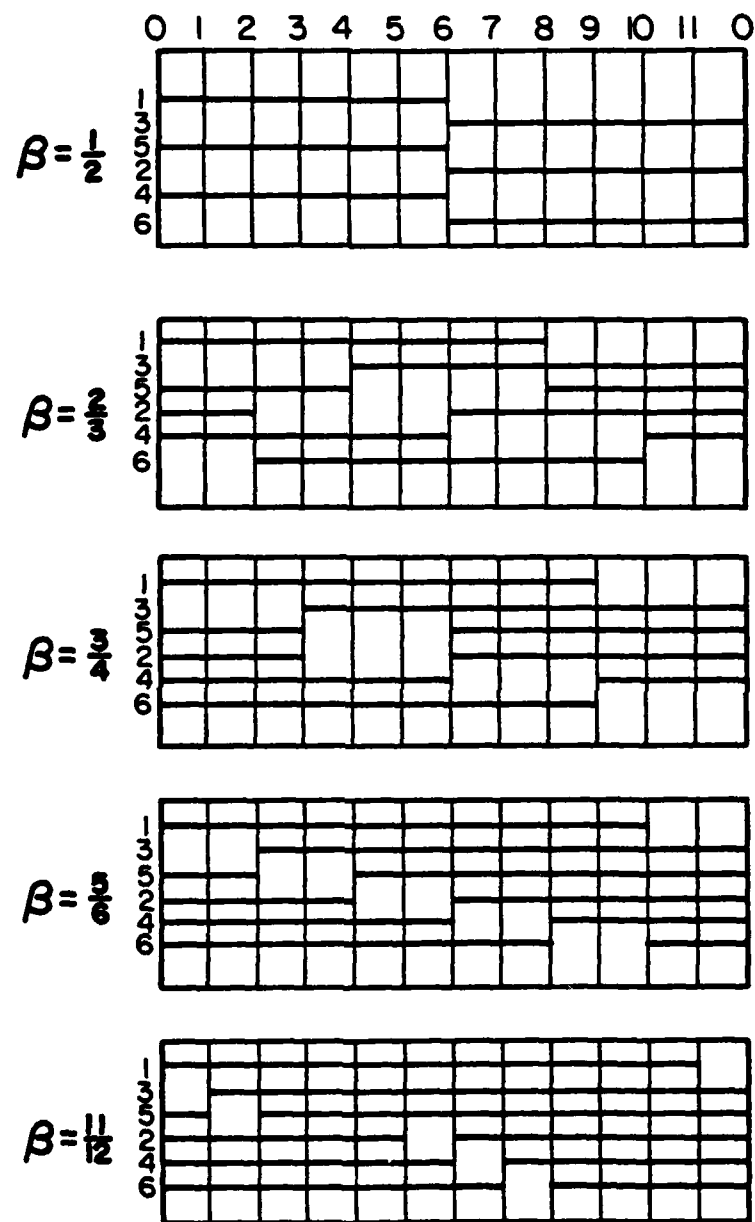


Figure 3.18: Gait diagrams of backward wave gaits.

The range of β for a stable backward EPH gait is less than that of a backward wave gait. It can be determined by studying the gait stability margin of a specific leg number. For a hexapod, the full cycle (120°) backward EPH gait and the half cycle (60°) backward EPH gait become

$$\phi_3 = 1/6, \quad \phi_5 = 2/6 \quad (3.39)$$

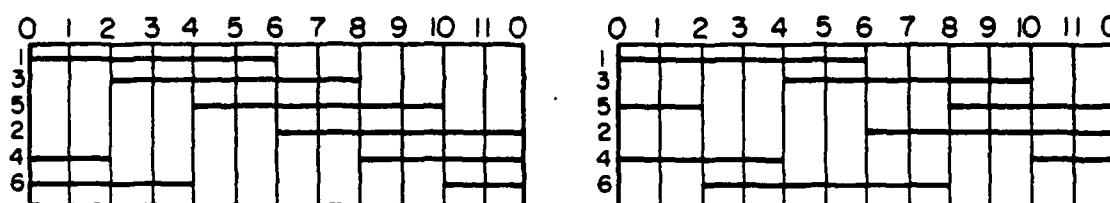
and

$$\phi_3 = 1/3, \quad \phi_5 = 2/3 \quad (3.40)$$

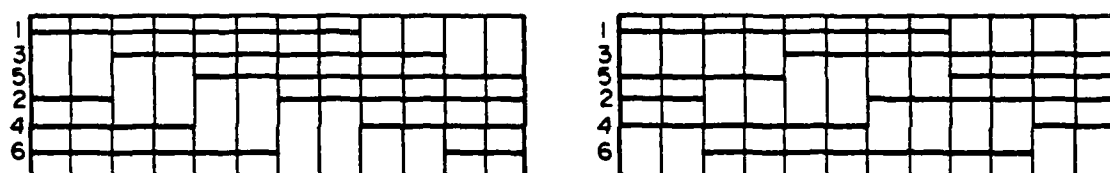
respectively. Figure 3.19 shows the gait diagrams of these two kinds of backward EPH gait with different duty factors. From the figure, the full cycle backward EPH gait at $\beta = 2/3$ and the half cycle backward EPH gait at $\beta = 5/6$ are identical to a backward wave gait.

The gait stability margins of 6-legged backward wave gait, full cycle backward EPH gait and half cycle backward EPH gait are computed by program HSM2 and are shown in Figure 3.20. The gait stability margin of a backward wave gait increases slowly along with the duty factor. By observing the gait diagrams of backward wave gaits, with the help of the stationary gait patterns, the only critical time is at the moment a rear leg is lifted. At this time, the leg ahead of it is being placed and the other rear leg is on the ground.

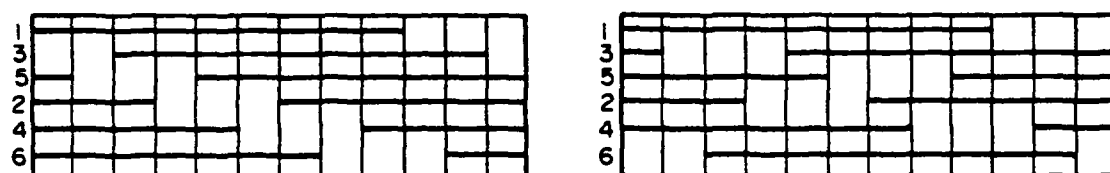
At this moment, for a specific duty factor and $\beta \geq 1$, the other rear leg is always at the same position due to symmetry. Hence, the position of the leg ahead of it would determine the gait stability. For a wave gait, since the leg ahead is at its most backward position,



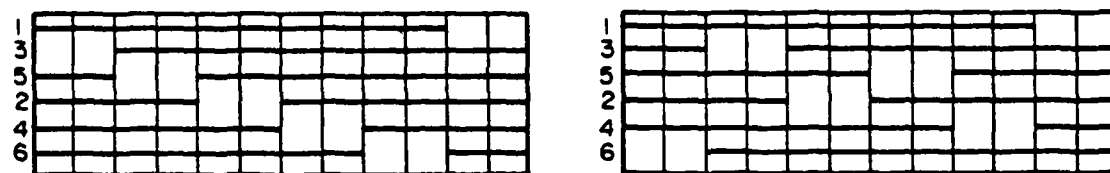
$$\beta = \frac{1}{2}$$



$$\beta = \frac{2}{3}$$



$$\beta = \frac{3}{4}$$



$$\beta = \frac{5}{6}$$

Figure 3.19: Gait diagrams of backward EPH gaits.

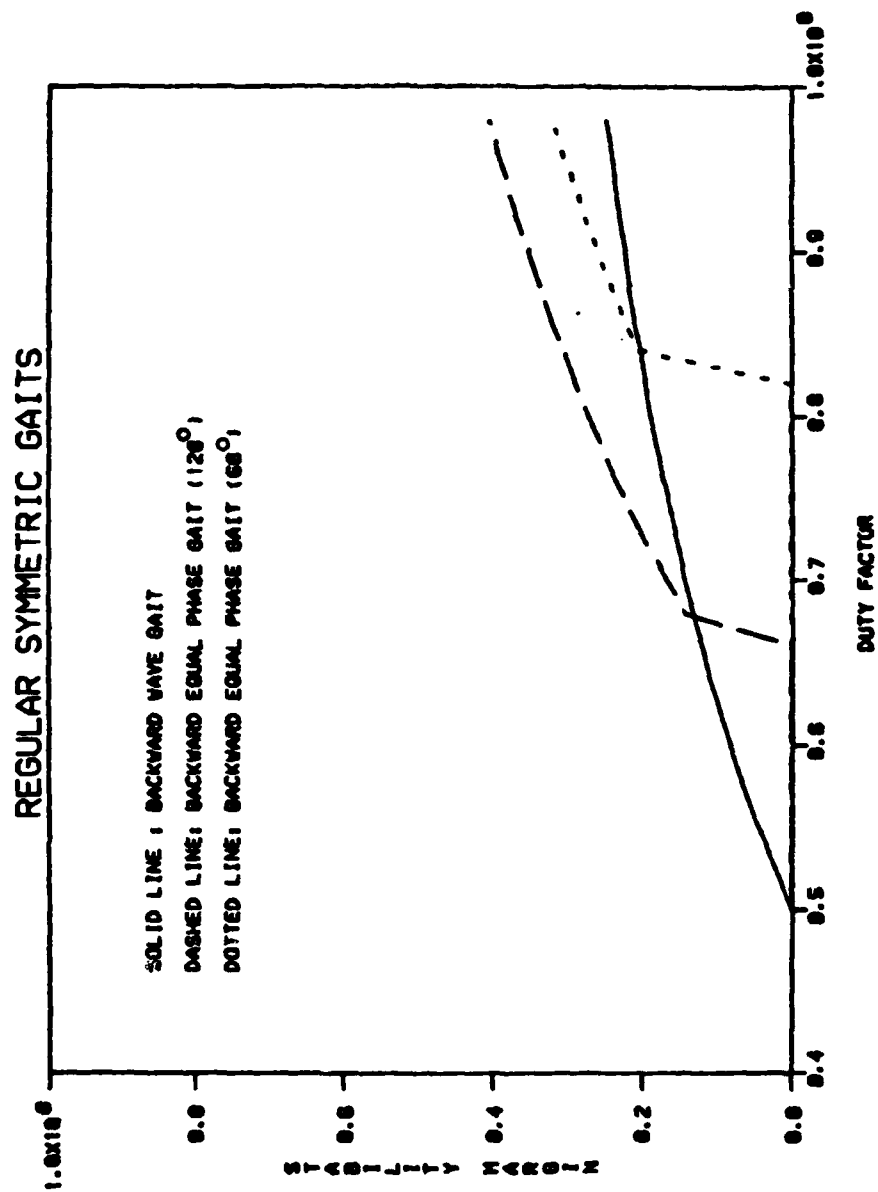


Figure 3.20: Gait stability margin of backward periodic gaits.

(any position further backward would cause this leg to be lifted before the rear leg is placed and lose stability), it has the maximal stability. On the contrary, for the backward wave gait, the leg ahead of the rear leg is at its most forward position. Hence, it has minimal stability for all gaits in which the minimal stability margin is determined by the same two legs. Figure 3.21 shows the gait stability margins of all the six periodic gaits. For any specific duty factor, the backward wave gait is at the lower margin of all the stable gaits while wave gait is at the higher margin.

In Figure 3.20, the full cycle backward EPH gait has a jump in stability margin to that of a backward wave gait at $\beta = 2/3$, and the half cycle EPH gait has a jump in stability margin to that of a backward wave gait at $\beta = 5/6$. The stability increases steadily after the jumps. The reasons for these two jumps can be understood by observing the gait diagrams and corresponding stationary gait patterns. The instability of the backward EPH gaits at lower duty factors is because the middle leg is not on the ground when the nearest rear leg is lifted. The rear boundary at this time, which is composed of the front leg on the same side and the other rear leg, is ahead of the center of gravity. This instability is removed by increasing the duty factor until the middle leg is being placed at the moment the rear leg is lifted. The rear boundary, which now is defined by the middle leg and the other rear leg, is behind the center of gravity giving positive stability. From the gait diagrams in Figure 3.19, the condition that leg 3 is being placed at the moment leg 5 is lifted occurs at $\beta = 2/3$ for full cycle backward EPH gait, and at $\beta = 5/6$ for half cycle backward EPH gait.

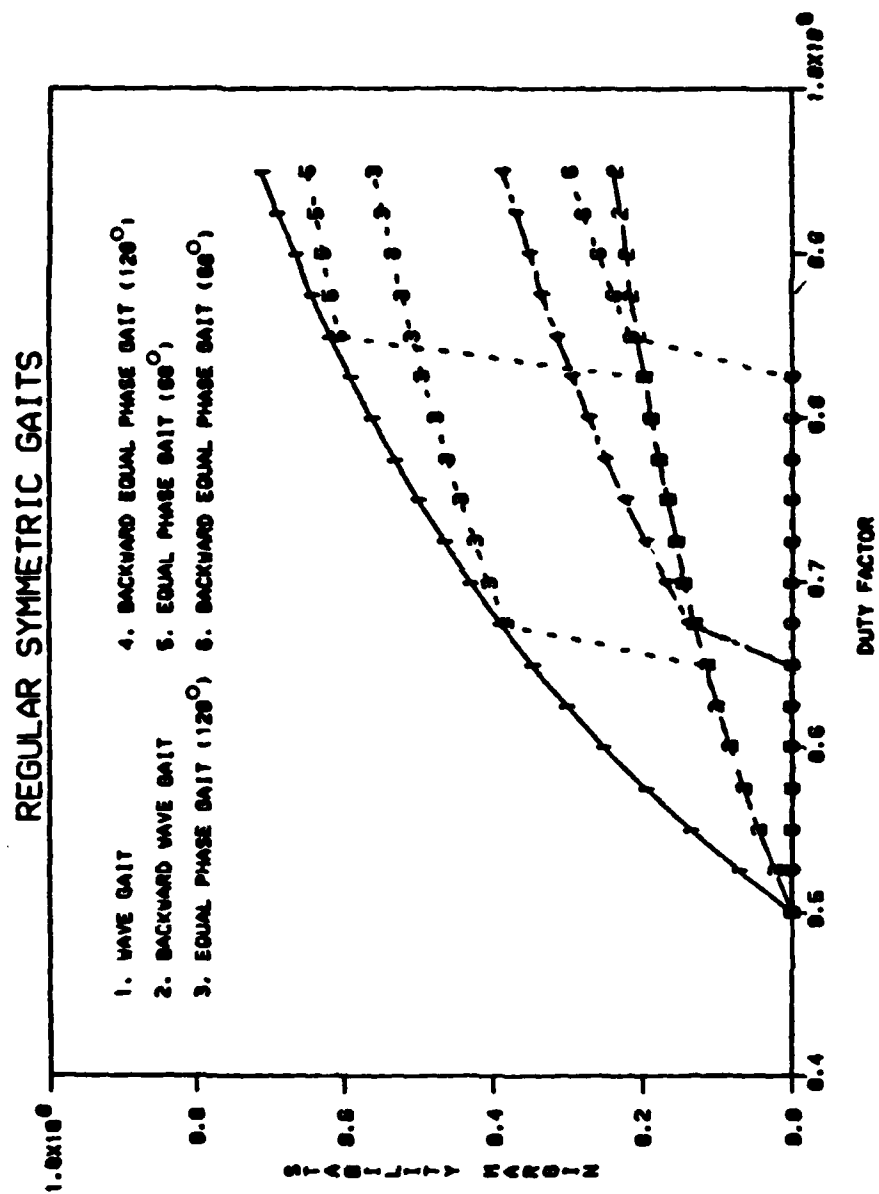


Figure 3.21: Gait stability margin of major periodic gaits.

Another feature shown in Figure 3.20 is that the gait stability margin of a full cycle backward gait is always greater than that of half cycle backward EPH gait. This is different from the forward EPH gaits. The following table shows some gait stability margins of backward gaits obtained by the stationary gait pattern method.

Table 3.3
Gait stability margin S of
backward periodic gaits

gait	duty factor, $\beta =$				
	1/2	2/3	3/4	5/6	11/12
backward wave gait	0	1/8	1/6	1/5	5/22
backward EPH gait (120°)	<0	1/8	2/9	3/10	----
backward EPH gait (60°)	<0	<0	<0	1/5	----

Since two cases of FTL gaits are discussed in the following two sections, and the algorithms developed there are available for the ASV to generate an appropriate FTL gait, the method to modify a backward gait to an FTL gait is not studied. This may be left for future research. This section is closed with an analytical study of the gait stability margin of the backward wave gait.

Theorem 10: For a $2n$ -legged backward wave gait, the gait stability margin is

$$S = (n/2 - 1) \cdot P - R/(4\beta) \quad \text{for } 1/2 \leq \beta < 1 \quad (3.41)$$

Proof: Since the backward wave gait is a periodic, regular, symmetric and constant phase increment gait, according to Theorems 3 and 4, it is sufficient to study the minimal rear SL in a half cycle. The negative phase difference is $1 - (1 - \beta) = \beta$. At the time rear leg $2n-1$ is lifted, the local phases of the leg before it, leg $2n-3$, and the other rear leg, leg $2n$, are

$$L\phi_{2n-3} = \beta - \beta = 0$$

and

$$L\phi_{2n} = \beta - 1/2$$

respectively. Since $\beta \geq 1/2$, $\beta - 1/2 < \beta$. This means leg $2n-3$ is being placed and leg $2n$ is on the ground. At the time leg $2n-1$ is placed, the local phases of these two legs become

$$L\phi_{2n-3} = 1 - \beta$$

and

$$L\phi_{2n} = 1 - 1/2 = 1/2$$

respectively. Since $\beta \geq 1/2$, $1 - \beta < \beta$. Thus both legs are on the ground. Since these two legs are on the ground at the beginning and end of the transfer phase of leg $2n-1$, and leg $2n-3$ and leg $2n$ cannot

be lifted and placed during this period of time, both legs $2n-3$ and leg $2n$ are on the ground throughout this interval. Thus, in one locomotion cycle, the minimal rear SL occurs at the time leg $2n-1$ is lifted. The positions of legs $2n-3$ and $2n$ are

$$P_{2n-3} = -[(n-3)/2] \cdot P + R/2$$

and

$$P_{2n} = -[(n-1)/2] \cdot P + R/2 - (\beta - 1/2) \cdot R/\beta$$

respectively. The gait stability margin is

$$\begin{aligned} S &= -(P_{2n-3} + P_{2n})/2 \\ &= (n/2 - 1) \cdot P - R/(4\beta) \end{aligned}$$

This completes the proof.

3.4.4 Discontinuous Follow-The-Leader (FTL) Gait

3.4.4.1 Introduction

The basic nature of an FTL gait is that the middle leg steps on the footprint made by the front leg, and the rear leg follows the footprint of the middle leg. The advantage of such a gait is that the human operator only needs to select the permitted footholds for the two front legs, then the rest of the legs automatically step on permitted cells. Therefore FTL gaits have very good terrain adaptability and can be used for walking in rough terrain.

FTL gaits can be divided into two types according to the smoothness of the body motion: continuous FTL gaits and discontinuous FTL gaits.

A continuous FTL gait is a periodic gait. Hence, the implementation of this gait is simpler and it generates continuous body motion and reaches higher speed. The disadvantage is that it has less stability due to a forward stepping sequence. Continuous FTL gaits should be used in fair terrain or rough terrain with more permitted cells. Detailed study of this gait is discussed in the next section. On the contrary, a discontinuous FTL gait is more complicated in implementation. It has a backward stepping sequence. Hence, it requires that only one leg move at a time to maintain good stability. Discontinuous FTL gaits may be the best gait for walking in rough terrain at the present time.

Discontinuous gaits are complicated because they combine leg motion with body motion. A complete step of a discontinuous gait is from a state in which all six legs are on the ground to the placement of the sixth leg. Each leg has one placing event and one lifting event in a complete step. Usually, leg 1 is always placed first, and only one event happens at a time. The leg motion is described as an event sequence. Tsai has pointed in [36] that the total number of possible event sequences with a backward stepping sequence is 20. These 20 event sequences are shown in Figure 3.22.

In order to describe the body motion, a body motion state is defined as follows. Between any two instants, the body motion state is 1 if the body has moved, and is 0 if the body has not moved. Since there are 12 events in one complete step, and the first body motion occurs between the current state and the first event, there are a total of 12 body motion states in one complete step. The number of

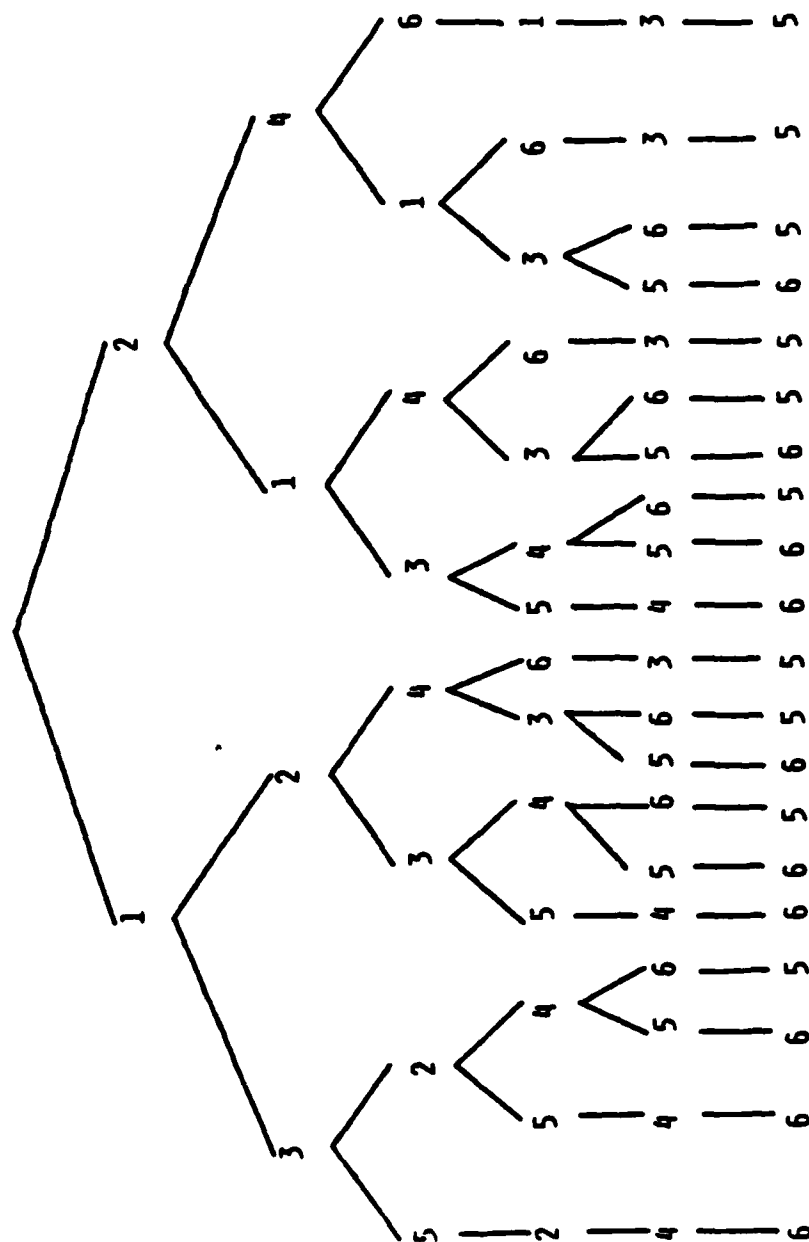


Figure 3.22: Possible event sequences with backward stepping sequence.

all combinations of body motion states is

$$2^{12} = 4096 \quad (3.42)$$

Since each combination of body motion states can be combined with a leg event sequence to be a discontinuous FTL gait, the number of discontinuous FTL gaits becomes

$$20 \cdot 4096 = 81920 \quad (3.43)$$

which is too large a number for a complete study. Moreover, this analysis has not included consideration of the distance of each body movement and the kinematic limits of the legs. At the present time, due to the needs of the ASV, it is adequate to select one out of the 81,920 possibilities and develop it into an implementable algorithm to generate a discontinuous FTL gait for the ASV. This work has been done by Tsai [36] and is described below.

Event sequence 1-3-5-2-4-6 was selected because of its physical symmetry. The body is restricted to two movements in a complete step. One body movement occurs after the placing of leg 3 and another occurs after the placing of leg 4. Only one leg at a time is moved, and the body moves only when all six legs are on the ground to ensure good stability. The human operator uses a laser beam to assign a foothold for leg 1. This foothold was located by triangulation using a two camera vision system. The coordinates of the selected foothold were computed and an optimal stability point (OSP) for the center of gravity of the new 6-vertex support pattern was also identified. Thus, the motion of the body can be pre-planned and a checking of kinematic limits for each leg is carried out. Any violation of kinematic limits

would require a reselection of the foothold before the foot actually moved. If the foothold is accepted, leg 1 is moved first, then leg 3 follows. Then the body next moves until the center of gravity is on the OSP. Finally leg 5 is moved. This is the first half cycle. The second half cycle is exactly the same of the first half cycle except it involves legs 2, 4 and 6 instead of 1, 3 and 5.

This algorithm has been implemented on the OSU Hexapod. Tests using the Hexapod have demonstrated the feasibility of the FTL gait for the ASV. This FTL gait permits the hexapod to walk over a three dimensional rough terrain since the body attitude can be maintained level automatically through its control systems. (For the ASV, the body attitude is maintained parallel to the average terrain gradient seen in the machine.) The stability margin SM is used in the algorithm instead of longitudinal stability margin SL. Hence, the vehicle maintains good stability in all directions. Therefore, this algorithm is for two dimensional body motion.

Although this FTL gait has been developed successfully, there are two aspects which can be improved. The first is that the reaching ability of the front legs are overly limited due to the constraint of the body motion. If the front legs are assisted by body motion, the reach is increased. The second is that the speed of the vehicle is slow. When the rough terrain in which the vehicle is walking has enough permitted cells, a higher speed should be reasonably expected. The first deficiency is removed by use of the general approach of discontinuous FTL gaits presented below. The second deficiency is alleviated by applying the continuous FTL gait.

3.4.4.2 A General Approach of Discontinuous FTL Gaits

Initially, only the longitudinal stability margin SL will be considered. In general, the lateral stability margin can be maintained satisfactorily by keeping the center of gravity equidistant from the two feet which determine the minimal SL. Later, A modification of this approach which considers the stability margin SM is also introduced. In the following discussion, stability margin is used to stand for longitudinal stability margin wherever there is no ambiguity.

Each one of the 20 possible event sequences can be used for a discontinuous FTL gait. If event sequence 1-3-5-2-4-6 is chosen for a discontinuous FTL gait, the complete event sequence which includes lifting and placing in one step becomes 7-1-9-3-11-5-8-2-10-4-12-6. A successive gait pattern of this FTL gait is shown in Figure 3.23. There are, in total, 13 support patterns. Let the first support pattern be designated as 0 and the rest of the support patterns be designated by the number of the last event. The 13 successive support patterns in order become 0, 7, 1, 9, 3, 11, 5, 8, 2, 10, 4, 12, 6. Similarly, the body motion state of each support pattern is designated as the same number. Since a step is completed at the placement of the sixth leg, the body motion state after it is considered in the next step. Hence, there are 12 body motion states in total: 0, 7, 1, 9, 3, 11, 5, 8, 2, 10, 4, 12.

Definition 29: A central segment, C' , of a support pattern is the longitudinal segment which passes through the center of gravity and is bounded by the front and the rear boundaries of the support pattern.

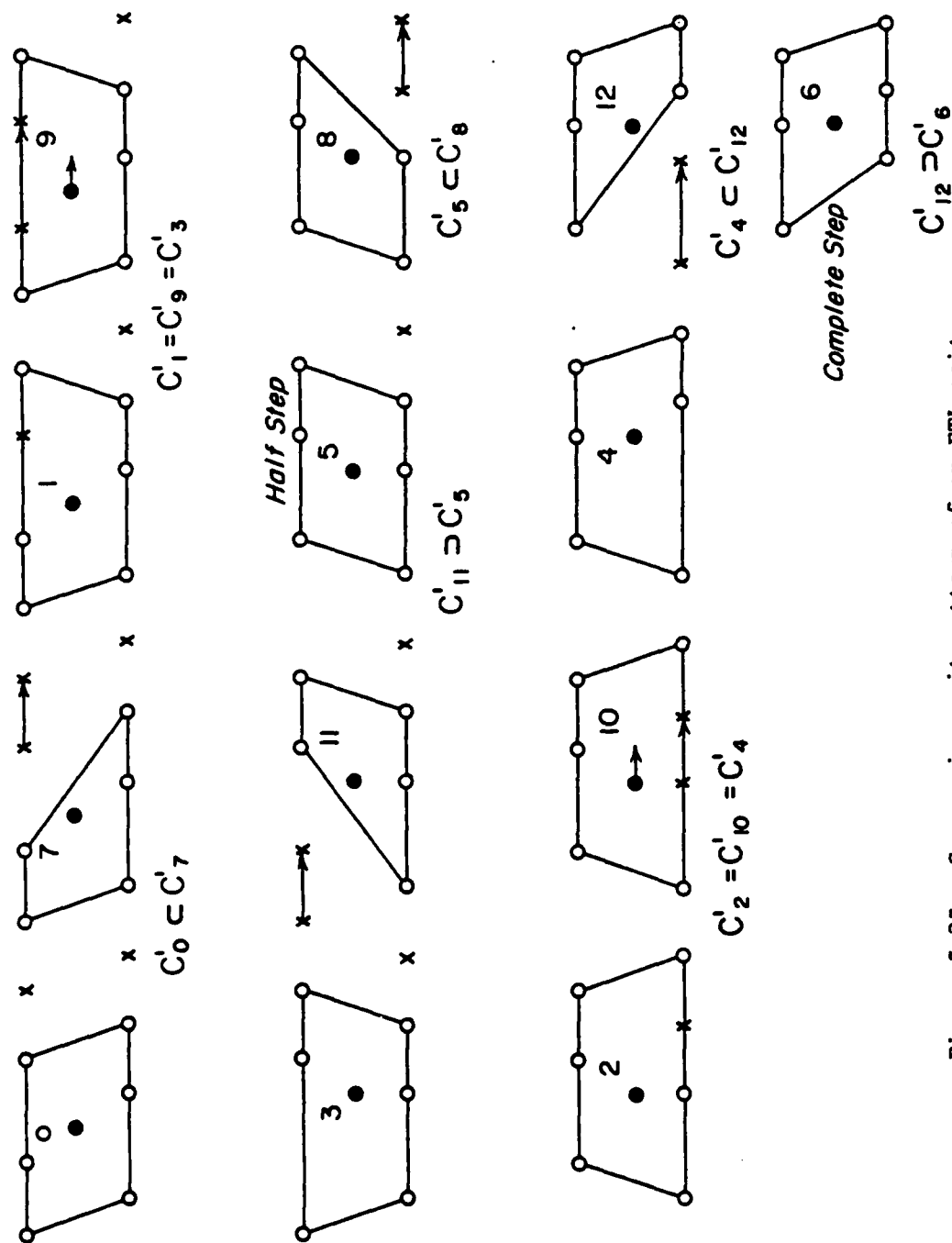


Figure 3.23: Successive gait pattern of an FTL gait with event sequence 1-3-5-2-4-6.

Definition 30: a stable segment, C , of a support pattern of a walking machine is the line segment generated by the center of gravity by moving the body in the longitudinal direction to its front and rear extremes without running into a stability problem or exceeding the kinematic limits of the legs.

From the definitions, C is always a subset of C' . For any support pattern n , the stable segment can be described as

$$X_{rn} \leq C_n \leq X_{fn} \quad (3.44)$$

where X_r and X_f denote the rear and front extreme points of the center of gravity. These two extreme points can be easily calculated by a computer program since the position of each foot on the ground and the kinematic limit of each leg are known.

In an FTL gait, the foothold of leg 1, say F_1 , is selected by the human operator. Leg 1 is then supposed to be lifted and to be placed on F_1 with either some or zero body movement. The accomplishment of event 7 depends on whether there is any overlap of C_0 and C_7 . If there is no overlap, the vehicle will either have a static stability problem by lifting leg 1 or a kinematic violation by moving the center of gravity into the stable segment of support pattern 7. On the contrary, an overlap of C_0 and C_7 would guarantee the accomplishment of event 7. A safety margin should also be considered. Figure 3.24 shows the successive central segments and corresponding stable segments of support patterns 0 and 7. AB is the overlap of these two stable segments. e is the safety margin and is measured from the two ends of a central segment. The darkened line is the truncated stable segment

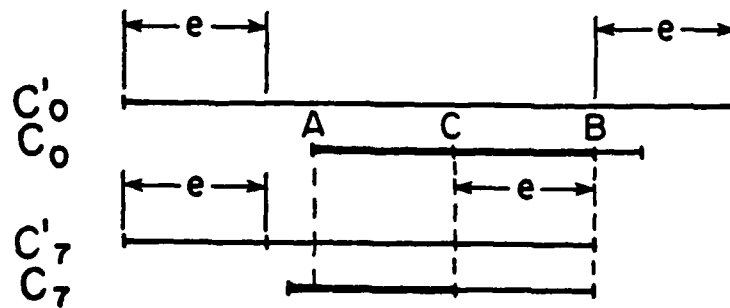


Figure 3.24: A pair of successive stable segments and central setments.

with the safety margin e . The overlap of the truncated stable segments becomes AC . Hence, the vehicle can proceed from event 0 to event 7 while maintaining the safety margin of stability. Similarly, an overlap of truncated C_7 and C_1 would guarantee the accomplishment of event 1, and an overlap of truncated C_1 and C_9 would guarantee the accomplishment of event 9...etc.

Events 7, 1, 9, 3, 11 and 5 are considered to be the first half step. After the foothold F_1 is chosen, the stable segments of the first half step can be computed as

$$x_{r0} \leq C_0 \leq x_{f0}$$

$$x_{r7} \leq C_7 \leq x_{f7}$$

$$\begin{aligned}
x_{r1} &\leq C_1 \leq x_{f1} \\
x_{r9} &\leq C_9 \leq x_{f9} \\
x_{r3} &\leq C_3 \leq x_{f3} \\
x_{r11} &\leq C_{11} \leq x_{f11} \\
x_{r5} &\leq C_5 \leq x_{f5}
\end{aligned}
\tag{3.45}$$

Figure 3.25 shows the central segments and the stable segments of a complete step. The accomplishments of events 7 through event 5 depend on whether there is an overlap between every two successive truncated stable segments. If it does, the first half step can be completed and the foothold F_1 is acceptable. If it does not, the foothold F_1 is unacceptable. The computer would then inform the human operator of the necessity of reselection of F_1 .

The second half step is similar to the first half step. After the selection of F_1 is accepted, the human operator should select a foothold F_2 for leg 2. For a selected F_2 , another set stable segments, $C_5, C_8, C_2, C_{10}, C_4, C_{12}$ and C_6 , for the second half step can be obtained. If there is an overlap between any two successive truncated stable segments, the foothold F_2 is acceptable. If not, F_2 is unacceptable and a reselection of F_2 is required.

If there is no acceptable F_2 available, a reselection of F_1 is required. This process of selection should continue until a set of cells F_1 and F_2 is found. Thus, a complete step which maintains the given safety stability margin is guaranteed to be accomplished. The

rest of this approach is the arrangement of the body motion.

3.4.4.3 The Schedule of Body Motions

There are many options for scheduling body motions. Generally speaking, there are two main strategies. The first is to keep the number of body movements to a minimum. One body movement simply means one body motion state is 1. The second is to maximize the stability margin by increasing the number of body movements. Since there are 12 body motion states in one complete step, the maximum number of body movements is 12, which means all 12 body motion states are 1, and the minimum number is 0, which means all 12 body motion state are 0.

The first strategy is to keep a minimum number of body movements. This strategy is shown by an example as in Figure 3.25. The heavy dot denotes the center of gravity. The truncated stable segments are the darkened lines. The method of finding common segments is used.

Definition 31: A common stable segment is the overlapped portion of several successive stable segments.

Compare the first truncated stable segment C_0 with the second one C_7 to find the common stable segment of these two. Then compare this common stable segment with the third truncated stable segment C_1 to find a new common stable segment. This process should be repeated until there is no more common segment between the existing one and the next stable segment. In Figure 3.25, a common stable segment I is found in the first five truncated stable segments. Then the same

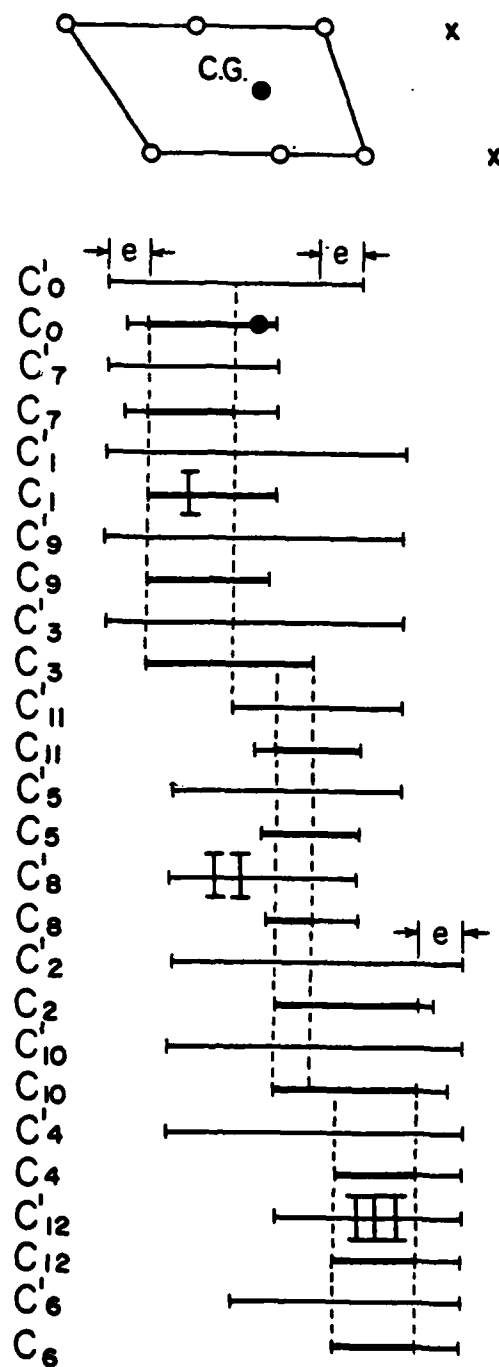


Figure 3.25: Stable segments and central segments of a step of an FTL gait.

procedure is repeated from the last stable segment C_3 toward the end of the step. Another common stable segment II is found in the next six truncated segments. Finally, a third common stable segment III is found in the last four truncated stable segments.

The minimum number of body movements is found as follows. During locomotion, the center of gravity should be in a common stable segment first, then the vehicle can proceed with leg motion to the last event of that group of stable segments. In the example, the vehicle should move the body backward so that the center of gravity is in the first common stable segment I. Then it can proceed to event 3. The body should then move to bring the center of gravity into common stable segment II. The vehicle can then proceed to event 10. Finally the body moves to bring the center of gravity to common stable segment III. The vehicle then proceeds to event 6 to complete the step. Three body movements are needed in this example. Let the number of common stable segments be N_c . If the center of gravity is already in the first common stable segment, the minimum number of body movements is $N_c - 1$. If not, it is N_c .

In the example, a larger reach of the front legs is demonstrated. If the body movements are restricted after event 3 and event 4, the selected footholds F_1 and F_2 are unacceptable since a body movement before event 7 is required. Since a flexible decision of the body movement, and only a safety margin is required during locomotion, the reach of the front legs is maximized.

In each body movement, the center of gravity should be moved to the position which gives the maximum stability margin. This point

is defined by applying the common central segment method.

Definition 32: A common central segment is the overlapped portion of several successive central segments.

For each group of truncated stable segments which share a common stable segment, the common central segment of the corresponding central segments should be found. If the center of gravity is on the center of this common central segment, it will give the maximal minimum stability margin for those support patterns. Hence, for each body movement, the center of gravity should be moved to this point of optimal stability, or as close as possible.

The second strategy is to maximize the stability margin by increasing the number of body movements. In this strategy, every two successive truncated stable segments are considered a group. A body movement is needed if the center of gravity is not on the point of optimal stability. The center of the common central segment of the two corresponding central segments is the point of optimal stability. In each body movement, the center of gravity should be moved to the point of optimal stability or as close as possible. By doing so, the stability margin of each two successive patterns is maximized. Hence, the gait stability margin is also maximized. The maximum number of body movements is 12, and the body may move forward and backward in order to have optimal stability.

The first strategy is preferable because fewer body movements are usually desirable. If the safety margin increases, the number of body movements may increase also. The extreme case is that of the second strategy. The maximum safety margin for a set of footholds is

when any one of the truncated common stable segments becomes a single point, under the condition that any more body movements would not help to increase its length.

3.4.4.4 Modification of the General Approach for Two Dimensional Body Motion

If the stability margin SM is considered, the general approach developed above is still applicable provided a few modifications are made. The stable segments are replaced by stable areas, and the central segments are replaced by central areas. The definitions of these two new terms are given below.

Definition 33: The central area, A' , of a support pattern is the area inside of the boundaries of the support pattern.

Definition 34: A stable area, A , of a support pattern of a walking machine is the composition of all the points on which the center of gravity would give the vehicle positive stability margin and would keep all the legs in their kinematic limits.

A stable area is a rectangle if the body is not allowed to rotate. All the common line segments mentioned above are replaced by common areas which are the overlapped areas of several successive stable areas or central areas. A safety margin should also be applied to the common central areas, and the truncated stable areas are used for those two strategies mentioned above (see Figure 3.26).

The point of optimal stability is no longer the center of the common central segment. It becomes the OSP which is defined as follows.

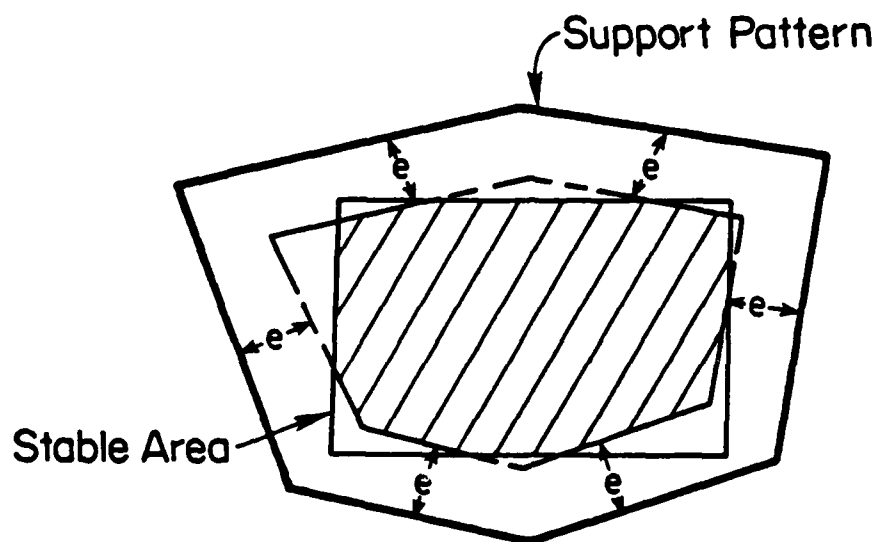


Figure 3.26: A truncated stable area (shaded area).

Definition 35: The optimally stable point, OSP, of a support pattern is the point inside the pattern that produces the maximal stability margin when the center of gravity is on it.

Since the central areas are polygons, the common central areas are also polygons. The method to find the OSP for a polygon is introduced in [36] by Tsai. In each body movement, the center of gravity is moved to the OSP of the common central areas, or as close as possible. Since the center of gravity does not have to be exactly on the OSP, and since the number and the time of body movements are flexible, this general approach constraints the selected footholds lease. The reach is maximized.

3.4.5 Continuous FTL Gait

3.4.5.1 Periodic Gaits with the Stepping Characteristic of FTL Gaits

The characteristic of an FTL gait is that the middle leg steps on the footprint made by the front leg, and the rear leg steps on the footprint made by the middle leg on both sides. Any gait with this stepping pattern can be an FTL gait, provided that the two front legs can be placed on the selected footholds without losing stability. In this section, a periodic gait with this stepping pattern is developed into a continuous FTL gait.

A hexapod with stroke R and stroke pitch P is walking in a periodic regular symmetric gait. The speed of the hexapod is R/β . Let the reference coordinate system be coincident with the body coordinate system at time 0, which is the time of the placement of leg 1. The positions of the footprints made by the legs on the left side are then:

$$P_{f1} = R/2 + P \quad (3.46)$$

$$P_{f3} = \phi_3 \cdot R/\beta + R/2 \quad (3.46)$$

$$P_{f5} = \phi_5 \cdot R/\beta + R/2 - P \quad (3.48)$$

If the gait has a backward stepping sequence 1-3-5, the condition of the phases is

$$0 < \phi_3 < \phi_5 < 1. \quad (3.49)$$

In order to guarantee that the leg which occupies a foothold is lifted before the next placement, the phases should satisfy the following inequalities:

$$\phi_7 < \phi_3 \quad (3.50)$$

$$\phi_9 < \phi_5 \quad (3.51)$$

For an FTL gait with a forward stepping sequence, leg 1 steps on a new foothold, then leg 3 steps on the old footprint of leg 1, which is one stride behind the new foothold, and finally leg 5 steps on the old footprint of leg 3, which is two strides behind the new foothold. Hence, the relationships between the footprints are as follows:

$$P_{f1} - R/\beta = P_{f3} \quad (3.52)$$

$$P_{f1} - 2R/\beta = P_{f5} \quad (3.53)$$

Substituting Equations (3.46) through (3.48) into Equations (3.52) and (3.53) gives

$$\phi_3 = (P/R) \cdot \beta - 1 \quad (3.54)$$

$$\phi_5 = 2[(P/R) \cdot \beta - 1] \quad (3.55)$$

Examining these two equations together with the conditions on the phases, Equation (3.49) gives

$$\phi_3 < 1/2$$

which leads to

$$P/R < 3/(2\beta) \quad (3.56)$$

Since $\phi_7 = \beta$ and $\phi_9 = \phi_3 + \beta$, Equations (3.50) and (3.51) give

$$(\beta + 1)/\beta < P/R \quad (3.57)$$

Since $1/2 \leq \beta$ for statically stable hexapod gait, Equation (3.57) becomes

$$3/(2\beta) < P/R \quad (3.58)$$

This is contradictory to Equation (3.56). Hence, it is impossible for a periodic regular symmetric gait with a backward stepping sequence to be an FTL gait.

If the gait has a forward stepping sequence 1-5-3, the phases should satisfy the following condition

$$0 < \phi_5 < \phi_3 < 1 \quad (3.59)$$

and also

$$\phi_7 < \phi_3 \quad (3.60)$$

$$\phi_9 < \phi_5 \quad (3.61)$$

For an FTL gait with a forward stepping sequence, leg 1 steps on a new foothold, then leg 5 steps on the footprint of leg 3 after leg 3 is lifted, which footprint is one stride behind the new foothold, and finally leg 3 steps on the footprint of leg 1 after leg 1 is lifted, which footprint is the new foothold. The footprints should satisfy the following equations.

$$P_{f1} = P_{f3} \quad (3.62)$$

$$P_{f1} - R/\beta = P_{f5} \quad (3.63)$$

Substituting Equations (3.46) through (3.48) into Equations (3.62) and (3.63) gives

$$\phi_3 = (P/R) \cdot \beta \quad (3.64)$$

$$\phi_5 = 2(P/R) \cdot \beta - 1 \quad (3.65)$$

Examining these two equations with the phase conditions, Equation (3.59) gives

$$1/2 < P/R < 1/\beta \quad (3.66)$$

and both Equations (3.50) and (3.51) give

$$1 < P/R \text{ or } 0 < P/R - 1 \quad (3.67)$$

Compare Equation (3.64) and (3.65) with a wave gait. The wave gait is an extreme of the continuous FTL gait with $P/R = 1$. The physical meaning of the term $P/R - 1$ is the time phase between the lifting of a leg and the next placement at one footfold. This time phase should not be too small in order to avoid any collision between legs. For instance, if the cycle time is one second and the time between the lifting of a leg and the next placement needs 0.2 second, the ratio of P/R should be 1.2.

A careful observation of the fast walking gait ($\beta < 3/4$) and the trotting gait of a horse shows they are continuous FTL gaits.

Several gait diagrams were drawn according to some selected plates³ made by Muybridge [22]. Although different horses may not behave exactly the same and each leg may have a slightly different duty factor, the constructed gait diagrams do closely follow the characteristics of continuous FTL gait. The duty factors of these gaits are in the range of 0.37 to 0.58. The values of P/R are in the range of 1.14 to 1.33. Figures 3.4 and 3.5 are the footfall formula and the gait diagram of a horse walking respectively. In this case, it is exactly a continuous FTL gait.

The stepping characteristics of these gaits are also examined. In some cases, the rear feet are placed ideally at the front footprints. In other cases, the rear feet are placed behind the front footprints. This is clearly obvious when the horse is hauling a heavy load. At other times, the rear feet are placed beside the front feet. The reason for this may be to avoid any possible interference between the feet.

Both the fast walking and trotting gaits are statically unstable. A horse can proceed from a slow walk (which is a wave gait) to a fast walk or trot by reducing the duty factor and adjusting the P/R ratio. This interesting fact shows that a continuous FTL gait may be developed into a statically unstable gait to reach higher speed.

Program HSM2 is used to study the gait stability margins of the continuous FTL gaits over a wide range of P/R ratios. Figure 3.27

³ Plate number 20, 33 and 39 in [22].

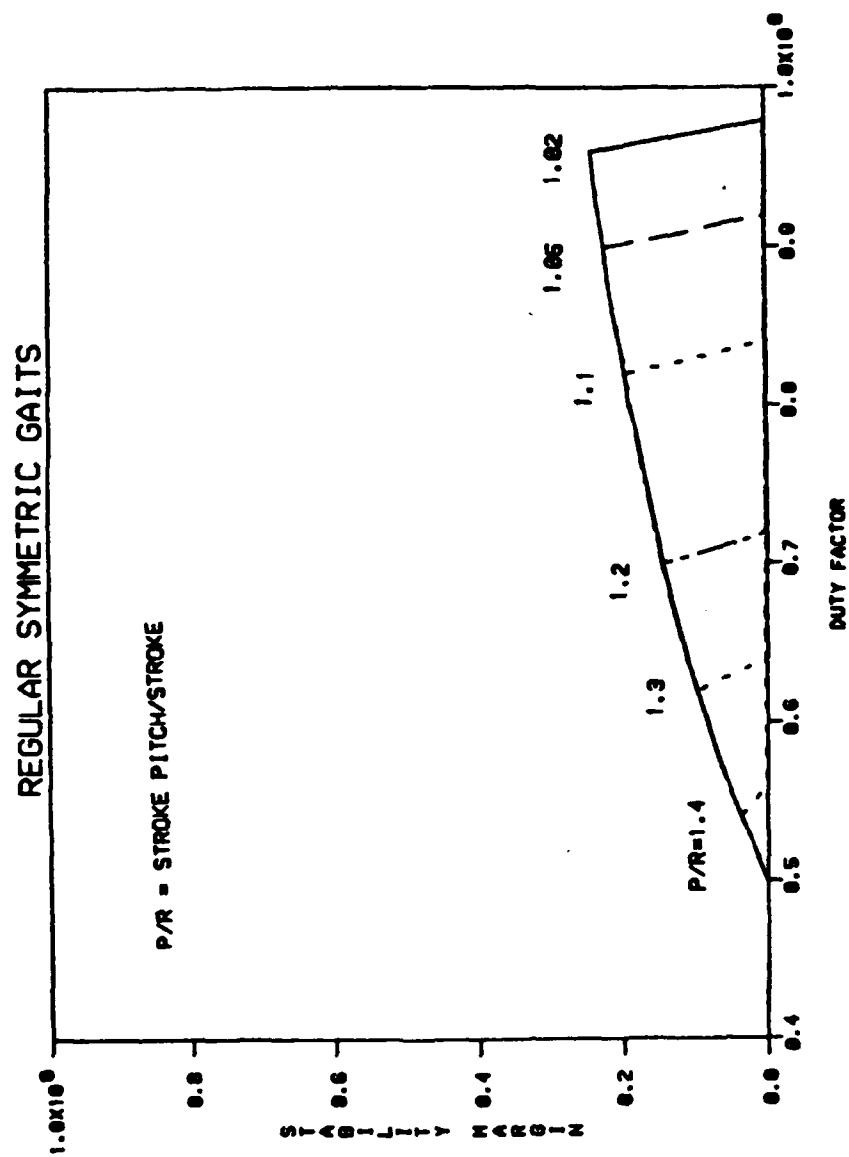
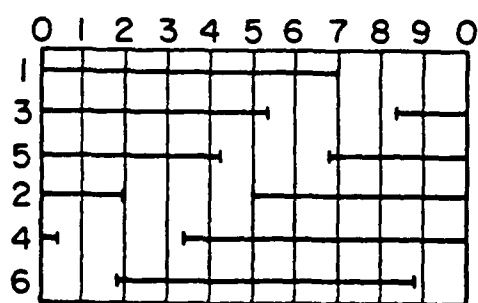


Figure 3.27: Gait stability margin of continuous FTL gaits.

shows the results. For each P/R ratio, the stability margin increases with the duty factor until it reaches a certain value. After this value the stability margin drops to zero abruptly. This phenomenon can be understood by examining gait diagrams of two continuous FTL gaits with the same P/R ratio. Figure 3.28a shows the one before this drop with $\beta = 0.7$ and Figure 3.28b shows the one after this drop with $\beta = 0.75$. The first one has a stability margin of about 1.8 while the second one is statically unstable. This is because that, at time 8, in the second case no leg on the left side is on the ground. This sudden drop happens at

$$\beta = \phi_5$$



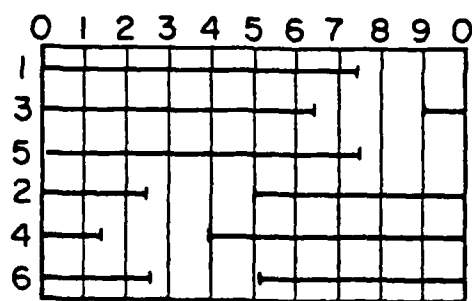
P/R=1.2

$\beta=0.7$

$\phi_3=0.84$

$\phi_5=0.68$

(a)



P/R=1.2

$\beta=0.75$

$\phi_3=0.1$

$\phi_5=0.08$

(b)

Figure 3.28: Gait diagrams of continuous FTL gaits.

This gives

$$\beta = 1/(2P/R - 1) \quad (3.68)$$

Figure 3.27 shows that the smaller the P/R is, the wider the range of duty factor for a statically stable gait. For the case of P/R larger than 1.4, there is hardly any value of duty factor which gives statically stable gait. For P/R = 1.02, almost all the values greater than 0.5 give statically stable gaits. Another fact shown in Figure 3.27 is that, before its sudden drop, the gait stability margins of all the continuous FTL gaits with different P/R ratios trace the same curve, and this part of the curve is identical to the gait stability margin of a backward wave gait.

3.4.5.2 Strategies to Avoid Forbidden Regions

For an FTL gait, the two front legs should be able to place on the selected footholds without losing stability. This is done by the four possible adjustments of the front legs. These four adjustments are placement of the front foot before, after, to the outside of and to the inside of the preplanned footprint while maintaining its stability. They are called the front adjustability (A_f), the rear adjustability (A_r), the abducted adjustability (A_b) and the adducted adjustability (A_d) respectively. After a front leg makes adjustment in these ranges, the middle and rear legs would follow it and maintain vehicle stability.

The method used to calculate these adjustments is shown by an example. Figure 3.29 shows the gait diagram and the stationary gait

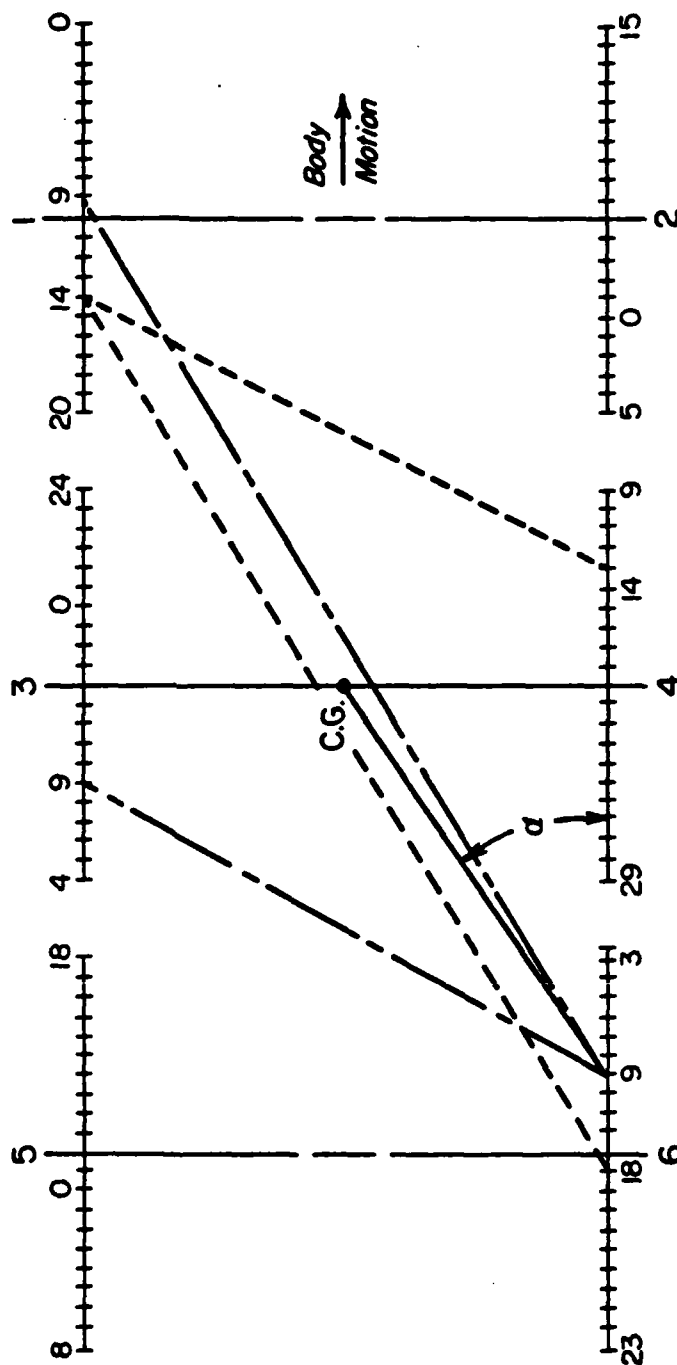
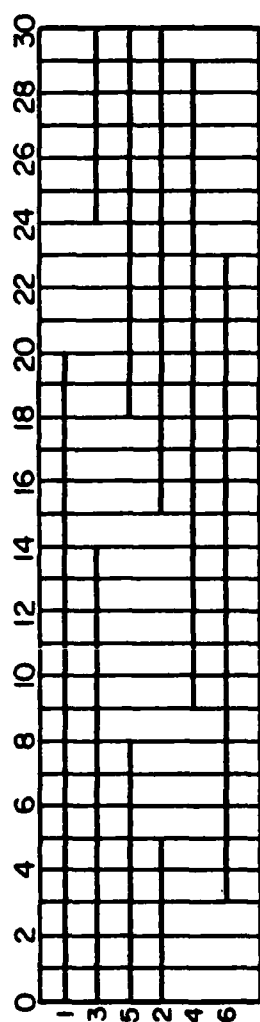


Figure 3.29: Stationary gait pattern of a continuous FTL gait with $P/R = 1.2$ and $\beta = 2/3$.

pattern of a continuous FTL gait with $P/R = 1.2$ and $\beta = 2/3$. The event sequence of this gait is 1-6-8-11-4-9-2-5-7-12-3-10. From the figure, in the first half cycle, the minimal front SL occurs at the moment before the middle foot 3 is placed, the minimal rear SL occurs at the moment after the middle foot 4 is lifted. At both times, the minimal SL is $0.125R$.

Let all the legs except leg 1 be placed on the preplanned footprints. If leg 1 is placed a distance ahead of the preplanned footprint and the gait stability margin is reduced to zero, this distance is the maximum front adjustment. From trigonometry, the maximum front and rear adjustments are

$$A_f = A_r = 2SL \quad (3.69)$$

In this example, it is $0.25R$. In a similar way, the abducted and adducted adjustabilities can be calculated as

$$A_b = A_d = 2SL \cdot \tan \alpha \quad (3.70)$$

where α is the angle of the line which goes through the center of gravity and the foot position of leg 6 at the time foot 4 is placed. At this time, the position of leg 6 is

$$P_6 = -P + R/2 - (\phi_4 - \phi_6) \cdot R/\beta \quad (3.71)$$

Since $\phi_4 - \phi_6 = \phi_3 - \phi_5$, Substituting Equation (3.64) and (3.65) into Equation (3.71) gives

$$P_6 = R \cdot (1/2 - 1/\beta) \quad (3.72)$$

Hence,

$$\alpha = \tan^{-1} \{W/[2R \cdot (1/\beta - 1/2)]\} \quad (3.73)$$

where W is the width between the footpaths. For the ASV with $P = 67.2$ inches, $R = 56$ inches and $W = 84$ inches, the maximum adjustments of this gait are: $A_r = A_f = 14$ inches, $A_b = A_d = 10.5$ inches. Although these may appear to be small, the vehicle can cross over large forbidden regions by using these adjustments. This is shown in the later examples.

There are two important features to be observed from Figure 3.29:

1. The boundary which determines the minimal SL in the first half cycle is bounded by feet 1 and 6. In the second half cycle, it is bounded by feet 2 and 5. The positions of middle legs do not affect the gait stability margin.
2. The time phase between the two placements of the two legs which determine the minimal SL is very short, and the two instants of the minimal SL occur after both legs have been placed. In the example, leg 6 is placed at $1/10$ after leg 1, and the time phases of the two instants of minimal SL are $3/10$ and $7/15$ respectively.

Hence, during walking, front leg 1 can be adjusted within the maximum adjustment as long as leg 6 is placed at the preplanned foothold. This is the same relationship as that of front leg 2 to leg 5. The middle legs simply follow the front legs and do not affect the stability. The following examples show how a hexapod avoids forbidden regions by these adjustments.

Figure 3.30 shows a hexapod cross over a narrow forbidden region in a continuous FTL gait. The pitch of footprints on the

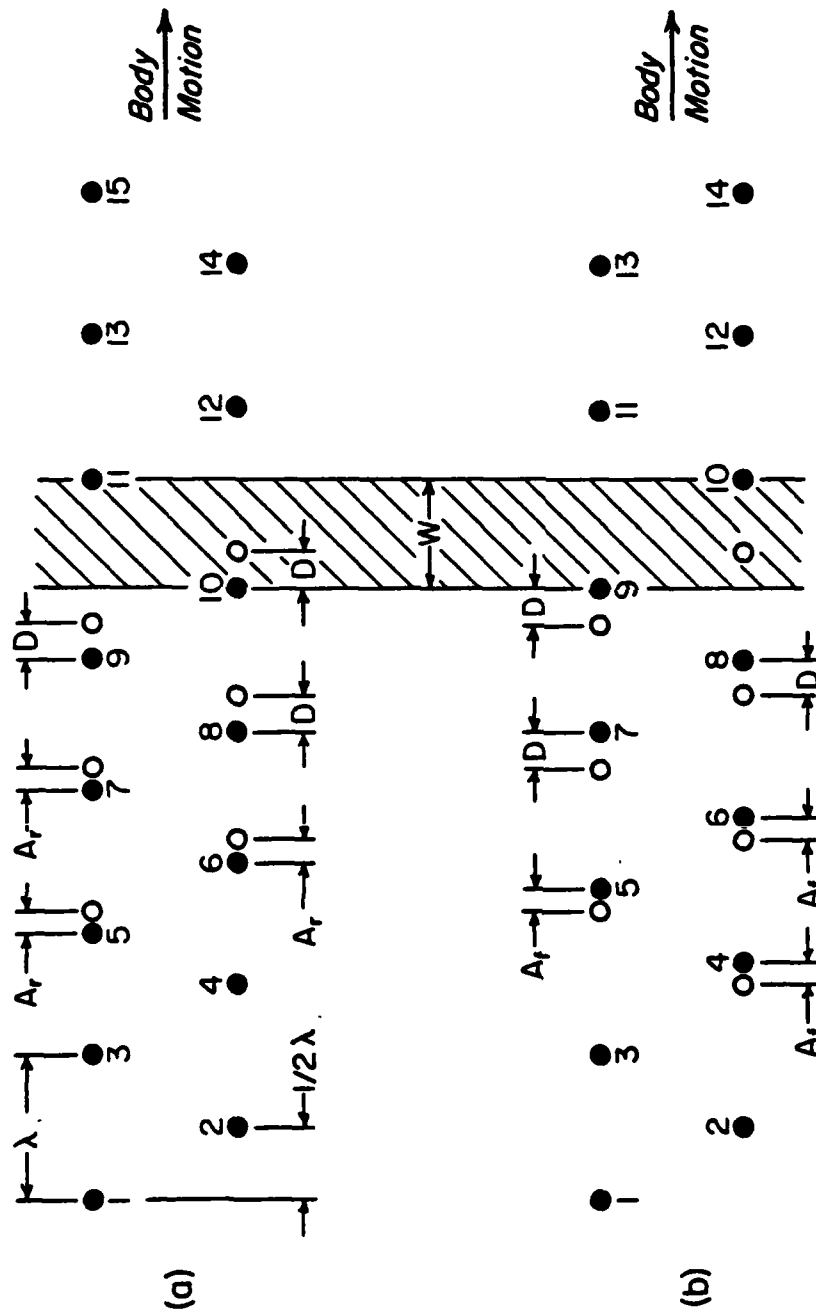


Figure 3.30: A hexapod crossing a ditch by front or rear foot adjustments in a continuous FTL gait.

same side is λ and the footprint on the right is 0.5λ ahead of that of the left. The maximal width region which can be crossed is the maximum of these two values: $0.5\lambda + A_f$ and $0.5\lambda + A_r$. The blank circles are the preplanned footholds and the darkened circles are the actual footprints. A preplanned foothold is in the forbidden region at a distance D from the edge. The vehicle should adjust its legs so that one of the front legs would step on the edge in order to gain the maximal crossing ability. Since D is large than A_r , two adjustments are needed.

In Figure 3.30a, the vehicle adjusts the legs by rear adjustment. It starts on leg 1 at footprint 5. Then leg 2 follows at footprint 6. At footprint 7, leg 1 can not adjust further because leg 6 is at footprint 4 where no adjustment has been made. At this time, the vehicle should slow down to readjust the center of gravity according to the positions of legs 1 and 2 so that the center of gravity is behind its original position by A_r . By doing this, the rear adjustment of the two front legs is compensated and the vehicle is ready for another rear adjustment. At footprint 8, leg 2 makes its second rear adjustment to D because leg 5 is at footprint 5 where one rear adjustment has been made already. Leg 1 makes its second adjustment at footprint 9. Leg 2 would then step on the edge of the forbidden region at footprint 10. At this time, the center of gravity should be readjusted again according to the two front legs. Then leg 1 can stretch out with its front adjustment to cross over the forbidden region. After both legs 5 and 6 pass over the forbidden region, the

center of gravity should be readjusted according to the two front legs in order to have optimal stability.

Figure 3.30b shows the vehicle crossing over the same forbidden region by front adjustment. It starts on leg 2 at footprint 4. After footprint 6, the center of gravity is readjusted. At footprint 9, leg 1 steps on the edge and the center of gravity is readjusted again. Then leg 2 stretches out to cross over the forbidden region. In both cases, six footprints are off the preplanned footprints. The method in Figure 3.30b starts the adjustment a half step earlier and has a half step less after the crossing.

Figure 3.31 shows a hexapod crossing over forbidden regions by lateral adjustments. In Figure 3.31a, the vehicle avoids some small longitudinal forbidden regions by lateral adjustments. In Figure 3.31b, the vehicle abducts the two front legs gradually to cross over a wide forbidden region. At footprint 5, leg 1 abducts by A_{b1} . Leg 2 then also abducts by A_{b1} at footprint 6. At footprint 7, leg 1 can not be further abducted since leg 6 is at footprint 4 where no abduction has been made. At footprint 8, leg 2 makes its second abduction by A_{b2} . Leg 1 makes its second abduction at footprint 9. By doing this, the leg on each side can make three abductions in five steps. This process proceeds until the width of the two foot paths is wider than the forbidden region. One thing noticeable is that the abducted adjustability increases as the path width increases (i.e., $A_{b3} > A_{b2} > A_{b1}$) since the angle α increases.

3.4.5.3 Special Methods for Large Leg Adjustments

If the terrain requires the vehicle to adjust its front legs abruptly, there are two methods available. The first method is to adjust the legs in cooperation with a body motion. The purpose of the body motion is to move the center of gravity and increase stability. The ways to move the body depend on the gaits and the adjustment made by the legs. The following is an example of this method.

Figure 3.32a shows a hexapod crossing over a large forbidden region by moving its body. The vehicle executes a large abduction of leg 1 at footprint 7. The center of gravity is moved to the left by half of the leg abduction. From the stationary gait pattern in Figure 3.29, the minimal SL determined by legs 1 and 6 does not change. However, the minimal SL determined by legs 2 and 5 in the second half step is negative. The body has to move back before this instability arises. Therefore, there are two body motions in the first step. In the second step, leg 1 is at footprint 9 and leg 6 is at footprint 6. The center of gravity has to move to the left again for the same reason. Leg 2 is then at footprint 10 and leg 5 is at footprint 7. Since footprint 7 has been abducted already, the center of gravity can be kept in its new position. After the vehicle passes the forbidden region, leg 1 adducts to its original path, and the body has to move laterally three times.

This method can also be used for a large longitudinal adjustment. In this case, the body has to move forward and backward. Hence, it becomes a discontinuous FTL gait.

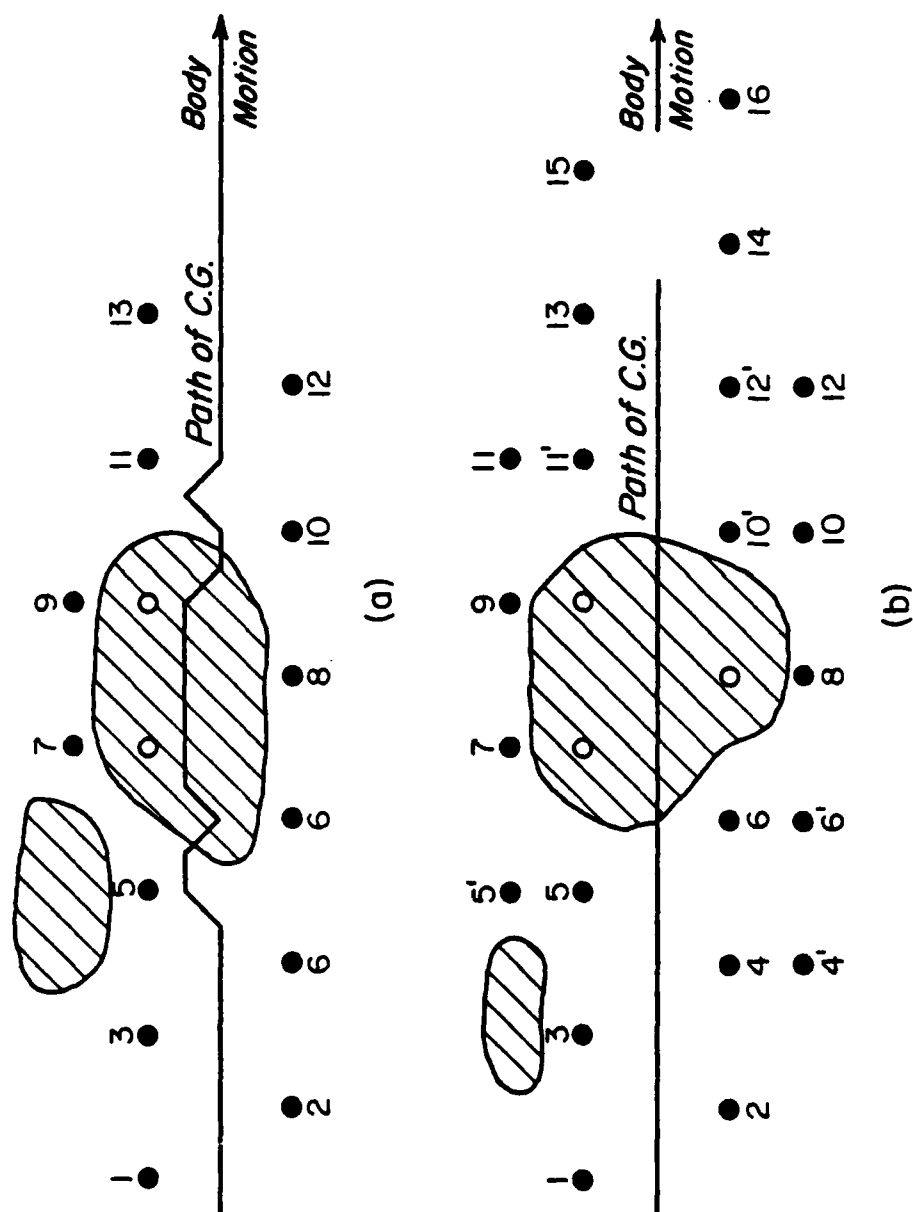


Figure 3.32: A hexapod crossing large forbidden regions by lateral foot adjustments incorporated with (a) lateral body motion, and (b) symmetric rear foot adjustments.

The second method is to adjust the two legs which determine the minimal SL together with the same adjustment in opposite directions. From Figure 3.29, since both the placements of legs 1 and 6 are before the moment of the minimal SL, if leg 1 has a large adjustment, leg 6 can follow immediately with an adjustment of the same distance but in the opposite direction. The resulting minimal SL is kept the same. This adjustment can be either longitudinal or lateral, or both.

Figure 3.32b shows a vehicle passing over a wide forbidden region by the second method. The vehicle performs a large abduction of leg 1 at footprint 7, leg 6 performs the same abduction in the opposite direction at footprint 4'. Leg 2 then performs a large abduction at footprint 8, followed by an abduction of leg 5 in the opposite direction at footprint 5'. The vehicle increases quickly its track width in a single step. After it passes the forbidden region, the same method is applied to adduct the legs on both sides to their original paths. The center of gravity is kept in the central line. The only disadvantage of this method is that it loses the nature of the FTL gait temporarily. The extra footprints at 4', 5', 6', 10', 11' and 12' have to be on permitted cells also.

3.4.5.4 Dexterous Periodic Gaits

As a summary of the above discussion, the principles of modification of a periodic gait into a continuous FTL gait are:

1. This periodic gait must possess the stepping characteristics of an FTL gait.
2. The maximum adjustments in longitudinal and lateral directions should be calculated. The vehicle can

adjust the two front legs to avoid forbidden regions.

3. The moments of the minimal SL and the legs which determine the minimal SL should be found. This information would provide the vehicle the strategies for leg adjustments, and special methods for large leg adjustments.

Many periodic gaits do not have the stepping characteristics of an FTL gait. However, it is possible for these gaits to possess the ability to avoid the forbidden regions through a similar development. A periodic gait with such ability is called a dexterous gait. The first step is to define the preplanned footholds before the vehicle. The locations of these preplanned footholds would tell whether any leg will fall into a forbidden region, and the necessary adjustments. The locations of the preplanned footholds can be calculated as follows.

$$\begin{aligned}
 P_{x1} &= R/2 + P + m \cdot R/\beta \\
 P_{x3} &= R/2 + (m + \phi_3) \cdot R/\beta \\
 P_{x5} &= R/2 - P + (m + \phi_5) \cdot R/\beta \\
 P_{x2} &= R/2 + P + (m + 1/2) \cdot R/\beta \\
 P_{x4} &= R/2 + (m + F[\phi_3 + 1/2]) \cdot R/\beta \\
 P_{x6} &= R/2 - P + (m + F[\phi_5 + 1/2]) \cdot R/\beta
 \end{aligned} \tag{3.74}$$

where $m = 1, 2, 3, 4, 5, \dots$ etc. and P_{xi} is the X-coordinate of the foothold of leg i and F is the fractional function.

The second step is to follow the principles 2 and 3 of the continuous FTL gait. The maximum adjustments of all six legs should

be calculated. A simple way to do it is by means of stationary gait pattern. The moments of minimal SL and the legs which determine the minimal SL are more complicated than those of continuous STL gait. For instance, for the wave gait, in the first half cycle, the minimal front SL and the minimal rear SL occur when leg 1 is placed and leg 5 is lifted respectively. The legs which determine the minimal front and rear SLs are legs 2 and 3 and legs 3 and 5 respectively. The strategies of avoiding forbidden regions and methods for large leg adjustments can be developed in a similar way to that of the continuous FTL gait. The detailed study of this development is left for future research.

3.5 Summary

In Chapter 3, analytical methods and graphical methods for gait analysis were introduced and demonstrated by many examples. The major gaits for level walking in different kinds of terrain were studied. From this analysis, the concluding points relating to leg design are:

1. For statically stable gait, a leg number of six seems to be appropriate because four legged gait has less stability and requires higher duty factor.
2. The improvement of stability by extending the stroke has a limit. A ratio $R/P = 1.2$ seems to appropriate. The break-point for $\beta = 11/12$ is $R/P = 1.22$.
3. In order to perform a large leg adjustment in rough terrain, which is desirable for discontinuous FTL gaits and continuous FTL gaits, the stroke in longitudinal and in lateral directions should be as large as possible.

The following are the main aspects of each gait.

Wave gaits have optimal stability among all periodic gaits. A simple formula for the gait stability margin with $\beta \geq 1/2$ was derived. Methods for wave gaits to increase stability by varying stroke and stroke pitch were studied in detail. Gait stability with $\beta < 1/2$ of wave gait for more than six legs is an interesting subject for the future research.

EPH gaits can equally distribute the placing events and/or the lifting events in one locomotion cycle. For $\beta < 5/6$, full cycle EPH gaits have better stability. For $\beta \geq 5/6$, half cycle EPH gaits have better stability.

Backward periodic gaits have a backward stepping sequence and have potential to be developed into discontinuous FTL gaits. Backward wave gaits have the minimal stability among all the periodic gaits in this chapter. Full cycle backward EPH gaits have better stability than half cycle backward EPH gaits. The method to develop a backward periodic gait into an FTL gait is a valuable topic for the future research.

The general approach of the discontinuous FTL gaits can maximize the reach of the two front legs. The reasons for this improvement are a flexible schedule of the body movements and a marginal stability. The longitudinal stability margin is used for this approach because it is easy for calculation, and lateral stability can be maintained simply by keeping the center of gravity between the two legs which determine the minimal stability margin. If optimal stability is required, a method to modify this approach by replacing the longitudinal stability margin with stability margin was also introduced.

Continuous FTL gaits have very good potential for the ASV to walk over most natural terrain. It has smooth body motion and can reach higher speed. No periodic gaits with backward stepping sequence can be a continuous FTL gait. The walk gait of horses is a continuous FTL gait. Several strategies of leg adjustments and special methods for large leg adjustments were introduced by examples. The methods used to develop a periodic gait into a dexterous periodic gait were discussed in principle. The detailed development of each dexterous periodic gait is a subject for future research.

Chapter 4

GAIT ANALYSIS PART II - GAITS FOR IRREGULAR TERRAIN

4.1 Introduction

In Chapter 3, gaits of a hexapod over level terrain were studied. In this chapter, gaits over three dimensional irregular terrain are studied. Since the variety of irregular terrain is unlimited, it is difficult to cover all the different cases of the walking over irregular terrain.

In order to study this problem the real terrain features are simplified into geometric features. The geometric feature types chosen for study are: slope, ditch, vertical step and isolated wall. The study presented in this chapter is concentrated on the walking of a hexapod over each irregularity.

In order to simplify the study, these irregularities are assumed to have simple geometry with sharp solid edges. Figure 4.1 shows the geometries of these features. Each can be described by one or two parameters. The last three irregularities are called obstacles.

In the following discussions, the dimensions of the ASV shown in Figure 3.1 are used to calculate the performance of the vehicle as references. In the figure, H is the height of the center of gravity. W is the width of the track. P is the stroke pitch and R is the stroke.

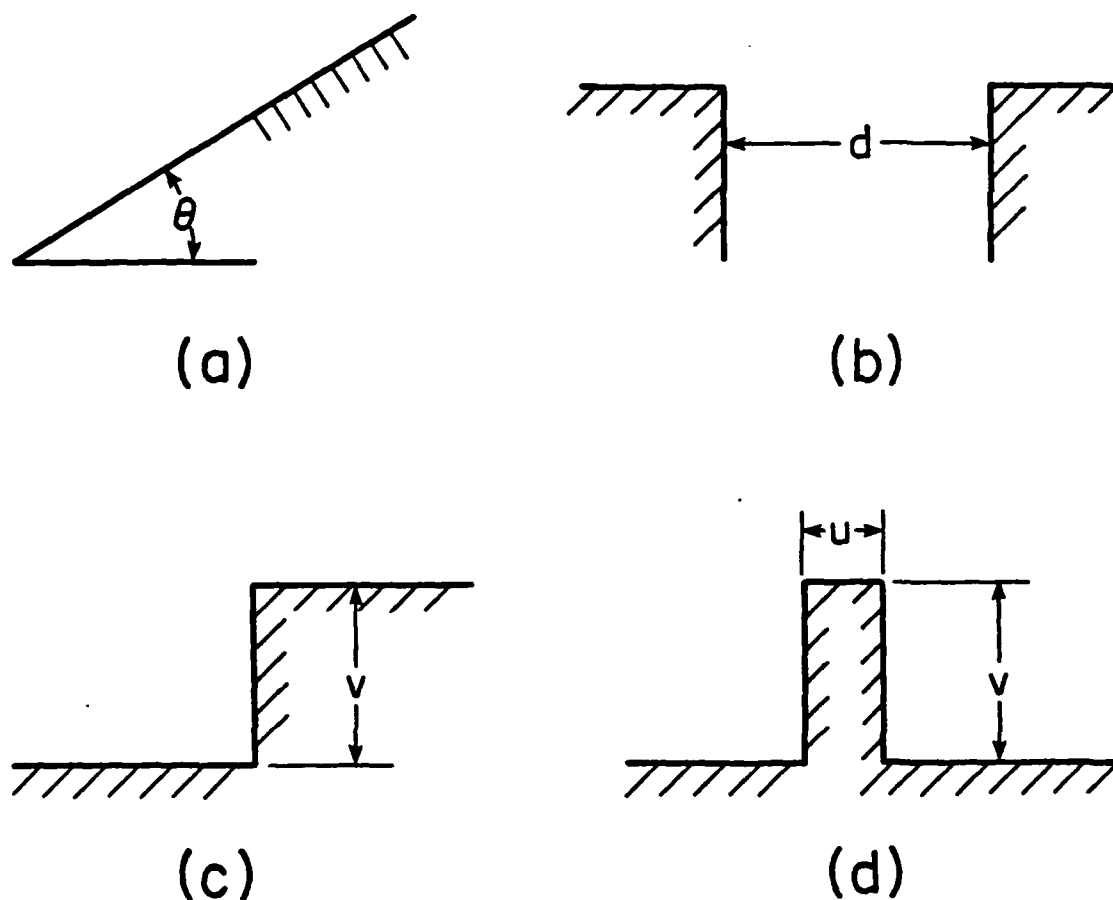


Figure 4.1: Major irregularities of a rough terrain,
 (a) a slope (b) a ditch (c) a vertical step
 (d) an isolated wall.

L is the length of the body. The body coordinate system X - Y - Z is attached on the body with the origin at the center of gravity. The directions of the X -axis, Y -axis and Z -axis are toward the front, the right and the ground respectively. R_x , R_y and R_z are the three dimensions of the walking volume in the X , Y and Z direction respectively. In the following discussion, a subscript "o" denotes

the normal dimensions, which are the values given in Figure 3.1, of the vehicle. For instance, H_0 denotes the normal height of the vehicle and $H_0 = 72$ inches.

The following assumptions are made for the simplicity of analysis:

1. Every point is a permitted cell except those on a vertical surface.
2. The contact between foot and the ground is a point contact.
3. There is no slip between foot and ground.
4. All the mass of the legs is lumped into the body. The center of gravity is assumed to be at the centroid of the body.
5. The motion is slow enough so that no dynamic effects need be considered.

In Section 4.2, gait stability for walking on a slope and strategies to improve the stability are studied. The maximum gradient which can be traversed in different cases of walking on a slope are also calculated.

In Section 4.3, ditch crossing of a hexapod with a periodic gait and a large obstacle gait is studied. A general introduction of obstacle crossing with a large obstacle gait is also given.

In Section 4.4, vertical step crossing of a hexapod with a large obstacle gait is studied. Both stepping up and stepping down are included.

In Section 4.5, isolated wall crossing of a hexapod with a large obstacle gait is studied.

In each of the obstacle crossing studies, the dimensions of the maximum obstacle which can be crossed are calculated and possible improvements obtained by modifying the walking volume are discussed.

4.2 Gaits for Walking on a Slope

The main difference between walking on a slope and level walking is that the projection of the center of gravity onto the support pattern is shifted. If a periodic gait is symmetric about the longitudinal and the lateral body axes, the minimal front SL and the minimal rear SL are the same in level walking. However, in walking on a slope, the shifted projection of the center of gravity would reduce the minimal SL on the downhill side, and hence reduce the gait stability margin.

There are two strategies which can be used to improve stability when walking on a slope. The first is to lower the walking height and/or to adjust the body attitude. The second is to change the beginning and the end of the stroke. In order to understand the effectiveness of each strategy, the upper limit of the maximum gradient which can be traversed in each case is calculated for comparison. The case when the stability margin becomes zero is the upper limit of the maximum gradient.

Wave gaits are selected as representative of periodic gaits because of their optimal stability. Precision footing gaits are also used for calculation because they give the maximum possible grade for each case.

In the following, parameters referring to operation on a slope are distinguished from the corresponding parameters for level walking by a prime. For instance, SL' denotes the longitudinal stability margin measured according to the support pattern on the sloping surface.

4.2.1 Walking on a Slope by Adjusting the Walking Height and/or the Body Attitude

4.2.1.1 Walking Along a Line of Maximum Gradient

The strategy of lowering the body height is studied first. The vehicle is walking in a condition in which the longitudinal body axis is aligned with the maximum gradient line. If the slope angle is θ , the offset of the projection of the center of gravity on the sloping surface is $H \cdot \tan \theta$. Referring to Figure 4.2, the stability margin SL can be calculated as

$$SL = SL' \cdot \cos \theta \quad (4.1)$$

Instability occurs if $SL < 0$ at any instant during a complete locomotion cycle. Hence, only the minimum longitudinal stability margin needs to be considered. Since wave gaits are symmetric about the lateral body axis, for the same slope angle, the effects on stability due to the shifted projection of the center of gravity in uphill and downhill walking are the same. These two cases are considered as one.

Let S_0 be the gait stability margin in level walking (i.e., slope angle $\theta = 0^\circ$). The gait stability margin for a walking on a

slope with slope angle θ becomes

$$S = (S_o - H \cdot \tan \theta) \cdot \cos \theta \quad (4.2)$$

The maximum walking height H_m can be determined by setting $S = 0$.

$$H_m = S_o \cdot \tan \theta \quad (4.3)$$

For a given body height H , the maximum slope angle is

$$\theta_m = \tan^{-1}(S_o/H) \quad (4.4)$$

Since the minimum body height is $H_o - Rz_o$, (it is here assumed that the vehicle belly height is greater than $H_o - Rz_o$), the maximum slope angle for the vehicle is

$$\theta_m = \tan^{-1}(S_o/(H_o - Rz_o)) \quad (4.5)$$

For a precision footing gait, the maximal stability margin can be obtained by extending the two legs on the downhill side to their limits. Hence,

$$S_o = P_o + Rx_o/2 \quad (4.6)$$

This gives $\theta_m = 76^\circ$.

From Table 3.2, the break-point is $R/P = 1.22$ for $\beta = 11/12$. For the hexapod, $R/P = 1.2$. If only the duty factors between $3/4$ and $11/12$ are considered, the gait stability margin of a wave gait is determined by Equation (3.20) alone, and increasing the stroke would increase the gait stability. Hence, for a hexapod, the gait stability margin is

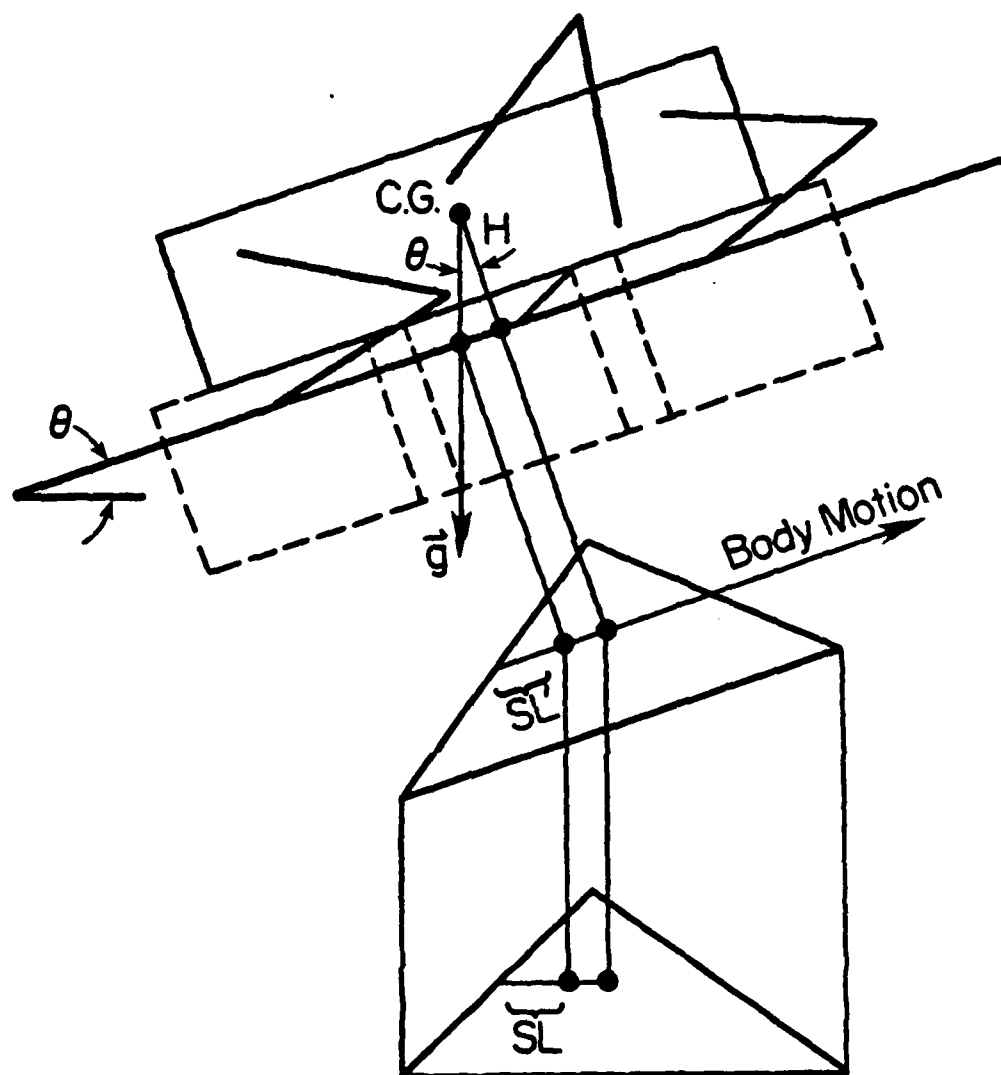


Figure 4.2: Support pattern of a hexapod walking on a slope by lowering the body height.

$$S_o = P/2 + (1 - 3/(4\beta)) \cdot R \quad (4.7)$$

For walking on a steep slope, a duty factor of $\beta = 11/12$ is reasonable. Substituting the dimensions of the hexapod and $\beta = 11/12$ into

Equation (4.7) gives

$$\text{For } P = R = 60, \quad S_o = 40.9 \quad (4.8)$$

$$\text{For } P = 60, R = 72, \quad S_o = 43.1 \quad (4.9)$$

These two values are used to calculate the maximum gradient for each case. Substituting these values of S_o into Equation (4.5) gives $\theta_m = 59.6^\circ$ for $P = R$ and $\theta_m = 60.9^\circ$ for $R/P = 1.2$.

The second strategy is to adjust the body attitude. Figure 4.3 shows that the projection of the center of gravity is not shifted if the body attitude is kept level. Hence, the gait stability margin is the same as it is in level walking. The body can be fully leveled only if the slope angle is less than a limiting angle ϕ_m . From Figure 4.3, this limiting angle ϕ_m is determined to be

$$\phi_m = \tan^{-1} [Rz_o / (L/2)] \quad (4.10)$$

Substituting the dimensions of the hexapod into Equation (4.10) gives $\phi_m = 31^\circ$.

In order that all six legs have the same stroke, the maximum slope which can be traversed with the body level is that of the line passing through A and B. This angle ϕ_o is

$$\phi_o = \tan^{-1} [Rz_o / (2P_o + Rx_o)] \quad (4.11)$$

For the ASV, $\phi_o = 14^\circ$. Let the gait stability margin on the sloping surface at this particular angle be S'_o , then

$$S'_o = S_o / \cos \phi_o \quad (4.12)$$

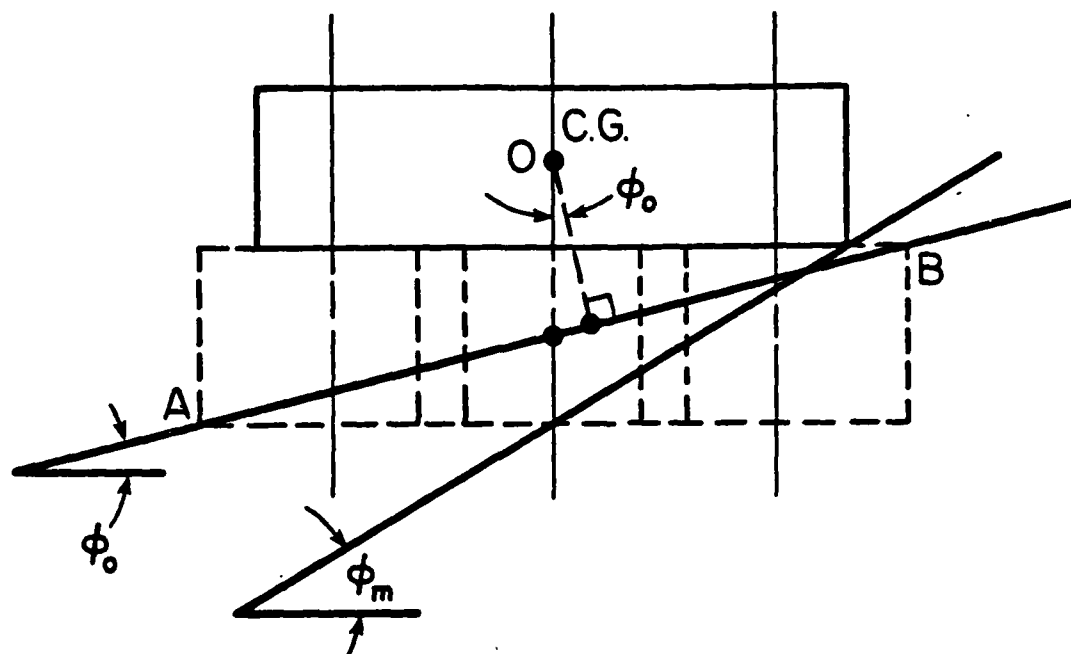


Figure 4.3: The maximum slope angle with level body attitude.

The distance between the center of gravity and the hypotenuse AB is

$$OC = (H_0 - Rz_0/2) \cdot \cos \phi_0 \quad (4.13)$$

If the slope angle θ is greater than the angle ϕ_0 , the body can not be fully leveled. Figure 4.4 shows such a case. The body angle θ' is equal to $\theta - \phi_0$. The intersection of the Z-axis with the sloping surface is at point E. This point E is called the geometric center of the support pattern. Since the support patterns are symmetric about the lateral body axis which goes through point E,

any offset of the center of the gravity should be measured according to point E.

The projection of center of gravity on the sloping surface is at point D. Hence, the offset of the projection on the slope is DE. From trigonometry,

$$\begin{aligned} DE &= DC - EC \\ &= OC \cdot (\tan \theta - \tan \phi_0) \end{aligned} \quad (4.14)$$

The gait stability margin on the slope, S' , is

$$S' = S'_0 - DE \quad (4.15)$$

and the gait stability margin becomes

$$S = S' \cdot \cos \theta \quad (4.16)$$

Substituting Equations (4.12), (4.14) and (4.15) into Equation (4.16) gives

$$S = [S'_0 / \cos \phi_0 - OC \cdot (\tan \theta - \tan \phi_0)] \cdot \cos \theta \quad (4.17)$$

The angle of maximum slope is reached when S becomes zero. This gives

$$\theta_m = \tan^{-1} [(S'_0 / \cos \phi_0 + OC \cdot \tan \phi_0) / OC] \quad (4.18)$$

for the hexapod, it becomes

$$\theta_m = \tan^{-1} [(1.03S'_0 + 11.61) / 46.57] \quad (4.19)$$

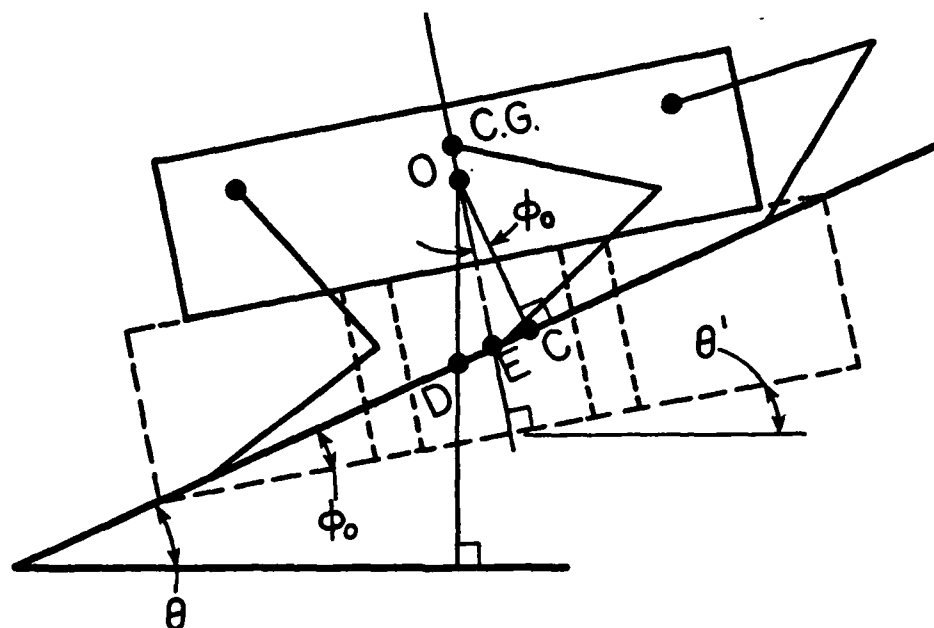


Figure 4.4: Walking on a slope of a hexapod with reduced body inclination, $\theta > \phi_0$.

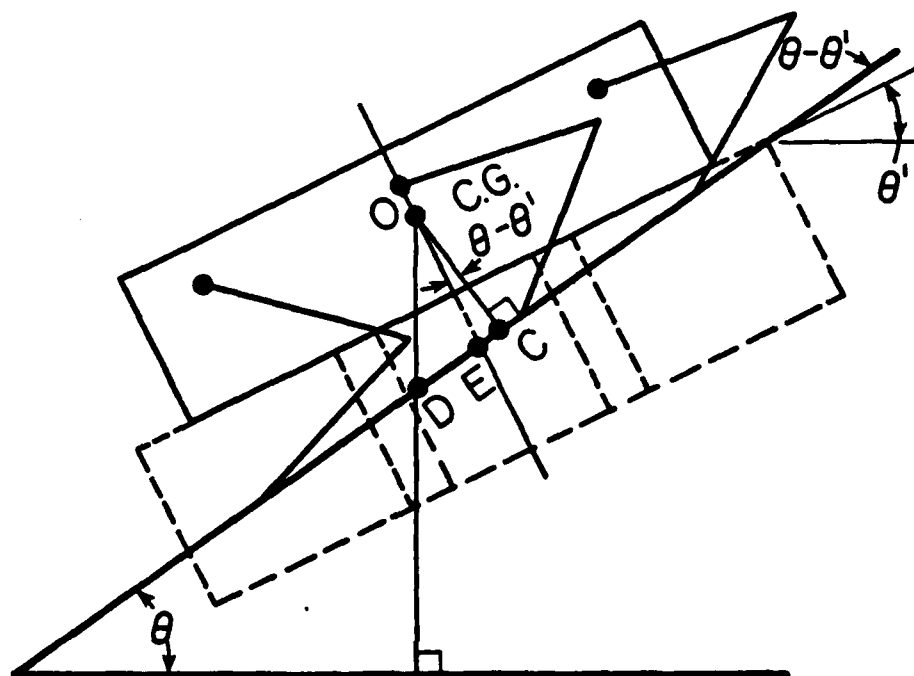


Figure 4.5: Walking on a slope of a hexapod by combining body inclination reduction and lowering of the body.

For a precision footing gait, substituting Equation (4.6) into Equation (4.19) gives $\theta_m = 67.1^\circ$. For wave gait with $\beta = 11/12$, $\theta_m = 49.1^\circ$ for $P = R$ and $\theta_m = 50.2^\circ$ for $R/P = 1/2$. Comparing these with the results of the first strategy shows that the first strategy is more effective.

Sometimes, both strategies might be combined for walking on a slope. The body attitude is first adjusted to a desired angle θ' . The body height is then reduced until the front upper corner of the walking envelope touches the ground (see Figure 4.5). The new body height OC is

$$OC = OE \cdot \cos (\theta - \theta') \quad (4.20)$$

$$= \{H_o - [Rz_o - (P_o + Rx_o/2) \cdot \tan (\theta - \theta')]\} \cdot \cos (\theta - \theta')$$

The geometric center of the gait is at point E, and OE intersects with OC at an angle $\theta - \theta'$. Hence, by replacing ϕ_o with $\theta - \theta'$ in Equation (4.17), the gait stability margin becomes

$$S = [S_o / \cos (\theta - \theta') - OC \cdot (\tan \theta - \tan (\theta - \theta'))] \cdot \cos \theta \quad (4.21)$$

4.2.1.2 Walking along a Zero Gradient Line

If a hexapod is walking along a zero gradient line on a slope with slope angle θ , and the body is kept parallel to the sloping surface, the projection of the center of gravity is shifted laterally to the downhill side by a distance $H \cdot \tan \theta$. Only if the legs are kept normal to the surface of the ground. Figure 4.6 shows such a case.

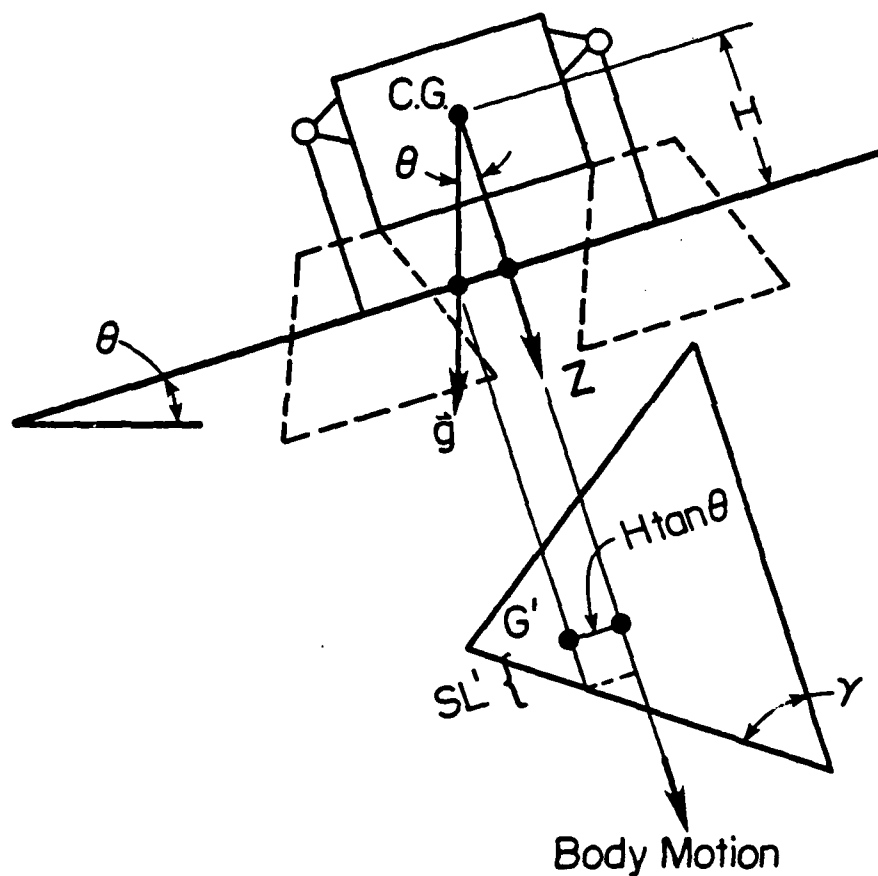


Figure 4.6: Walking on a slope along a zero gradient line by lowering the body height.

For a precision footing gait, the maximum grade which can be handled by this strategy occurs when the offset of the projection of the center of gravity is equal to $W/2$. That is,

$$H \cdot \tan \theta = W/2 \quad (4.22)$$

If the body height is lowered to the minimum, Equation (4.22) gives

$$\theta_m = \tan^{-1}(W/(2H)) \quad (4.23)$$

For the hexapod, $\theta_m = 60.2^\circ$.

If the legs on the downhill side are fully abducted, the maximum gradient becomes

$$\theta_m = \tan^{-1}[(W + Ry_t)/2] \quad (4.24)$$

where Ry_t is the lateral stroke on the top of the walking volume.

For the ASV with minimal body height, $\theta_m = 66^\circ$.

For a wave gait, the stability margin on the sloping surface is

$$S' = S_0 - H \cdot \tan \theta / \tan \gamma \quad \text{for } H \cdot \tan \theta \leq W/2 \quad (4.25)$$

where γ is the angle of the boundary which determines the minimal SL relative to the longitudinal body axis. This can be calculated as follows:

From the proof of Theorem 6 in Chapter 3, the moment of the minimal SL of a wave gait is when a rear leg is lifted. For a hexapod, the foot positions of legs 3 and 6 at the moment leg 5 is lifted are

$$P(3) = R/2 - (2\beta - 1) \cdot R/\beta \quad (4.26)$$

$$P(6) = -P + R/2 - (\beta - 1/2) \cdot R/\beta \quad (4.27)$$

The width of the track is W . Hence, the angle γ is

$$\begin{aligned} \gamma &= \tan^{-1} \{W/[P(3) - P(6)]\} \\ &= \tan^{-1} \{W/[P + (1/(2\beta) - 1) \cdot R]\} \end{aligned} \quad (4.28)$$

Since the longitudinal body axis is parallel to the horizontal plane, S' is equal to S . Hence,

$$S = S_0 - H \cdot \tan \theta / \tan \gamma \quad \text{for } H \cdot \tan \theta \leq W/2 \quad (4.29)$$

For a given slope angle θ , the maximum body height H_m is

$$H_m = S_0 \cdot \tan \gamma / \tan \theta \quad (4.30)$$

Since the minimal body height is $H_0 - Rz_0$, the maximum slope angle for this case is the minimum of Equation (4.23) and the following equation

$$\theta_m = \tan^{-1} [S_0 \cdot \tan \gamma / (H_0 - Rz_0)] \quad (4.31)$$

For a wave gait with $\beta = 11/12$ and $P = R = 60$, $\gamma = 65.6^\circ$. Substituting this value into Equation (4.31) gives $\theta_m = 75.1^\circ$. Hence, the maximal gradability of the wave gait is the same as that of a precision footing gait. This gives $\theta_m = 60.2^\circ$. If the legs on the downhill side are fully abducted, $\theta_m = 66^\circ$.

The second strategy is to adjust the body attitude. In Figure 4.7a, the body attitude is leveled by extending the legs on one side and shortening the legs on the other side. The projection of the center of gravity is kept on the center line. Thus, there is no change in the gait stability margin. The maximal slope angle on which the body can be fully leveled is

$$\alpha_0 = \tan^{-1} (Rz_0 / W) \quad (4.32)$$

For the hexapod, $\alpha_0 = 33.7^\circ$.

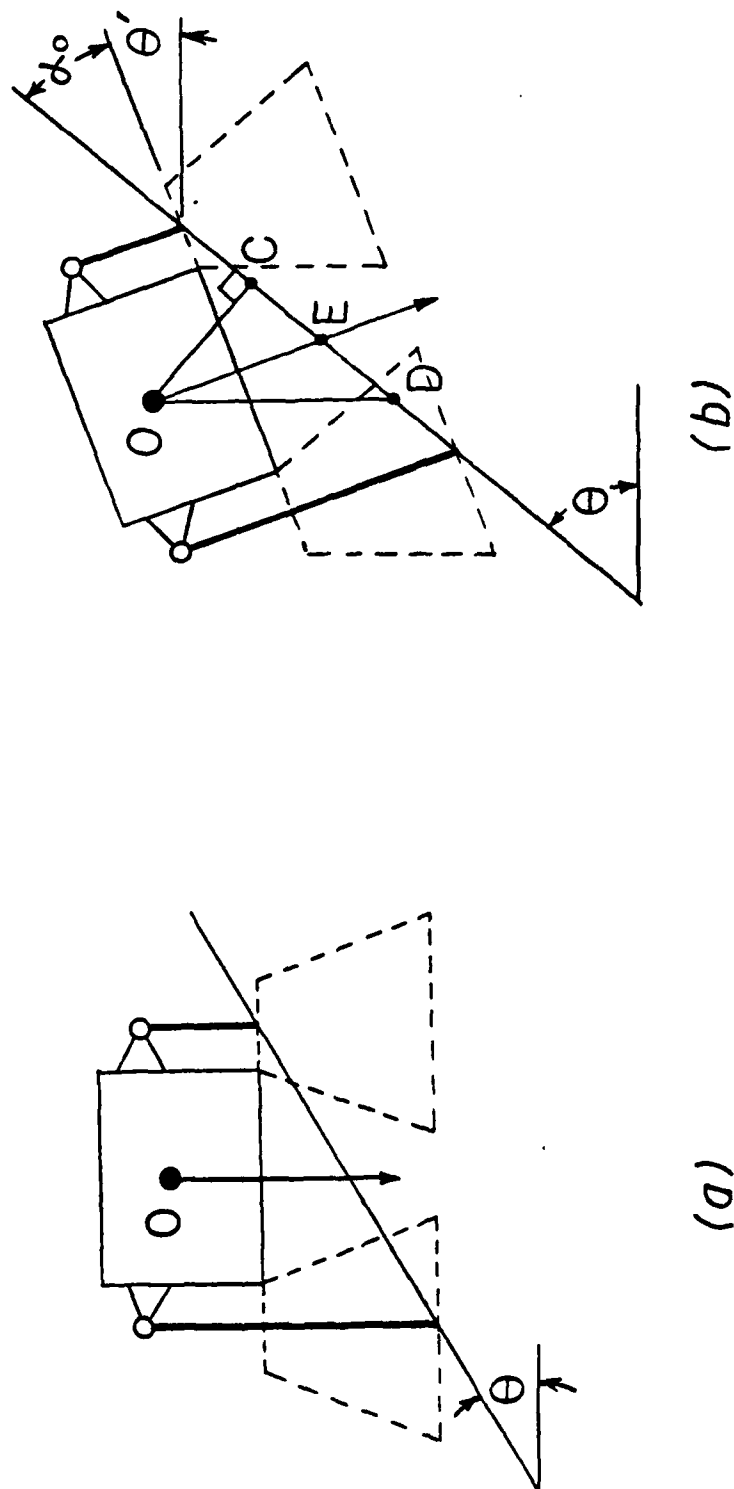


Figure 4.7: Walking on a slope along a zero gradient line by leveling the body attitude.

If the slope angle is greater than α_o , the body can not be fully leveled. Figure 4.7b shows such a case. The distance apart on the sloping surface of the foot trajectories is:

$$W' = W/\cos \alpha_o \quad (4.33)$$

The geometric center of the support pattern is at point E. The offset of the projection of the center of gravity is

$$\begin{aligned} DE &= DC - EC \\ &= OC \cdot (\tan \theta - \tan \alpha_o) \end{aligned} \quad (4.34)$$

and

$$OC = (H_o - R_z_o/2) \cdot \cos \alpha_o \quad (4.35)$$

For a precision footing gait, the maximum slope angle occurs when the offset is equal to $W'/2$. Hence,

$$\theta_m = \tan^{-1}[(W'/2)/OC + \tan \alpha_o] \quad (4.36)$$

For the ASV, $\theta_m = 65.1^\circ$.

If the legs on the uphill side are adducted and the legs on the downhill side are abducted the same distance Ry_t , the projection of the center of gravity is moved up a distance $Ry_t \cdot \cos \alpha_o$. The offset becomes

$$DE = OC \cdot (\tan \theta - \tan \alpha_o) - (Ry_t/2) \cdot \cos \alpha_o \quad (4.37)$$

and OC becomes

$$OC = (H_o - Rz_o/2) \cdot \cos \alpha_o - (Ry_t/2) \cdot \sin \alpha_o \quad (4.38)$$

Setting the right hand side of Equation (4.37) equal to $W'/2$, the maximum slope angle θ_m becomes

$$\theta_m = \tan^{-1} \{ [W'/2 + (Ry_t/2) \cdot \cos \alpha_o] / OC + \tan \alpha_o \} \quad (4.39)$$

For the ASV, $\theta_m = 76^\circ$.

For a wave gait, the gait stability margin on the slope is

$$S' = S'_o - DE/\tan \gamma \quad (4.40)$$

where γ is the angle of the boundary which determines the minimal SL relative to the longitudinal body axis. For $\beta = 11/12$ and $P = R = 60$, substituting W' into Equation (4.28) gives $\gamma = 72^\circ$. Since the longitudinal body axis is parallel to the horizontal plane, $S = S'$ and $S_o = S'_o$. Hence, the gait stability margin is

$$S = S_o - DE/\tan \gamma \quad \text{for } DE \leq W'/2 \quad (4.41)$$

Substituting for DE from Equation (4.34) into Equation (4.40) gives

$$\theta_m = \tan^{-1} [(S_o \cdot \tan \gamma + OC \cdot \tan \alpha_o) / OC] \quad (4.42)$$

The maximum slope angle is the minimum of the values given by Equations (4.36) and (4.42). For the ASV, Equation (4.36) gives $\theta_m = 75.3^\circ$. Hence, the maximum slope angle is equal to that of a precision footing gait. This gives $\theta_m = 65.1^\circ$. Similarly, if the legs on both sides are abducted and adducted to the downhill side the same distance $Ry_t/2$, the maximum slope angle becomes $\theta_m = 76^\circ$.

4.2.1.3 Relationship to the Walking Volume

The gradability of each case calculated in the previous sections are tabulated in Table 4.1.

Table 4.1
Gradability of the ASV

		First strategy	Second strategy
Along a maximum gradient line	PFG	76.0°	67.0°
	WG P = R	59.6°	49.1°
	WG R/P = 1.2	60.9°	50.2°
Along a zero gradient line	PFG normal	60.2°	65.1°
	PFG ab/ad	66.0°	76.0°
	WG normal	60.2°	65.1°
	WG AB/ad	66.0°	76.0°

PFG : precision footing gait
 WG : wave gait with $\beta = 11/12$
 ab/ad: abduction/adduction

In the case of walking along a maximum gradient line, the first strategy, which is to lower the body height, is more effective than the second strategy, which is to adjust the body attitude. By examining the related equations, it is concluded that the gradability using the first strategy is very closely related to the minimal body height $H_0 - R z_0$ and the stability margin. The gradability using the second strategy is very closely related to the minimal body height, the stability margin and the angle ϕ_0 , which is defined in Equation (4.11).

For a precision footing gait, the stability margin is determined by P_0 and Rx_0 . Increasing either of these two values would increase the stability margin. For a wave gait, the gait stability margin depends on P_0 , Rx_0 and the ratio R/P . It can be optimized according to Table 3.2.

If ϕ_0 increases, the gradability given by the second strategy increases too. The angle ϕ_0 is only 14° for the ASV. This is the reason that the second strategy gives smaller gradability. ϕ_0 can be increased by increasing Rz_0 or by reducing P_0 or Rx_0 . The reduction of P_0 or Rx_0 has negative effect in stability. Hence, the best way to increase ϕ_0 is to increase Rz_0 .

In the case of walking along a zero gradient line, the first strategy has the same effect as the second strategy on gradability. The gradability given by the first strategy depends on the minimal body height and the stability margin. The gradability given by the second strategy depends on the minimal body height, the stability margin and the angle α_0 , which is defined in Equation (4.32).

For a precision footing gait, the stability margin is determined by the distance between the foot trajectories on the two sides of the vehicle. For a wave gait, the gait stability margin is determined by P_0 , Rx_0 and the ratio R/P . The reduction of the longitudinal stability due to the offset of the projection of the center of gravity depends on the angle γ , which is defined in Equation (4.28). Since γ is very large for a large duty factor, the wave gait has the same gradability as the precision footing gait.

The angle α_0 has the same effect on gradability as ϕ_0 in the previous case. Since α_0 is 33.7° for the ASV, it causes the second strategy to give a greater gradability.

4.2.1.4 Walking in an Arbitrary Direction

In practice, a walking machine will not usually go uphill or downhill along a maximum gradient line. At this time, the projection of the center of gravity has offsets in both the longitudinal and lateral directions.

Figure 4.8 shows a walking machine walking in an arbitrary direction on a sloping surface with slope angle θ . The body is kept parallel to the sloping surface. O is the center of gravity. G' is the projection of O on the sloping surface. O' is the intersection of the Z-axis and the sloping surface. If there is no abduction or adduction of the legs, O' is the geometric center. X' and Y' are two coordinate axes with the origin at O' and are respectively parallel to the X-axis and the Y-axis of the body reference frame. θ_x and θ_y are the angles of X' -axis and the Y' -axis relative to the horizontal plane respectively. ψ is the angle between the maximum gradient line and the X' -axis. α_x , α_y and α_z are the angles between the direction of gravity and the X-axis, Y-axis and Z-axis respectively.

From the above discussion, the longitudinal gait stability margin of a periodic gait on the sloping surface is

$$S' = S_0 / \cos \theta_x - E_x - E_y / \tan \gamma \quad (4.43)$$

and the gait stability margin is

where $SGX = 1$ if $\alpha_x \leq \pi/2$, and $SGX = -1$ if $\alpha_x > \pi/2$

$SGY = 1$ if $\alpha_y \leq \pi/2$, and $SGY = -1$ if $\alpha_y > \pi/2$

If α_x , α_y , α_z and ψ are known, E_x and E_y can be calculated. Substituting these values into Equations (4.43) and (4.44), the gait stability margin can be found. The following shows a way to calculate these angles:

Given the angle α_x between the direction of gravity and X-axis and the angle α_y between the direction of gravity and Y-axis, the third angle α_z can be calculated according to the directional cosines.

$$\cos^2 \alpha_x + \cos^2 \alpha_y + \cos^2 \alpha_z = 1 \quad (4.47)$$

It is assumed that the machine will have a vertical gyro, or other instrumentation, to enable at least two of α_x , α_y and α_z to be measured. This gives

$$\alpha_z = \cos^{-1} [(1 - \cos^2 \alpha_x - \cos^2 \alpha_y)^{1/2}] \quad (4.48)$$

Figure 4.9 shows the relationship of these angles. O is the center of the gravity of the machine. A and C are the respective intersections of the X and Y axes with a zero gradient line. D is the projection of O on the horizontal plane which contains line AC. BO is the maximum gradient line. Since the X-Y plane is parallel to the sloping surface, and the Z-axis is perpendicular to the sloping surface, from trigonometry

$$\alpha_z + \delta = \pi/2 = \delta + \theta \quad (4.49)$$

This gives

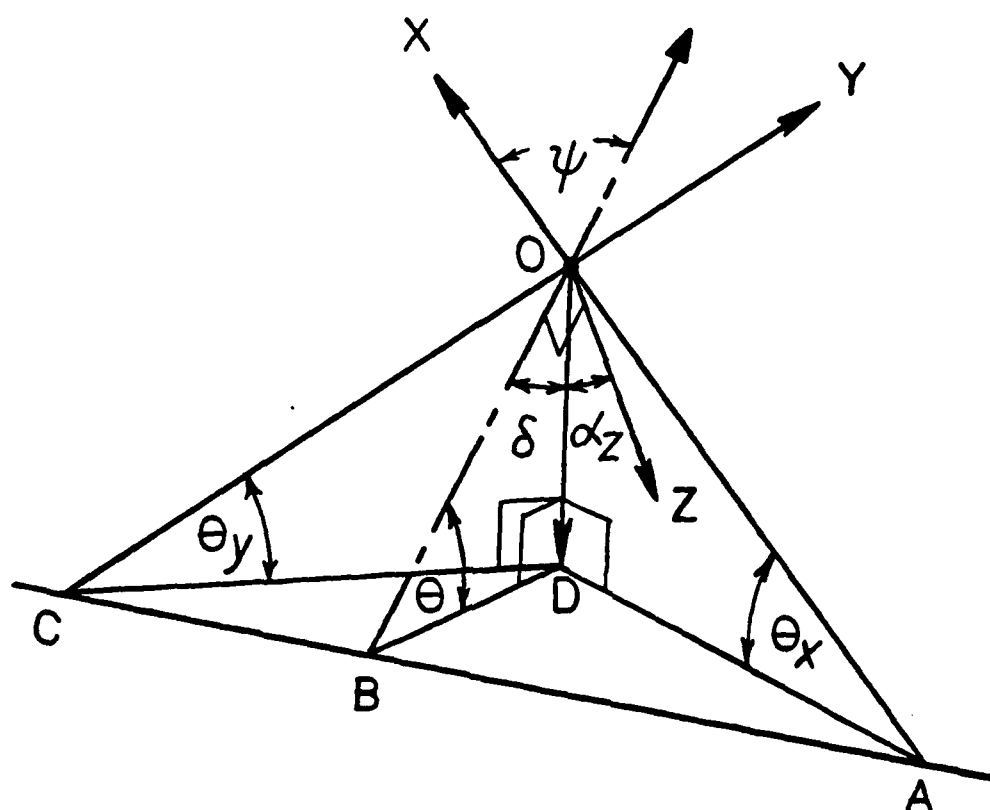


Figure 4.9: Relationship of angles for walking on a slope.

$$\alpha_z = \theta \quad (4.50)$$

This indicates that α_z is equal to the slope angle whenever the body is kept parallel to the ground. Similarly,

$$\theta_x = \alpha_x - \pi/2 \quad (4.51)$$

$$\theta_y = \alpha_y - \pi/2 \quad (4.52)$$

From trigonometry,

$$\sin \theta_x = OD/AO \quad (4.53)$$

$$\sin \theta = OD/BO \quad (4.54)$$

Dividing Equation (4.53) with Equation (4.54) on both sides gives

$$\frac{\sin \theta_x}{\sin \theta} = \frac{BO}{AO} = \cos \psi \quad (4.55)$$

Substituting Equation (4.50) and (4.51) into Equation (4.55) gives

$$\psi = \cos^{-1} \left(\frac{\sin(\alpha_x - \pi/2)}{\sin \alpha_z} \right) \quad (4.56)$$

This completes the calculation.

4.2.2 Walking on a Slope by Adjusting the Beginning and the End of the Stroke

A walking machine can increase its gait stability by adjusting the positions of beginning and end of the stroke relative to the body. Since the general equations for walking on a slope along a maximum gradient line, along a zero gradient line or in an arbitrary direction have been derived in the last section, the improvement in stability given by this strategy can be substituted into the proper equations according to the walking conditions. Hence, the study in this section is concentrated on the improvements of the gait stability margin given

by different methods.

The adjustment of the beginning and the end of the stroke includes the following four methods: the adjustment of the stroke only, the adjustment of stroke pitch only, the adjustment of both stroke and stroke pitch simultaneously and the shifting of the centers of the strokes. In order to have these adjustments, the walking machine must have overlap between the walking envelopes of adjacent legs. The overlap between two adjacent envelopes is $Rx_0 - P_0$.

The first method is to adjust the stroke only. Since higher stability is required for walking on a gradient, a higher duty factor is expected to be used. From Table 3.2, for $\beta \geq 3/4$, increasing stroke would increase stability. From Equation (4.7), the gait stability margin of a wave gait with maximum stroke Rx_0 is

$$S_0 = P_0/2 + (1 - 3/(4\beta)) \cdot Rx_0 \quad (4.57)$$

The second method is to adjust the stroke pitch only. If the stroke is kept to be equal to P_0 , the maximal stroke pitch is $(Rx_0 - P_0)/2$. The gait stability margin becomes

$$S_0 = [P_0 + (Rx_0 - P_0)/2]/2 + (1 - 3/(4\beta)) \cdot P_0 \quad (4.58)$$

The third method is to increase Rx and P simultaneously. If $Rx = P$, the maximum value of Rx and P become

$$Rx = P = (2P_0 + Rx_0)/3 \quad (4.59)$$

Substituting this value into Equation (4.7) gives

$$\begin{aligned}
 S_o &= (2P_o + Rx_o)/6 + (1 - 3/(4\beta)) \cdot (2P_o + Rx_o)/3 \\
 &= (1 - 1/(2\beta)) \cdot P_o + (1/2 - 1/(4\beta)) \cdot Rx_o
 \end{aligned}
 \tag{4.60}$$

Subtracting Equation (4.60) from Equation (4.57) gives

$$\Delta S = (1/\beta - 1) \cdot (Rx_o - P_o)/2 \tag{4.61}$$

Since $\beta < 1$, $Rx_o > P_o$, $\Delta S > 0$ always. Hence, the third method gives a better improvement in stability than the first method.

Subtracting Equation (4.58) from Equation (4.60) gives

$$\Delta S = (1/\beta - 1) \cdot (Rx_o - P_o)/4 \tag{4.62}$$

Again, $\Delta S > 0$ since $\beta < 1$. Hence, the second method gives the best improvement in stability of these three. The improvement of the stability of the second method is $(Rx_o - P_o)/4$.

The fourth method is to shift all the centers of the strokes to the downhill side. The improvement in stability is due to the reduction of the offset in the longitudinal direction. Figure 4.10 shows that the maximum shifted distance is $(Rx_o - P_o)/2$. If the longitudinal offset of the projection of the center of gravity is greater than this value, the improvement of the gait stability margin on the sloping surface is also $(Rx_o - P_o)/2$.

The fourth method has double the improvement of that of the second method. Hence, the fourth method is the most effective. In order to understand the extent of the improvement, the gradability of the fourth method is calculated as below.

Assume that the vehicle is walking along a maximum gradient line. The gait stability margin of a wave gait with $\beta = 11/12$ with $P = Rx = 60$ is 40.9 inches. After the centers of the strokes are shifted, the

AD-A159 147

AN EXPERIMENTAL STUDY OF AN ULTRA-MOBILE VEHICLE FOR
OFF-ROAD TRANSPORTAT. (U) OHIO STATE UNIV RESEARCH
FOUNDATION COLUMBUS R B MCGHEE ET AL. MAY 85

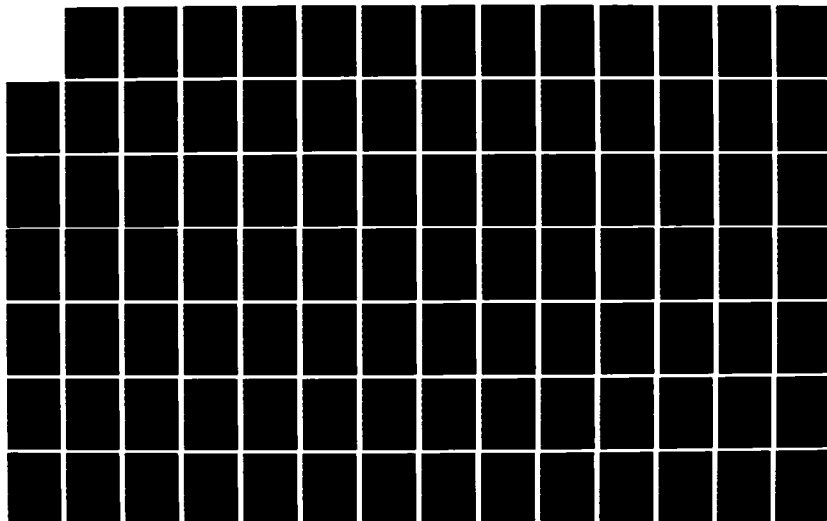
3/5

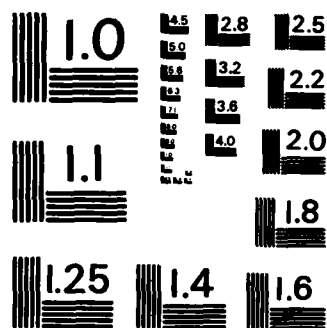
UNCLASSIFIED

MDA903-82-K-0058

F/G 13/6

NL





MICROCOPY RESOLUTION TEST CHART
NATIONAL BUREAU OF STANDARDS - 1963 - A

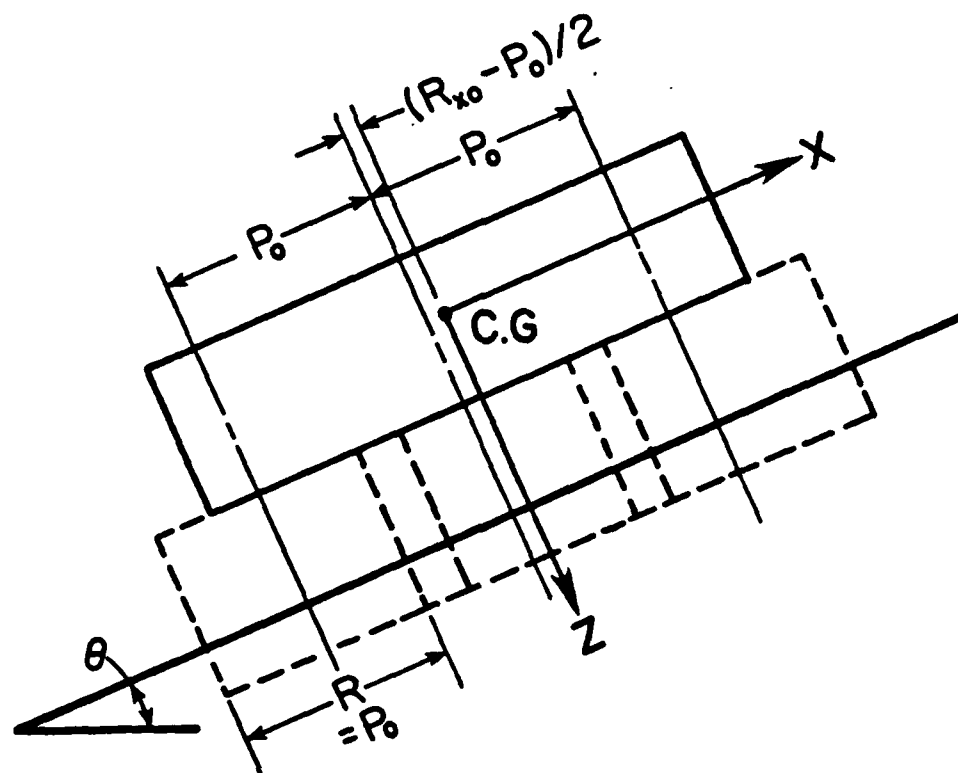


Figure 4.10: Walking on a slope by shifting the centers of strokes to the downhill side.

equivalent gait stability margin on the slope becomes 46.9 inches. Substituting this value into Equation (4.5), the gradability obtained by lowering the body height is $\theta_m = 62.9^\circ$. Substituting this value into Equation (4.19), the gradability obtained by leveling the body attitude is $\theta_m = 52.1^\circ$. Comparing these values to the results in Table 4.1, the improvement is about 2° . If the vehicle is walking along a zero gradient line, the strategy in this section has no effect on the gradability since the gradability is determined by the lateral stability margin.

4.3 Ditch Crossing

An idealized ditch was shown in Figure 4.1b. It is completely described by one parameter, d , which is the width of the ditch. The land on the two sides of the ditch is assumed to be on the same level. The bottom of the ditch and the vertical wall are considered as forbidden regions.

Generally speaking, there are two methods for a walking machine to cross a ditch. If the ditch width is relatively narrow, a walking machine can cross it with a periodic gait. An example of this method was shown in Figure 3.30. If a ditch is wider than can be handled using a periodic gait, a large obstacle gait (LOG) should be used. In the following, ditch crossing using periodic gaits is studied first. A general introduction of the obstacle crossing with a LOG is then given. Finally, ditch crossing with a LOG is studied.

4.3.1 Ditch Crossing with a Periodic Gait

The continuous FTL gaits and the dexterous wave gaits are the two periodic gaits which are suitable for ditch crossing. An example of a ditch crossing with a continuous FTL gait has been shown in Figure 3.30. In the example, the vehicle adjusts its footholds a few steps before the ditch so that one of the front legs would step on the edge of the ditch. The other front leg is then stretched to step on the far side of the ditch. Since the two front legs do not fall into the ditch, the rest of the legs will not fall into the ditch because they follow the steps of the two front legs.

The maximal width can be crossed by this method is $0.5\lambda + A_f$, where A_f is the front adjustability. For $\beta = 2/3$ and $P/R = 1.2$, $A_f = 0.25R$. Since $\lambda = R/\beta$, the maximal ditch width for this particular case is R , which is 60 inches or 5 feet for the ASV. If the ditch width is less than 0.5λ , the vehicle can cross it without extending its front leg. The value of 0.5λ for different duty factors are given in Table 4.2. It shows that the smaller the duty factor is, the wider the ditch which can be crossed.

Table 4.2

Maximal ditch width can be crossed by a periodic gait in normal walking mode.

duty factor β	ditch width 0.5λ
1/2	R
2/3	(3/4)R
3/4	(2/3)R
5/6	(3/5)R
11/12	(6/11)R

For a wave gait, if the middle legs are abducted a foot width during walking, the footprints would be like those in Figure 4.11. This is almost like the footprints of a continuous FTL gait except that each footprint is doubled. The longitudinal distance between footprints of each pair of legs is also 0.5λ . If the wave gait is modified into a dexterous wave gait to possess some adjustability in the legs, it can cross a ditch just like a continuous FTL gait. The vehicle adjusts its front legs so that one front leg would step

on the edge of the ditch. The other front leg is then stretched to cross over the ditch. The maximal ditch width which can be crossed is also $0.5\lambda + A_f$. However, the adjustability A_f is different from that of a continuous FTL gait.

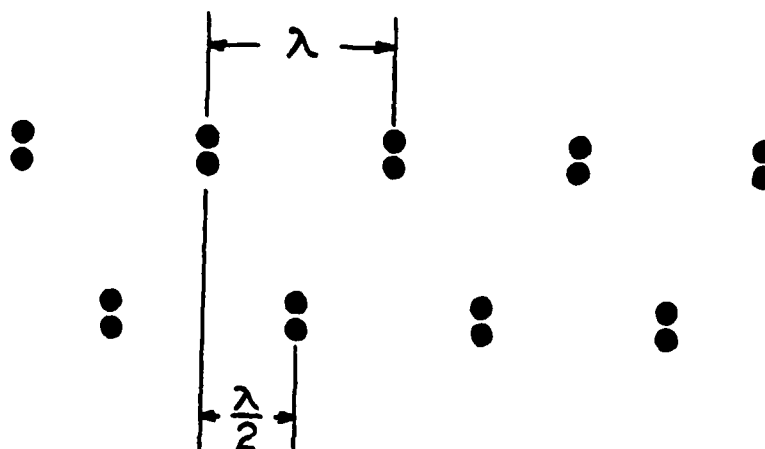


Figure 4.11: Footprints of dexterous wave gait.

Other dexterous periodic gaits may also be used for ditch crossing. However, the control algorithm is more complicated because all legs have different footprints. The maximal width which can be crossed will be less than that of the two gaits mentioned above.

4.3.2 Introduction to Large Obstacle Gait (LOG)

4.3.2.1 Programable Features of LOGs

The gait used by a walking machine to cross large obstacles is called a large obstacle gait (LOG). Usually, similar LOGs are suitable

for one type of obstacle. If LOGs used to cross different sized obstacles of the same type share the same motion characteristics, and these characteristics are simple and well defined, this LOG can be automatically generated by a computer program. Hence, an obstacle crossing may be performed according to a pre-implemented program which only receives limited information, such as ditch width, from the human operator or a vision system. One example of these motion characteristics observed in ditch crossing were presented in reference [52] and are summarized below.

Referring to Figure 4.12, the whole motion of a complete ditch crossing can be categorized into three motion cycles. In each motion cycle, the hexapod repeats the following four similar movements:

1. Movement of the body to bring the center of gravity forward of the middle feet.
2. Movement of the rear legs accompanied by further body movement.
3. Movement of the middle legs.
4. Movement of the front legs accompanied with body movement.

It was also noticed that the rear to front cycle is similar to the rear to front cycles found in optimally stable wave gaits. (The only difference is that the opposite legs are in phase rather than 180° out of phase in a wave gait.). Moreover, the most interesting feature is, similar motion cycles can be found in other kinds of obstacle crossing such as in a short vertical step crossing. These motion features, like other common features found in legged locomotion, may be implemented into a program. Based on the study of obstacle

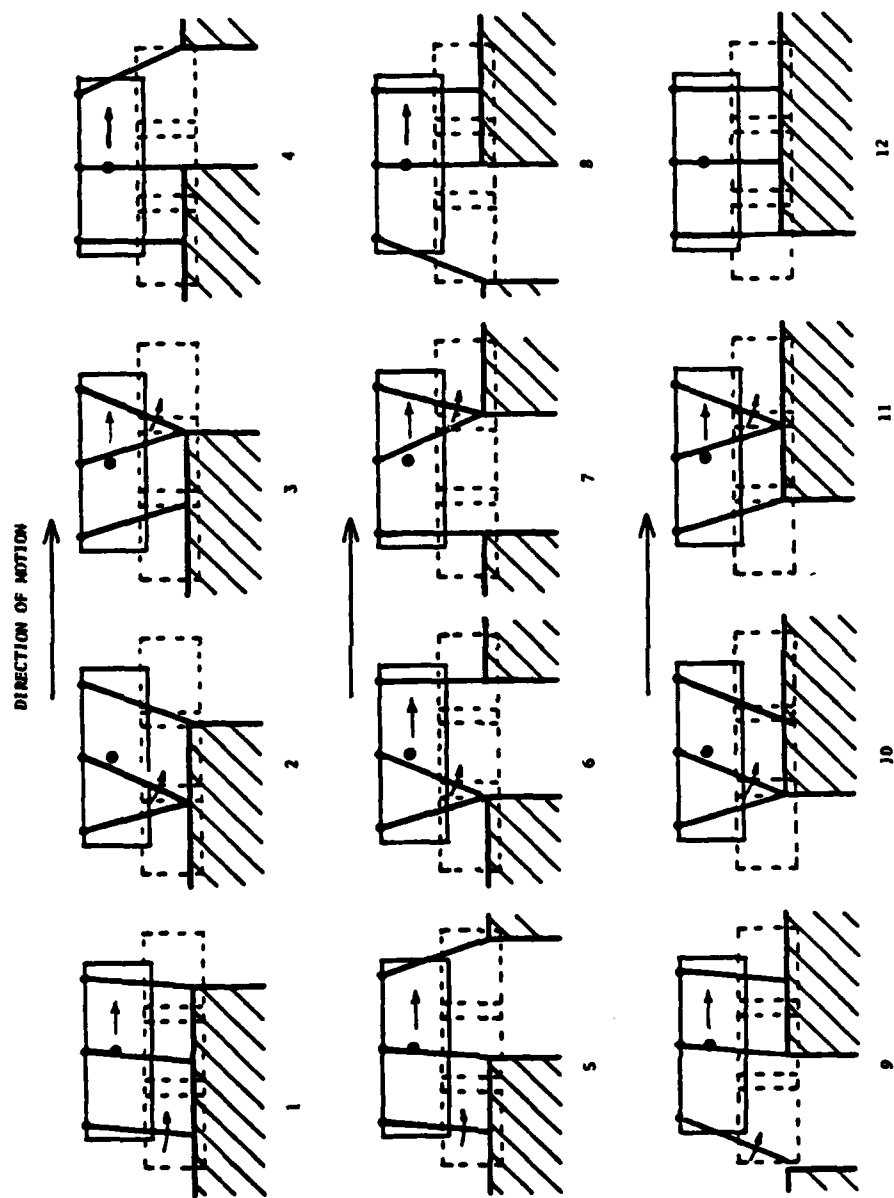


Figure 4.12: Lateral motion sequence of a complete ditch crossing.

crossing presented in [52,53,54] and in this chapter, accompanied with more further research, it is expected that many LOGs will be fully automated in the near future.

However, at the present time, due to the complexity of the terrain condition and the safety requirement, the human operator should have control of each foot placement as well as each body motion. A possible application of the common motion features is shown as follow: The human operator selects a pre-programmed LOG for the obstacle in front of the vehicle. Then he enters some necessary information. The program then suggests a motion to perform the selected LOG. The human operator then decides either to accept it or to adjust it according to the specific terrain condition before the execution.

4.3.2.2 General Approach to Formulize a LOG

A complete obstacle crossing is to move the vehicle entirely from the present plane to the destination plane. (Some obstacles, such as the isolated walls, have a middle plane between these two planes.). For the convenience of study, a complete obstacle crossing maneuver of a hexapod is divided into three successive phases. In each phase, one leg pair is transferred from the present plane to the destination plane. The first phase starts from the initial position on the present plane and ends at the placements of the two front legs on the destination plane. The second phase starts from the completion of the front-leg placements and ends at the placements of the two middle legs on the destination plane. The third phase starts from the completion of the middle-leg placements and ends at placements of the

two rear legs on the destination plane. This is demonstrated in the following example of ditch crossing:

Referring to Figure 4.12, the initial position is that in which all six legs are at their mid-positions with the front feet at the edge of the ditch. The first phase includes sequences 1 through 4. The second phase includes sequences 4 through 7. The third phase includes sequences 7 through 10. At sequence 10, the ditch crossing is considered to be completed. The rest of the movements, sequences 11 and 12, are to restore the legs to be at their mid-positions.

In general, the legs are moved by pairs in each phase. Each pair of legs are moved simultaneously in principle, although a human operator would, using the planned control modes, move them sequentially. This type of paired leg motion is not only simple for analysis, it is also very effective [53]. Paired leg movements are used by insects when crossing obstacles [54].

It is helpful to define the foot range and the corner distance for further study and discussion. The foot range is the maximal distance which a pair of legs can be extended with the help of the body motion while the other legs remain on the ground and maintain statical stability. This maximal distance is measured from the edge of the present plane. Hence, the foot range depends on the positions of the legs on the ground, which is called the foot conditions. The maximal foot range is obtained if the legs which are on the ground are optimally placed. In the following, foot range is used to indicate the maximal foot range for convenience.

The corner distance is the distance of the position of a leg relative to a corner of the obstacle. This corner can be the edge of either the present plane, the middle plane, or the destination plane. In the following discussion, corner distances are used to define the foot positions.

A general approach to definition of the maximal mobility over an obstacle is to find out the foot range of the transferring leg pair and the corresponding foot conditions in each stage. The maximal mobility is the minimal foot range of these three phases provided that the legs can be placed to satisfy the corresponding foot conditions. If there is any difficulty in fulfilling the foot conditions, the foot range should be modified according to the available foot positions. Then the maximal mobility becomes the modified foot range. This general approach will be demonstrated in many examples.

4.3.3 Ditch Crossing with a LOG

The general approach in the last section is applied to find the maximal ditch crossing ability. The three foot ranges with their corresponding foot conditions are defined first.

If the body of the hexapod is kept level, the three foot ranges are shown in Figure 4.13. Figure 4.13a shows the foot conditions of the front-foot range. The middle legs step on the edge of the ditch and the rear legs step a distance about P_0 behind the middle legs. Then the center of gravity is brought right behind the middle legs. The range is $P_0 + R_{x_0}/2$. The rear-foot range is also $R_0 + R_{x_0}/2$. This can be visualized by reversing the body motion in Figure 4.13a.

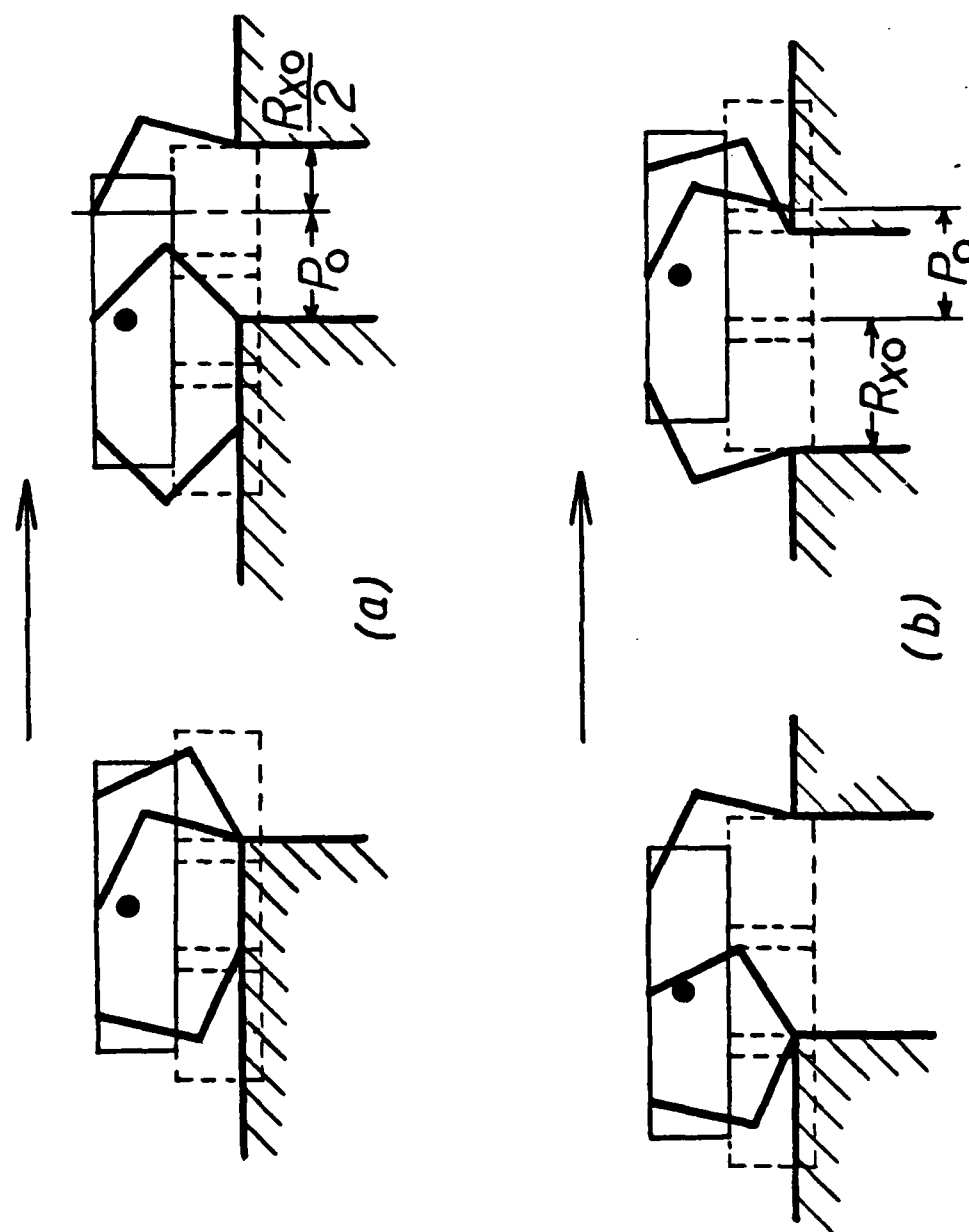


Figure 4.13: Ranges of a hexapod in ditch crossing, (a) front foot and rear foot (b) middle foot.

Figure 4.13b shows the foot conditions of the middle-foot range. The front legs and the rear legs step on the two sides of the ditch separately. The distance between them is $2P_0$. The range of the middle feet is $P_0 + Rx_0$.

Therefore, the maximal ditch which can be crossed by the hexapod is the minimum of these three foot ranges provided the foot conditions of the front-foot and the rear-foot ranges can be fulfilled. The following shows how the hexapod place its legs to satisfy foot conditions in three phases. In each phase, the legs are placed to satisfy the foot conditions first, then one leg pair is extended to place on the far side of the ditch with the help of the body movement.

In the first phase, the body is moved forward so that the center of gravity is brought over the middle legs, and the rear legs are lifted and placed alongside the middle feet. The middle legs are then lifted and placed alongside the front feet. This accomplishes the foot conditions of the front-foot range. The body is then moved forward and the front legs are extended and placed on the edge of the far side.

In the second phase, the body is moved forward again and the center of gravity is brought over the middle legs. The rear legs are then lifted and placed alongside the middle feet. This fulfills the foot conditions. The body is then moved forward and the middle legs are extended and placed on the far side of the ditch. In this phase, the front and rear legs do not have to be placed exactly according to the foot conditions because the middle-foot range is more than needed.

In the third phase, the front legs are lifted and placed at a distance P_0 in front of the middle legs. The body is then moved

forward and the center of gravity is brought ahead of the middle legs to satisfy the leg conditions. The rear legs are then lifted and placed alongside the middle feet with the help of body movement.

Since there is no difficulty fulfilling the foot conditions of the minimum range, $P_O + R_{x_O}/2$ is the maximum ditch width. For the ASV, the maximal ditch width is 96 inches or 8 feet.

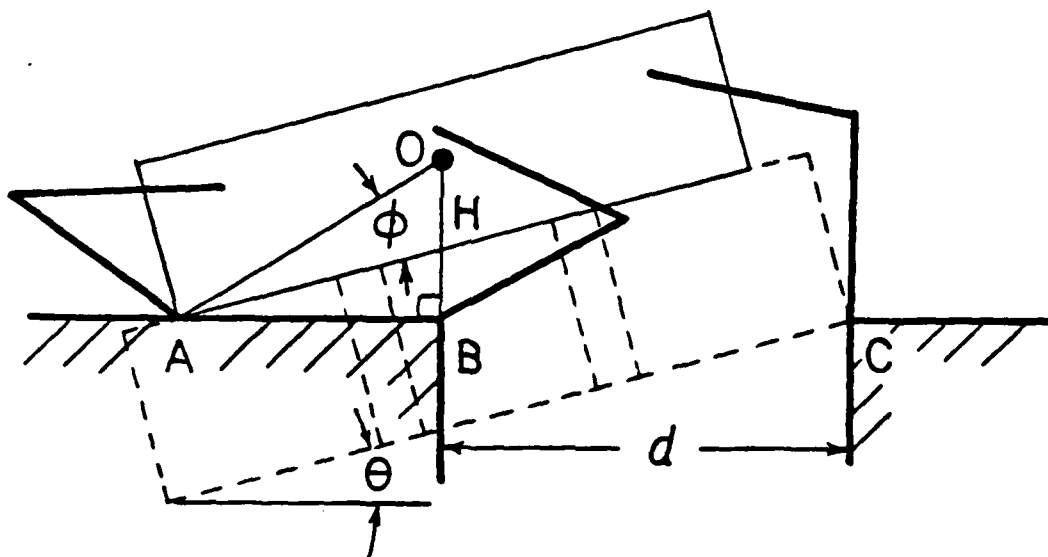


Figure 4.14: Ditch crossing by tilting the body attitude.

If the body is tilted so that the bottom corner of the body touches the ground (see Figure 4.14), both the front-foot range and

the rear-foot range become

$$BC = (P_o + Rx_o/2)/\cos \theta + [H_o - (P_o + Rx_o/2) \cdot \tan \theta] \cdot \sin \theta \quad (4.63)$$

where

$$\theta = \tan^{-1} [Rz_o / (L/2 + P_o + Rx_o/2)] \quad (4.64)$$

For the ASV, $\theta = 15.3^\circ$ and $BC = 111$ inches. Since the middle-foot range remains the same as $P_o + Rx_o = 132$ inches. The maximum ditch width which can be crossed by this method is 111 inches or 9.3 feet. Comparing this to the maximum ditch width above, the improvement is significant. The motion sequence for this method is similar to that in Figure 4.12.

4.3.4 Relationship to Walking Volume

From the above discussion, the ditch crossing ability can be increased by increasing both the front-foot and the rear-foot ranges. One effective way to do this is to increase the stroke pitch while keeping the stroke the same. Another way is to increase the strokes of the front legs and the rear legs in the front and rear directions respectively.

A small overstroke is required for the legs to be placed alongside the adjacent feet. But a large overstroke does not help in increasing the ditch crossing ability.

4.4 Vertical Step Crossing

A configuration of a vertical step was shown in Figure 4.1c. It is fully defined by one parameter V , which is the step height. The vertical step crossing is more complicated than a ditch crossing. According to the general approach, the foot ranges in the vertical direction, which is called the vertical ranges in the following, in which the three phases and their foot conditions are studied first. Then the motion between these foot conditions is studied. The case of stepping down is also studied. Finally, the relationship between vertical step crossing ability and the walking volume is discussed.

4.4.1 Vertical Ranges

Figures 4.15 and 4.16 show the two conditions of the front-foot vertical range. The body is tilted by an angle θ . The angle γ is the angle of a line which passes through point 0 and a bottom corner of the walking envelope of the middle leg relative to the body Z-axis. Hence,

$$\gamma = \tan^{-1} [(Rx_0/2)/H_0] \quad (4.65)$$

For the ASV, $\gamma = 26.5^\circ$.

Figure 4.15 shows the case of $\theta > \gamma$. The center of gravity falls behind the middle legs. The vertical range is V_1 . In order for V_1 to be maximized, the middle legs are fully extended and placed at a corner distance C_{m1} from the corner C. The subscript "m1" denotes the middle legs and the first phase. The rear legs can be placed anywhere behind the projection of the center of gravity, N. Hence, $C_{r1} = CN$.

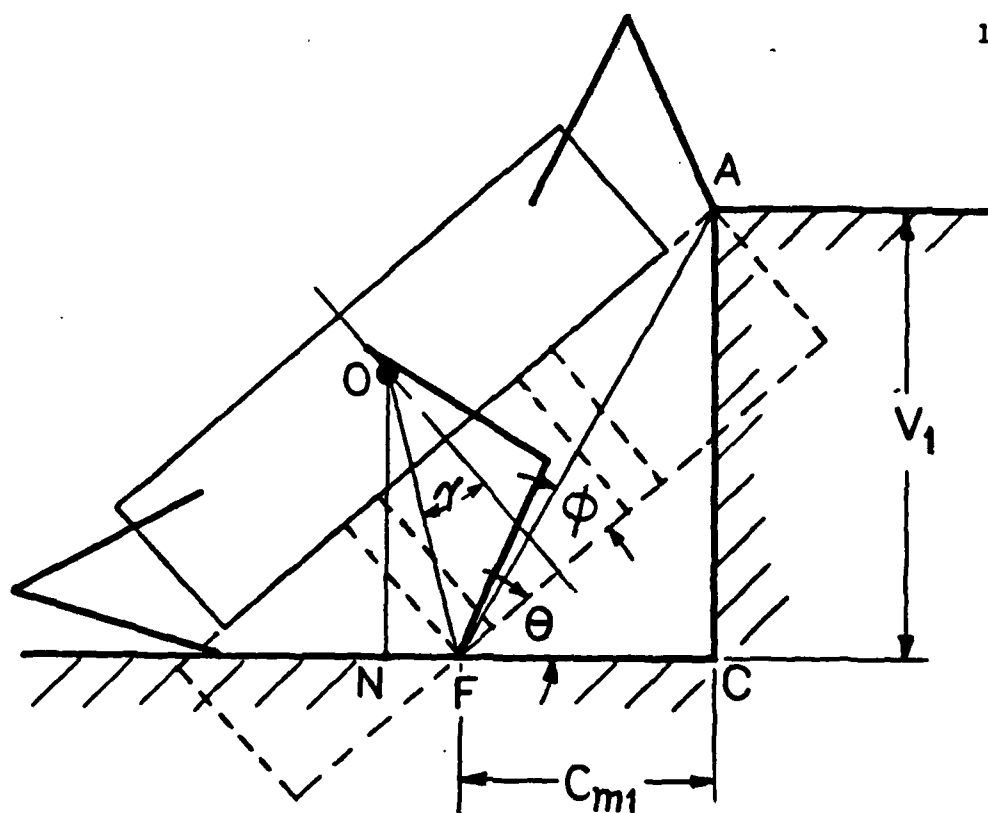


Figure 4.15: Front-foot vertical range, $\theta > \gamma$.

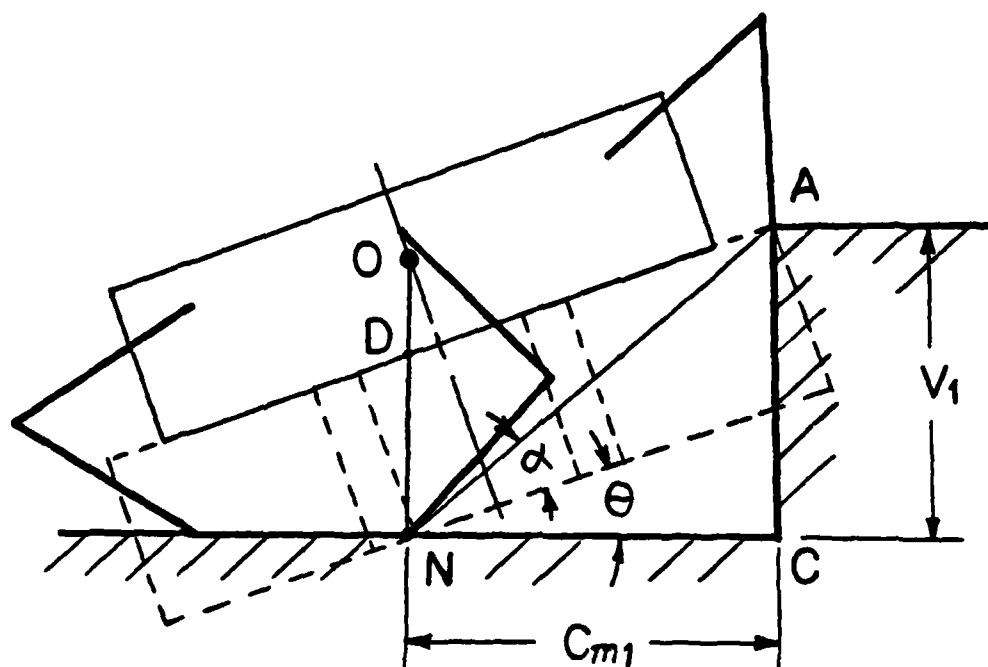


Figure 4.16: Front-foot vertical range, $\theta \leq \gamma$.

From trigonometry,

$$V_1 = AF \cdot \sin(\theta + \phi) \quad (4.66)$$

$$C_{m1} = AF \cdot \cos(\theta + \phi) \quad (4.67)$$

where

$$\phi = \tan^{-1} [Rz_o / (P_o + Rx_o)] \quad (4.68)$$

$$AF = Rz_o / \sin \phi \quad (4.69)$$

For the ASV, $\phi = 20^\circ$ and $AF = 140.4$.

$$CN = C_{m1} + OF \cdot \sin(\theta - \gamma) \quad (4.70)$$

Hence,

$$C_{r1} = C_{m1} + (H_o / \cos \gamma) \cdot \sin(\theta - \gamma) \quad (4.71)$$

The maximal body angle θ_m occurs when the bottom corner of the body touches the ground.

$$\theta_m = \tan^{-1} [2Rz_o / (L - Rx_o)] \quad (4.72)$$

For the ASV, $\theta_m = 47.5^\circ$.

Figure 4.16 shows the case of $\theta \leq \gamma$. The center of gravity is right behind the middle legs. The vertical range and the corner distances are

$$V_1 = AN \cdot \sin(\theta + \alpha) \quad (4.73)$$

$$C_{m1} = AN \cdot \cos(\theta + \alpha) \quad (4.74)$$

$$C_{r1} = AN \cdot \cos(\theta + \alpha) \quad (4.75)$$

where

$$\alpha = \tan^{-1} [Rz_o / (P_o + Rx_o/2 + H_o \cdot \tan \theta)] \quad (4.76)$$

$$AN = Rz_o / \sin \alpha \quad (4.77)$$

A set of V_1 and C_{m1} for different body angles is given in Table 4.3. From this table, increasing θ would increase V_1 and decrease C_{m1} . (In the range of $\theta \leq 15^\circ$, C_{m1} is increased when θ is increased. However, C_{m1} is very large in this range and does not constrain the leg placement.). For a given step V_1 , if the middle legs are placed outside C_{m1} , the front legs can never reach the upper corner. If the middle legs are placed within C_{m1} , the front legs can still reach the upper corner. However, the body angle will be greater than the θ corresponding to the given V_1 .

Figure 4.17 shows the conditions of the middle-foot vertical range. The front legs are placed at the upper corner A. The middle legs are moved up to be placed at A. The center of gravity is between the upper corner A and the rear legs. From trigonometry,

$$V_2 = AF \cdot \sin(\theta + \phi) \quad (4.78)$$

$$C_{r2} = AF \cdot \cos(\theta + \phi) \quad (4.79)$$

where ϕ and AF were defined as in Equations (4.68) and (4.69) respectively. Notice that these two equations are the same as Equations (4.66) and (4.67) respectively. In order to keep the rear

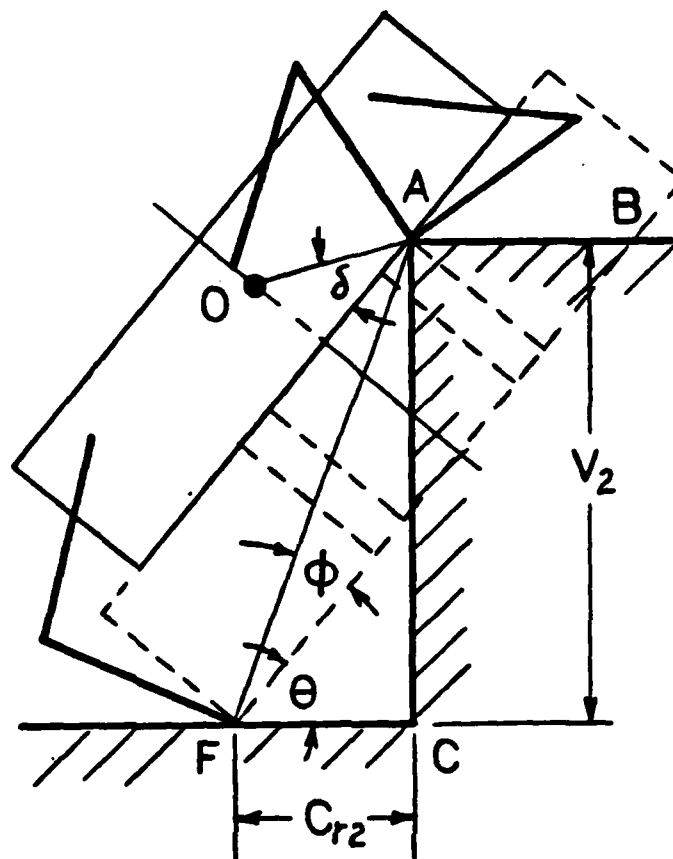


Figure 4.17: Middle-foot vertical range.

legs behind the center of gravity, the following relationship has to be kept.

$$C_{r2} > OA \cdot \cos(\theta - \delta) \quad (4.80)$$

where

$$\delta = \tan^{-1} [2(H_o - Rz_o)Rx_o] \quad (4.81)$$

$$OA = Rx_o / (2\cos \delta) \quad (4.82)$$

For the ASV, $\delta = 33.7^\circ$ and $OA = 43.3$. The maximal body angle θ_m

moving the body forward. Hence, the rear-foot vertical range is the distance V_3 when the center of gravity is above the upper corner and the rear legs are fully extended. Figure 4.18 shows the conditions of the rear-foot vertical range. From trigonometry,

$$V_3 = AF \cdot \sin(\theta + \alpha) \quad (4.83)$$

$$C_{r3} = AF \cdot \cos(\theta + \alpha) \quad (4.84)$$

where

$$\alpha = \tan^{-1} \{Rz_0 / [P_0 + Rx_0/2 - (H_0 - Rz_0) \cdot \tan \theta]\} \quad (4.85)$$

$$AF = Rz_0 / \sin \alpha \quad (4.86)$$

The maximal body angle θ_m occurs when $C_{r3} = 0$. For the ASV, $\theta_m = 53^\circ$. The front legs should be placed outside the corner distance c_{f3} in order to be kept within their walking envelopes.

$$C_{f3} = [(H_0 - Rz_0) \cdot \tan \theta + P_0 - Rx_0/2] / \cos \theta \quad (4.87)$$

Compare Figure 4.18 with Figures 4.17 and 4.15. For the same body angle θ , the vertical range of the third phase is less by a distance $DA \cdot \sin \theta$ where

$$DA = Rx_0/2 + (H_0 - Rz_0) \cdot \tan \theta \quad (4.88)$$

Hence, the rear-foot vertical range is the smallest of the three vertical ranges.

A set of V_3 , C_{r3} and C_{f3} for different θ is listed in Table 4.3. Unlike the front-foot and the middle-foot vertical range, when θ is

increased, the rear-foot vertical range reaches a maximum value of 85.5 at $\theta = 40^\circ$, then it decreases afterward. Since a smaller body angle is preferable, only the range of $\theta \leq 40^\circ$ should be used. Hence, the rear legs should not be placed within a corner distance 27.3 inches. For a given vertical step V_3 , if the rear legs are placed outside C_{r3} , the center of gravity can never pass the upper corner. If the rear legs are placed between C_{r3} and 27.3 inches from the corner, the center of gravity can pass the upper corner with a body angle which is greater than the θ corresponding to the given V_3 .

Table 4.3

Vertical ranges and corner distances of all three phases in vertical step crossing.

θ	V_1	C_{m1}	C_{r1}	V_2	C_{r2}	$OA \cdot \cos(\theta - \delta)$	V_3	C_{r3}	C_{f3}
0	48.0	96.0	96.0	48.0	131.9	36.0	48.0	96.0	24.0
10	66.1	98.7	98.7	70.2	121.6	39.6	63.2	82.0	28.7
15	76.2	98.9	98.9	80.5	115.0	41.0	69.5	74.1	31.5
20	86.9	98.4	98.4	90.2	107.6	42.0	74.9	65.6	34.8
25	98.3	97.1	97.1	99.3	99.3	42.8	79.3	56.6	38.8
26.5	101.8	96.6	96.6	101.8	96.6	43.0	80.4	53.8	40.2
30	107.6	90.2	95.2	107.6	90.2	43.2	82.6	47.1	43.7
35	115.0	80.5	92.4	115.0	80.5	43.3	84.7	37.3	49.8
40	121.6	70.2	89.0	121.6	70.2	43.0	85.5*	27.3	57.6
45	127.2	59.3	84.9	127.2	59.3	42.5	84.8	17.0	67.9
47.5	129.7*	53.7	82.6	129.7	53.7	42.0	83.9	11.8	74.3
50	---	---	---	131.9	48.0	41.6	82.5	6.6	81.8
53	---	---	---	134.3*	41.0	40.9	80.1	0.3	92.8

"*" = maximum V

From Table 4.3, the maximal vertical step which can be crossed by the ASV is determined by V_3 . If there is no difficulty in fulfilling the foot conditions, the maximal vertical step which can be crossed by the ASV is 85.5 inches or 7.1 feet.

4.2.2 Leg and Body Motion

The leg and body motion in a complete vertical step climb is studied in an example. A body angle $\theta = 30^\circ$ is chosen to climb up a vertical step. According to Table 4.3, the three vertical ranges at $\theta = 30^\circ$ are $V_1 = V_2 = 107.6$ inches and $V_3 = 82.6$ inches. Hence, the maximal vertical step which can be crossed is 82.6 inches.

Figure 4.19 shows a lateral motion sequence of a hexapod climbing up a 86.2 inch step with 30° body angle. The first phase includes sequences 1 through 4. The second phase includes sequences 4 through 7. The third phase includes sequences 7 through 12. After sequence 12, the rear legs can be lifted and placed on the upper corner by leveling the body and moving the body forward. The vertical step climbing is considered to be completed at this stage. The rest of motion is to replace the legs at ready positions for the next movement.

During the motion at these three phases, legs are moved in pairs. Each pair of legs are moved simultaneously as long as such a movement would not cause static instability. If a paired movement would result in instability, alternating short steps may be used.

In this example, corner distances at $\theta = 30^\circ$ are used for the placement of the feet. According to Table 4.3, the minimal body angles corresponding to the step height at phases 1 and 2 are about 20° and 18° respectively. C_{m1} and C_{r2} of the step height are longer than the C_{m1} and C_{r2} of $\theta = 30^\circ$. Hence, if the legs are placed at C_{m1} and C_{r2} of $\theta = 30^\circ$, they are automatically within the C_{m1} and C_{r2} of the step height. C_{r1} is usually trivial because the available foot positions

of the rear legs are usually outside the range of C_{r1} at the first phase.

Sequence 1 shows the initial position of the hexapod. The initial position is that all the legs are in their mid-positions and the center of gravity is slightly ahead of the middle legs, and there is some clearance between the front end of the vehicle and the wall to avoid any interference between the two when the vehicle is tilted. The rear legs are lifted and placed outside the corner distance C_{r1} . A place with 152 inches corner distance is chosen for the placement.

Sequence 2 shows that the middle legs are lifted and placed at a corner distance of $C_{m1} = 90.2$ inches. Then the body is tilted to a 30° body angle. The body is moved back-upward so that the bottom corner of the body would not touch the ground.

Sequence 3 shows that the body is moved forward along a 30° direction. The front legs are lifted and placed at the upper corner of the step.

In sequence 4, the front legs are placed at the upper corner. Notice that the front legs are not fully lifted and the body has not reached its motion limit yet. This is because the step height is less than V_1 of $\theta = 30^\circ$. This completes the first phase. Now the legs should be re-placed to satisfy the foot conditions for the second phase. Since there is little stroke left in the middle legs and the rear legs, the body is moved forward to bring the center of gravity ahead of the middle legs.

Figure 4.20 shows a criterion to check whether this is feasible or not. If $L_2 > L_1$, the center of gravity can be brought ahead of the

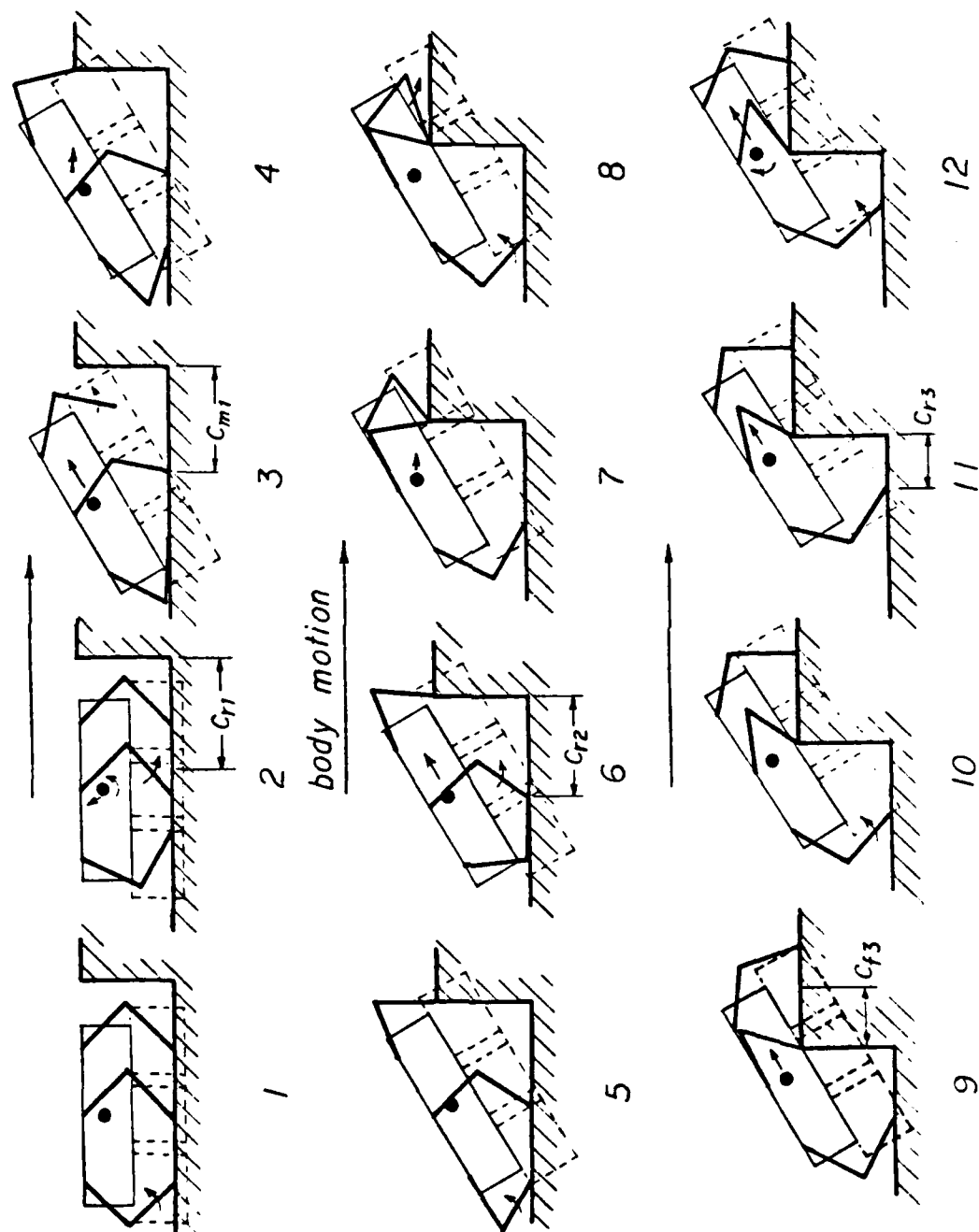


Figure 4.19: Lateral motion sequence of a stepping up.

middle legs by adjusting the body height, which is $H/\cos \theta$. If $L_2 < L_1$, the body angle has to be reduced until $L_2 > L_1$. If the vehicle can not bring the center of gravity ahead of the middle legs, a tetrapod walking mode, which will be discussed shortly, should be used to move the rear legs to a corner distance of C_{r2} .

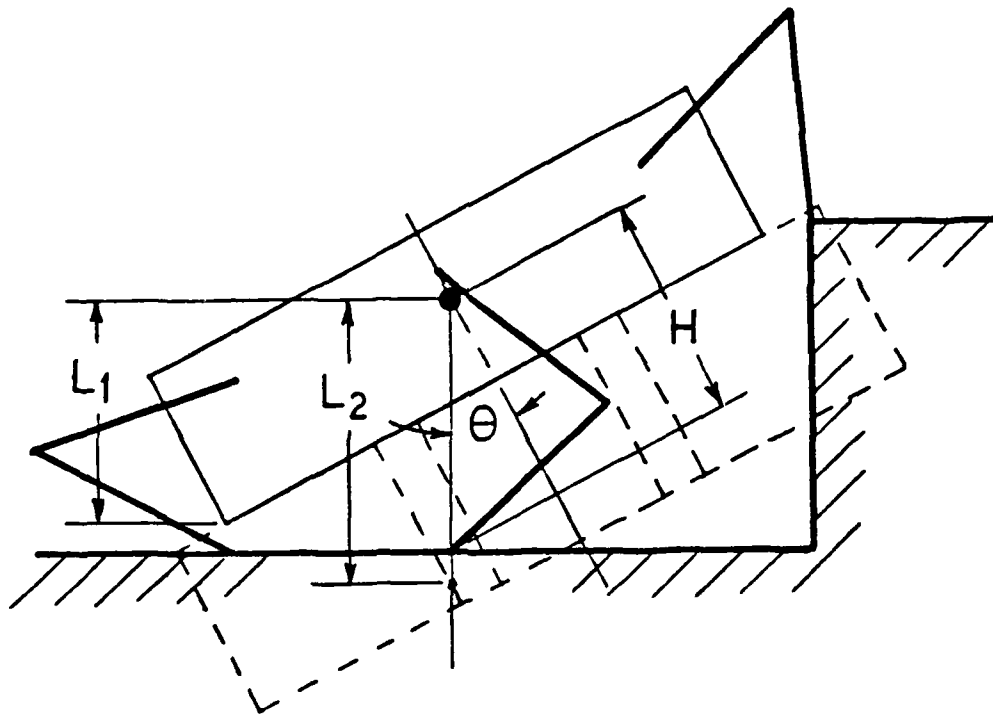


Figure 4.20: A criterion of tetrapod walking mode at the second phase.

Sequence 5 shows that the center of gravity is slightly ahead of the middle legs and the rear legs are lifted and placed alongside with

the middle feet since $C_{r2} = C_{m1}$.

Sequence 6 shows that the body is moved upward along a 30° direction and the middle legs are lifted and placed alongside the front feet at the upper corner of the step.

Sequence 7 shows the completion of the second phase. The body is then moved forward to prepare to meet the foot conditions for the third phase.

In sequence 8, the two rear legs can not be moved at the same time because of stability. A tetrapod walking mode is used to place the rear legs at the corner distance C_{r3} . In a tetrapod walking mode, one leg is moved at a time through a limited distance to maintain stability. The body may be simultaneously moved to bring the center of mass forward if other legs are not at the limits of their stroke. Hence, the rear legs can not be placed at the corner distance C_{r3} directly. The rear legs are lifted and placed as forward as possible without causing instability. The front legs are lifted and placed at a place outside the corner distance C_{f3} .

A detailed description of the tetrapod walking mode from sequence 7 through sequence 12 is given in Figure 4.21. This tetrapod walking mode can be avoided only when the middle legs can be placed within a corner distance of $C_{r3} + (Rx_0 - P_0)/\cos \theta$ while the center of gravity is ahead of C_{r3} . At this time, the rear leg can be placed directly at C_{r3} . This may happen when θ is small and C_{r3} is relatively large.

Sequence 9 shows that the body is moved forward along a 30° direction until the rear legs reach their limits.

Sequence 10 shows that the rear legs are lifted and placed at the corner distance C_{r3} alternately in a tetrapod walking mode.

Sequence 11 shows that the rear legs are at the ready positions for the rear-leg placement. The body is moved upward along a 30° direction until the center of gravity passes the upper corner.

Sequence 12 shows that the center of gravity has already passed the upper corner. The body is leveled and moved forward, and the rear legs are lifted and placed on the upper corner. This completes the third phase and also the vertical step climb.

4.4.2.1 Tetrapod Walking Mode

When a hexapod has only four legs which are effective in maintaining stability, (the other two legs are either in the air or in positions which do not affect stability), the hexapod can still be moved by these four legs. The method for such a movement is called the tetrapod walking mode by Wang [51]. Successive support patterns of the tetrapod walking mode used in sequence 7 through 12 in Figure 4.19 are shown in Figure 4.21. The same labels are used to indicate the corresponding motion sequence.

In pattern 7, the middle legs are placed alongside and outside the front feet. The body is moved forward. The dashed lines indicate the support pattern.

In pattern 8a, the left rear leg is lifted and placed as forward as possible. The dashed-dotted line is the rear boundary after the rear leg is lifted. The placement should ensure stability while the right rear leg is lifted in pattern 8b.

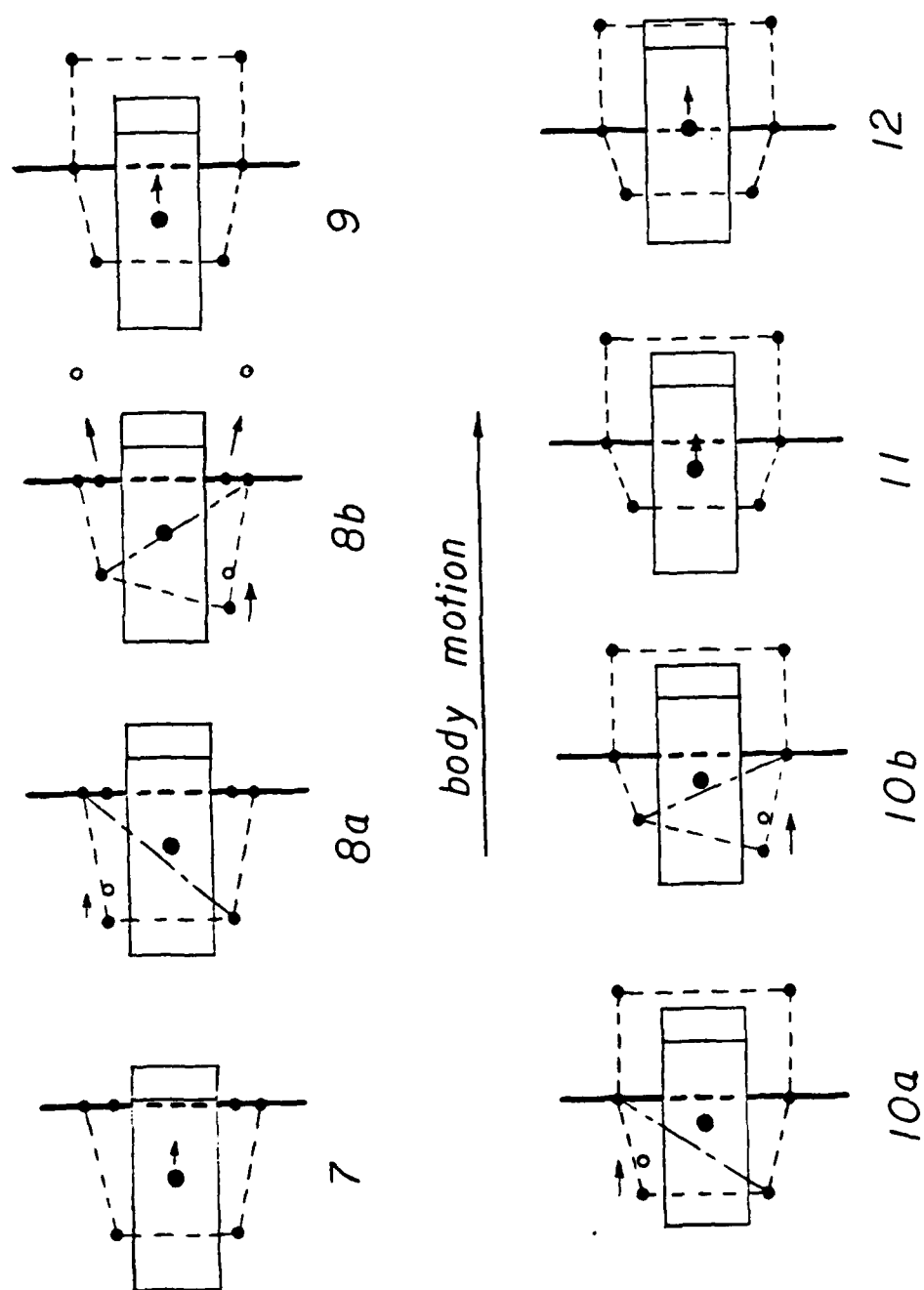


Figure 4.21: Tetrapod walking mode.

In pattern 8b, the right rear leg is lifted and placed at the same corner distance as the left rear leg. Patterns 8a and 8b are considered one step of tetrapod walking mode.

In pattern 9, the body is moved forward as much as possible so that the rear legs can be moved further.

In pattern 10a, the left rear leg is lifted and placed at the corner distance c_{r3} . In pattern 10b, the right rear leg is lifted and placed at the same corner distance.

In pattern 11, the body is moved forward to bring the center of gravity ahead of the upper corner of the step.

In pattern 12, the foot conditions for the rear-leg placement are fulfilled and the body is moved forward and leveled to complete the third phase.

Hence, it takes two tetrapod steps to move the rear legs to a corner distance of C_{r3} . The number of steps depends on the positions of the rear legs and of the center of gravity. The farther these positions are from the corner, the more steps are needed.

4.4.2.2 Tetrapod Walking Mode With Lateral Body Motion

Sometimes, the body is moved in a lateral direction in order to increase the step length in a tetrapod walking mode. Figure 4.22 shows that the same motion as that in Figure 4.21 can be completed in one tetrapod step with the help of lateral body motion. Both the lateral motion sequence and the successive support patterns are shown. Sequences 1 through 6 in Figure 4.22 can replace sequences 7 through 12 in Figure 4.20.

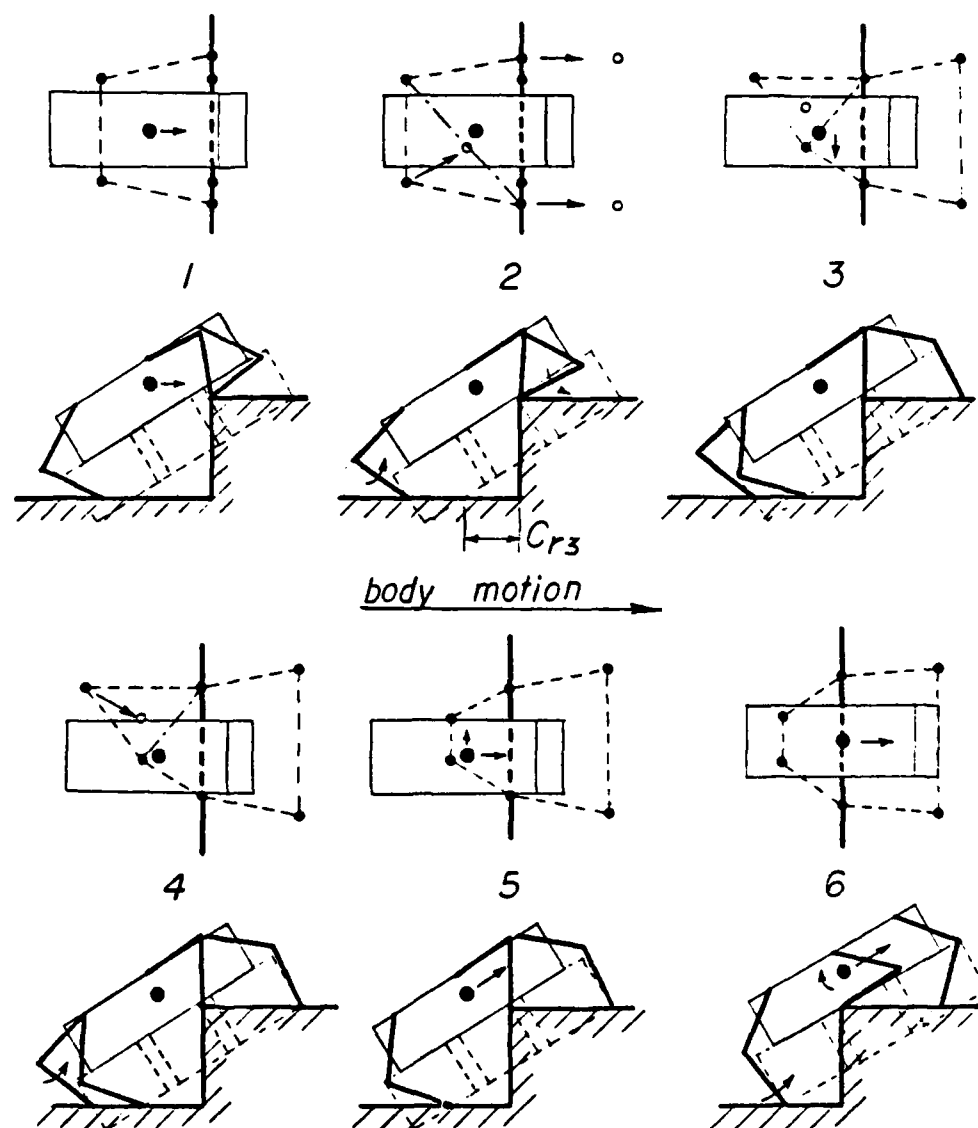


Figure 4.22: Tetrapod walking mode with lateral body motion.

Sequence 1 shows that the middle legs are placed alongside and inside the front legs at the upper corner of the step. The body is moved forward until it is against the upper corner.

Sequence 2 shows that the right rear leg is lifted and adducted, then is placed at the corner distance C_{r3} . The two front legs are lifted and placed outside the corner distance C_{f3} . Notice that the middle legs are not abducted or adducted so that a maximal lateral body motion can be performed.

Sequence 3 shows that the body is moved to the left to increase the stability margin after the left rear leg is lifted.

Sequence 4 shows that left rear leg is lifted and placed adducted, it is then placed at the corner distance C_{r3} .

Sequence 5 shows that the body is moved to the left, it is then moved forward to bring the center of gravity over the upper corner.

Sequence 6 shows that the body is leveled and moved forward so that the rear legs can be placed at the upper corner. This completes the vertical step climb in one tetrapod step.

When the body angle is large and a better stability margin is required, a combination of these two types of tetrapod walking mode should be used.

4.4.3 Stepping Down

A stepping down maneuver can be obtained by reversing the motion of a stepping up. For example, for a 86.2 inch vertical step, the motion of a hexapod to step down with a 30° body angle can be visualized by reading Figure 4.19 with a reversed body motion and

sequence. Hence, all the corner distances of stepping up are also available for stepping down. In both cases, most of the major constraints of corner distances are in the lower plane. In the following, a prime denotes the corner distances for stepping down.

Due to gravity, stepping down is easier than stepping up. Also, a larger step can be negotiated. This will be shown in a later example. Figure 4.23 shows a lateral motion sequence for a hexapod climbing down a 86.2 inch vertical step with varying body angle.

Sequence 1 shows the initial position of the hexapod with all the legs in their mid-positions and the front feet at the edge of the step. The rear legs are lifted and placed within a corner distance C'_{r1} . From Figure 4.18, C'_{r1} is the distance AB. If the bottom corner of the walking envelope is above the upper plane,

$$C'_{r1} = R z_o / \sin \theta \quad (4.89)$$

If the bottom corner is below the upper plane,

$$C'_{r1} = [(H_o - R z_o) \cdot \tan \theta + P_o + R x_o / 2] / \cos \theta \quad (4.90)$$

Also, the rear legs should not be placed within the corner distance C_{f3} .

Sequence 2 shows that the middle legs are lifted and placed at the edge with the help of the body movement.

Sequence 3 shows that the front legs are lifted and extended to the front lower extremes, then the body is rotated until it reaches 30° body angle. The body is then lowered until the bottom touches the edge. The body is moved along a 30° direction until the front

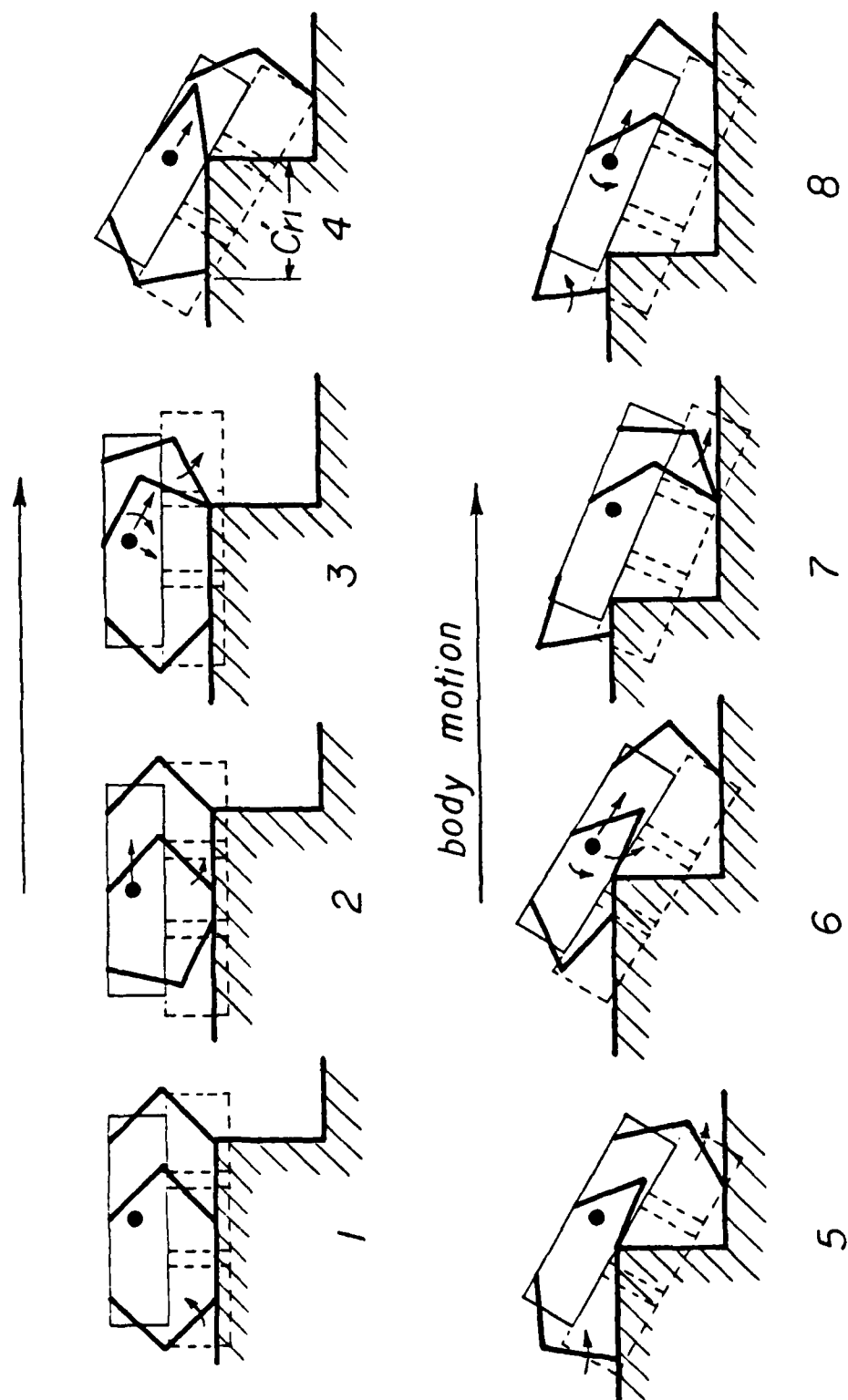


Figure 4.23: Lateral motion sequence of stepping down with varying body angle.

legs touch the lower plane. The corner distance of the front legs should be C_{r3} . This completes the first phase.

Sequence 4 shows the body moved further down along a 30° direction. The purpose of this movement is so that the two front legs may have available foot positions ahead of the feet so that a tetrapod walking maneuver can be performed later. The center of gravity can not be too close to the front legs since tetrapod walking would not then be possible.

Sequence 5 shows the rear legs lifted and placed close to the upper corner. The two front legs are moved alternatively in a tetrapod walking mode.

Sequence 6 shows the front legs placed within and close to C_{r2} . The body is moved down and rotated until the bottom corner of the walking envelope of the middle legs touches the lower plane. This touch point should be ahead of the center of gravity. The middle legs are lifted during the body movement.

Sequence 7 shows that the middle legs are placed alongside the front feet. Notice that the body angle is less than 30° . This completes the second phase. The front legs are lifted and placed at their front extremes.

Sequence 8 shows the center of gravity moved ahead of the middle legs. The rear legs are then lifted. The body is moved forward and leveled gradually until the rear legs touch the ground. The reason that the middle legs should be close to C_{r2} at sequence 7 is that interference between the rear part of the body and the wall can then be avoided.

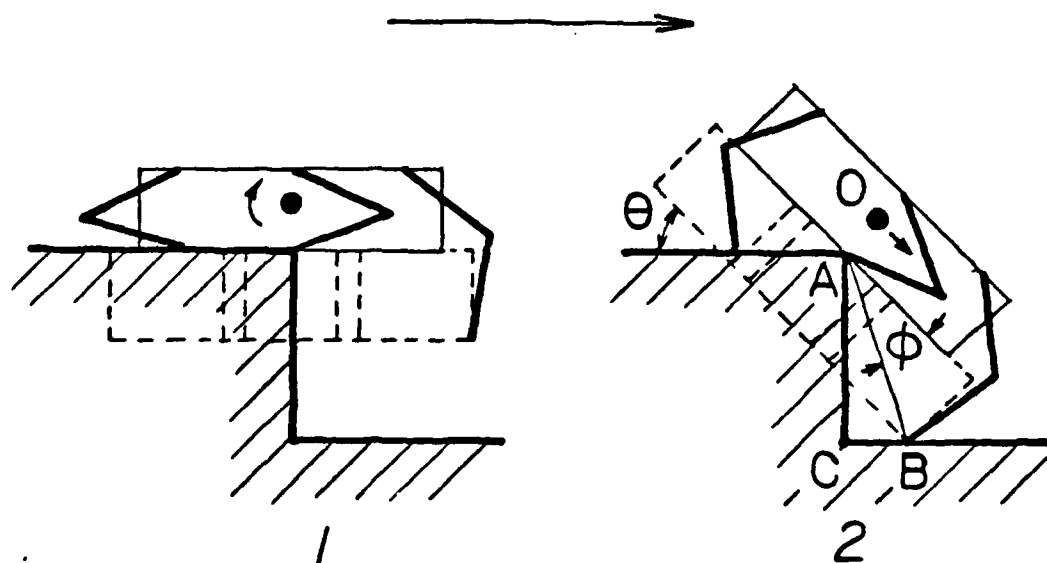


Figure 4.24: To step down a large step.

4.4.3.1 Stepping Down by Gravity

If the step is higher than the rear-foot range, the hexapod can not climb up it. But it can climb down it. Figure 4.24 shows a method of climbing down a step which is higher than the rear-foot range.

Sequence 1 shows the hexapod lowered to its limit and the center of gravity moved to the edge of the step. The front legs are fully extended to their front limits.

Sequence 2 shows that the body is rotated about the middle legs and the center of gravity is brought over the upper corner. The vehicle is then rotated down by gravity about the middle legs until

the front legs fall onto the lower plane. The vehicle can then move its front legs in the tetrapod walking mode. The step height is

$$V = AB \cdot \cos(\pi/2 - \phi - \theta) \quad (4.91)$$

where

$$\phi = \tan^{-1} [Rz_o / (P_o + Rx_o/2)] \quad (4.29)$$

and

$$AB = Rz_o / \sin \phi \quad (4.93)$$

In order to perform a tetrapod walking maneuver easily, the projection of the center of gravity should be on the middle point of CB. The body angle at this condition is

$$AB \cdot \sin(\pi/2 - \phi - \theta) = 2(H_o - Rz_o) \cdot \sin \theta \quad (4.94)$$

for the ASV, $\theta = 45^\circ$. The maximal step height which can be handled by this method is 101.7 inches or 8.5 feet.

The rest of the motion is similar to that of sequences 5 through 8 in Figure 4.23.

4.4.4 Relationship to Walking Volume

Several features are observed in the above examples of stepping up, stepping down and the tetrapod walking maneuver.

1. For stepping up, the rear-foot range is the minimum among all three vertical ranges. It determines the maximal crossing ability.

2. For stepping up, the third phase is the most difficult. This difficulty is due to the small value of C_{r3} . The rear legs are usually placed within C_{r3} in a tetrapod walking mode.
3. For stepping up, a tetrapod walking maneuver may be used to bring the center of gravity over the middle legs at the second phase if condition $L_2 > L_1$ can not be fulfilled by reducing the body height and the body angle.
4. A constant body angle in all three phases is not necessary. For stepping up, the body angle at phases 1 and 2 can be less than that at the third phase.
5. By reversing the body motion and sequence, the principles and corner distances of stepping up can be applied to stepping down.
6. When stepping down it is possible to cross a higher step than stepping up with the help of gravity. That is, by deliberately using a statically unstable maneuver.
7. The placements of the legs on the lower plane at each phase should be as close to the corner as possible. A closer placement would ease the placements which follow it.
8. Abduction and adduction are helpful in increasing stability. They are especially helpful in the tetrapod walking maneuver.

According to these features a vertical step crossing may be improved by modifying the walking volumes of the legs.

Longitudinal and vertical strokes: For stepping up, since the rear-foot range determines the maximal step height, an additional stroke of the rear legs in both the backward and downward directions would increase V_3 and C_{r3} . The following table shows the effectiveness of the additional stroke in both directions.

From the table, the additional stroke in the backward direction is more effective in C_{r3} while the additional stroke in the downward

direction is more effective in V_3 . An additional stroke in both directions is given in the last column. As it is shown, a longer rear leg improves the stepping up capability significantly. The rear legs should also be stronger because they provide most of the propulsion force to push the body up. This characteristic is also found in living creatures. Many six-legged insects, such as ants, have stronger and longer rear legs.

For stepping down, a similar improvement can be obtained by increasing the strokes of the front legs. However, the same improvement can be achieved with the help of gravity using a statically unstable maneuver. A longer front leg is not as crucial as a longer rear leg.

Table 4.4

Rear-foot vertical range of a hexapod with
Additional strokes of rear legs.

(unit: inch)

θ	no change		$\Delta R_{x_o} = 12$		$\Delta R_{x_o} = 24$	
	V_3	C_{r3}	V_3	C_{r3}	V_3	C_{r3}
0	48.0	96.0	48.0	108.0	48.0	120.0
10	63.2	82.0	65.3	93.8	67.4	105.6
20	74.9	65.6	79.0	76.7	83.2	88.1
30	82.6	47.1	88.6	57.5	94.6	67.9
40	85.5*	27.3	93.2*	36.4	100.9	45.6
47.5	83.9	11.8	92.7	19.9	101.6*	27.3
θ	no change		$\Delta R_{z_o} = 12$		$\Delta R_{z_o} = 12$	
	V_3	C_{r3}	V_3	C_{r3}	V_3	C_{r3}
0	48.0	96.0	60.0	96.0	60.0	108.0
10	63.2	82.0	75.0	80.0	77.1	91.7
20	74.9	65.6	86.2	61.5	90.3	72.7
30	82.6	47.1	93.0	41.1	99.0	51.5
40	85.5*	27.3	94.7*	19.5	102.0*	28.7
47.5	83.9	11.8	92.0	2.9	100.8	11.0

"*" = maximum value of V_3

Abduction and adduction: In a tetrapod walking maneuver, abduction of the legs on the upper corner increases stability. If a lateral body motion is used to increase stability, equal and large abductions and adductions on opposite sides of the body are desirable. For the ASV, R_y is smaller at the top of the walking volume. Hence, a longer R_y on the top in both abduction and adduction would improve the stability in a tetrapod walking maneuver.

4.5 Isolated Wall Crossing

A general configuration of an isolated wall is shown in Figure 4.1d. An isolated wall is defined by two parameters: the thickness U and the vertical height V . In general, an isolated wall crossing, or a wall crossing in brief, is a combination of a step up and a step down. If the thickness is wide enough for two pairs of legs to stand on the top simultaneously, the wall crossing is exactly the same as stepping up followed by stepping down. If the thickness is smaller, a special method is needed for the crossing.

4.5.1 General Approach

Figure 4.25 shows the general method of a wall crossing. The motion before sequence 1 is the same as when stepping up. The motion after sequence 5 is the same as when stepping down. This figure only describes the motion between these two stages.

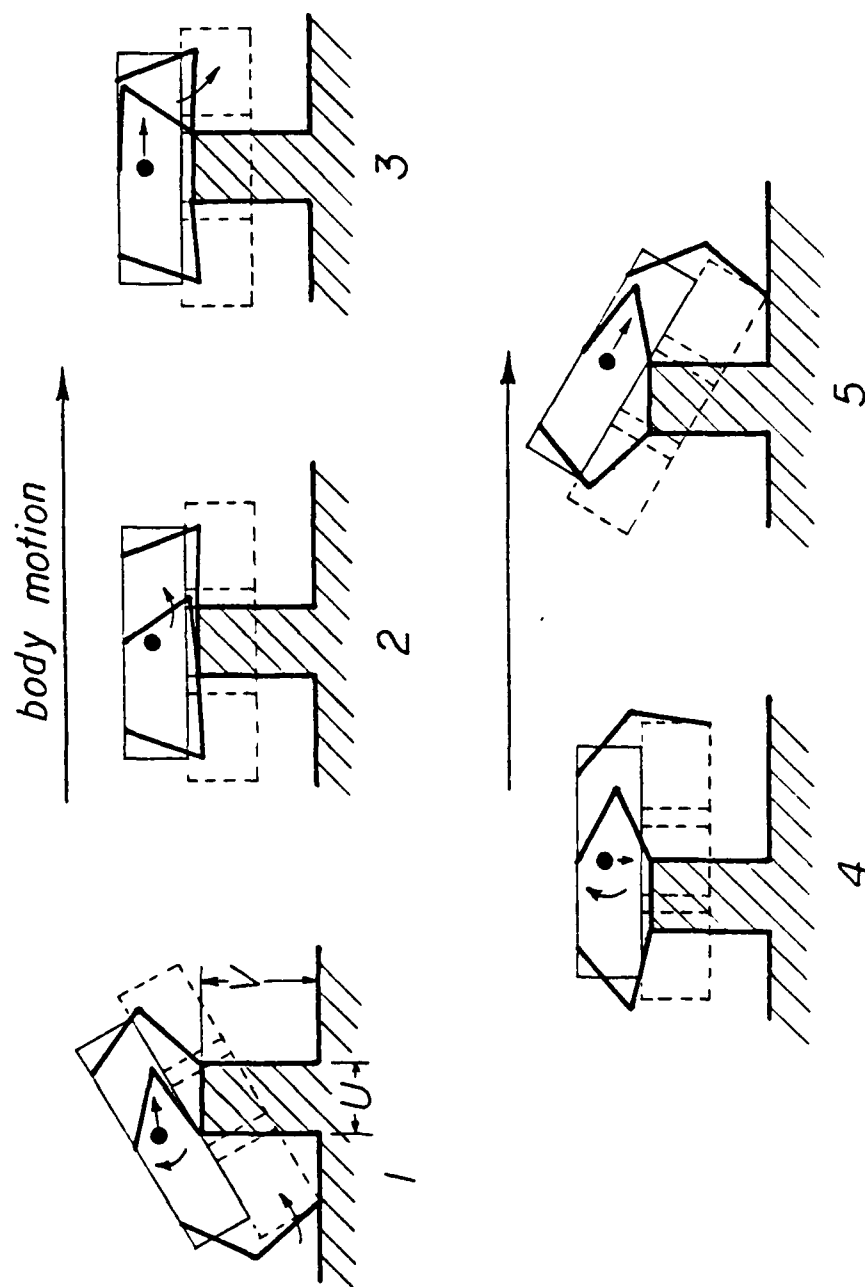


Figure 4.25: A wall crossing.

Sequence 1 is the foot conditions of the rear-leg placement at the third phase of stepping up. In order for the front legs to be placed on the top, the minimum thickness U_1 is

$$U_1 = C_{f3} \quad (4.95)$$

The body is moved forward and is leveled about the middle legs. The rear legs are lifted and placed alongside the middle feet at the near side corner.

Sequence 2 shows that the middle legs are lifted and placed alongside the front feet at the far side corner. Since both the front legs and the rear legs stand on the top simultaneously, the minimum thickness of the isolated wall is

$$U_2 = 2P_0 - Rx_0 \quad (4.96)$$

Sequence 3 shows that the center of gravity is moved to be right behind the far side corner. The front legs are lifted and fully extended to their front limits.

Sequence 4 shows that the body is rotated about the center of gravity to reach the same body angle of the stepping up. Then the body is lowered until the bottom touches the far side corner. The front legs should touch the ground at this time because of symmetric walking envelopes.

Sequence 5 is the front-leg placement at the first phase of stepping down. The body is moved down along the direction of the body angle. Aince the walking envelopes are symmetric, the minimum thickness for both the rear legs and the middles legs to step on the

top simultaneously is

$$U_3 = C_{f3} \quad (4.97)$$

The minimum thickness U_{\min} is the maximum of U_1 , U_2 and U_3 . According to Table 4.3, U_{\min} is equal to U_2 for $\theta \leq 30^\circ$, and it is equal to C_{f3} for $\theta \geq 35^\circ$. For the ASV, U_2 is 48 inches or 4 feet. The maximal obstacle height which can be crossed is equal to the rear-foot range. For the ASV, the maximal height is 85.5 inches or 7.1 feet

4.5.2 Narrow Wall Crossing

If U is less than U_{\min} , the general method can not be applied. A special method with the help of ground contact with the belly of the body is shown in Figure 4.26. Again, this figure only shows the motion between stepping up and stepping down.

Sequence 1 shows the rear legs placed to fulfill the foot conditions of the rear-leg placement. The two middle legs step on the two corners of the top respectively. The dashed leg is the middle leg on the far side of the body. The belly of the body is against the near side corner. The body is leveled gradually about the near side corner by lifting the middle leg on the far side.

Sequence 2 shows the body is fully leveled. The weight of the vehicle is mainly supported by the belly of the body. The body is rotated about the far side corner by extending the middle leg on the near side. The front legs should touch ground when the center of gravity is right above the far side corner.

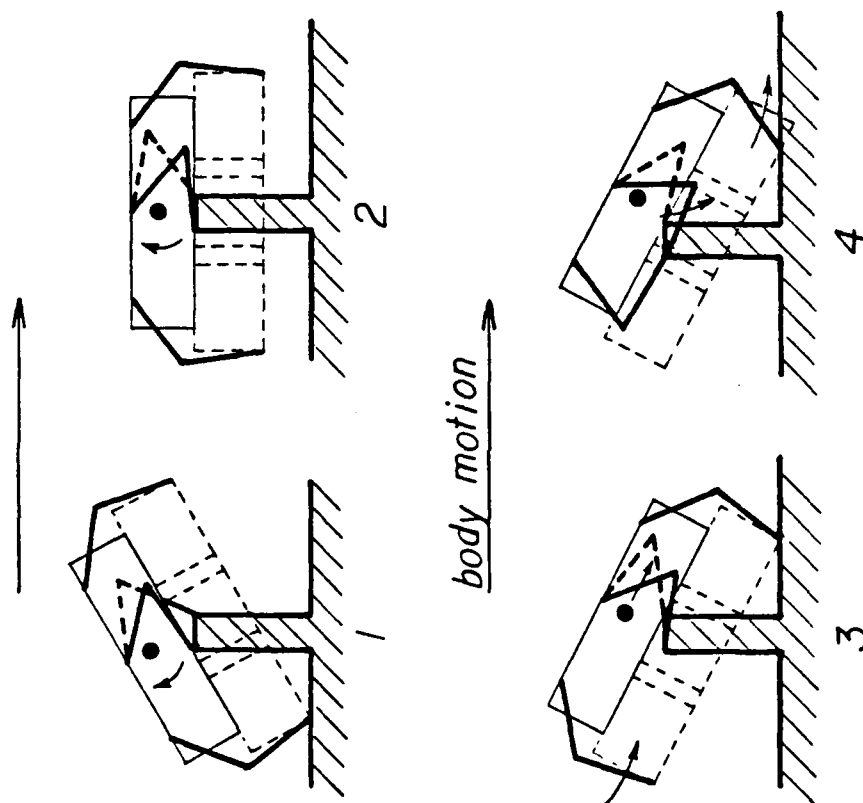


Figure 4.26: A narrow wall crossing.

Sequence 3 shows the body moved down and the rear legs lifted to be ready for placement on the top of the obstacle.

Sequence 4 shows the rear legs placed at the near side corner. The front legs are lifted and placed alternately in a tetrapod walking maneuver. The middle legs are lifted to be ready for the middle-leg placement.

Using this method, there is no lower limit of the thickness of the isolated wall. If the thickness U is 0, the whole body would roll over about the top edge and the front legs would take a small landing shock due to the statically unstable motion from sequence 1 to sequence 3. Since the center of gravity does not deviate from the top edge much, the shock at landing should be small.

4.5.3 Relationship to Walking Volume and Body Structure

Wall crossing ability is determined by step crossing ability. Hence, the relationship between wall crossing ability and walking volumes is the same as it is in step crossing.

The minimum thickness of the wall crossing is determined by either U_2 or C_{f3} . Both of U_2 and C_{f3} can be reduced by increasing the overstroke between adjacent legs.

The special method for a narrow wall crossing requires strong and smooth belly skids which can support the weight of the vehicle.

4.6 Overall Walking Volume of the ASV

All of the analysis above is based on the assumption of a perfectly rectangular walking envelope. This may not be feasible in

leg design. The walking envelope is constrained by the kinematic limits of the leg linkage. From the study in Chapter 6, the walking envelope of the pantograph leg is a rectangle with one upper corner truncated. Hence, the overall arrangement of the walking volumes of the legs should minimize the loss of mobility due to this truncated corner.

Figure 4.27 shows an overall arrangement of the walking envelope of the ASV. The front legs and the rear legs are mounted in opposite directions, and the middle legs are mounted to be the same as the front legs. The truncated corner is the rear upper corner for the front and the middle legs, and it is the front upper corner for the rear legs.

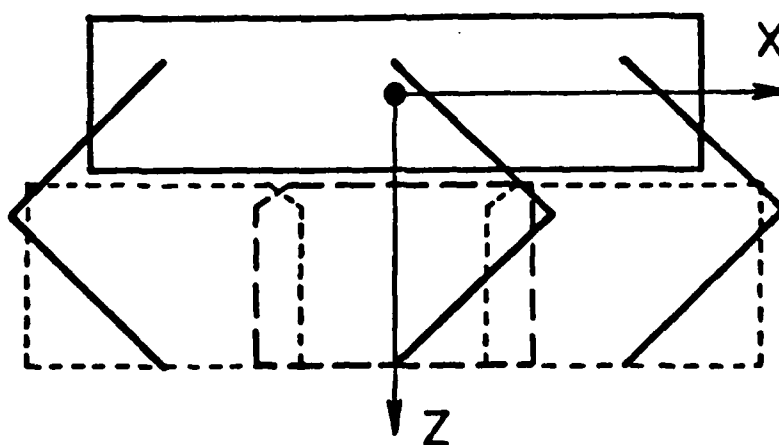


Figure 4.27: Overall walking volume of the ASV.

The reason for the different mountings of the front and the rear legs are: first, in a ditch crossing, the ASV usually lowers its body height in order to have better resistance to disturbance. The front upper corner of the front legs and the rear upper corner of the rear legs should not be truncated so that the front-foot and rear-foot ranges are not reduced at lower body height. Hence, the ditch crossing ability is not reduced. Second, a truncated front upper corner would reduce the front-foot vertical range, and hence reduce stepping up capability.

The reason for the mounting of the middle legs is that a truncated front upper corner of the walking envelope of the middle leg would reduce the middle-foot range and C_{r2} . This will put more constraints on a stepping up maneuver. It may take more than one step to place the rear legs within C_{r2} at stage 2. If the rear upper corner is truncated, from Figure 4.18, the rear-foot range is reduced only if the truncated corner exceeds point A.

In the earlier pantograph leg design, the truncated corner was very large, and this truncated corner did exceed point A and reduce the rear-foot range. Hence, the middle legs should be turned around because the rear-foot range is more important than the middle-foot range in stepping up. Later, through much optimization, a large walking envelope with a small truncated upper corner became available. The middle legs are mounted as in Figure 4.27 in order to maximize mobility.

The advantages of this arrangement when stepping up are disadvantages when stepping down. However, stepping down is easier and a larger obstacle can be handled better than when stepping up. The

mounting of the middle leg should be selected to the benefit the performance when stepping up.

4.7 Summary

In this chapter, hexapod walking over a slope, a ditch, a vertical step and an isolated wall was studied. In the study of slope walking, gradability of the ASV obtained by lowering the body height and by leveling the body attitude was calculated. The results were tabulated in Table 4.1. The first method is more effective for walking along a maximum gradient line, and the second method is more effective for walking along a zero gradient line. Methods of improving the stability by changing the beginning and the end of the stroke were also studied.

Table 4.5
Mobility of the ASV.

	obstacle dimension (feet)	minimum body angle (degree)
ditch crossing		
1. Continuous FTL gait, $\beta = 2/3$	5.0	0
2. body leveled	8.0	0
3. body tilted	9.3	15
vertical step crossing		
1. stepping up	7.1	40
2. stepping down	7.1	40
3. stepping down by gravity	8.5	45
isolated wall crossing	7.1	40

A general approach was used to study large obstacle gaits for ditch crossing, vertical step crossing and wall crossing. The entire obstacle crossing was divided into three phases. The range at each phase was calculated. The minimum of these three was the maximal possible crossing ability. The leg motion and body motions needed to fulfill the foot conditions of the minimum range were then studied. If there is no difficulty in fulfilling these foot conditions, the maximal crossing ability is thus determined. The maximal crossing ability for these obstacle types were calculated and are tabulated in Table 4.5.

In each obstacle crossing, the relationship between the crossing ability and the walking volume was discussed. Methods to improve the crossing ability by modifying the walking volume were also suggested. According to these relationships, the overall walking volume of the ASV was designed.

Chapter 5

LEG DESIGN BY FOUR-BAR LINKAGE SYNTHESIS

5.1 Introduction

Due to lack of full understanding of the ideal performance of a walking machine, the preliminary design goals of the ASV were not completely defined. However, a set of design criteria was established as follows:

- A vehicle cruise speed of 5 mph and a sprint speed of 8 mph.
- A grade climb capability of a 50% slope.
- The vehicle should possess good mobility, close to that of a horse, in rough terrain.
- The vehicle energy efficiency should be better than conventional off-road vehicles in rough terrain.
- The vehicle shall carry a 200 pound human driver and 500 pound payload. The dry weight of the vehicle will be 3000 pounds.
- The vehicle overall dimensions shall be 12 feet in length, 8 feet in height, and 4 feet in width (from center to center of foot paths).

The leg design is the most crucial aspect of a walking machine since it strongly influences the mobility, the energy efficiency, the speed and the control algorithm of the machine. The leg design, like any other design, should be based on the design specifications.

The design specifications of the leg were modified continually during the design process due to increasingly understanding of gait and mobility of a hexapod. Hence, leg geometries were designed and modified according to different specifications at different stages. The major steps of leg design are presented in this chapter and the next chapter.

At the beginning of the leg design, it was not completely clear what kind of performance an ideal leg should have. Hence, the design goal at that time was to prove that it is possible to build a practical walking machine as specified above. The major difficulty found in walking machines built in the past was poor energy efficiency. Therefore, the primary goal at that time was to prove that an energy efficient leg is possible with proper kinematic and mechanical design.

The poor energy efficiency is mainly due to inappropriate leg design. Considerable refinement is necessary both in leg geometry and in the method of power transmission and actuation. An extensive discussion of conceptual designs of a leg for a walking machine was given by Shigley in 1961 [4]. He gave several possible leg configurations which generate good foot trajectories with respect to basic considerations in geometry and in efficiency. However, most of the walking machines built since that time were intended for the study of control algorithms. Little consideration was given to the relationship of leg geometry to energy efficiency in those leg designs. As a result, these machines have poor energy efficiency. The only exception may be the PV II built by Hirose and Umetani [21].

However, the small scale and low speed of this machine makes comparison difficult.

The PV II has four three-dimensional pantograph legs. Each leg is actuated by three independent linear actuators which are DC motors with screw actuators. Two of the screws are ball screws while the third (lateral motion) is a plain power screw. The vehicle can walk at a speed of 2 centimeters per second with a 10 Watt power consumption. The vehicle weight is only 10 kilograms. This energy efficiency is considered to be relatively higher than previously built walking machines. However, the size, weight and speed of this machine make it an impractical walking machine. It did not provide adequate evidence that an energy efficient leg was possible for a full scale practical walking machine. In fact, due to its extremely low speed, the specific resistance¹ of the PV II was much greater than those of biological or other practical mechanical locomotion systems.

In recent years, Waldron and Kinzel gave an overall explanation of the poor energy efficiency found in walking machines as well as industrial robots² [44]. They also suggested a simple leg configuration

¹ This is a dimensionless coefficient defined by Gabrielli and Von Karman [45]. The specific resistance is used to compare the efficiency of different biological and mechanical locomotion systems regardless of their weight.

² A more detailed review of their argument is given in the next section.

based on a four-bar linkage which would eliminate the dynamic reasons for poor energy efficiency. Their study provides the initial direction for the leg design presented in this chapter.

A simple four-bar leg with a variable length driven-crank was designed in the first stage. This leg could only provide a small amount of vertical stroke. Hence, it is only suitable for smooth terrain. The primary purpose of this leg design was to test the energy efficiency of the leg. Two small scale walking machines were built using this design and were tested for energy efficiency [47,48]. The results of these tests showed it was possible to achieve low specific resistance in an artificial legged system.

Further research revealed that at least a two foot vertical stroke was required in order to gain minimum mobility in rough terrain. The original four-bar leg was modified in order to provide this vertical stroke. This led to a different design for lifting the foot in which a variable shank length was used.

Finally, the mobility of the ASV was determined to be:

- Grade climb ability: > 60%, 70% for cross slope.
- Ditch crossing ability: 6 feet.
- Vertical step crossing ability: 5.5 feet.
- Isolated wall crossing ability: 4.5 feet.
- Fording depth: 4 feet.

The relationship of mobility and walking volume was better understood after a careful gait study (see Chapter 4). According to this study, the walking volume of the leg for the ASV was defined as below.

1. Longitudinal stroke: > 5 feet, 6 feet is preferable.
2. Vertical stroke: 4 feet.
3. Lateral stroke: 4 feet.
4. Longitudinal overlap between strokes of adjacent legs:
 $\geq .5$ feet, 1 foot is preferable.

The major difficulty in designing a leg according to these specifications is the increased vertical stroke. The four-bar leg was further modified to satisfy the vertical stroke requirement. Although a long linear shank actuator could generate a satisfactory walking volume, it was found that such a mechanism was not practical from the mechanical design point of view. Hence, a seven-bar leg with no sliding joints was designed to replace the four-bar leg. However, this left several mechanical design problems unsolved. As a result, a completely different leg mechanism: the pantograph leg, which will be discussed in the next chapter was adopted.

5.1.1 Energy Efficiency in Robots and Walking Machines

In reference [44], Waldron and Kinzel showed that one reason for the poor energy efficiency of robots and walking machines is the use of the actuators as brakes. That is, the actuators are "back-driven." The energy consumed when the actuator is back-driven converted into heat with no provision for recycling. There are two reasons for back-driving. The first occurs in the usual case in which each joint is driven directly by a separate actuator. Figure 5.1 shows a two link leg actuated by two actuators placed at the hip H and at the knee K, respectively. In Figure 5.1a, the contact point P is ahead of H.

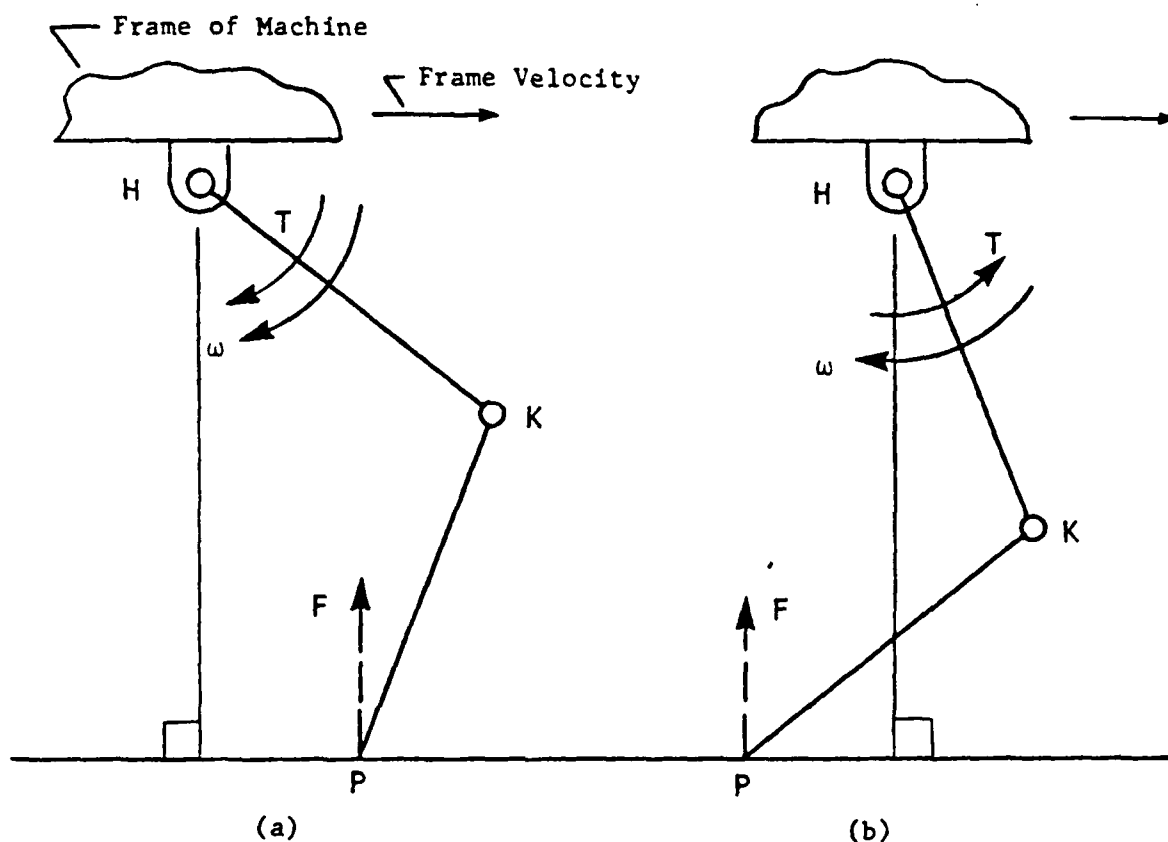


Figure 5.1: Back-drive in one-joint actuator system

Hence, the actuating torque T_H is in the same direction as the rotation of the joint H (ω) and the actuator is doing positive work. In Figure 5.1b, the point P is behind H, and T_H is in the opposite direction to ω . In this case the actuator at H is acting as a brake, or it is back-driven. By observing the arrangement of muscles in biological systems, there is an indication that an alternative actuator arrangement might avoid this situation. Some major muscles act across two joints while others act across only one joint. Evidence of improvement in mechanical efficiency can be found by

this use of two-joint muscles [49]. Hence, a two-joint actuator may avoid this problem.

The second reason for the existence of back-drive is mainly found in walking machines. Most walking machines in the past have adopted an "insect" type leg. Due to the oscillatory nature of leg movement during walking, leg kinetic energy fluctuates periodically from near zero to a substantial value. The leg is braked at the end of the stroke and leg kinetic energy is converted into heat. The obvious solution is to use gravity to brake the leg at the end of stroke. The leg kinetic energy is then converted to potential energy and can be recovered during the return phase. The leg acts as a pendulum swinging in a vertical plane. Hence, a "mammal" type leg, instead of an "insect" type leg, can avoid this kind of loss mechanism.

Alternatively, if there is a well defined primary working cycle it is possible to minimize wasted energy by optimizing the system geometry. In walking machines, the primary working cycle is a load-bearing, level and straight line followed by a relatively arbitrary return path.

Figure 5.2 shows a "mammal" type leg mechanism with a two-joint actuator. Joint H is driven directly by linear actuator $O_A A$. The second actuator $O_B B$ acts across both joints H and K. In support phase, the length of $O_B B$ is kept constant and it does no work. $O_A A$ is always doing positive work to overcome the environmental resistance.

At the end of the stroke, $O_B B$ is shortened and the leg is braked by gravity. It then reverses direction and swings forward as a pendulum. Hence, back-driving does not occur. Moreover, the four-bar linkages $HKBO_B$ can be proportioned so that point P approximately generates a segment of a straight line. This would minimize the work done in the support phase. A remarkable good approximation to a straight line can be obtained if the support portion of a step is limited in range [46]. Another advantage of this mechanism is that its simple structure allows good mechanical reliability.

5.1.2 Contents of Sections

In Section 5.2, an introduction to the program RECSYN is given. RECSYN was used to generate all of the four-bar linkages in the following design procedure.

In Section 5.3, the design of the four-bar leg is described. Several major techniques for the optimization of leg geometry are also introduced. The analysis of bearing loads, actuating torque, and mounting positions for the main actuator is given. Finally, the interference between adjacent legs is studied by graphical methods and the load distribution of an abducted or adducted leg is studied by finite element methods.

In Section 5.4, the design of a seven-bar leg is described. This design is based mainly on the concept of a shank linkage which is used to replace the linear shank actuator of the four-bar leg.

5.2 An Introduction to RECSYN

5.2.1 Functions of the Program

RECSYN is an acronym for RECTified SYNthesis. It is an interactive graphics program which synthesizes mechanical linkages with nominated irregular motions of a machine member while avoiding (rectifying) the spurious solutions which are generated by traditional procedures. The spurious solutions eliminated are of two types designated by the terms "branch problem" or "order problem." The branch problem, if present, requires the solution linkage to be disassembled and reassembled in order to reach some of the design positions. The order problem causes the solution linkage to pass through the design positions in an order different from that specified. With the rectification capability a designer using RECSYN is able to synthesize a mechanical linkage more efficiently than when using other linkage synthesis programs.

The primary mechanical linkage type synthesized by the program is a four-bar linkage (see Figure 5.3a). The four-bar linkage is a simple mechanism. Nevertheless, it is capable of generating a great variety of irregular motions. The program can also synthesize two additional linkage types: the slider-crank (see Figure 5.3b) and the elliptic trammel (see Figure 5.3c). Usually, it is impossible to design a linkage which passes along an exact trajectory. However, a solution linkage should conform to design positions selected to be on the trajectory.

According to the method of defining design positions, there are three different basic kinds of synthesis problem: motion generation

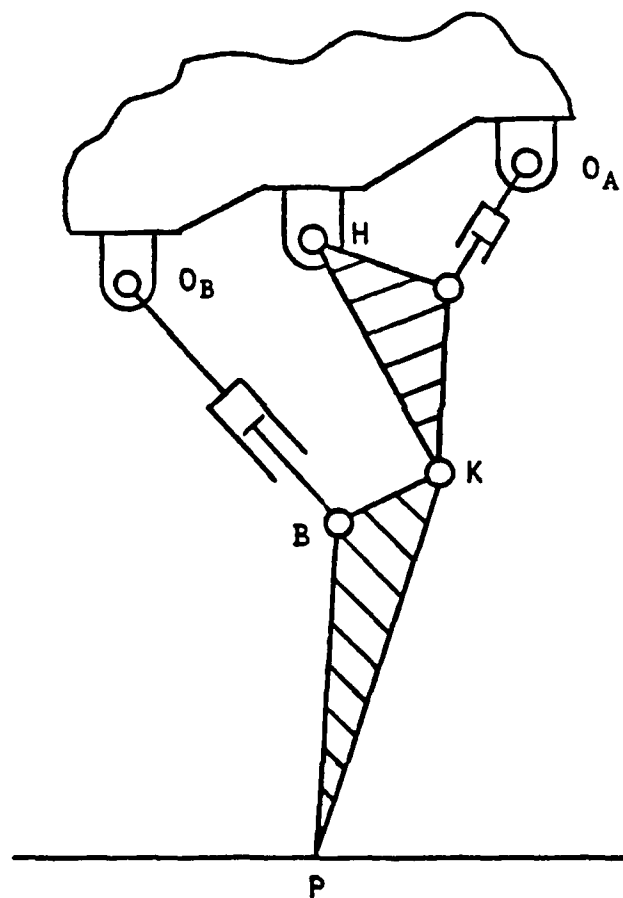


Figure 5.2: A "mammal" type leg with a two-joint actuator.

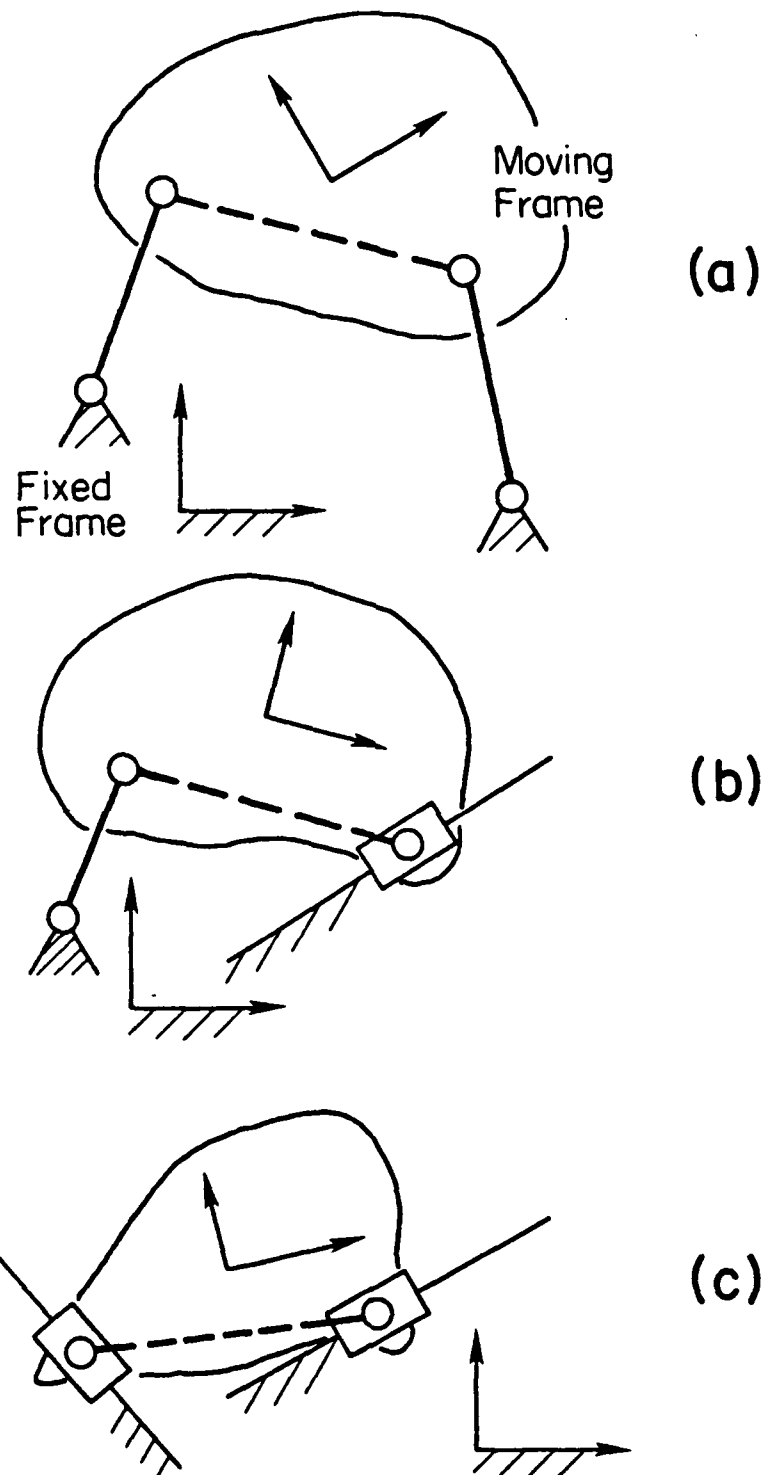


Figure 5.3: Linkage types designed by RECSYN.

problems, function generation problems and path-angle generation problems. RECSYN is written specifically with the intention of solving motion generation problems. The other two problem types can be transformed into motion generation problems, allowing them to be synthesized by the same approach.

The program is constructed to generate solution linkages which pass exactly through either 2, 3, 4 or 5 design positions. Although this seems too small a number of design positions to obtain a good approximation of an irregular plane trajectory, experience shows that the trajectory between design positions can be very close to the desired trajectory, provided a good selection is made of the design positions. Moreover, many practical design problems do not require the solution linkage to follow the desired trajectory exactly.

The number of the design positions required is related to the accuracy of the generated trajectory. In general, the larger the number of design positions, the better the accuracy of the trajectory. The number of design positions is also related to the dimensions of the solution space. The larger the number of design positions, the smaller will dimensions of the solution space be. For a five position specification the solution linkages number 6, 1 or 0 and are calculated directly from the input design positions without giving any freedom to the designer for optimization except in the case in which there are six real solutions to select from. Therefore, the dimension of the solution space is 0. On the other hand, the dimensions of the solution space are larger for smaller numbers of design positions. There are 6 dimensions for 2 positions, 4 for 3 positions and 2 for

4 positions. That is, there are two disposable parameters for, four design positions; four for three design positions; and six for two design positions. The more the dimensions of solution space are, the more freedom the designer has to optimize the solution linkage according to this design constraints. One can select the number of design positions by considering the accuracy of the trajectory and the freedom of optimization. This interaction between the program and the designer becomes an essential factor for the optimization.

5.2.2 Operation of the Program

With the exception of five position case, in which the few possible solution linkages [6, 1 or 0] are defined automatically by the entered design positions, the design process is divided into two major stages: the selections of the driven and driving-crank respectively. Since the theories developed for the rectification of the spurious solutions provide the available solution space for the circle-point of the driven-crank, the designer is asked to select the driven-crank first.

The design procedure can best be shown by giving an example of a four position case. After the design positions have been entered, four L shaped symbols appear on the screen to indicate the four design positions (see Figure 5.4). The L shaped symbol, which is attached to the coupler of the solution linkage, should pass exactly through these four design positions. A circle-point curve is also generated on the screen. Any circle-point of the driven-crank selected on the dotted segments will result in a spurious solution

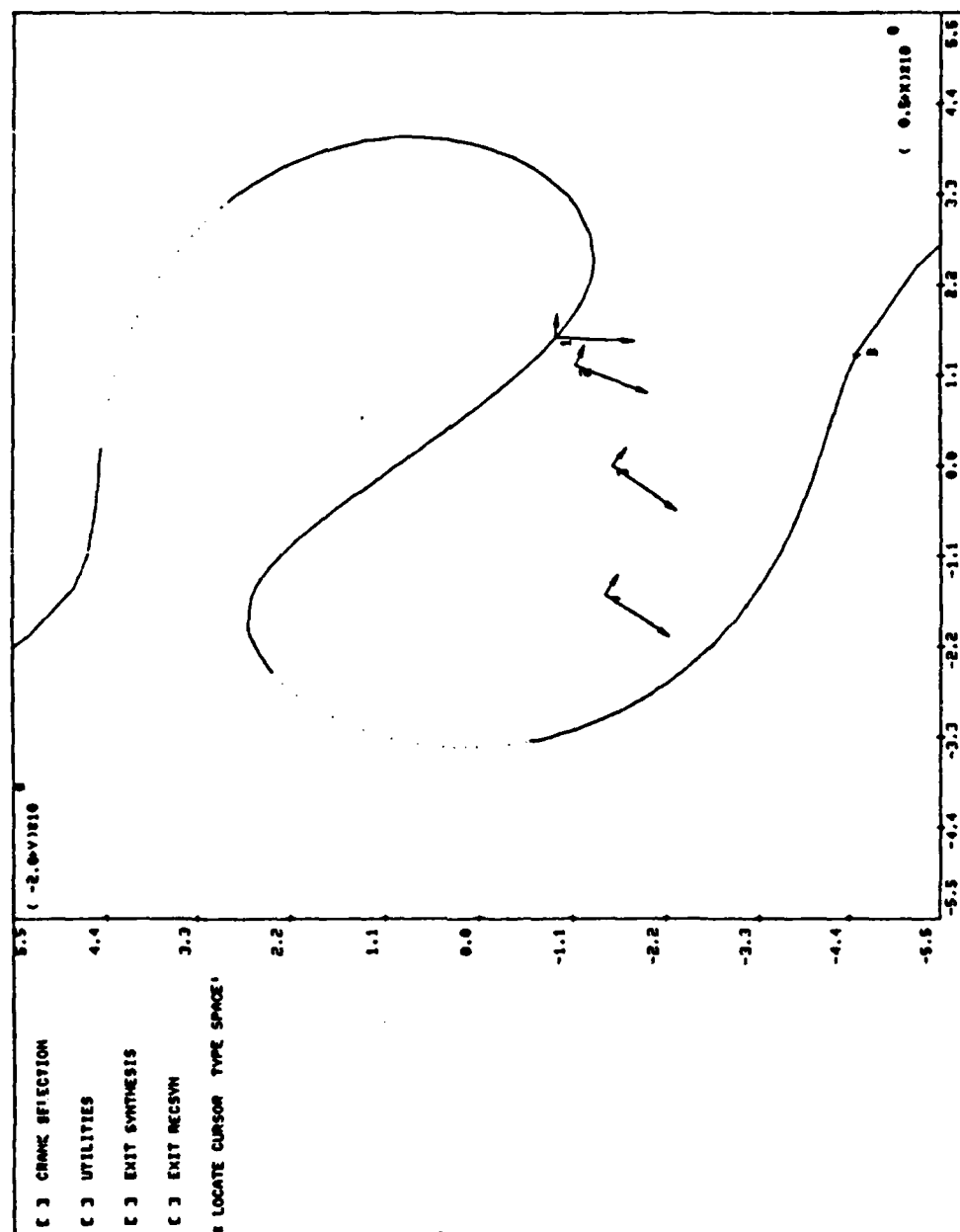


Figure 5.4: The display for the selection of driven-crank -- before selection.

linkage of the branch problem type. Therefore, the designer should select a circle-point (either by cursor or by keypad) on the solid segment of the curve for the driven-crank. The corresponding center-point, with crank and a hatched area, is then shown on the screen (see Figure 5.5). The hatched area indicates the solution space for the circle-points of the driving-crank which result in a solution linkage with branch problems. The designer can estimate the possibility of obtaining a desired solution linkage at this time and decide whether to proceed to the next stage or reselect the driven-crank.

After the driven-crank design has been completed, the screen is erased and another display is shown (see Figure 5.6). The dotted segments of the circle-point curve are different from those of the previous display. In this display, they indicate the solution space of circle-points for the driving-crank which result in solution linkages with order problems. Therefore, the designer should select a circle-point on the solid segments which are outside the hatched area. For any such selection, the corresponding center point and crank, and the linkage type are shown on the screen (see Figure 5.6). The designer can reselect the driving-crank or go back to the previous display to reselect the driven-crank. The designer can complete the design if the selection is satisfactory. The screen is then erased and the solution linkage with the data of the pivot positions are shown (see Figure 5.7). The designer can animate the solution linkage to check his results. The design process can be repeated many times until an optimal solution linkage is obtained.

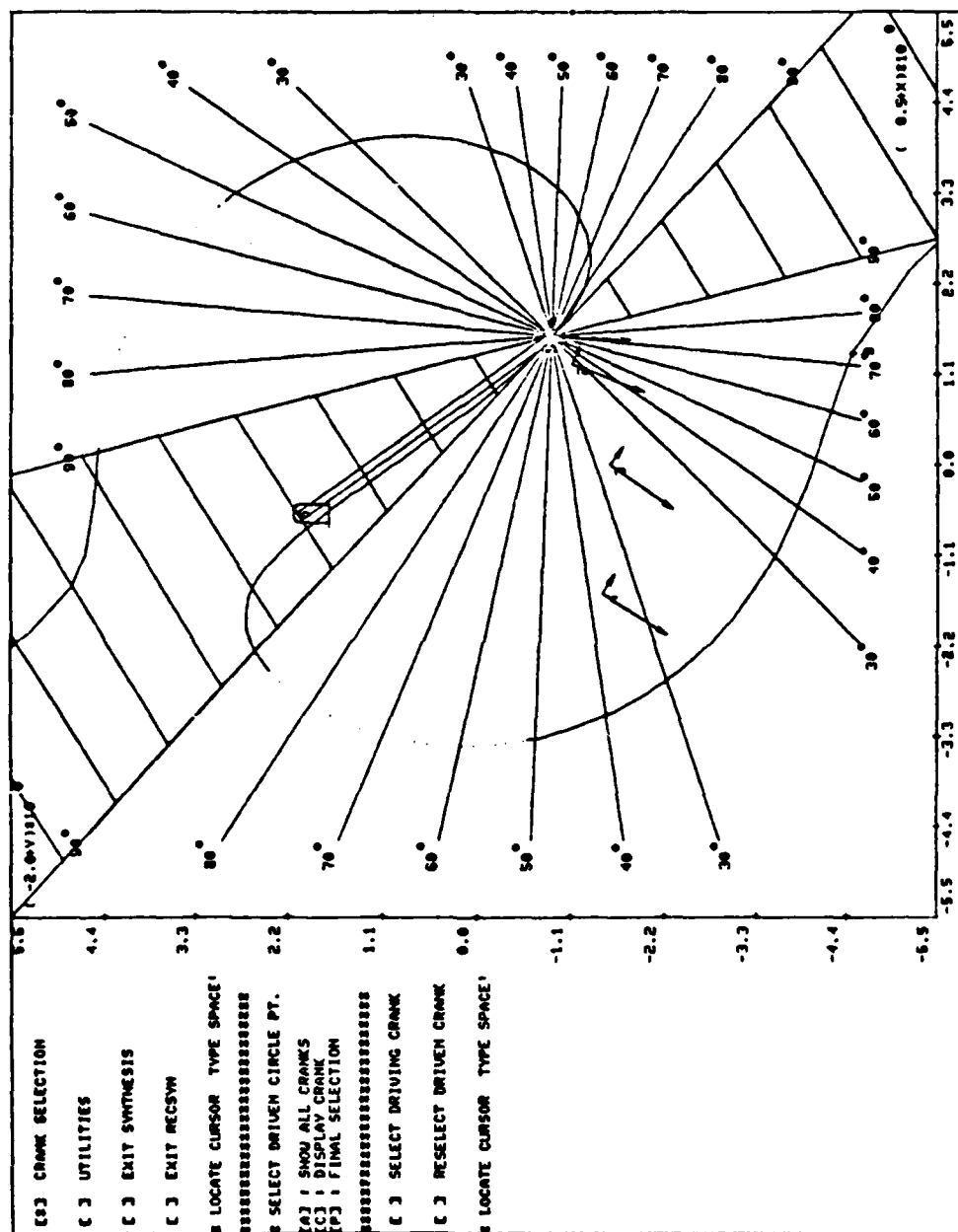


Figure 5.5: The display for the selection of driven-crank -- after selection.

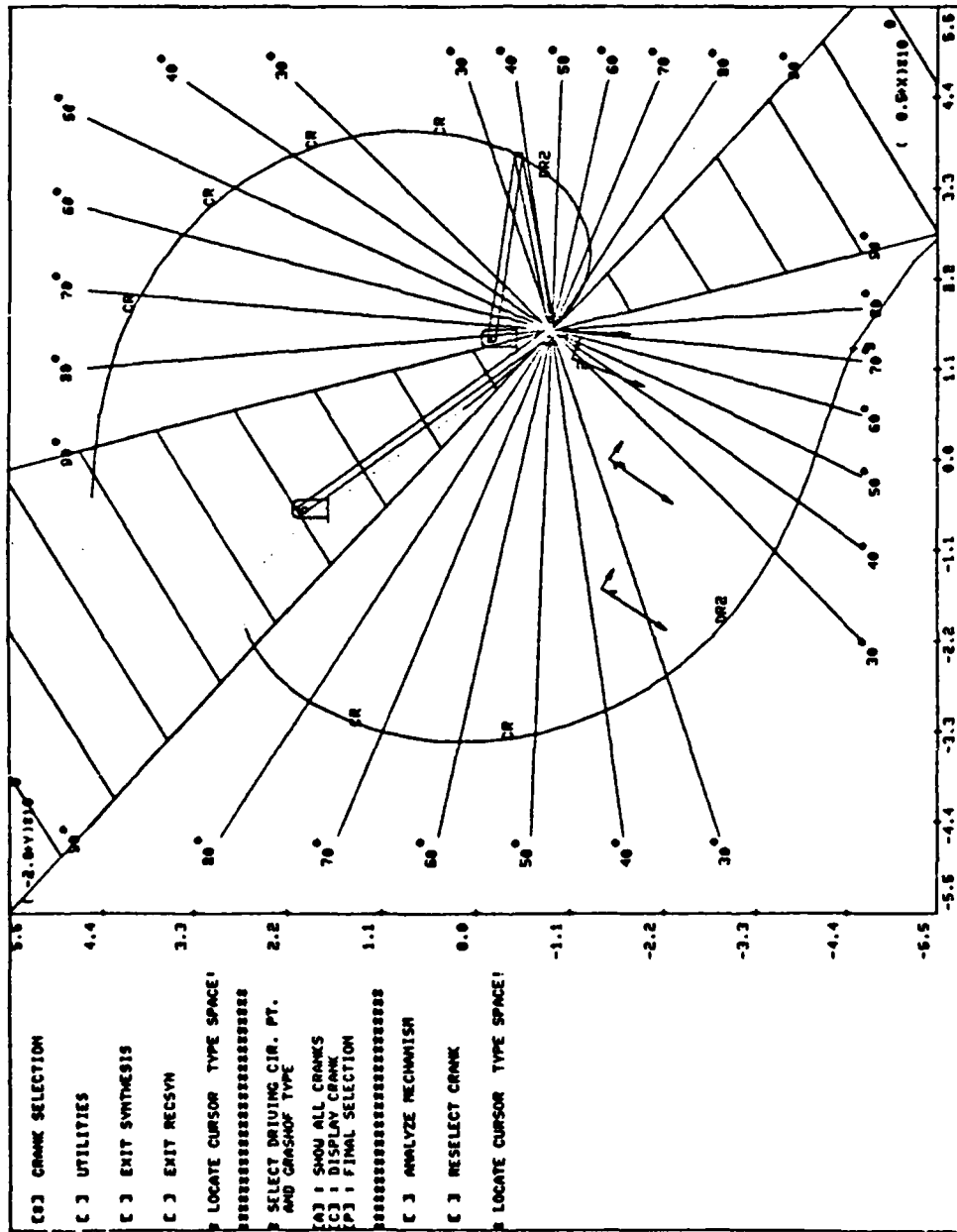


Figure 5.6: The display for the selection of driving-crank .

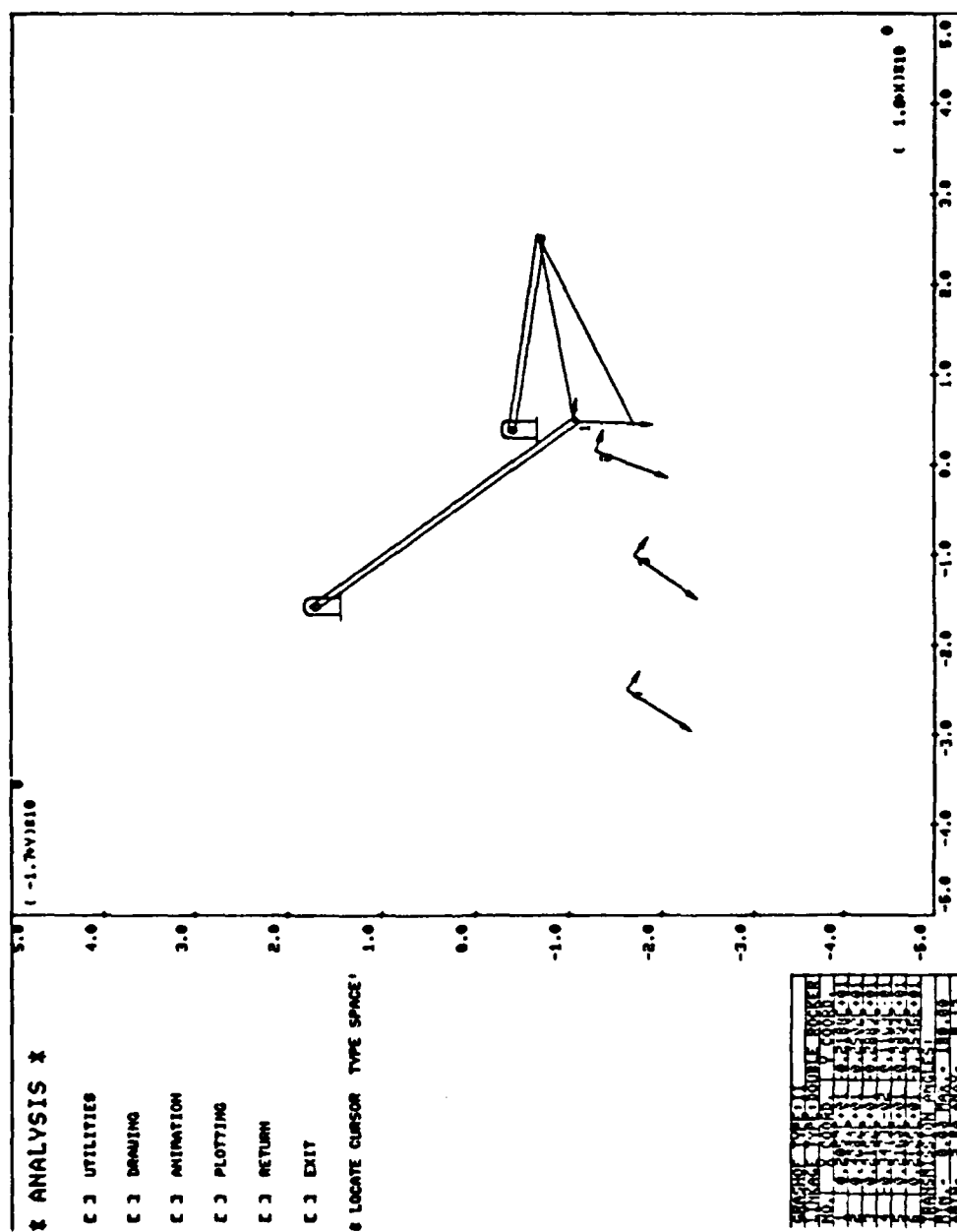


Figure 5.7: Solution linkage generated by RECSYN.

5.3 Design of a Four-Bar Leg

5.3.1 Design Specification

The design specifications of the leg have been modified several times during the design process. Only the specifications related to the design of the four-bar leg are described below.

The first stage of leg design is to design a four-bar leg as shown in Figure 5.2. In support phase, the four-bar linkage $HKBO_B$ is driven by the main actuator $O_A A$ only. The foot path should be an approximation of a horizontal straight line. At the end of the stroke, the foot is lifted by the lifting actuator $O_B B$ and moved back to the front by the main actuator with the help of gravity. The frame of the four-bar leg is rotated by a third actuator called the lateral actuator. This actuator rotates the leg frame about an axis which is parallel to the longitudinal body axis and provides abduction and adduction so the vehicle can change direction.

The foot of the leg was considered as a rigid body attached to the shank at this stage³. The foot profile was circular and the foot reference point was at the center of the circle. The foot was to roll on the ground during walking. The radius of the foot circle depended on the soil conditions and was to be selected to provide

³ A foot with a passive ankle is also designed for the ASV legs. However, the foot-ankle system can be separated from the leg design. A brief discussion of foot-ankle system is given in Chapter 7.

proper contact pressure. A radius of .6 feet was selected for a bare foot. Different shoes could be put on when the vehicle was operating in different soil conditions.

The leg of a walking machine serves two major functions. The first is to provide a desired walking volume, which is the three-dimensional reachable space of the foot reference point. The second is to carry the weight of the vehicle. Also, interference between links and among legs should be avoided. Considering these three aspects, the design specification of the four-bar leg was determined as follows:

Leg strokes: The stroke pitch was selected to be 5 feet since the predetermined maximum length of the vehicle was 12 feet. The overstroke between adjacent legs was not recognized to be necessary at the beginning. Hence, the leg stroke was selected to be 4 feet in order to avoid any interference between the feet. The lateral stroke was selected to be 4 feet.

The vertical stroke was originally used to lift the foot in transfer phase only. Hence, a small amount of vertical stroke, such as 3 inches, was sufficient. This was suitable for walking on smooth terrain only. Later, the vertical stroke was increased to 2 feet in order to be able to walk in rough terrain. After the mobility requirement was finally determined, the vertical stroke was increased to 4 feet to satisfy the requirement of vertical step crossing ability. While the vehicle is walking in a tripod wave gait, a four foot stroke results in less than one Hertz cycling frequency at cruise speed,

which is 7.3 feet/second. The dynamic effects were considered insignificant in this design due to the low frequency.

The maximum vertical variation of the trajectory in one step is an interesting subject. If the legs contact the ground at different times, the leg height of each supporting leg is not the same at one instance due to this vertical variation. This different leg height will contribute to the vehicle's undesired pitching and rolling and will result in energy losses. Therefore, the vertical variation should be as small as possible. In reference [42], test results show that the maximum amplitude of sinusoidal and vertical body motion at which a human feels discomfort is 4 inches at one Hertz, .5 inches at two Hertz, and .05 inches at four Hertz, respectively. When the ASV is walking at cruise speed in an alternating tripod wave gait, the human body is moved up and down with a four Hertz sinusoidal motion. This can be understood by referring to Figure 5.13 where two peaks exist in one limited variation stroke, and the vehicle experiences two strokes in one motion cycle. Hence, the maximum vertical variation should not be more than .05 inches. However, comfort is not the essential goal of the ASV, and terrain factors may increase the vertical variation to a couple of inches even for an exact straight-line stroke. A one inch maximum variation of the foot trajectory was selected for the leg design.

Loads: When the center of gravity is kept in the center line of the support pattern, the supporting legs on each side bear half the vehicle weight. In an alternating tripod gait, at any time, one

side of the machine is supported by only one leg. In this case, the maximum vertical load on that leg is half the vehicle weight. Hence, the leg was to be able to take a vertical load of 1500 pounds at all positions in its walking volume (at that time the projected vehicle weight was 3000 lbs.). The maximum horizontal load was taken to be the longitudinal component of half the weight when the vehicle is walking on a 50% slope and was found to be 671 pounds. Later, the grade climbing performance goal became 60% and the maximal horizontal load became 772 pounds. The leg bears lateral load when it is abducted or adducted. The maximal angle in abduction was 20° and the maximal lateral load was 513 pounds.

Leg size: The dimension of the leg was determined by the dimensions of the ASV. Since the stroke pitch was 5 feet, the maximum width in the longitudinal direction for one leg to move between its two extreme positions was about 4.5 feet in order to avoid interference between legs. The maximal leg height was determined to be 7 feet. Since the foot radius was about six inches, a leg height of 6.5 feet was used for the linkage synthesis. The leg thickness should be as small as possible and the maximum thickness was temporarily determined to be 2 feet.

5.3.2 Basic Geometric Design

Figure 5.8 shows a general construction of a walking machine with four-bar legs. The entire leg below the hip joint is composed of a four-bar linkage. The thigh is the two cranks and the shank is the

coupler. The primary objective was to design a four-bar linkage with a foot point (a point in the coupler) moving along a good approximation to a level straight line relative to the body. RECSYN was used to synthesize such a four-bar linkage.

Since close approximation of a straight line is required, a large number of design positions should be used. Five position synthesis does not allow the designer to optimize the solution linkage. Hence, a four position synthesis is proper for this design. Another

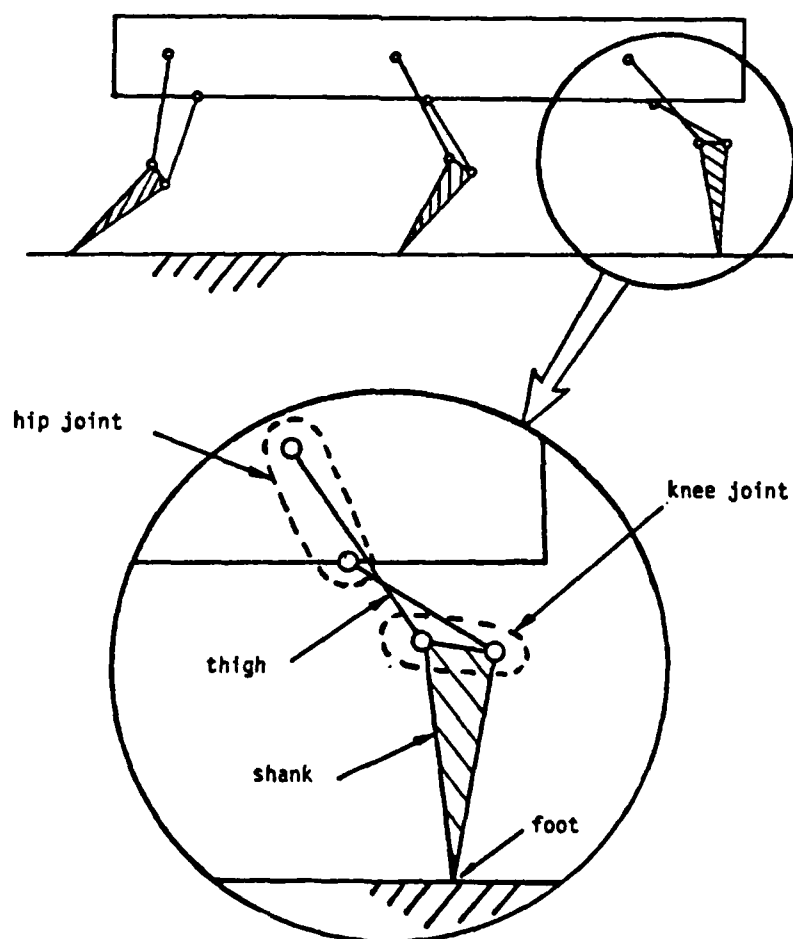


Figure 5.8: Structure of a walking machine leg.

reason for using four position synthesis is that it results in a relatively symmetric trajectory of the foot point, while a three position specification usually results in an asymmetric foot trajectory. Figures 5.9a and 5.9b show these two different shapes of trajectory.

5.3.2.1 Calculation of Design Positions

The four design positions are calculated as follows. Let the reference frame be attached to the machine body as shown in Figure 5.10. Link OQ is a driven crank with length a , and link QP with length b is a part of the coupler. Points O, Q and P are the driven-crank-center point, the driven-crank circle-point and the foot point, respectively. If the foot point P moves on a horizontal straight line relative to the body, the hip joint O will also move on a straight line if P is fixed on the ground. From Figure 5.10, the position of point P can be defined according to the reference frame as

$$h = a \cdot \sin \phi + b \cdot \sin \theta \quad (5.1)$$

$$X = a \cdot \cos \phi + b \cdot \cos \theta \quad (5.2)$$

These equations can be combined to eliminate ϕ as follows:

$$(h - a \cdot \sin \phi)^2 + (X - a \cdot \cos \phi)^2 = b^2 \quad (5.3)$$

which can be expanded and reduced to the following form:

$$A \cdot \cos \phi + B \cdot \sin \phi + C = 0 \quad (5.4)$$

where

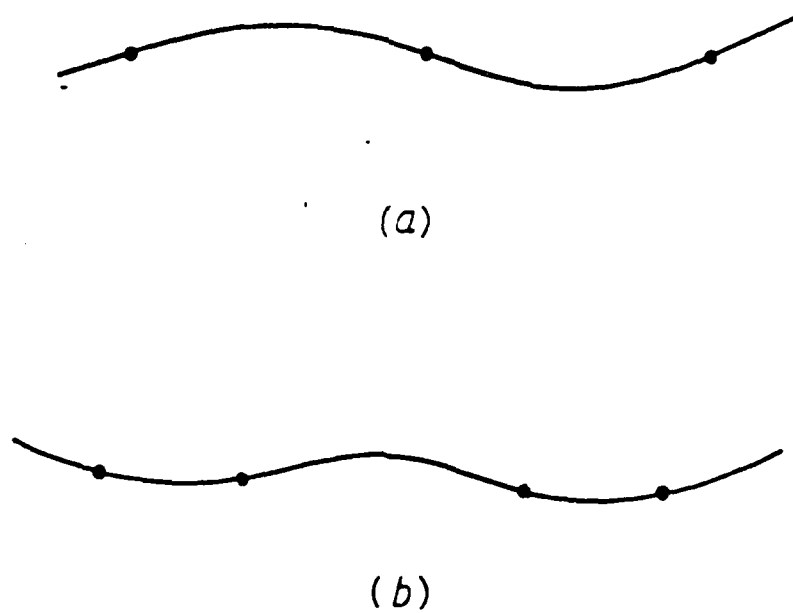


Figure 5.9: Trajectories of three and four position synthesis.

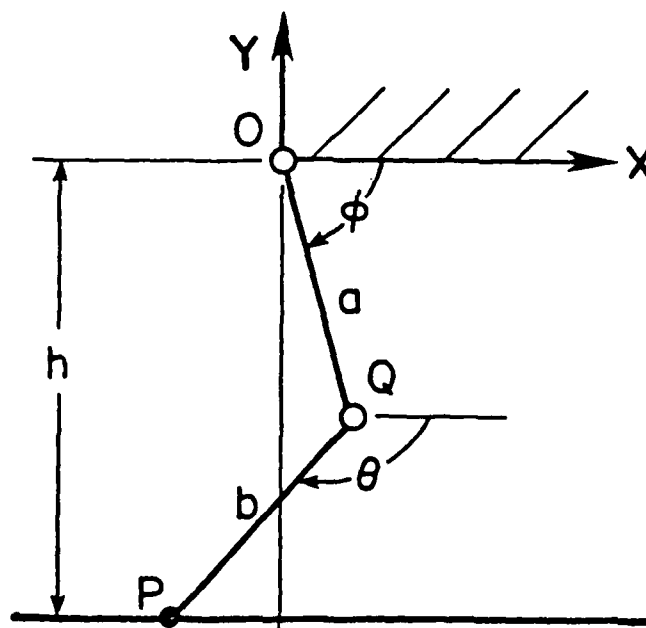


Figure 5.10: Symbols to define a position of the foot point P.

$$A = -2a \cdot X$$

$$B = -2a \cdot h$$

$$C = a^2 + h^2 - b^2 + X^2$$

If $U = \tan(\phi/2)$, equation (5.4) can be rewritten as

$$A(1 - U^2) + 2B \cdot U + C(1 + U^2) = 0 \quad (5.5)$$

or

$$(C - A)U^2 + 2B \cdot U + C + A = 0 \quad (5.6)$$

The solution to this quadratic equation is

$$U = \frac{-B + \sigma(A^2 + B^2 - C^2)^{1/2}}{C - A} \quad (5.7)$$

where $\sigma = \pm 1$. For the leg design, $b < h$ and length a is positive.

This means

$$-B = 2a \cdot h > 0$$

and

$$\begin{aligned} C - A &= a^2 + h^2 - b^2 + X^2 - 2a \cdot X \\ &= (a - X)^2 + h^2 - b^2 > 0 \end{aligned}$$

Since the smaller value of ϕ is expected, $\sigma = -1$, and the value of ϕ is obtained from

$$\tan \frac{\phi}{2} = \frac{B + (A^2 + B^2 - C^2)^{1/2}}{A - C} \quad (5.8)$$

Elimination of ϕ from Equations (5.1) and (5.2) yields

$$(h - b \cdot \sin \theta)^2 + (X - b \cdot \cos \theta)^2 = a^2 \quad (5.9)$$

which can be expanded and reduced to the form

$$A' \cdot \cos \theta + B' \cdot \sin \theta + C' = 0 \quad (5.10)$$

where

$$A' = -2b \cdot X$$

$$B' = -2b \cdot h$$

$$C' = b^2 + h^2 - a^2 + X^2$$

After a similar process to that used for $\tan(\phi/2)$, an expression for $\tan(\theta/2)$ is given by

$$\tan \frac{\theta}{2} = \frac{B' - (A'^2 + B'^2 - C'^2)^{1/2}}{A' - C'} \quad (5.11)$$

The full foot step length is shown in Figure 5.11. The minimum and maximum coupler-point displacements in the X direction are

$$X_{\max} = -(a^2 - (h - b)^2)^{1/2} \quad (5.12)$$

and

$$X_{\min} = ((a + b)^2 - h^2)^{1/2} \quad (5.13)$$

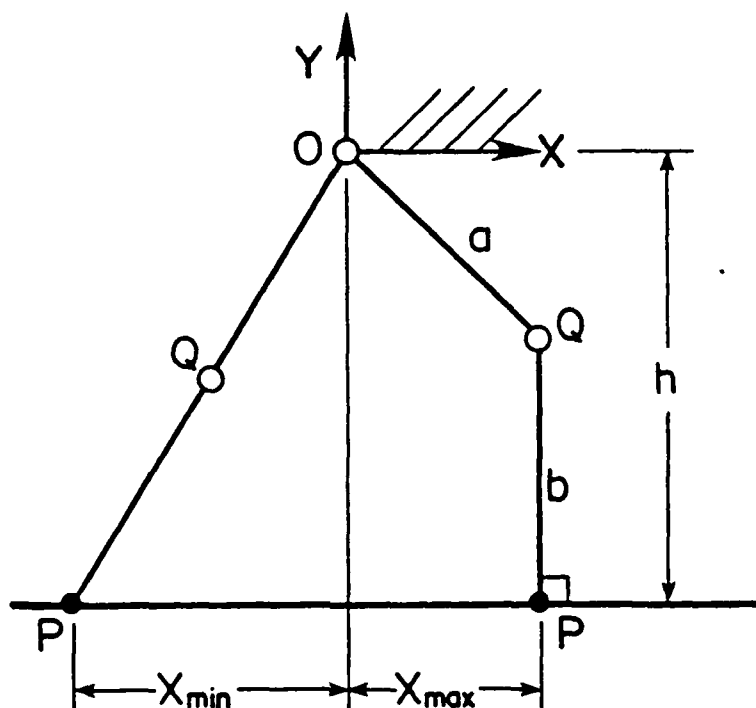


Figure S.11: A full step used for the calculation of design positions.

For a good estimate of optimum design point spacing, four position Chebychev spacing can be specified as follows:

$$\begin{aligned}
 X_1 &= X_a - X_r \cdot \cos (22.5^\circ) \\
 X_2 &= X_a - X_r \cdot \cos (67.5^\circ) \\
 X_3 &= X_a + X_r \cdot \cos (67.5^\circ) \\
 X_4 &= X_a + X_r \cdot \cos (22.5^\circ)
 \end{aligned}
 \tag{5.14}$$

where $X_a = (X_{\max} + X_{\min})/2$

$X_r = (X_{\max} - X_{\min})/2$

Since X_1 , X_2 , X_3 and X_4 are the four positions of point P, Equations (5.8) and (5.11) can be used to compute the values of ϕ

and θ at these four positions. The coordinates of point Q at the four positions can then be computed using elementary trigonometry. The locations of Q and values of θ , which are in terms of a , b , and h , provide the design positions for the four position synthesis problem. This set of design positions is called the knee design positions because point Q is one of the knee joints.

A program LEG was written to calculate the design positions. Table 5.1 is an example of knee design positions with $a = 1$, $b = 1$, and $h = 1$. The leg height h corresponds to the real leg height which is 6.5 feet. This set of knee design positions is also used in the example of linkage synthesis in the next section.

Another alternative is to use the four foot positions with corresponding shank angles as the four design positions. Table 5.2 is the foot design positions of the same example of Table 5.1.

Table 5.1

Knee design positions with $a = 1$, $b = 1$ and
 $h = 1.8$, the leg height is 6.5 feet.

position	X	Y	θ
1	2.160	-2.894	-93.099°
2	1.810	-3.125	-110.824°
3	0.592	-3.562	-125.557°
4	-0.967	-3.479	-123.223°

Table 5.2

Foot design positions with $a = 1$, $b = 1$ and
 $h = 1.8$, the leg height is 6.5 feet.

position	X	X	θ
1	1.964	-6.500	86.901°
2	0.526	-6.500	69.176°
3	-1.508	-6.500	54.443°
4	-2.946	-6.500	56.777°

5.3.2.2 Design Procedure

After the design positions in Table 5.1 are entered into the program RECSYN, the circle-point curve with four design positions will appear on the screen as shown in Figure 5.4. Notice that the circle-point curve passes through the first design position A_1 because A_1 is the moving pivot. Hence, the circle-point of the driven-crank has to be at A_1 . After a selection at A_1 is made, the driven-crank C*C with hatched areas are displayed as in Figure 5.5. The screen is then erased and the program proceeds to the next step.

Figure 5.6 shows the display for the selection for the driven-crank. Any point on the solid line and outside the hatched area can be the second circle-point. Since the primary motion cycle is oscillatory, the linkage type is not important⁴. The main concern in

⁴ If the main actuator is a linear actuator, the maximum crank angle should be limited to less than 120 degrees for good efficiency. Crank-rocker type linkages usually need a crank angle larger than this limit. Hence, a crank-rocker is not desired. More discussion of the influence of crank selections on the solution linkage is given in Section 5.3.1.

this selection is the compactness of the leg and the foot trajectory. The temporary selection feature can be used to generate many cranks at different locations (see Figure 5.6). A solution linkage with proper compactness is selected and the solution linkage is shown in Figure 5.7.

The solution linkage is entered into another computer program FORBAR⁵ to study the foot trajectory⁶. Figure 5.12 shows this foot trajectory. By observing the coordinates of the foot points, the smoothness and the available stroke is known. If the maximal variation is one inch, the available stroke of this leg is 5.5 feet. Strokes defined by this method are called limited variation strokes.

One important feature of body motion should be considered here. The foot path has two height extreme points due to the characteristics of a four position synthesis solution (see Figure 5.13a). A break point occurs at the connection if consecutive foot paths are linked together. Since velocity is the derivative of displacement, this break point will cause a sudden change of the vertical velocity of the body. This indicates that a substantial energy loss will occur at this point. Therefore a smooth connection between two foot paths is more energy efficient. This can be obtained by reducing the full

⁵ FORBAR is an interactive graphics program. It was developed originally by V.J. Vohnout for the analysis of the four-bar leg used in the Monopod. The program was modified substantially by the author to study various aspects of the leg design.

⁶ In the later version of RECSYN, foot trajectory can be generated right after the solution linkage is obtained within the same program.

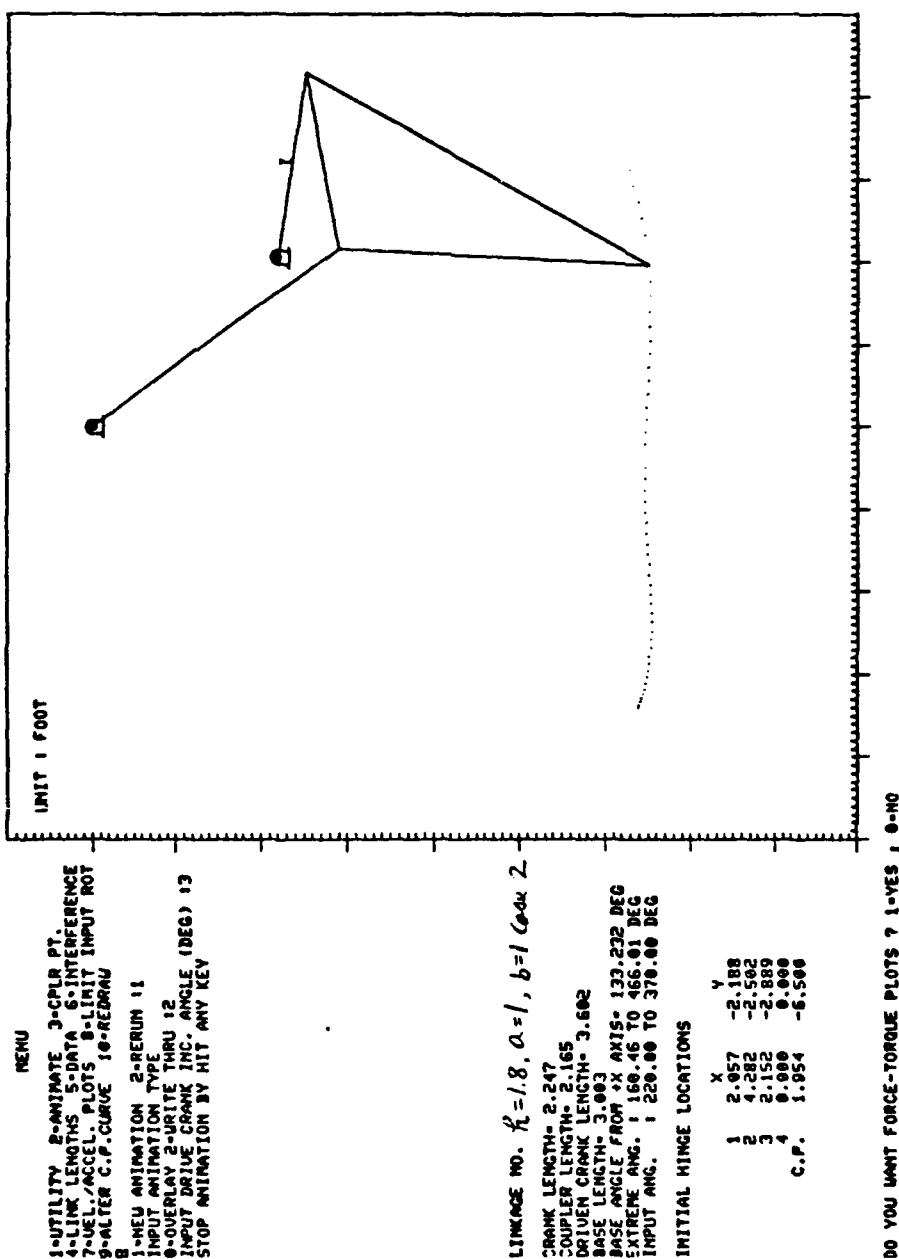
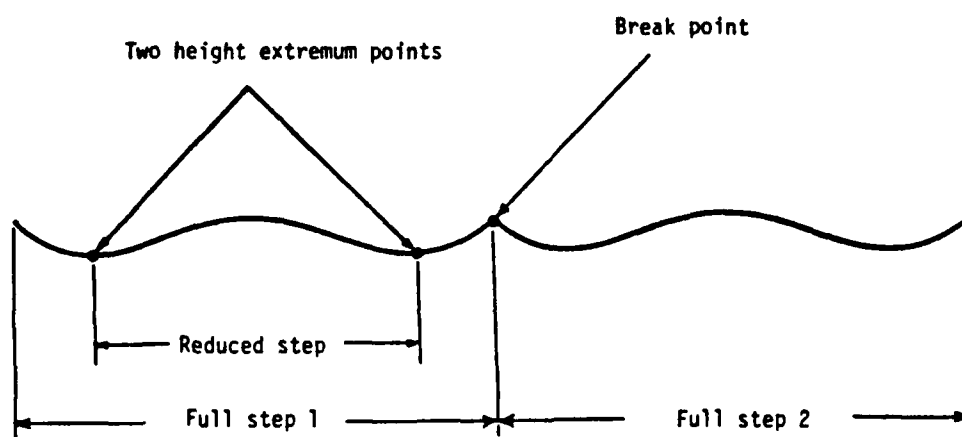


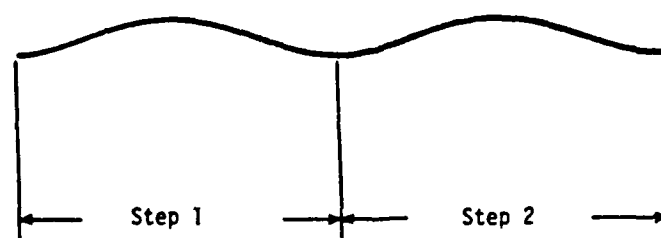
Figure 5.12: Foot trajectory of a four-bar leg.

step to a segment bounded by the two height extreme points. The result is shown as in Figure 5.13b.

However, the available stroke of this smooth consecutive footpath, which is called a smooth footpath stroke, is shorter than the limited variation stroke. In the above example, the stroke of the smooth footpath is only 3.37 feet. Since a longer stroke is usually hard to obtain, the limited variation stroke is used in the later sections.



(a)



(b)

Figure 5.13: Consecutive footpaths of the four-bar leg, the vertical variation is exaggerated.

5.3.3 Optimization of Leg Linkages

The optimization work goes along with the leg design and is carried out in two major steps. Figure 5.14 shows a general flow chart of the procedure of the leg design and its optimization. The first major step is to design and optimize a four-bar linkage with optimal foot trajectory. Some other design aspects such as crank angle and compactness are also considered. This step is indicated on the part of the flow chart above the dashed line in Figure 5.14. Usually, a batch of four-bar linkages are generated and optimized at one time. All the good linkages are stored in a "warehouse." The major optimization techniques used in this step will be discussed shortly.

The second major step is directed at other aspects such as load distribution and interference avoidance, and is indicated on the part of the flow chart under the dashed line. In this step, a good linkage is selected from the "warehouse." The optimal mounting positions of the main actuator are then determined. Following this, the bearing loads and actuator loads are determined. The interference between legs is also checked. If one linkage can not satisfy all the design criteria after all possible optimization work has been completed, a new linkage is selected and the procedure is repeated. If none of the linkages can satisfy all the design criteria, the first step must be repeated in order to generate more linkages. The experience gained in trying to optimize the first batch was a great help in the design of the second batch of linkages. This procedure was repeated until a

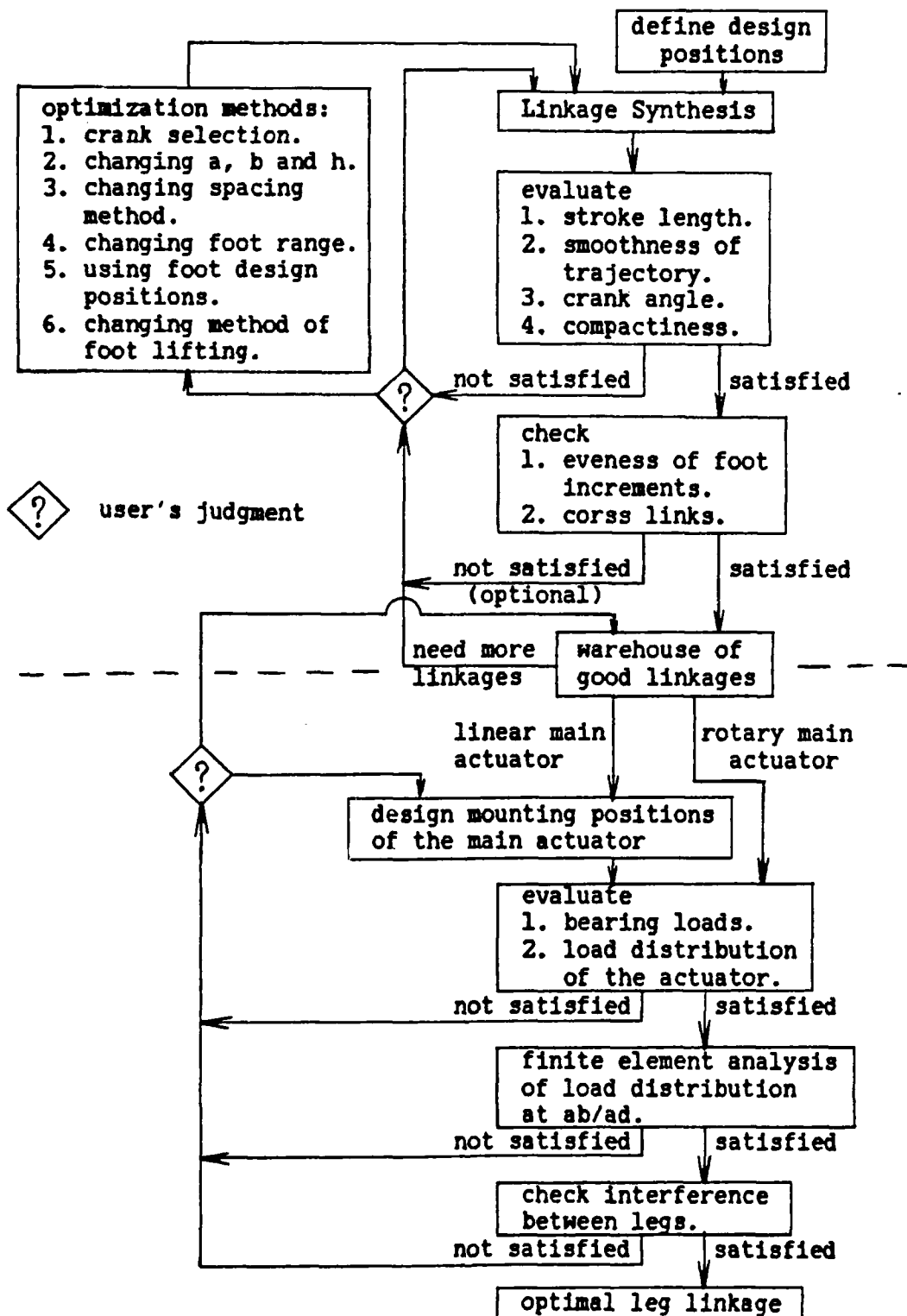


Figure 5.14: Design procedure of a four-bar leg.

few optimal leg linkages are obtained. The design steps in the second step are discussed in the later sections.

In the first major step, the selection of the leg linkage is based on six factors listed below in descending order of importance.

1. The available stroke length.
2. The smoothness of the foot trajectory.
3. The crank rotation angle.
4. The compactness of the leg.
5. The evenness of foot increments for constant crank angle increments.
6. The absence of crossed positions of the two cranks.

The first four factors must be controlled to meet the design specifications. The last two are preferable if they can be obtained without sacrificing the first four factors.

The requirement of stroke length in both horizontal and vertical directions was defined in Section 5.3.1. The foot trajectory is expected to be the smoother the better for the sake of good efficiency. A one inch vertical variation of the foot path in support phase was considered to be acceptable. If the main driver is linear, the crank rotation angle is directly related to its mechanical efficiency. The crank angle should not exceed 120° in one cycle and, in order to maintain a good transmission angle, the portion of the crank rotation which corresponds to support phase should not exceed 100° . The compactness of the leg in the longitudinal direction should be such as to avoid any interference between legs. The compactness in the vertical and lateral directions should be such that the vehicle does not exceed

its dimension limits. More even foot increments mean that the crank rotates at a more constant speed. This is important in equalizing the hydraulic flow rate of the main actuator. The crossed positions of the cranks should be avoided if possible because increased thickness of the leg may be needed to avoid interference.

In order to have an optimal four-bar leg, several methods were used to optimize the leg linkages obtained from RECSYN. The following describe the most effective techniques used in this optimization.

5.3.3.1 Crank Selections

Crank selections in linkage synthesis strongly affect the leg performance. Figure 5.15 is a duplication of Figure 5.6. Theoretically speaking, any point on the solid curve segments and outside the hatched area can be selected as the second circle-point to form a four-bar linkage. However, experience showed that only selections on the solid curve segment to the right of the first circle-point and between the two dashed-dotted lines may result in good leg linkages. The reasons for this conclusion are given below.

Any selection on the curve above the first center-point would result in a violation of the leg height limit. Hence, the upper dashed-dotted line is the upper limit of circle-point for crank selection. Any selection on the curve lower than the design positions results in a very long crank length, and the solution linkage has both compactness problems and interference problems between the links and the ground due to too low a position. Hence, the lower dashed-dotted line is the lower limit of the crank selection. In the region between

the two dashed-dotted lines, the selection on the lower part of the curve segment to the left of the first circle-point still results in linkages with compactness problems. Selection on the upper part of the same segment results in a crank rocker with a short driving crank. The compactness of the solution linkage is roughly acceptable. (The corresponding center-point is at the upper left corner relative to the selected circle-point, and it may be slightly higher than the upper dashed-dotted line.). However, the length of the coupler becomes very long and a very large crank angle ($\geq 180^\circ$) is required because the linkage type is always crank-rocker. Since a linear main actuator is eventually proposed, requiring a crank angle which is less than 120° , the selections in this area are still unacceptable.

The selections on the solid curve to the right of the first circle-point and between the two dashed-dotted lines result in two types of linkages: a crank-rocker and a non-Grashof double-rocker. Selection close to the first circle-point results in a crank length similar to the first crank and the solution linkage is a non-Grashof double-rocker. When the selection is moved farther from the first circle-point, the crank length becomes shorter. After the selection passes a break point, the solution linkage becomes a crank-rocker. Three points on the solid curve in this region are selected to examine the difference in leg performance. One point is close to the first circle-point, the second point is close to the break point and the third point is to the right of the break point. These three points are marked as 1, 2 and 3 in Figure 5.15, respectively. The foot

Figure 5.15: Crank selections in RECSYN.

trajectories of these three leg linkages are generated by FORBAR and are shown in Figures 5.16, 5.12 and 5.17, respectively. The output data of these leg linkages are examined and the characteristics of each leg are tabulated below.

From Table 5.3, the leg width and the crank angle increase as the selected point moves away from the first circle-point. Case 1 has the minimum leg width and crank angle. Case 2 has the maximum stroke. Case 3 has the minimum variation in foot trajectory. Later, interference study show that the leg width should be less than 4 feet in order to avoid interference between the legs. Hence, the selection should be in the neighborhood of point 1. The smooth footpath strokes are less than 4 feet in all three cases. Therefore, the limited variation stroke should be used in the leg design.

Table 5.3

Characteristics of legs obtained by different crank selections.

Case	Leg Width*	Stroke	Vertical Variation	Crank Angle	Smooth Footpath Stroke	Linkage Type
1	3.6'	4.8'	1.0"	78°	3.7'	DR2
2	4.3'	5.5'	1.0"	123°	3.4'	DR2
3	4.6'	4.9'	0.5"	153°	3.6'	CR

* : the longitudinal distance between the two extreme nodes at the first design position.

DR2 : non-Grashof double-rocker

CR : crank-rocker

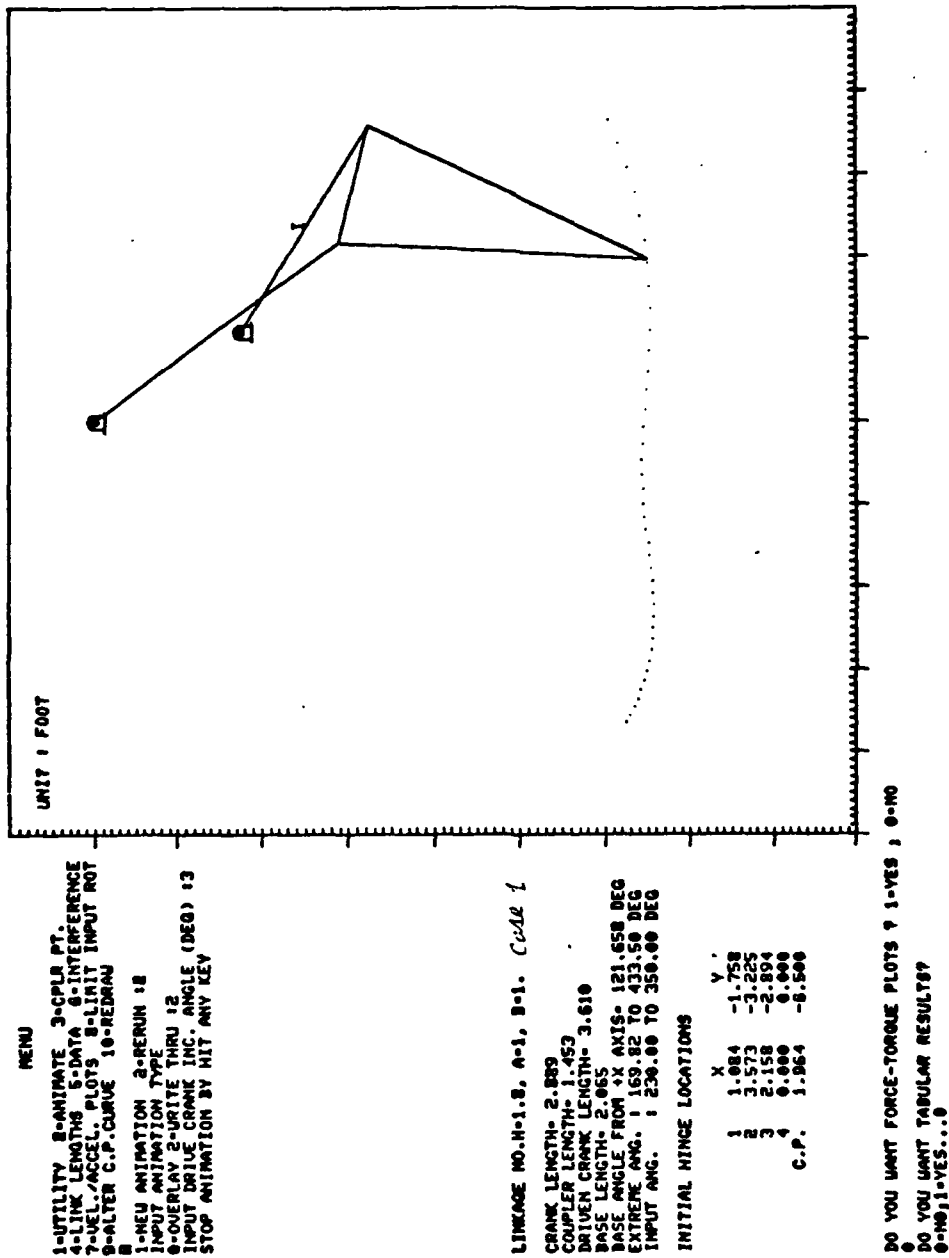


Figure 5.16: Foot trajectory of leg linkage with $h = 1.8$, $a = 1$, $b = 1$, and crank selection case 1.

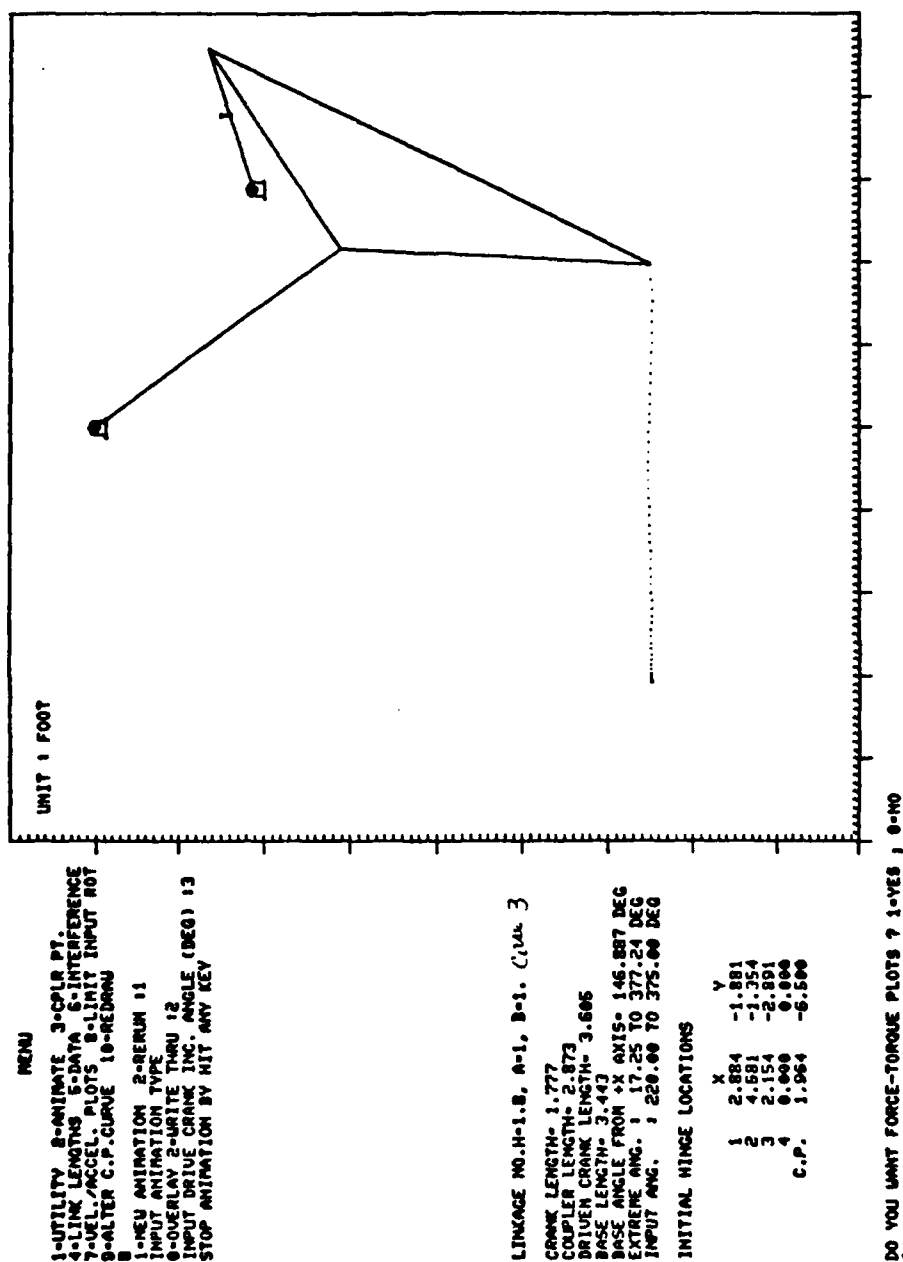
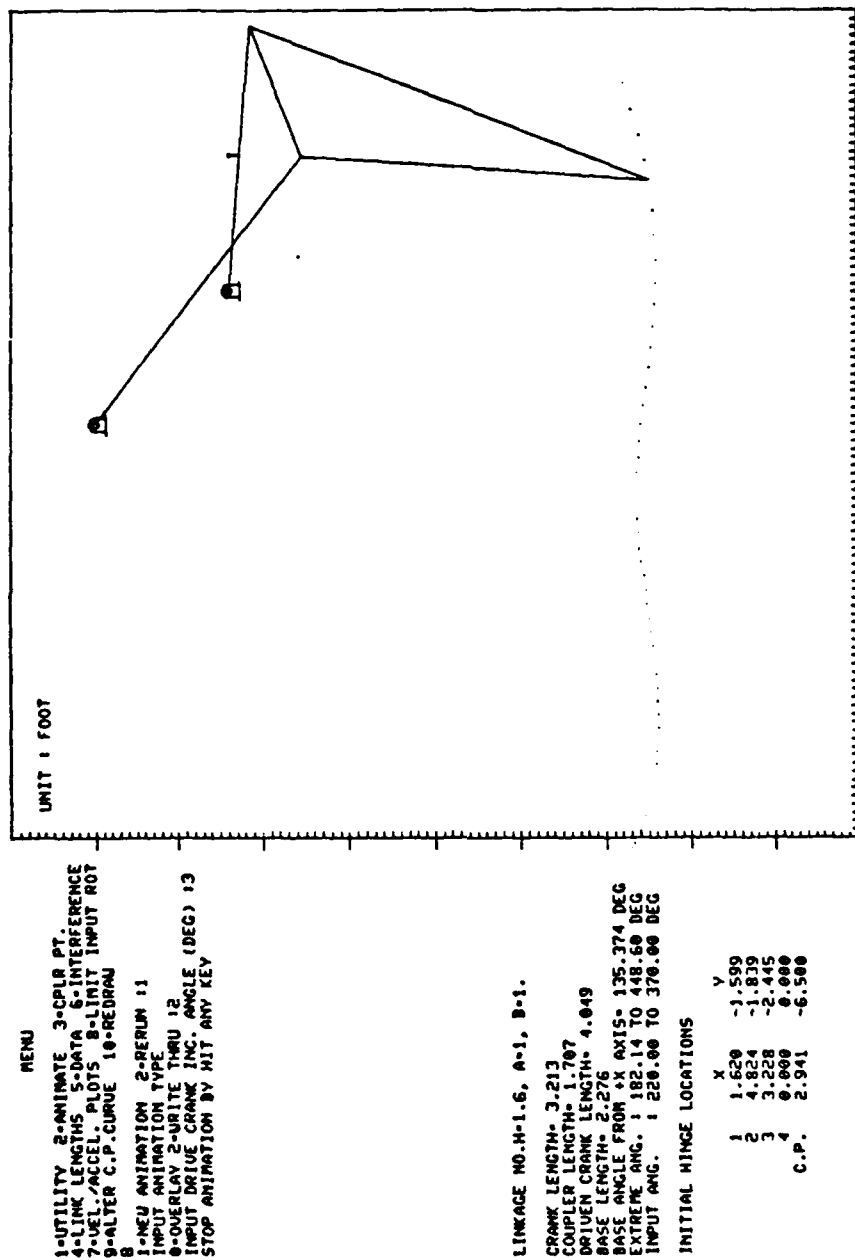


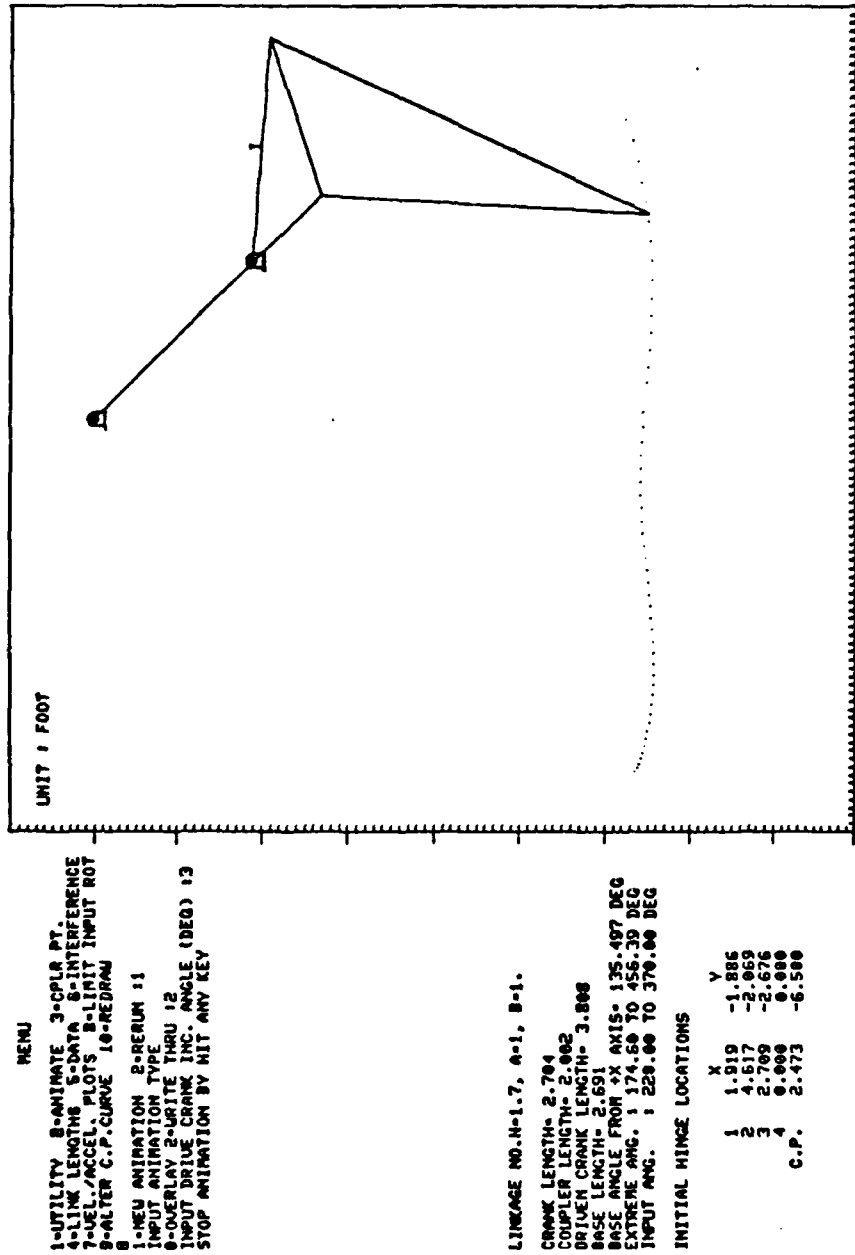
Figure 5.17: Foot trajectory of leg linkage with $h = 1.8$, $a = 1$, $b = 1$, and crank selection case 3.

5.3.3.2 Varying a , b and h

The foot trajectory is dependent on the design positions of the four-bar linkage as well as on the crank selections. The design positions are dependent on the values of a , b and h discussed in Section 5.3.2. The first choice is to let $a = b = 1$ and vary the value of h . The leg height is kept the same. The range of h is from 1.3 to 1.9. RECSYN is used to generate several four-bar linkages for each set of design positions. The breakpoints of non-Grashof double-rocker and crank-rocker solutions move toward the first circle point as h increases. For each case, a selection which results in a similar slope angle of the driving-crank is made. The foot trajectories were generated by the program FOURBAR.

The results show a value of h between 1.6 and 1.9 gives fairly straight line sections. Smaller values of h result in a longer available stroke and in more evenness of foot increments. For larger values of h , the smoothness of the trajectory is better. In all cases, crossing of the cranks can be avoided if a wider linkage is selected. However, because of the width limit of the leg, crank crossing is almost unavoidable. Figures 5.18, 5.19 and 5.20 show the foot trajectories for $h = 1.6$, $h = 1.7$ and $h = 1.9$, respectively. The foot trajectory for $h = 1.8$ has already been shown in Figure 5.12. The characteristics of these leg linkages are tabulated as follows:

Figure 5.18: Foot trajectory of leg with $h = 1.6$.

Figure 5.19: Foot trajectory of leg with $h = 1.7$.

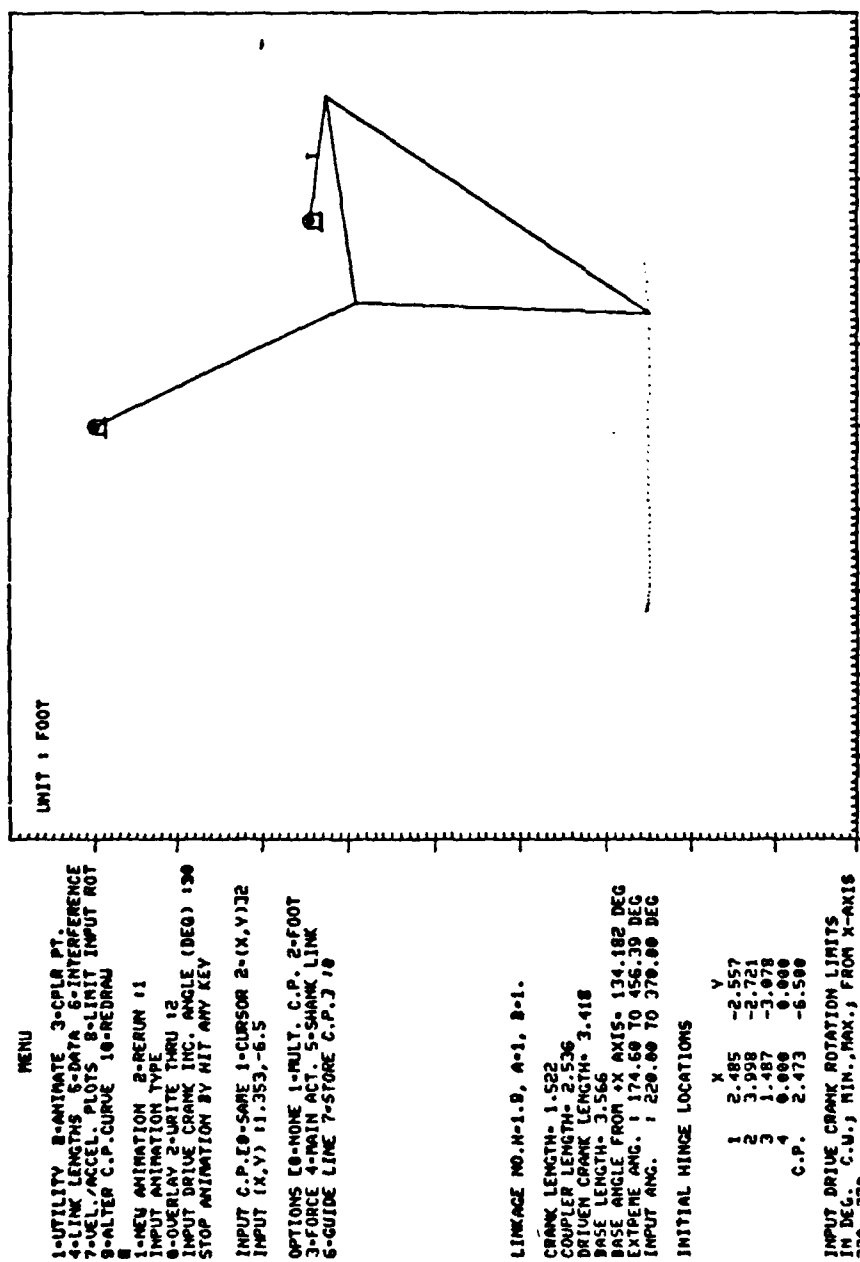
Figure 5.20: Foot trajectory of leg with $h = 1.9$.

Table 5.4

Characteristics of legs with different values of h

h	Leg Width*	Stroke	Vertical Variation	Crank Angle	Smooth Footpath Stroke	Linkage Type
1.6	4.8'	6.9'	1.0"	108°	5.5'	DR2
1.7	4.6'	6.2'	1.0"	114°	4.6'	DR2
1.8	4.3'	5.5'	1.0"	123°	3.4'	DR2
1.9	4.0'	4.2'	0.9"	150°	2.5'	CR

* : the longitudinal distance between the two extreme nodes at the first design position.

DR2 : non-Grashof double-rocker

CR : crank-rocker

Although a smaller value of h has better characteristics in most respects except for leg width. By considering all the aspects of the design specifications of the leg, a value of $h = 1.8$ was selected for further analysis.

The second choice was to leg $h = 1.8$ and vary the proportionality of a to b . Arbitrarily, the sum of the thigh and shank lengths was set to be close to a constant ($a + b \rightarrow 2$). The range of the values of the pair a and b is from $a = 1.3$, $b = 0.6$ to $a = 0.6$, $b = 1.4$. The results showed that the step length increases 9% when the thigh is 2.2 times as long as the shank ($a = 1.3$, $b = 0.6$), and the step length decreases 10% when the shank is 2.3 times as long as the thigh ($a = 0.6$, $b = 1.4$). After tracing the foot trajectories of these legs, it was found that most of these cases do give a good approximation of a straight line. However, because there is no compelling reason to make the length of the thigh different from that of the shank, $a = b$

has been retained in the basic design.

5.3.3.3. Varying Spacing Angles

One other method of redefining the design positions is to use a different spacing approach to Chebychev spacing in Equation (5.14). For instance, a pair of spacing angles, 0° and 50° , can be substituted into Equation (5.14) to obtain a new set of design positions. By this spacing method, the first two and the last two design positions are shifted toward the two end points of a full step. Since the two lower extremes of a foot trajectory are between positions 1 and 2 and positions 3 and 4, respectively, this new set of design positions should result in a longer smooth footpath stroke. The following are a set of knee design positions with spacing angles of 0° and 50° . One of the solution linkage generated from this set of design positions with its foot trajectory is shown in Figure 5.21. The characteristics of this leg linkage are: 4.6 foot smooth footpath stroke, 4.46 inch variation, 102° crank angle and 4 foot leg width. Comparing this data to that of Table 5.3 shows that the smooth footpath stroke is improved significantly. However, the price of this improvement is a large vertical variation.

Table 5.5

Design positions with $a = 1$, $b = 1$, $h = 1$,
and spacing angles of 0° and 50° .

Position	X	Y	θ
1	2.167	-2.889	-90.000°
2	2.035	-2.983	-103.094°
3	-0.032	-3.611	-126.866°
4	-1.573	-3.250	-115.859°

AD-A159 147

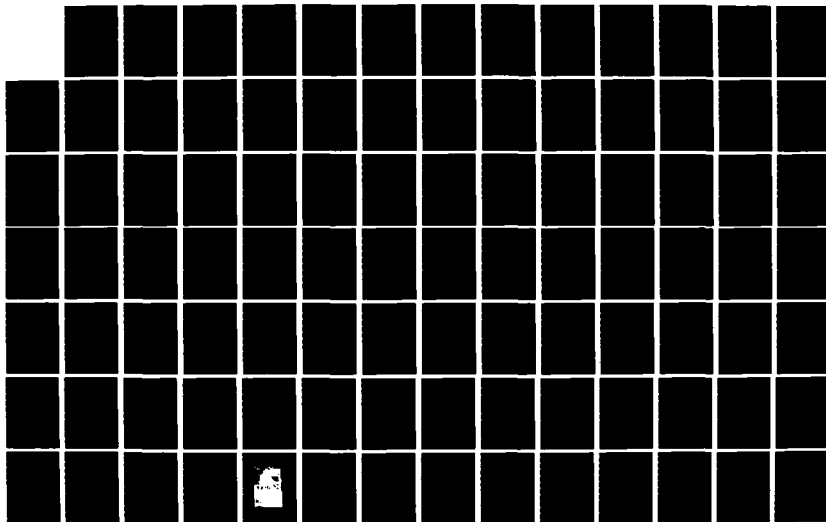
AN EXPERIMENTAL STUDY OF AN ULTRA-MOBILE VEHICLE FOR
OFF-ROAD TRANSPORTAT. (U) OHIO STATE UNIV RESEARCH
FOUNDATION COLUMBUS R B MCGHEE ET AL. MAY 85
MDA903-82-K-0058

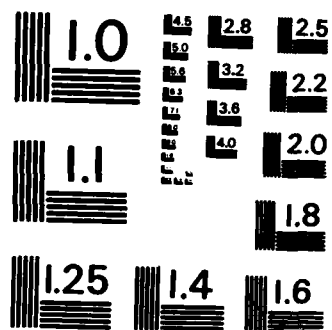
4/5

UNCLASSIFIED

F/G 13/6

NL





MICROCOPY RESOLUTION TEST CHART
NATIONAL BUREAU OF STANDARDS-1963-A

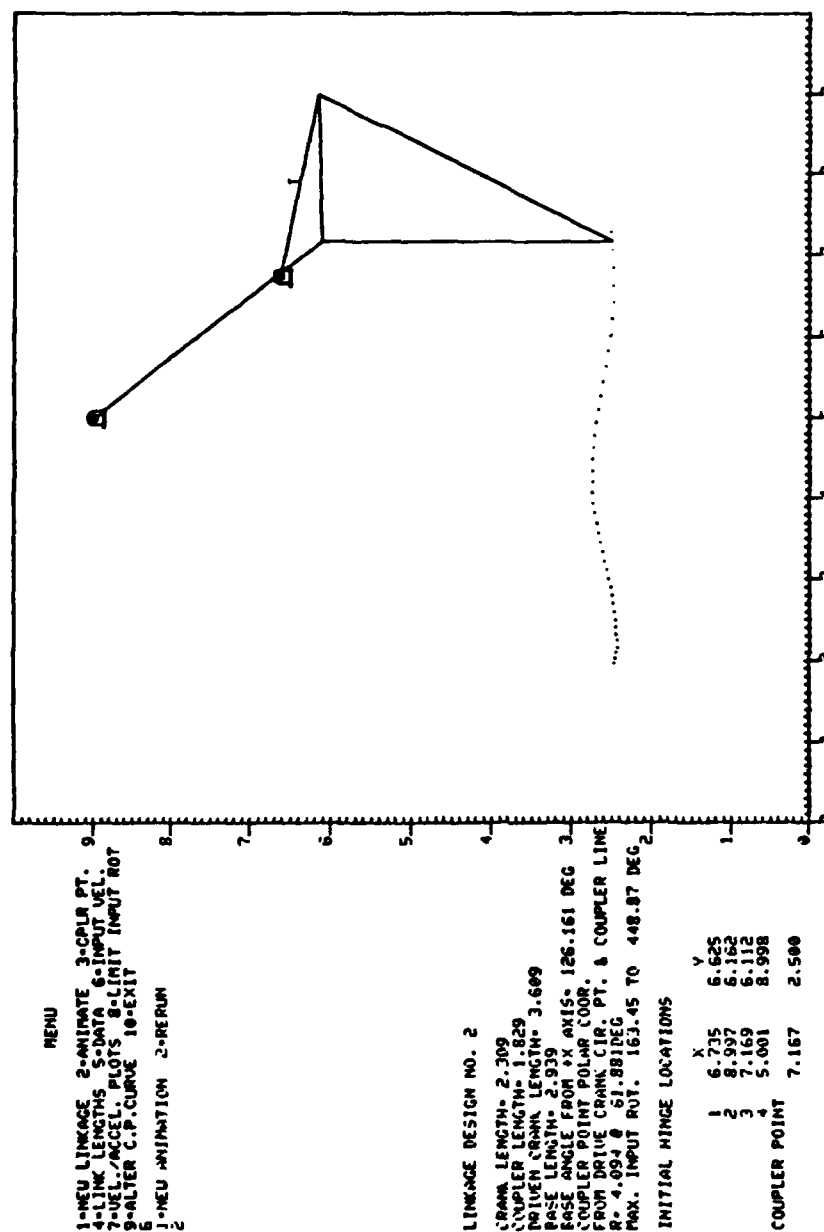


Figure 5.21: Foot trajectory of the leg linkage generated from design positions with spacing angles of 0° and 50° .

5.3.3.4 Varying the Beginning and the End of a Full Step

The beginning and end of a full step shown in Figure 5.4 may be changed. A shorter full step usually results in a smoother trajectory between the two end points of the defined step. However, the trajectory outside those two end points will vary quickly, and the price of a shorter stroke has to be paid. Hence, if the stroke length is long enough, this method can be used to improve the smoothness of trajectories. For instance, the smoothness of the trajectory of the case of $h = 1.6$ (see Figure 5.18) can be improved by this method.

5.3.3.5 Using Foot Design Positions

The design positions used in the previous sections are knee design positions. In the design procedure, only one crank, the driving-crank, is selected by the designer. As mentioned in Section 5.3.2.1, foot design positions can also be used for linkage synthesis. The two obvious advantages of this approach are that both cranks are selected by the designer and the design positions can be modified directly according to the resulting trajectory and improve the foot trajectory. Figure 5.22 shows a solution linkage obtained by specifying foot design positions. The approach to improvement of a trajectory by using modified foot design positions is demonstrated in the following example.

The trajectory in Figure 5.21 has a bump in the middle. This bump can be smoothed by adjusting the foot design positions according to the following two methods. The first method is to move the second and third design positions toward the center. The second is to move these two design

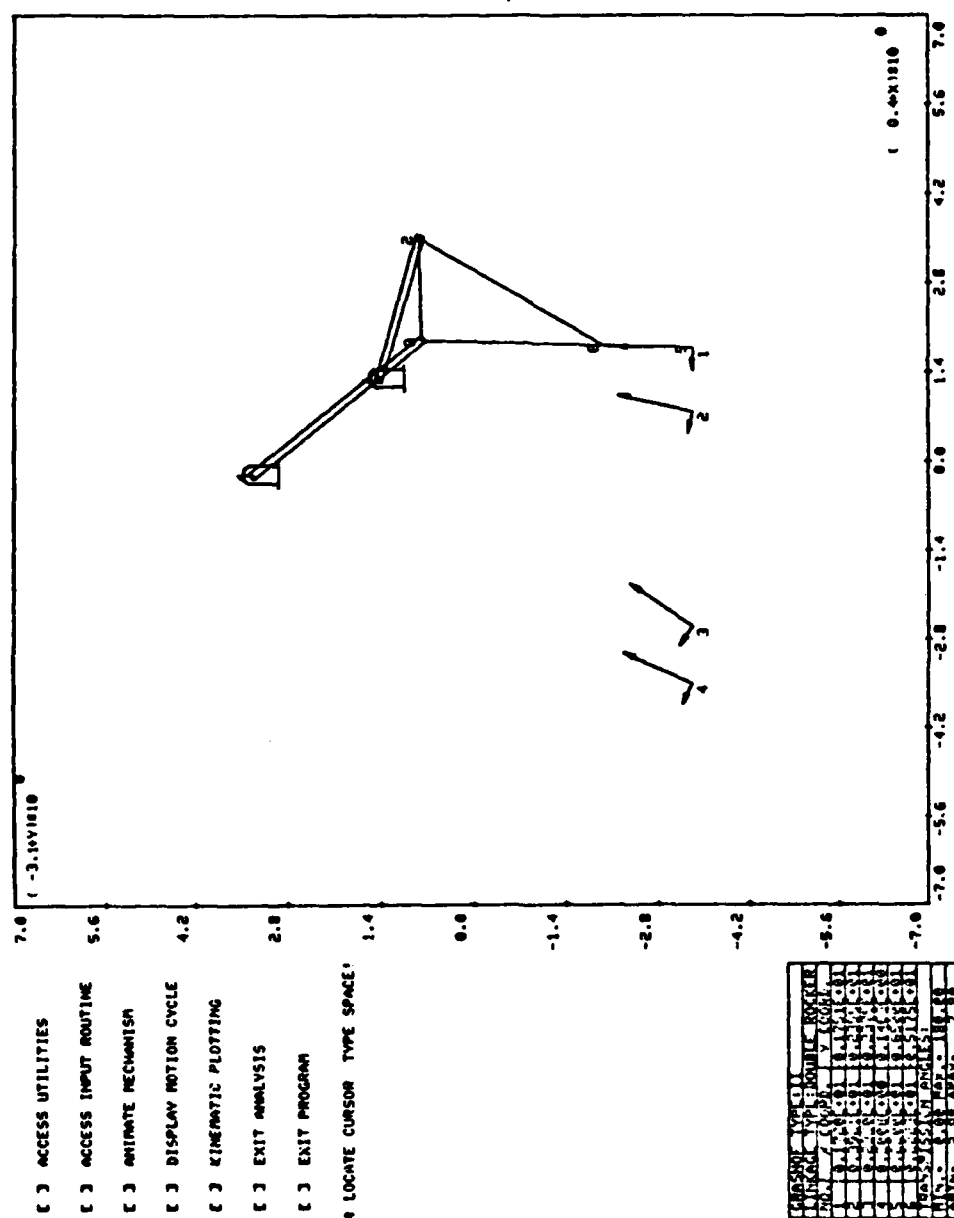


Figure 5.22: Foot trajectory of a leg linkage design by foot design positions.

positions downward. Both methods will result in a reduced smooth footpath stroke. The second method is used in this example. After both of the two central design positions were moved down by 0.07 feet, the set of foot design positions corresponding to Table 5.5 was obtained and is tabulated below. The resultant solution linkages have much less variation than the original one. One of the leg linkages with its trajectory is shown in Figure 5.23. The characteristics of this leg linkage are: 3.6 foot leg width, 4.55 stroke length, 0.45 inch variation, 3.17 foot smooth footpath stroke, and 96° crank rotation angle. The smoothness of this trajectory is remarkably good. If a one inch variation is used, the stroke length becomes 5.3 feet and the crank angle becomes 124° . This leg meets all the design specifications for a 4-foot stroke four-bar leg except that the smooth footpath stroke is reduced significantly after modification. This is the reason that the concept of smooth footpath stroke is eventually given up.

Table 5.6

Foot design positions according to Table 5.5, the two central design positions are moved down by .07 feet.

position	X	Y	θ
1	2.167	-6.500	89.8°
2	-1.217	-6.570	76.9°
3	-2.199	-6.570	53.1°
4	-3.148	-6.500	64.1°

5.3.3.6 Vertical Leg Stroke

At the end of the support phase, the foot is lifted and returned to the initial position without touching the ground. A very small

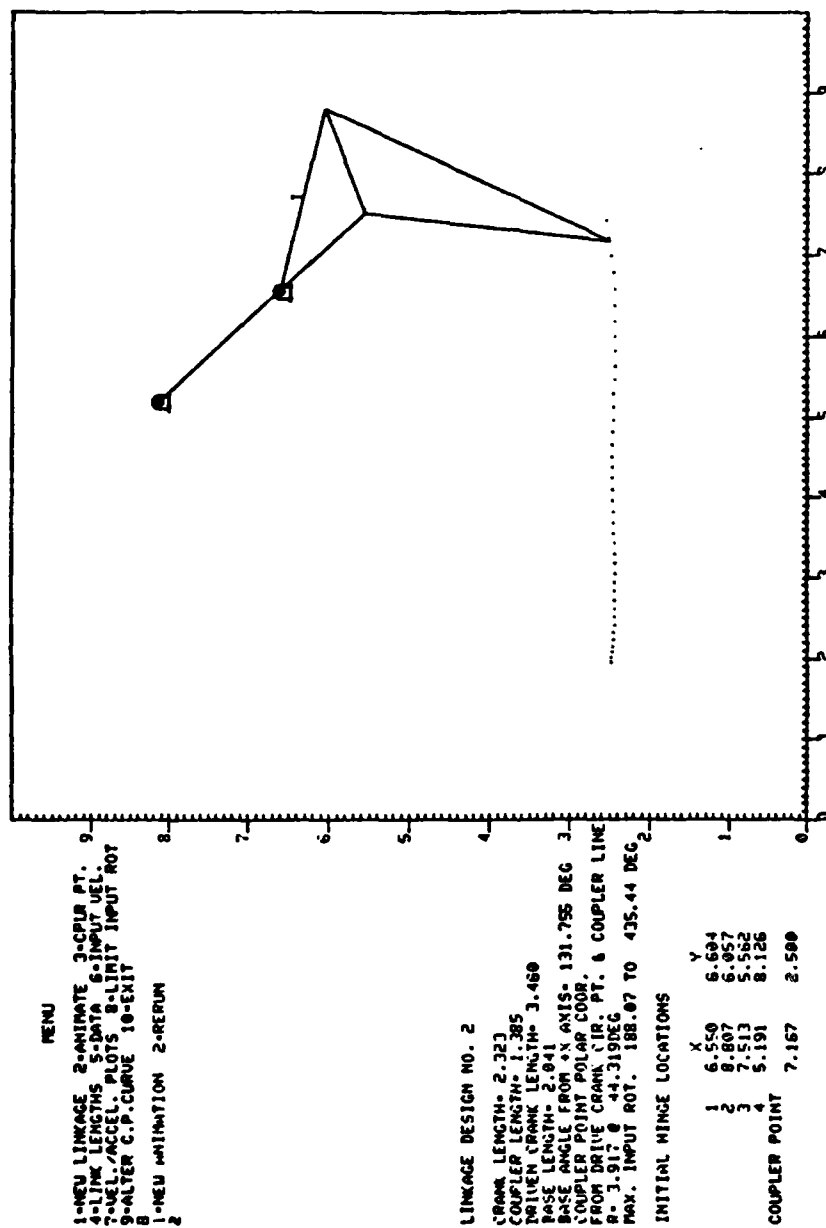


Figure 5.23: Foot trajectory obtained from the modified foot design positions.

vertical stroke should satisfy this leg motion. When a leg steps on a hump or a depression, the walking height of that leg is different from the other legs. The foot trajectory of this leg should still be an approximation of a straight line so that the overall mechanical efficiency will not be substantially degraded. Hence, foot points within the range of vertical stroke should generate a set of appropriate straight lines which are parallel to the original foot trajectory. The vertical stroke was selected to be two feet in order to walk in rough terrain. After the mobility requirements of the ASV were set, the requirement for vertical stroke became four feet in order to pass major obstacles. Different approaches were developed in order to provide different vertical strokes.

There are three simple methods to vary the walking height of a leg. One method is to vary the driving-crank length. The second is to vary the driven-crank length. The third is to vary the shank length. The foot trajectory of several sample legs with varying walking heights were studied using all three methods.

The first and the second methods gave similar results. After one crank is shortened or lengthened, the foot trajectory becomes closer to, or farther from the two fixed pivots. If the change of crank length exceeds some limit, the trajectory is altered and no longer approximates a straight line. Figures 5.24 and 5.25 show two examples of foot trajectories generated by leg linkages with a variable driving-crank and with a variable driven-crank, respectively. The vertical range in which a foot point generates an acceptable foot trajectory is about 15%

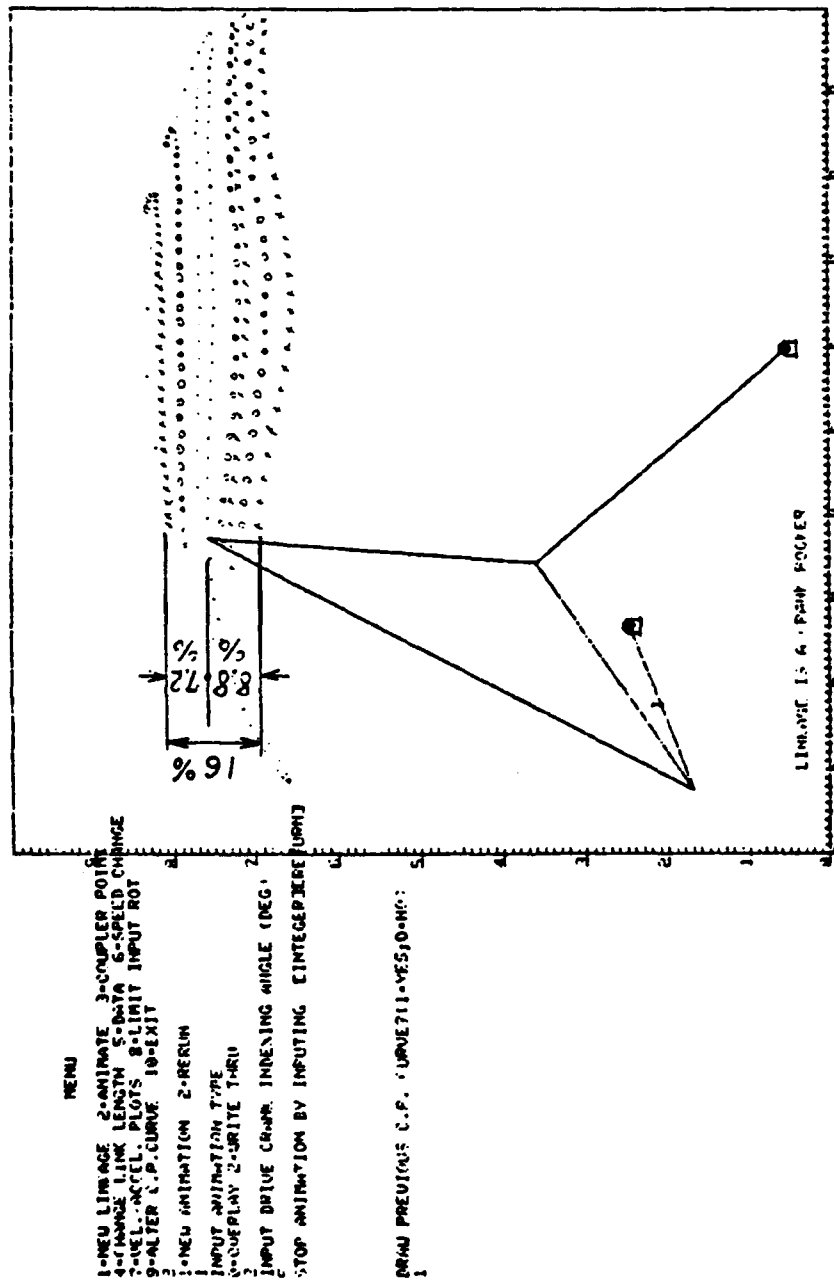


Figure 5.24: Foot trajectories of a four-bar leg with variable driving-crank.

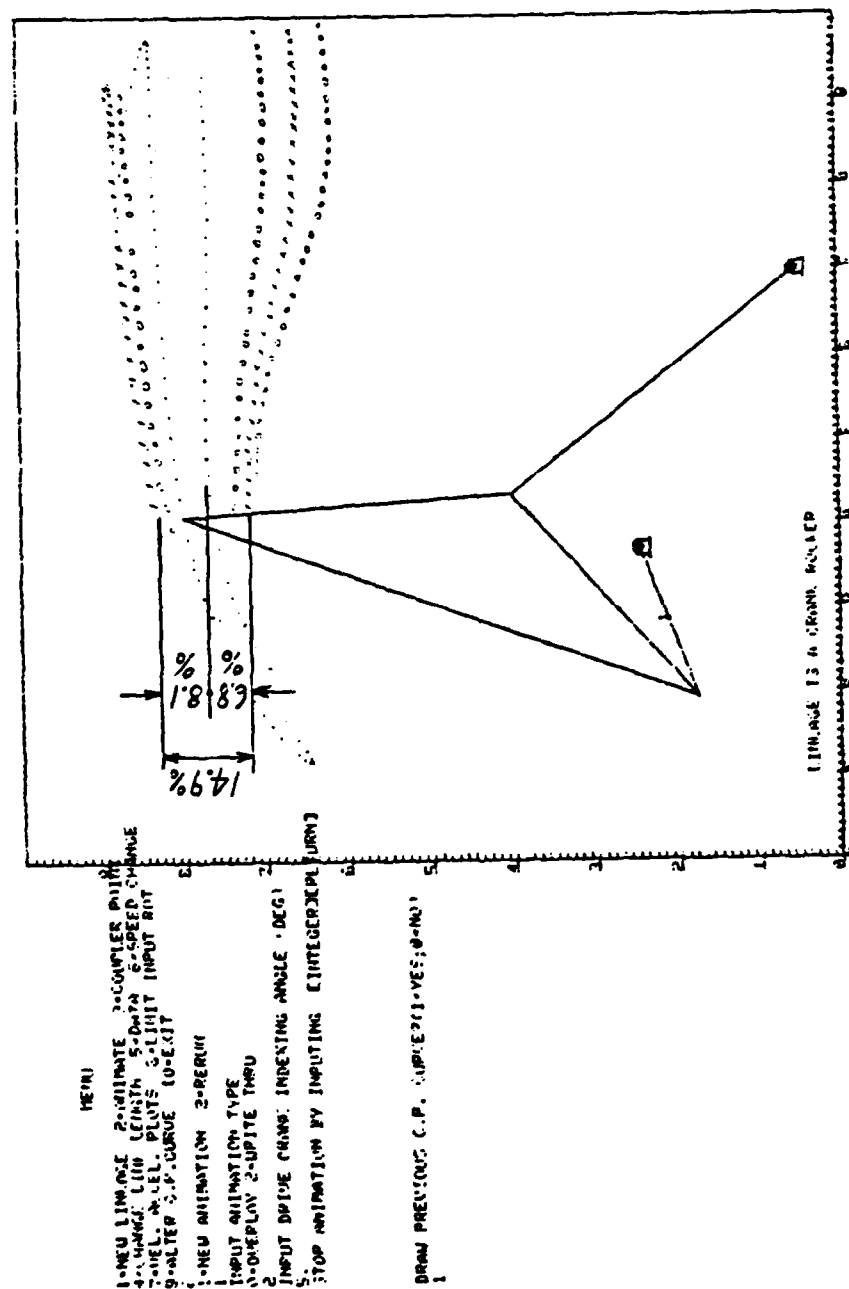


Figure 5.25: Foot trajectories of a four-bar leg with variable driven-crank.

of the leg height. For a 6.5 foot leg, the available vertical stroke is only 1 foot. Hence, methods of varying a crank are only good for walking in smooth terrain.

The third method generates good trajectories in a much wider range of vertical strokes. Many coupler-point curves of the coupler points in different walking heights were generated by FORBAR. It was found that coupler points which generate good trajectories are in the neighborhood of a straight line. Figure 5.26 shows an example of foot trajectories generated by this method. In this case, the straight line on which a coupler point will generate good trajectories is inclined at about 20° relative to the vertical at the specified position. Hence, if a linear actuator is attached to the coupler and aligned with this straight line, a wide range of vertical stroke is obtained. The range of vertical stroke which generates good trajectories can be as wide as 90% of the leg height.

If a two foot vertical stroke is required, a leg linkage attached with a two foot linear actuator on the coupler would provide it. If a four foot vertical stroke is required, a four foot linear shank actuator can still generate a satisfactory walking volume. However, it was found not to be practical from the mechanical design point of view. This impracticality leads to the design of a seven-bar leg in which the linear shank actuator is replaced by a four-bar shank linkage. The reasons that the slide design is not satisfactory will be discussed in the section on seven-bar leg design.

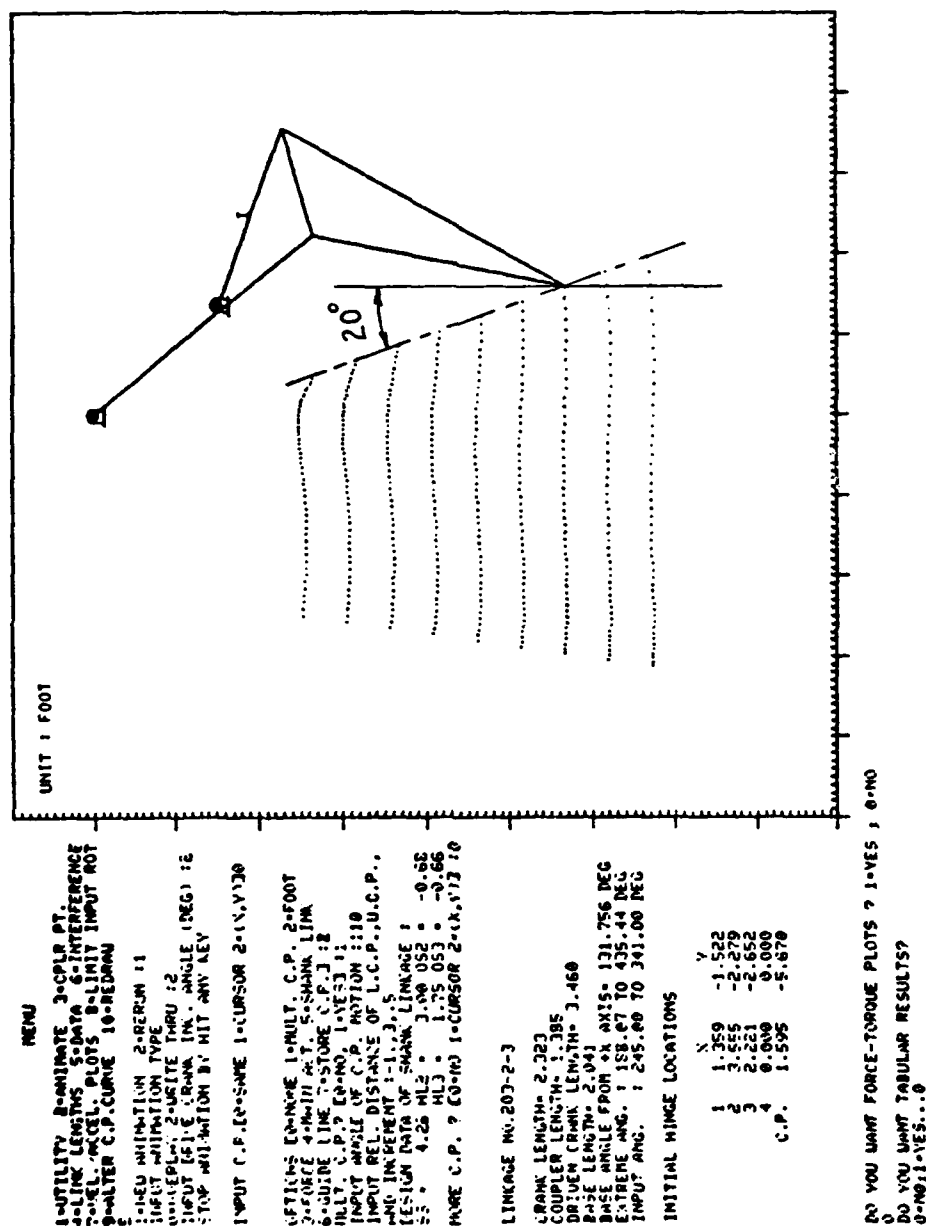


Figure 5.26: Foot trajectories of a four-bar leg with variable shank.

5.3.4 Bearing Loads, Actuating Torque and Mounting Positions of the Main Actuator

If the main actuator is a rotary actuator, there are two moving bearings and two fixed bearings in a four-bar leg. In the program FORBAR, the crank angle θ is incremented by a small number and the positions of the pivot points and foot point are calculated for each crank angle. For each leg position, the bearing loads and the actuating torque can be calculated as follows.

Due to low speed motion and small weight of the link member relative to the vehicle weight, the following assumptions can be made:

1. The friction in the bearings is negligible.
2. The inertial forces due to leg segment or body movements are negligible.
3. Leg weight can be lumped into the body weight.

The free body diagrams of the leg links are shown in Figure 5.27.

Applying static equilibrium to the coupler gives

$$F_{ey} \cdot |X_e - X_b| + F_{ex} \cdot |Y_e - Y_b| + F_{cy} \cdot |X_c - X_b| + F_{cx} \cdot |Y_c - Y_b| = 0 \quad (5.15)$$

$$F_{cy}/F_{cx} = \tan \phi \quad (5.16)$$

$$F_{ex} + F_{cx} + F_{bx} = 0 \quad (5.17)$$

$$F_{ey} + F_{cy} + F_{by} = 0 \quad (5.18)$$

Since F_{ex} and F_{ey} are known, F_{cx} and F_{cy} can be calculated from the

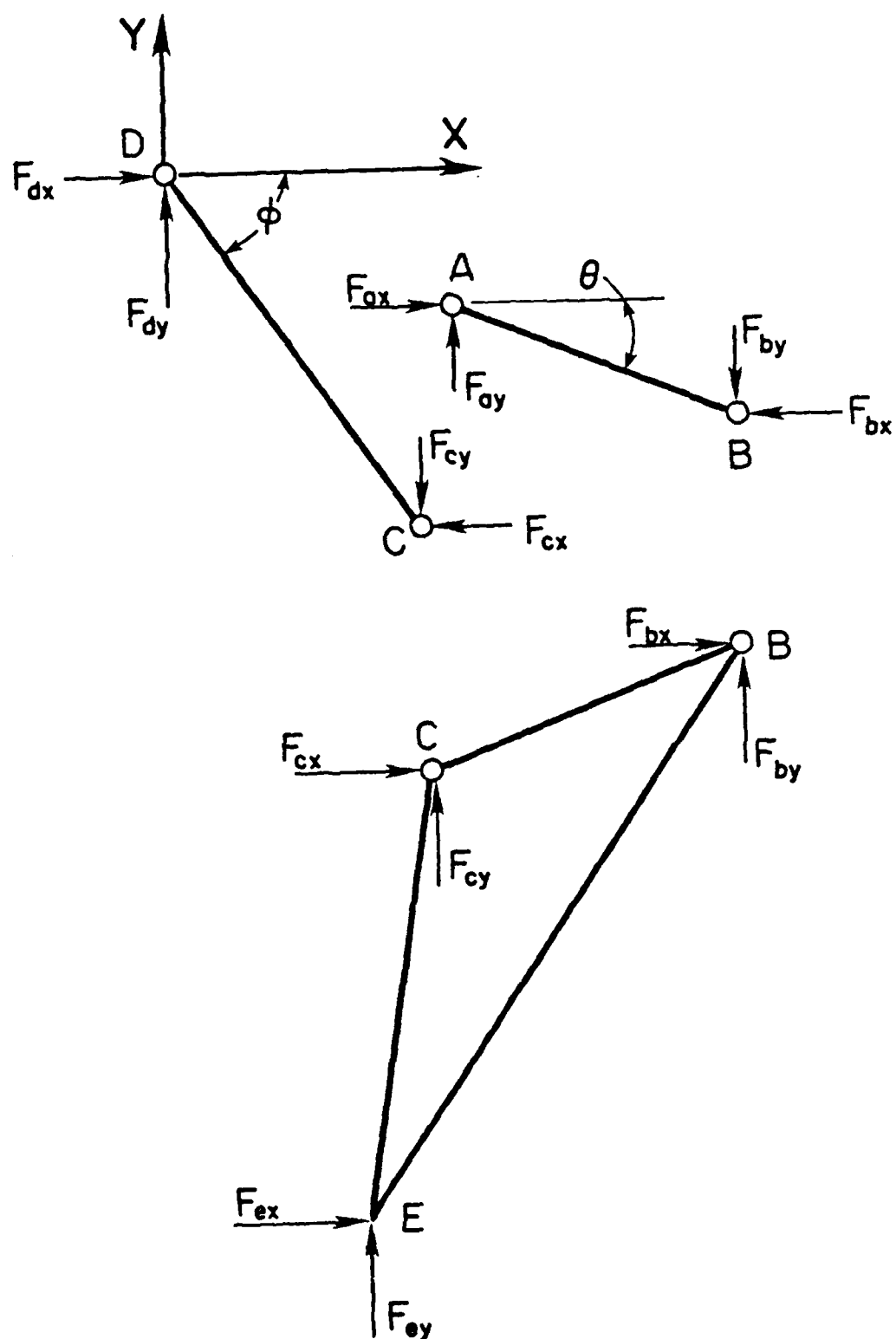


Figure 5.27: Free Body diagrams of a four-bar leg.

first two equations. The resultant force at C is the bearing load at C. The bearing load at D is opposite in direction and has the same magnitude as the bearing load at C. By substituting F_{cx} and F_{cy} into Equations (5.17) and (5.18), F_{bx} and F_{by} can be solved for. The resultant force is the bearing load at B. The bearing load at A is opposite in direction and has the same magnitude as the bearing load at B. The actuating torque T_a can be found by solving the following equation.

$$T_a - F_{bx} \cdot |Y_b - Y_a| - F_{by} \cdot |X_b - X_a| = 0 \quad (5.19)$$

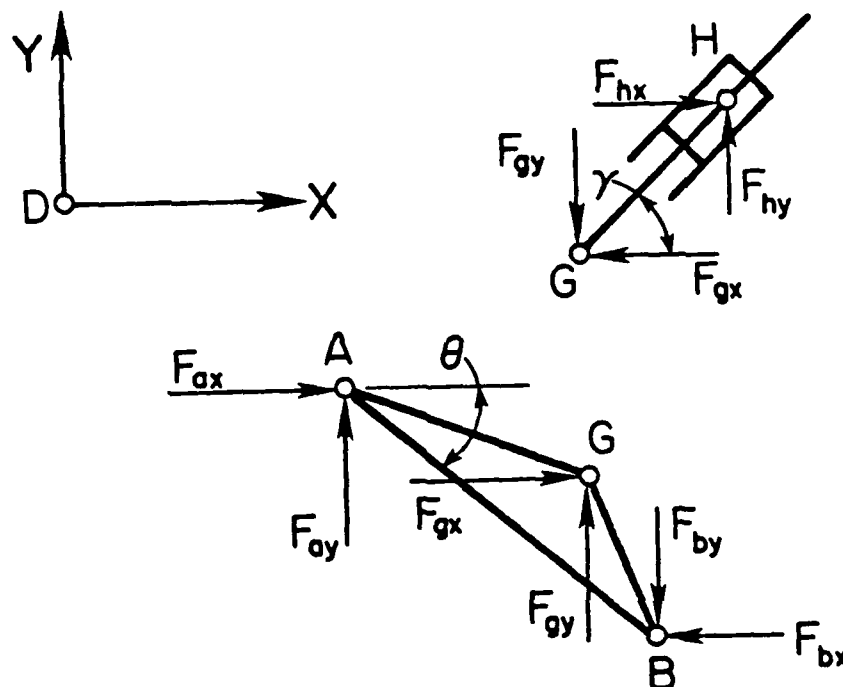


Figure 5.28: Free body diagram of the driving crank with linear actuator.

Figure 5.29 shows an example of the actuating torque of an four-bar leg in one step. The maximum actuating torque is at the level of 17,000 inch-pounds. Since the weights of commercial rotary actuators capable of this torque are too large to be acceptable, a linear actuator is selected as the main actuator.

The mounting positions of the linear actuator are selected according to the compactness requirement and the load distribution over a step. An even load distribution is desirable because it gives the least energy waste, especially when a constant pressure hydraulic power source is used. The bearing loads and the actuating force are calculated as follows: from Figure 5.28, applying static equilibrium gives

$$F_{by} \cdot |X_b - X_a| + F_{bx} \cdot |Y_b - Y_a| + F_{gy} \cdot |X_g - X_a| + F_{gx} \cdot |Y_g - Y_a| = 0 \quad (5.20)$$

$$F_{gy}/F_{gx} = \tan \gamma \quad (5.21)$$

$$F_{bx} + F_{gx} + F_{ax} = 0 \quad (5.22)$$

$$F_{by} + F_{gy} + F_{ay} = 0 \quad (5.23)$$

The load at pivot G can be found by solving equations (5.20) and (5.21). The resultant force is the bearing load at G and also the actuating force. Substituting these values into equations (5.22) and (5.23), F_{ax} and F_{ay} can be found. The resultant force is the bearing load at A. The stroke of the linear actuator is the length difference of GH at the two extreme positions in one cycle.

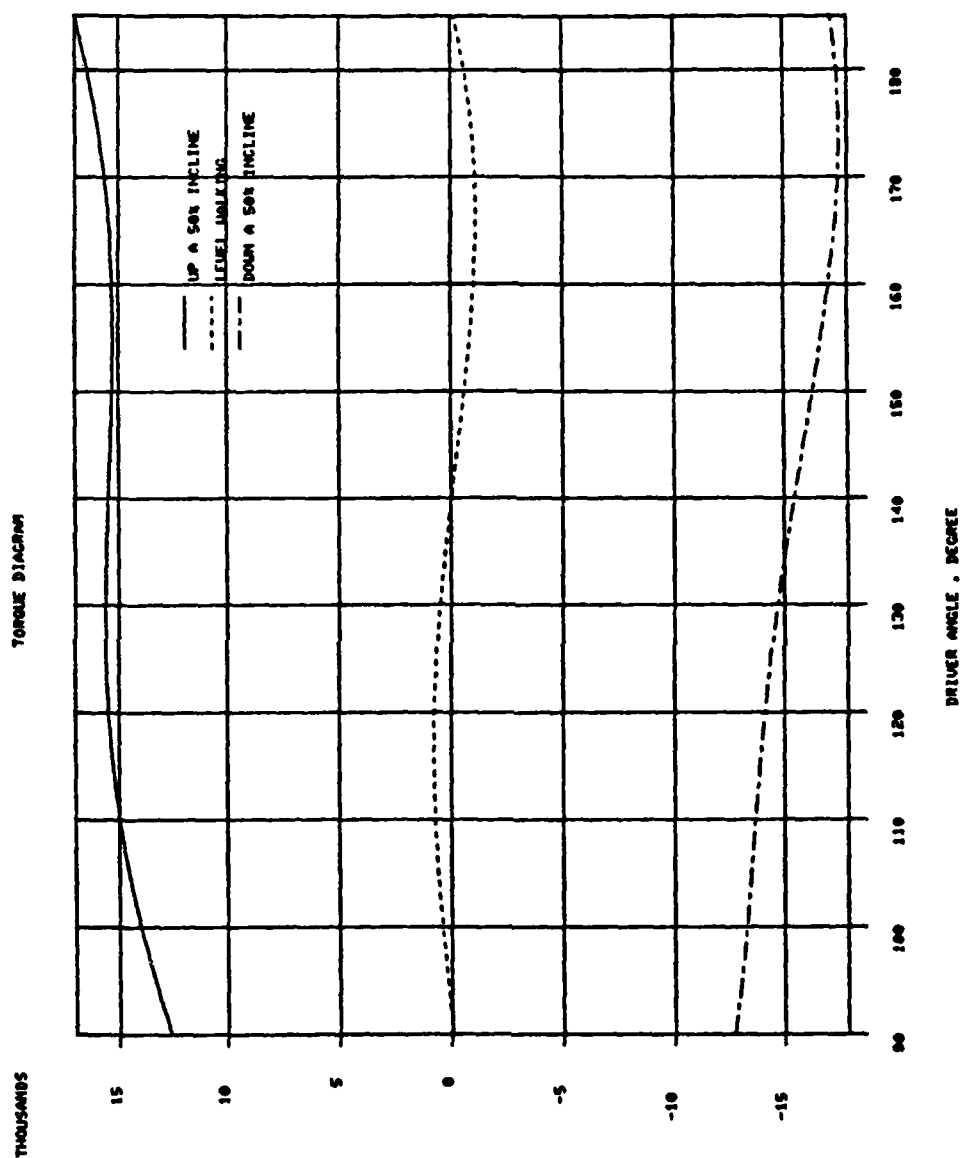


Figure 5.29: Actuating torque of a four-bar leg in one step.

In the program FORBAR, two mounting positions can be selected interactively by either keyboard or cursor. The bearing loads and the actuating force in one step are then calculated. By the method of trial and error with the help of experience, a set of optimal mounting positions can be located. If none of the mounting positions is satisfactory, a new leg linkage should be used.

5.3.5 Interference

After the leg linkage and mounting positions of the main actuator have been determined, the critical positions of the two adjacent legs during walking are studied by a graphical method. If any interference occurs, actions such as changing the leg linkage and/or mounting positions are taken to eliminate this problem. Figure 5.30 shows the critical positions of the leg linkage in Figure 5.23 with an optimal mounting position of the main actuator. The knee joint of the rear leg may interfere with the shank of the leg ahead of it. Hence, the stroke pitch should be extended to 5.4 feet in order to avoid this interference. The leg width of this linkage is 3.6 feet. Experience shows that leg linkages with a leg width greater than 3.5 feet have little chance of avoiding such interference. This interference study can also be done in FORBAR.

5.3.6 Abduction and Adduction

In order to change the direction of the walking machine, the leg should be able to swing laterally or, using biological terminology, to adduct and abduct. One easy way to do this is to mount the entire leg

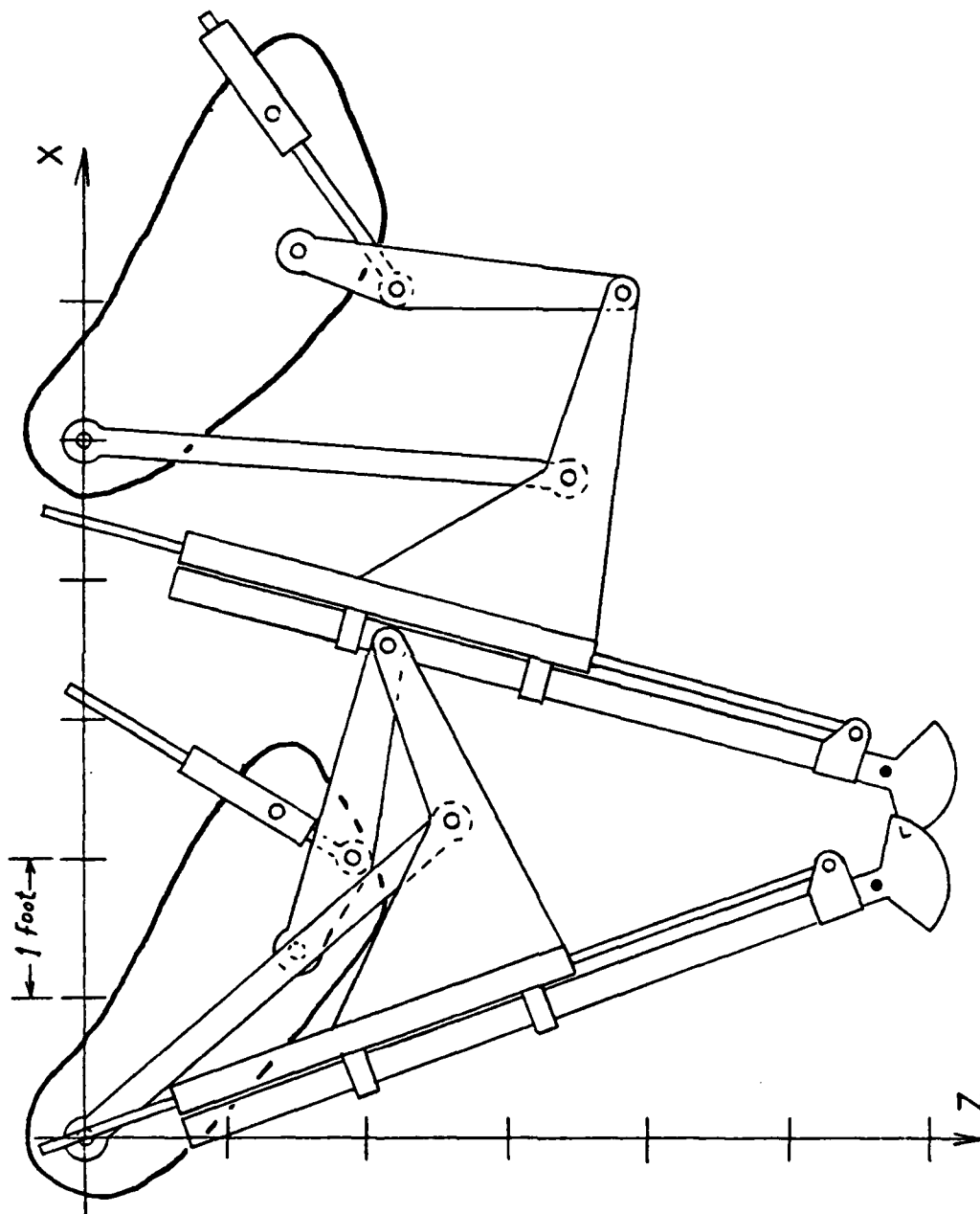


Figure 5.30: Interference study of a pair of four-bar legs, the three foot stroke of the shank is strengthened by a slide mechanism.

on a member which is mounted on a longitudinal horizontal hinge on the frame of the body. A linear actuator is then used to rotate this member inward or outward. The positions of the hinged axis and the linear actuator depend on the body structure of the ASV. However, the rotation angle for abduction and adduction should not be excessive because of the resulting large bending moments on the leg links and slide mechanisms.

The bearing loads when the leg is abducted or adducted are different from those when the leg is standing vertically. Since lateral deflection of the links is significant at abduction and adduction, and since the load distribution is very sensitive to the lateral distribution, the load distribution on each joint can not be solved for analytically. In this case, a finite element program is required to calculate the load distribution.

A finite element program SUPERB⁷ was used for this analysis. Models of the four-bar leg at five critical positions were made of space beam elements. These five critical positions are the four corners of the walking envelope and the normal position. The detailed information of one of the models, the input file and the results of the analysis are shown in Appendix C. These results were reviewed by the engineer who did the design of the mechanical parts of the leg. If any load is found to be excessive, the leg has to be redesigned.

⁷ SUPERB is a product of the Structural Dynamics Research Corp., Milford, Ohio.

A maximum crank angle of 20° in both abduction and adduction was found to be acceptable in both load distribution and lateral stroke. The mounting and the selection of the lateral actuator should provide both the required stroke and the actuating force.

5.4 Design of a seven-Bar Leg

As mentioned in Section 5.3.3, a four foot vertical stroke was required in order to satisfy the mobility requirement of the ASV. The vertical stroke can be obtained by attaching a linear shank actuator to the coupler of the four-bar leg. It was also pointed out that such an arrangement was not practical from the mechanical design point of view. The reasons for this are that this long shank actuator, at least four feet in stroke, raises two problems: mechanical strength and the compactness.

The foot should bear the shock load which results when it kicks any obstacle during walking. The load condition at this time is like a long and slim cantilever beam struck by a heavy shock load. This load condition becomes even more serious when the shank actuator is fully extended. Hence, excessive care is needed in designing this linear actuator. The shank should be as light as possible because it strongly affects the inertia of the leg, and hence the energy efficiency. Under this constraint, the design of the shank actuator becomes difficult.

In order to have good actuator control, a double ended actuator is required. For a 4-foot linear actuator, a 13-foot space is needed for full extension and contraction. Obviously, this length is too

long for the ASV. Figure 5.31 shows an overall arrangement of the ASV with four-bar legs. It appears that the legs are too bulky. Remember that the stroke of these legs is 4 feet with no overstroke between legs. Later, the results of gait analysis showed that a 6 foot stroke was preferable and overstroke between legs was required. The legs should be magnified by a factor of 1.5 in order to have 6 foot stroke. Therefore, the compactness of the legs becomes a serious problem.

Both problems mentioned above indicate that different mechanisms should be designed to replace the long shank actuator. Fortunately, the vertical motion of the foot does not have to be an exact straight line. Therefore, a four-bar linkage which generates an approximate straight line can be used again for this purpose. The main concern here is whether this four-bar linkage, referred to as the "shank linkage" from now on, is compact enough to fit within the space constraints without causing an interference problem. Again, RECSYN was used to design the shank linkage. When the shank linkage is mounted on the coupler of the four-bar leg, the leg becomes a seven-bar leg. In the following, the design procedure for a seven-bar leg is described.

5.4.1 Calculation of Design Positions

For a selected main linkage, the design positions of the foot for the shank linkage are calculated as follows. Due to the size constraints of the leg, it is more economic in the usage of space to put one of the fixed pivots of the shank linkage on a moving pivot

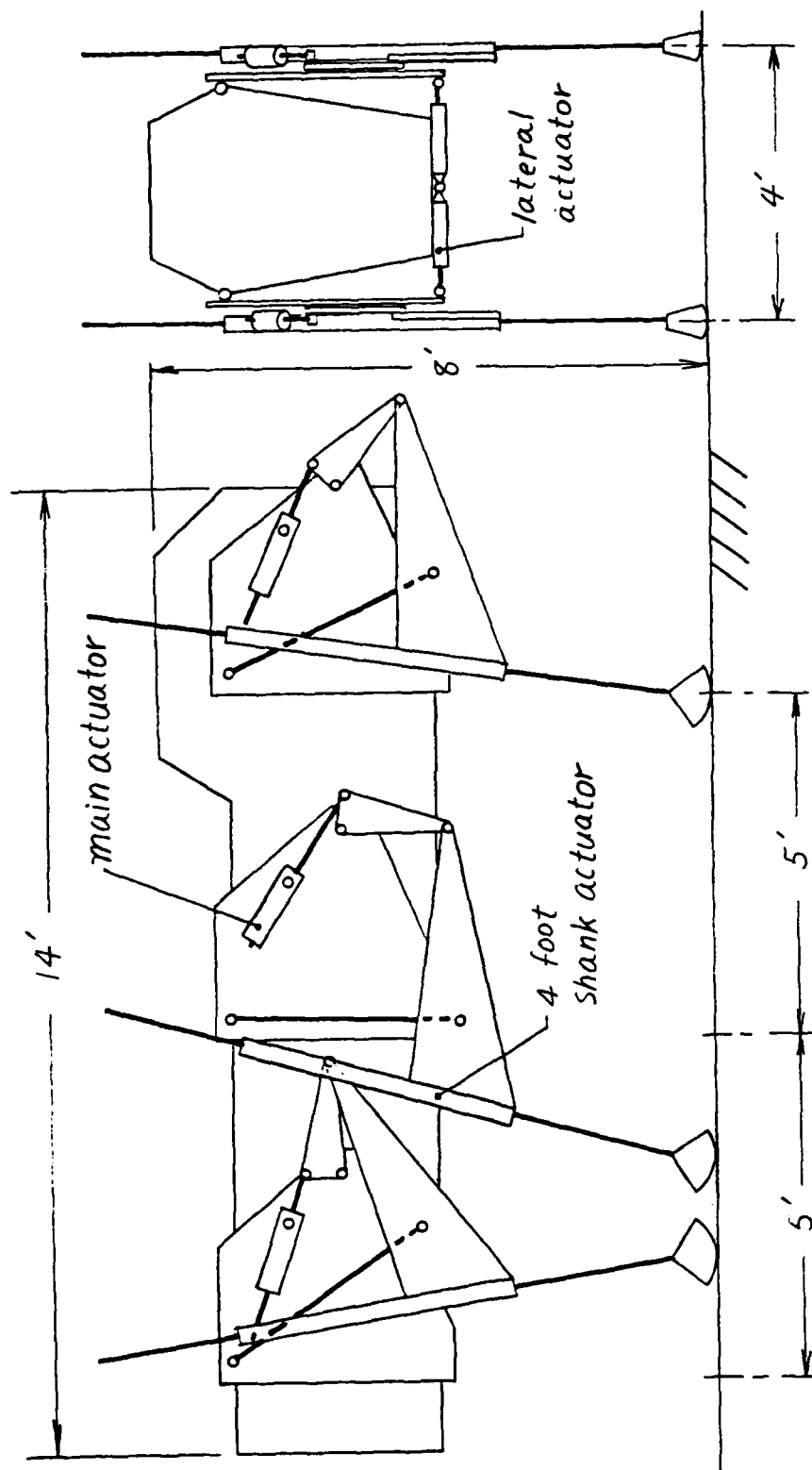


Figure 5.31: The ASV with four-bar legs.

of the main linkage. The linkage height h can then be calculated as the distance from the moving pivot to the desired foot path (see Figure 5.32). The maximal joint angle, α , and the length, a , of the crank are then chosen. The four design points on the foot path are selected using Chebychev spacing. Hence,

$$\begin{aligned} X_1 &= X_a - X_r \cdot \cos 22.5^\circ \\ X_2 &= X_a - X_r \cdot \cos 67.5^\circ \\ X_3 &= X_a + X_r \cdot \cos 67.5^\circ \\ X_4 &= X_a + X_r \cdot \cos 22.5^\circ \end{aligned} \quad (5.24)$$

where

$$X_a = [f + (f-s)]/2$$

$$X_r = [f - (f-s)]/2$$

The angles θ_1 through θ_4 corresponding to X_1 through X_4 , respectively, can be calculated⁸ according to the geometry shown in Figure 5.32. The equation for θ is :

$$\tan \frac{\theta}{2} = \frac{B - (A^2 + B^2 - C^2)^{1/2}}{A - C} \quad (5.25)$$

where

⁸ For detailed derivation, please refer to Section 5.3.2.1.

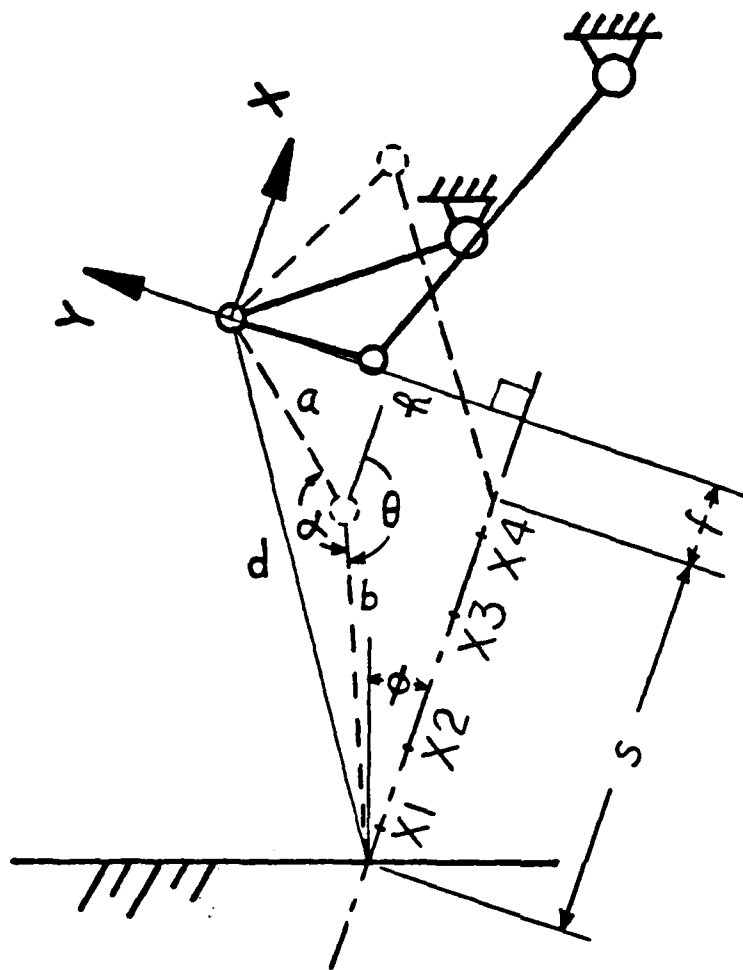


Figure 5.32: Design positions of shank linkage

$$A = -2b \cdot X$$

$$B = -2b \cdot h$$

$$C = b^2 + h^2 - a^2 + X^2$$

5.4.2 Shank Linkage Design

The design procedure is similar to that for the design of the main linkage. Figure 5.33 shows one of the shank linkages generated by RECSYN. This shank linkage was entered into FORBAR and a foot trajectory was generated (see Figure 5.34). The shank linkage was then

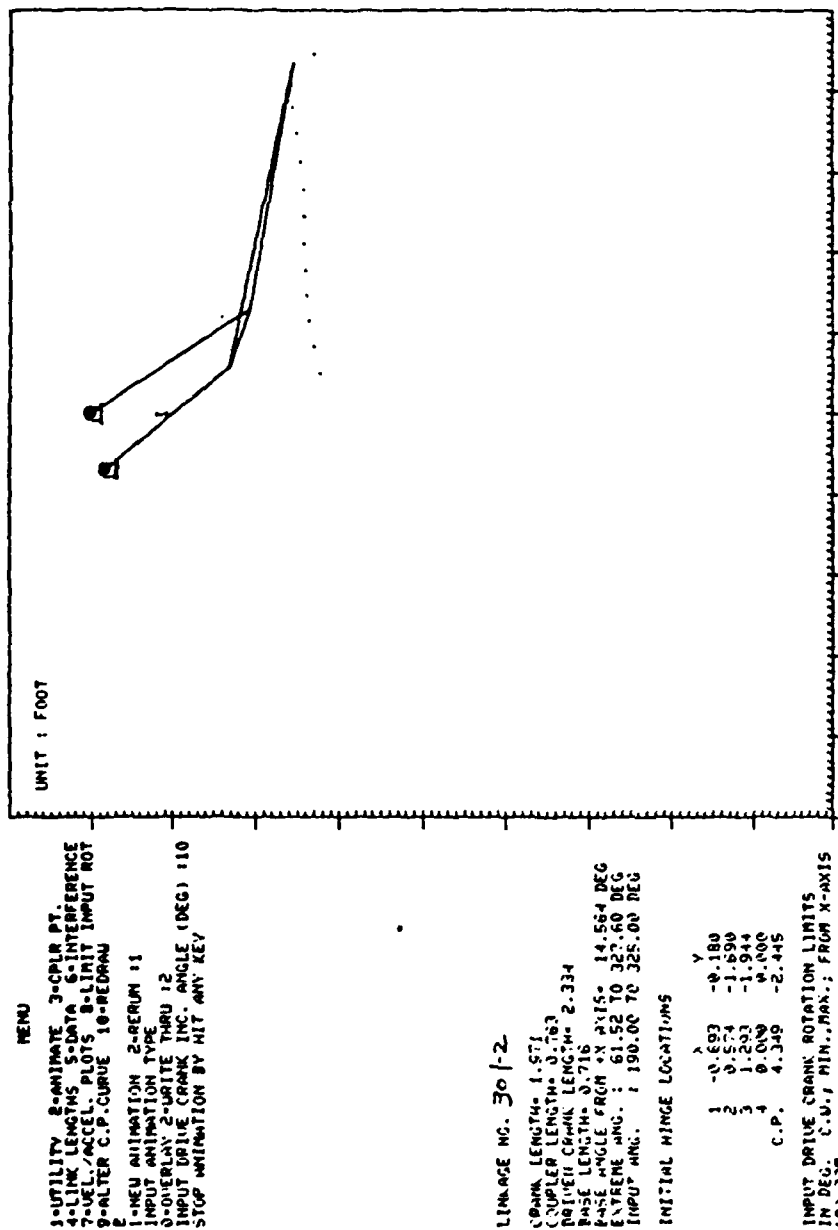


Figure 5.34: Foot trajectories of a shank linkage.

mounted on the main linkage to form a seven-bar linkage. Figure 5.35 shows that the coupler of the four-bar leg is replaced by the shank linkage. This seven-bar linkage was then animated to generate the walking envelope and is shown in Figure 5.36. Good foot trajectories could be obtained provided appropriate linkage designs are used. The compactness in the vertical direction is much better than that of a four-bar leg.

FORBAR was also used to study the interference problem between legs. Figures 5.37a, 5.37b and 5.37c show the pictures of two legs at their extreme positions when the legs are fully raised, are in the normal height, and are fully extended, respectively. The interference problem is less serious than it is for the four-bar legs. (If the stroke is magnified to 6 feet, interference between the legs will appear.). A small overstroke exists when the legs are fully extended. The rest of the design, such as the optimization of the shank linkage, determination of bearing load and actuating load, selection of mounting positions of the main actuator, stress analysis using finite element methods...etc., are similar to those used for the four-bar leg. Many iterations on the leg design were made in order to obtain a few seven-bar legs which satisfy all design specifications.

Figure 5.38 shows the final design of the seven-bar leg. Notice that one crank of the shank linkage is bent in order to avoid interference between the links. The shank drive system was selected to be a short linear actuator with a gear and rack system because a large

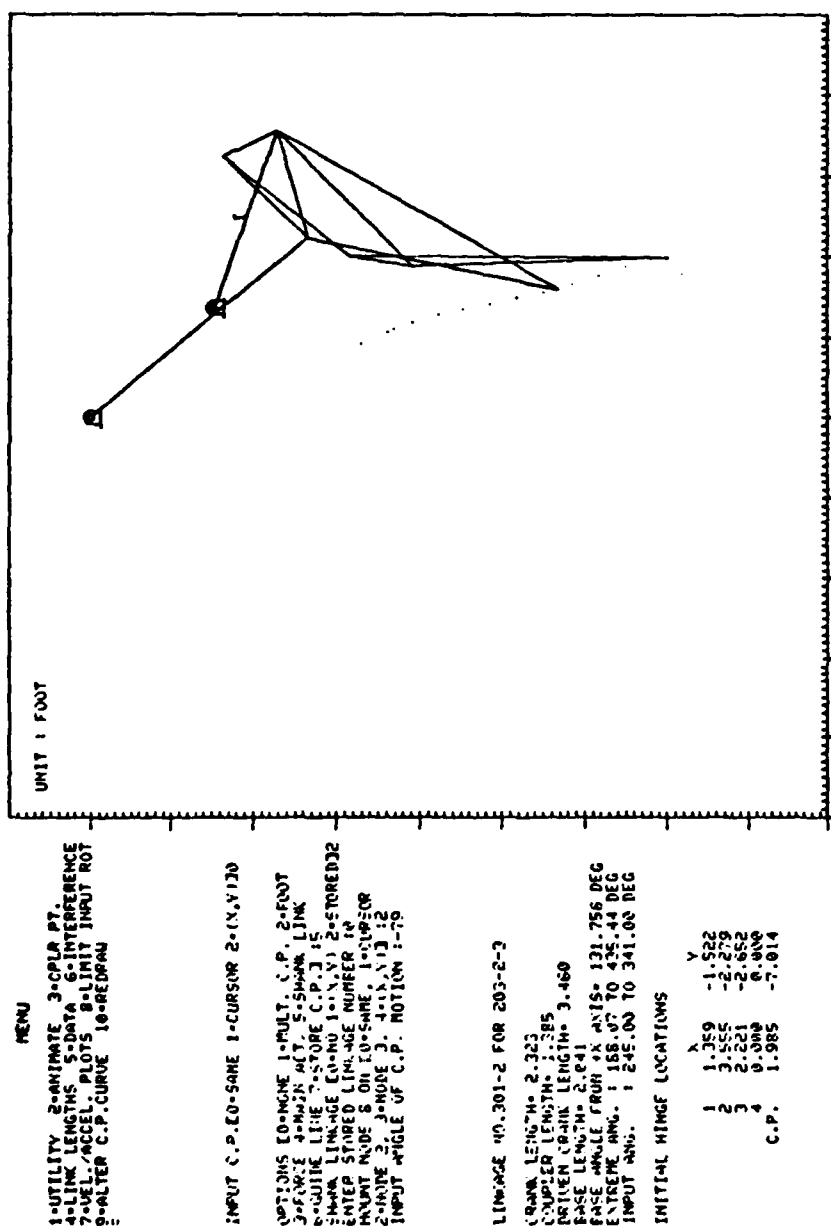
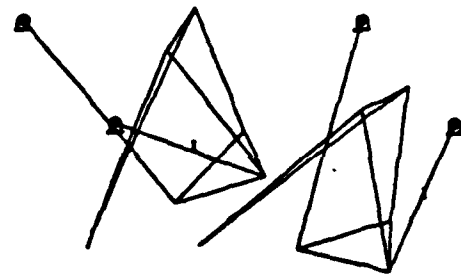
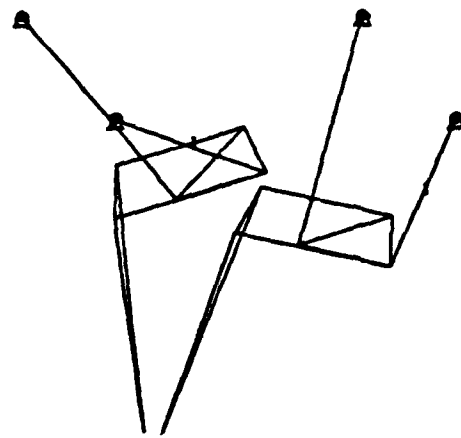


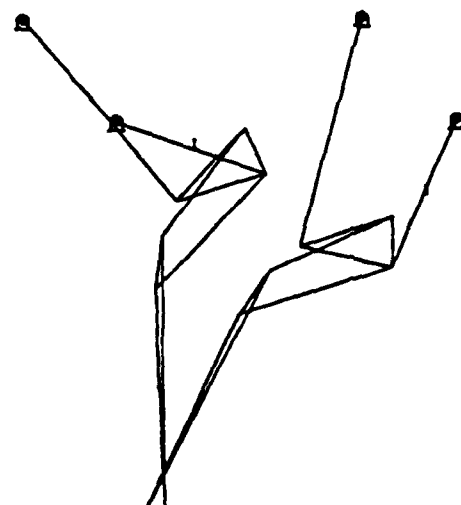
Figure 5.35: A seven-bar leg generated by FORBAR.



(a)



(b)



(c)

Figure 5.37: Interference study of seven-bar legs.

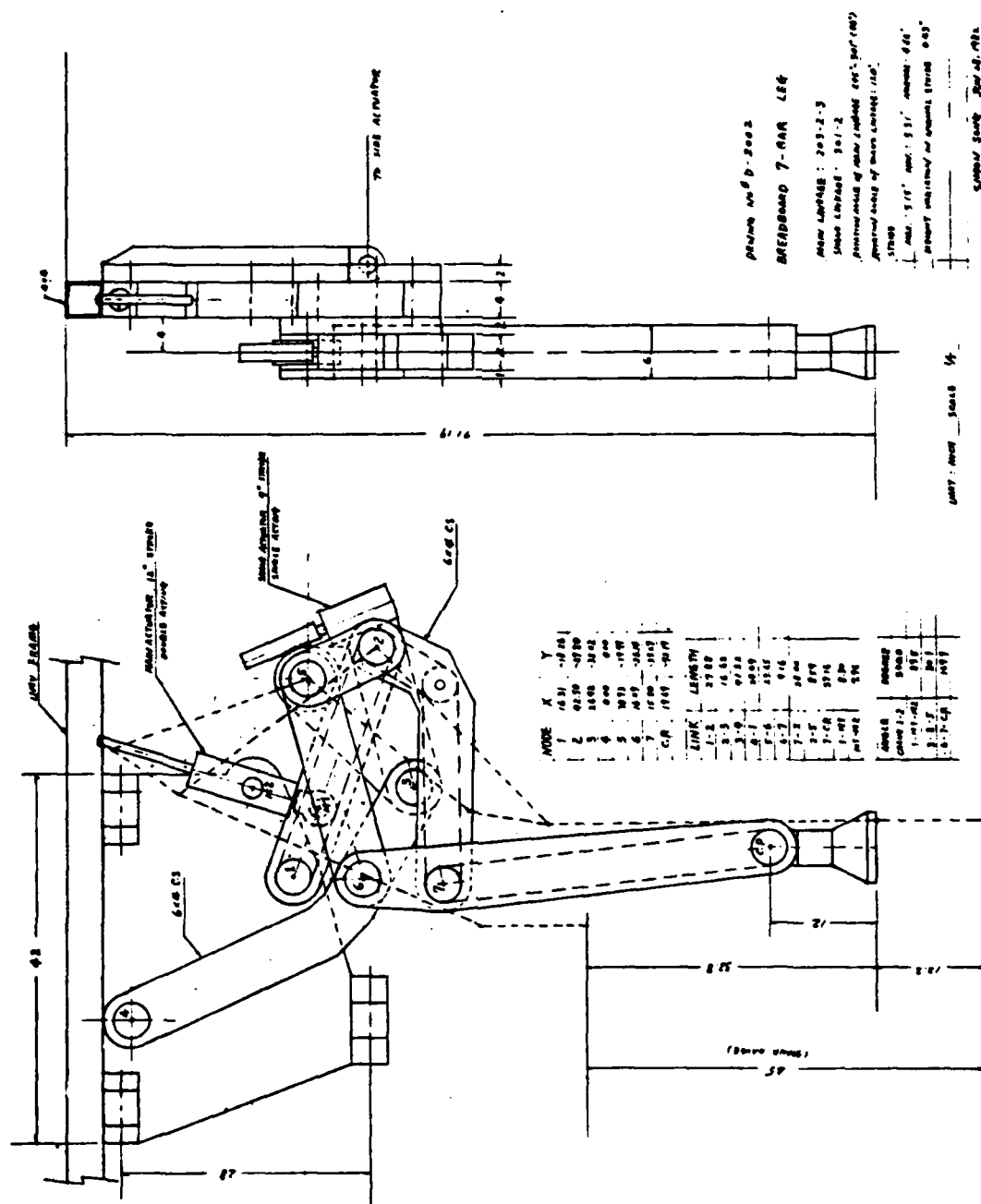


Figure 5.38: A design of the seven-bar leg.

crank rotation angle is required for the full stroke motion.

Although the seven-bar leg partially solved the design problems inherent in the four-bar leg, a few design problem characteristics of the seven-bar leg remained to be overcome. One was that the thickness of the leg increased due to the fact that many links overlap the same space. The second was that the lateral rigidity was degraded due to a longer stress path from the ground to the frame of the body. The third was that the compactness of the leg in the longitudinal direction was left unsolved.

5.5 Summary

In this chapter, principles to improve the poor energy efficiency of existing walking machines were introduced. In consideration of these principles, a "mammal" type four-bar leg was designed. This design procedure began with a four-bar linkage synthesis and its geometric optimization. Several linkages which generate good approximations to a straight line section were obtained. Methods of generating a vertical stroke were also studied. A four-bar leg with a variable crank can generate a vertical stroke of about 15% of the leg height while the same linkage with a variable shank can generate a vertical stroke of about 90% of the leg height. Hence, a four-bar linkage with a variable shank was selected for the ASV. Following this decision, analysis of bearing loads, actuating torque and mounting positions of the main actuator, interference study and stress analysis by finite element methods were carried out. Methods for abduction and adduction were also discussed.

Two small scale machines using four-bar legs were built to test the energy efficiency. The results of these tests were discussed elsewhere [47, 48] and a comparison of the machine efficiencies to that of the OSU Hexapod was made. It showed that significant improvement in energy efficiency had been achieved. However, a four-bar leg with a long linear shank actuator was found lacking in mechanical strength and compactness.

A seven-bar leg was designed to diminish the shortcomings found in four-bar legs. Several four-bar shank linkages were designed using a similar procedure to that used in designing the main linkage. These shank linkages were mounted on the coupler of the main linkage to form a seven-bar leg in a computer program. The geometrical optimization and design process, which are similar to those used in four-bar leg design, were carried out for the seven-bar leg. Although the mechanical strength and the vertical compactness were improved, the seven-bar leg gave rise to some other minor problems such as thickness and lateral deflection of the leg. The compactness in the longitudinal direction of the leg was not as good as desired. Due to these difficulties, a different leg mechanism was sought and will be discussed in the next chapter.

Chapter 6

DESIGN OF A PANTOGRAPH LEG

6.1 Introduction

In Chapter 5, the design of leg geometry for a walking machine using linkage synthesis was presented, and a four-bar leg and a seven-bar leg were designed. Both leg geometries were able to generate an acceptable walking volume. However, both types of leg have mechanical design problems and compactness problems. Although these problems might be solved by intelligent design, the construction schedule of the ASV did not permit further time to be spent on uncertain design concepts. A definite and functional leg geometry was required for detailed mechanical design and manufacturing within a limited time period. Hence, while some efforts were devoted to solution of those problems, several other linkages which generate straight line segments were also studied at the same time.

Among those linkages, pantograph mechanisms exhibited the most potential as a suitable leg linkage and was selected for detailed analysis after a short time. This selection was based on the following reasons:

1. The input motions can be mechanically decoupled. The least effort needed for foot trajectory control is expected.

2. An exact-straight-line foot trajectory can be obtained by actuating only one linear actuator. A high energy efficiency is expected.
3. The leg geometry can be as compact as wished by adjusting the magnification ratio.
4. Successful examples were demonstrated by the small scale quadruped PV II and the hexapod constructed by Kessis and his colleagues [60].

The pantograph leg mechanisms of the PV II¹ is a three dimensional pantograph mechanism (see Figure 6.1). The leg is mounted as an "insect" type leg. In each leg, three linear actuators were designed to provide the three degree-of-freedom motion of the foot. At both points R and Q, each has a vertical joint between the actuating system and the leg joint. The actuator in the Y direction does not have a guideway system. When the actuator is extended, the load condition that of a cantilever beam under lateral load. This structure is suitable for a light weight vehicle (The PV II weighs 22 pounds.). However, for a vehicle as heavy as the ASV (at least 3000 pounds), serious structural problems would be raised if the leg mechanism of the PV II were to be directly applied.

The history of pantograph mechanisms can be traced back to the Seventeenth Century [55]. Pantographs have been used extensively in embroidering machines, copying machines and magnifying mechanisms since then. In the Nineteenth Century, a more general case of pantograph, the skew pantograph or the plagograph, was introduced by

¹ The PV II was built by Hirose and Umetani [21]. Some related aspects of this machine were also discussed in Sections 2.2 and 5.1.

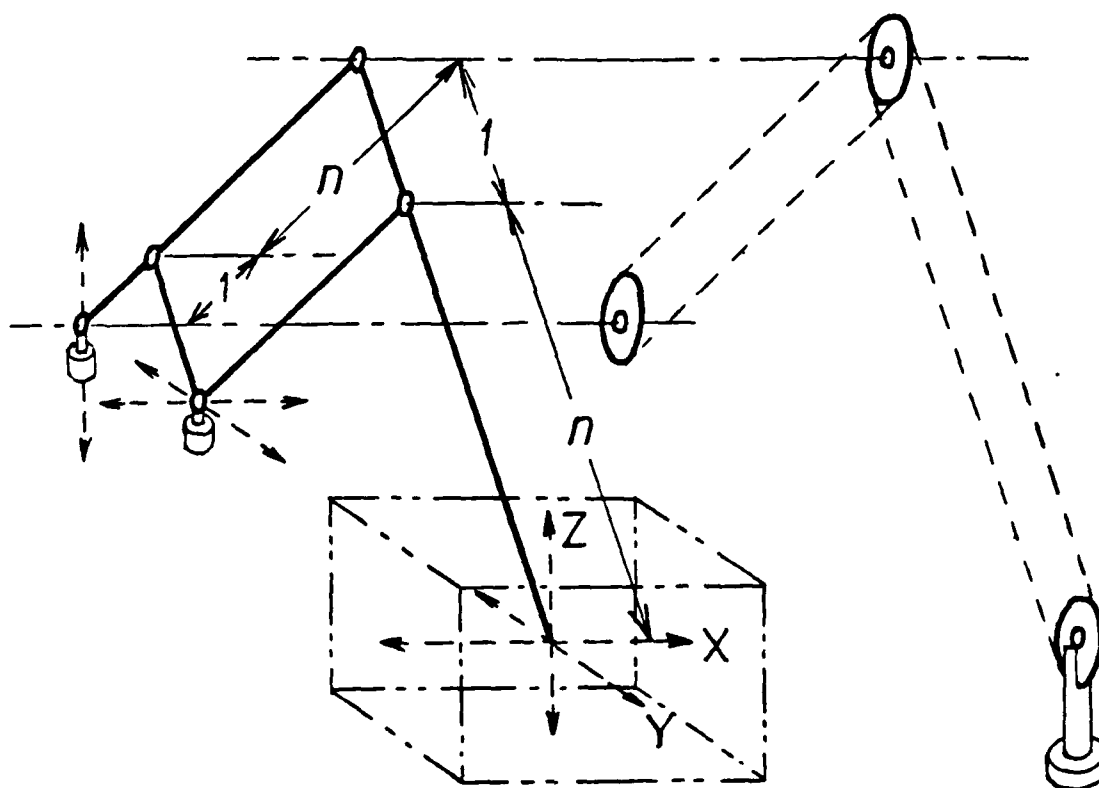


Figure 6.1: The three dimensional pantograph mechanisms used in PV II.

Sylvester [56, 57]. Both pantograph and skew pantograph are planar mechanisms. Although pantograph mechanisms have been in use for such a long time, the literature available on the geometric design of pantographs is surprisingly sparse.

In Section 6.2, a theoretical background to pantographs is given. Two basic theorems applying to planar pantographs are reviewed first. The theorems applicable to three dimensional pantographs are then developed. In order to generate decoupled motion of the foot point,

the properties of different sets of principal axes are studied. The singularities of pantographs are also discussed.

In Section 6.3, the detailed design procedure for a pantograph leg is given. In a preliminary design study, a two dimensional pantograph leg with a special frame structure is found to be suitable for the ASV. The leg design is mostly done by graphical and experimental methods due to the limited understanding of pantograph mechanism design methods. A computer program PANTO was developed to assist the design. Methods for the optimization of walking envelopes were also introduced. These methods include the changing of the skew angle, different actuator arrangements, different offsets of the walking envelopes and the changing of the ratio of upper to lower links.

In Section 6.4, an analytical study of the pantograph mechanism is given. The analytical results are used to confirm the leg geometry designed by graphical and experimental methods. This analysis can be extended to design a pantograph manipulator.

In Section 6.5, a comparison between a pantograph leg and a seven-bar leg is made. The possible mechanical design problems in both cases are also discussed. After all factor were considered, the pantograph leg was selected to be the leg for the ASV.

6.2 Motion Characteristics of Pantographs

6.2.1 Nomenclature of Pantographs

Figure 6.2 shows a tow dimensional pantograph manipulator mounted on a frame which rotates on a base. In order to provide a suitable

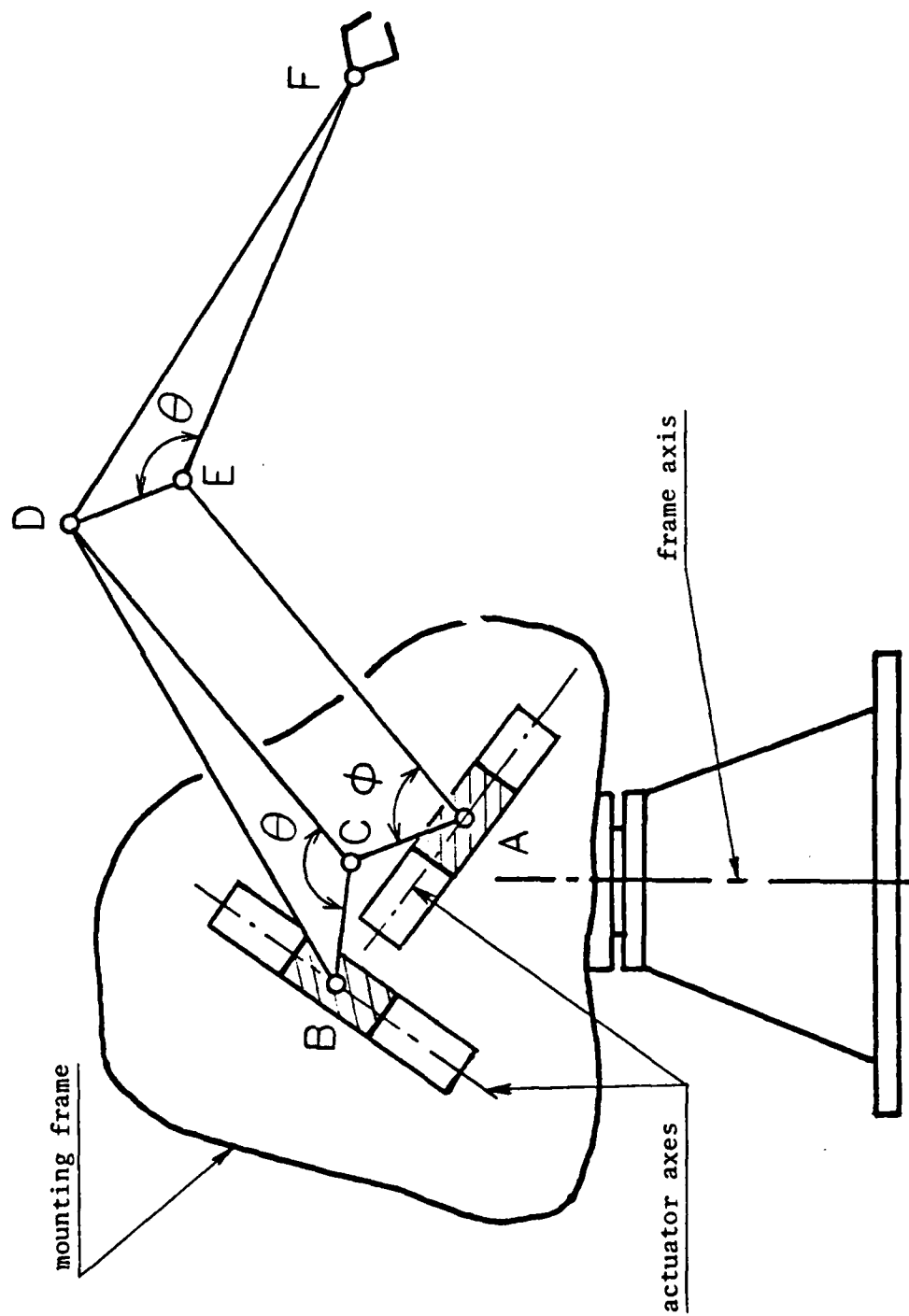


Figure 6.2: A general configuration of a pantograph manipulator.

background to study the motion characteristics of pantographs, several important terms are defined and are listed in the following in an alphabetical order:

- Actuator axes:** In a pantograph, each input linear actuator is assumed to act along a fixed axis. These axes are the actuator axes.
- Equivalent triangle:** The triangle defined by points A, B and F in Figure 6.2. Because of the motion geometry of the pantograph, the equivalent triangles are similar triangles in all positions during motion.
- Fixed point:** A point in the pantograph which does not move relative to the frame during motion. There is no fixed point in Figure 6.2.
- Following point:** This point (point F in Figure 6.2) follows the input motion of the guiding point or points and generates the desired output motion of the pantograph.
- Frame axis:** The axis on which the mounting frame rotates (see Figure 6.2).
- Guiding point:** The point or points which are connected to the actuators which generate input motions. In Figure 6.2, both A and B are guiding points.
- Mounting frame:** The frame on which a pantograph is mounted (see Figure 6.2).
- Plane axis:** The axis on which the principal plane rotates. The plane axis should pass through either the guiding point or the reference point.
- Principal angle:** The angle between the two adjacent links of the parallelgram. It is $\angle CAE$ in Figure 6.2.
- Principal axes:** The unique subset of all actuator axes that result in fully decoupled motion.
- Principal parallelgram:** The parallelgram linkage of a pantograph. It is linkage ACDE in Figure 6.2.
- Principal plane:** The plane in which a planar pantograph operates; a plane defined by the guiding point, the reference point and the following point.

- Reference point: The point to which the input motion and output motion are referred. It may be a fixed point or a moving point. In Figure 6.2, points A and B are both reference points and guiding points.
- Skew angle: Angle θ in Figure 6.2.

6.2.2 Two Dimensional (2D) Pantographs

6.2.2.1 Basic Theorems

Figure 6.3 shows a two dimensional skew pantograph mechanism. Two similar triangular rigid bodies BCD and DEF are attached on the principal parallelogram ACDE. Therefore, the following relationship holds.

$$\frac{BC}{DE} = \frac{CD}{EF} = \frac{BD}{DF} \quad (6.1)$$

The angle ϕ is the principal angle. The angle θ is the skew angle and is in the range of $0^\circ \leq \theta < 360^\circ$. When this angle is either 0° or 180° the pantograph is called the simple pantograph. Figure 6.4 shows these two special cases. In the following, two theorems of planar pantographs are introduced first, then more theoretical development of both planar and three dimensional pantographs are presented.

Theorem 1 is the most basic theorem of planar skew pantographs and was introduced by Sylvester [56,57]. In reference [59], Roth applied this theorem to his study of some other motion features of skew pantographs.

Theorem 1: In Figure 6.3, if point A is a revolute joint fixed on the frame, then if any curve is traced by point B, a similar curve

will be traced by point F. The curve will be magnified by the ratio R and will rotate through an angle θ , where

$$R = \frac{AF}{AB} \quad (6.2)$$

Theorem 2: In Figure 6.3, if point A is released and point B is a revolute joint fixed on the frame, then if any curve is traced by point A, a similar curve will be traced by point F. The curve will be magnified by the ratio R' and rotate through angle ψ , where

$$R' = (R^2 + 1 - 2R \cdot \cos \theta)^{1/2} \quad (6.3)$$

$$\psi = \tan^{-1} \left(\frac{R \cdot \sin \theta}{1 - R \cdot \cos \theta} \right)$$

Proof: From Figure 6.3 we have

$$\angle ACB = 2\pi - (\pi - \phi + \theta) = \pi + \phi - \theta = \angle AEF$$

Since

$$\frac{BC}{DE} = \frac{CD}{EF}, \text{ and } AC = DE, CD = AE$$

This gives

$$\frac{BC}{AC} = \frac{BC}{DE} = \frac{CD}{EF} = \frac{AE}{EF}$$

Hence, $\triangle ABC$ is similar to $\triangle AEF$. This gives

$$\frac{AB}{AF} = \frac{BC}{AE} = \frac{BC}{CD} = \frac{DE}{EF}$$

Also,

$$\begin{aligned}
 \angle BAF &= \angle CAE + \angle BAC + \angle EAF \\
 &= \angle CAE + \angle BAC + \angle ABC \\
 &= \phi + [\pi - (\pi + \phi - \theta)] \\
 &= \theta
 \end{aligned}$$

Therefore, ΔABF is similar to ΔBCD and ΔDEF during tracing. Since point B is the fixed reference point and point A is the guiding point, the motion of F is magnified by the factor BF/AB and is rotated through $\angle ABF$. According to the law of cosines

$$BF^2 = AB^2 + AF^2 - 2AB \cdot AF \cdot \cos \theta$$

so that

$$(BF/AB)^2 = 1 + (AF/AB)^2 - 2(AF/AB) \cdot \cos \theta$$

Now

$$R' = BF/AB = (1 + R^2 - 2R \cdot \cos \theta)^{1/2}$$

and from the law of sines,

$$\sin \psi = (AF/BF) \cdot \sin \theta$$

From the law of cosines,

$$\cos \psi = \frac{BF^2 + AB^2 - AF^2}{2BF \cdot AB}$$

Hence

$$\begin{aligned}\tan \psi &= \sin \psi / \cos \psi \\ &= \frac{(AF/BF) \cdot \sin \theta}{(BF^2 + AB^2 - AF^2)/(2BF \cdot AB)} \\ &= \frac{2(AF \cdot AB) \cdot \sin \theta}{BF^2 + AB^2 - AF^2}\end{aligned}$$

Both the numerator and denominator are divided by AB^2 to give

$$\begin{aligned}\tan \psi &= \frac{2(AF/AB) \cdot \sin \theta}{(BF/AB)^2 + 1 - (AF/AB)^2} \\ &= \frac{2R \cdot \sin \theta}{1 + R^2 - 2R \cdot \cos \theta + 1 - R^2}\end{aligned}$$

which reduces to

$$\tan \phi = \frac{R \cdot \sin \theta}{1 - R \cdot \cos \theta}$$

Thus Theorem 2 is proved.

The Concept of Equivalent Triangle: From Theorem 1, the motion of B and F can be visualized by replacing the whole pantograph by a magnifiable triangle BAF, which is indicated by the dashed triangle in Figure 6.3. This triangle can rotate on the reference point A and expand or contract to a similar triangle simultaneously. Therefore, wherever the guiding point B moves, the position of the following point

can be found by constructing a new triangle BAF which is similar to the original one. This triangle is called the equivalent triangle. The same concept can be applied to the case in which point B is the reference point. This concept is very important and helpful in the following analysis

6.2.2.2 Principal Axes and Actuator Arrangements

In order to produce decoupled rectilinear output motions, linear actuators should be used to actuate the input motions of a pantograph. A decoupled rectilinear motion is described as follows: For a selected reference frame X-Y-Z, an X-movement of the following point can be generated by actuating only one actuator. Similarly, a Y-movement and a Z-movement can be generated by actuating respectively only the second and the third actuator. The actuators which generate the X-movement, Y-movement and Z-movement of the following point are called the X-actuator, Y-actuator and Z-actuator, respectively. For a planar pantograph, two linear actuators are necessary. The directions of these two actuators are arbitrary except they may not be parallel to one another. However, only one unique set of actuator axes can generate decoupled motions. These special actuator axes are the principal axes.

Let the following point of a pantograph be point F. Since both points A and B can be a guiding point, there are four types of actuator arrangement which generate decoupled motion (see Figure 6.5). For each type of actuator arrangement, one unique set of principal

axes can be defined. The way to locate the principal axes is by applying the concept of equivalent triangles.

In Case 1 (see Figure 6.5a), X-Y is a chosen reference coordinate system, and U-V is the principal axes to be defined. Let counter-clockwise be the positive direction of angles. Then the angle θ from the guiding vector AB to the following vector AF is negative. Since the trajectory of F is obtained by rotating the trajectory of B through angle θ , the motion of point B should be in a direction which is at angle $-\theta$ from the positive X-axis if a positive X-movement of point F is desired. The direction of axis U is thus defined. Likewise, B should move in a direction which is at angle $-\theta$ from the positive Y-axis if a positive Y-movement of point F is desired. The direction of axis V is thus defined. The origin of the principal axes U-V does not have to be at point A.

In Case 2 (see Figure 6.5b), B is the fixed reference point. The following vector BF is the direction found by rotating the guiding vector BA through the angle ψ . ψ is positive in this case. By the same argument given for Case 1, U is in the direction given by rotating an angle $-\psi$ from the positive X-axis and V is in the direction given by rotating $-\psi$ from the positive Y-axis.

In Case 3 (see Figure 6.5c), the X-movement of F is generated by A and the Y-movement of F is generated by B separately. The axes U and V can be determined by taking separated reference points, in this case B and A, respectively. Thus axis U is determined by rotating an angle $-\psi$ from positive X-axis about point A, and V is determined by rotating an angle $-\psi$ from positive Y-axis about point B.

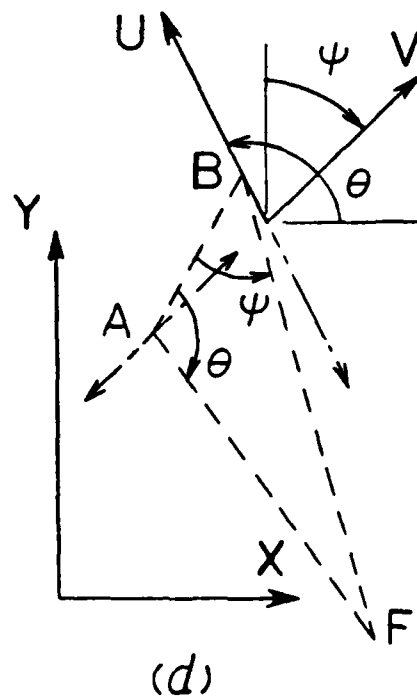
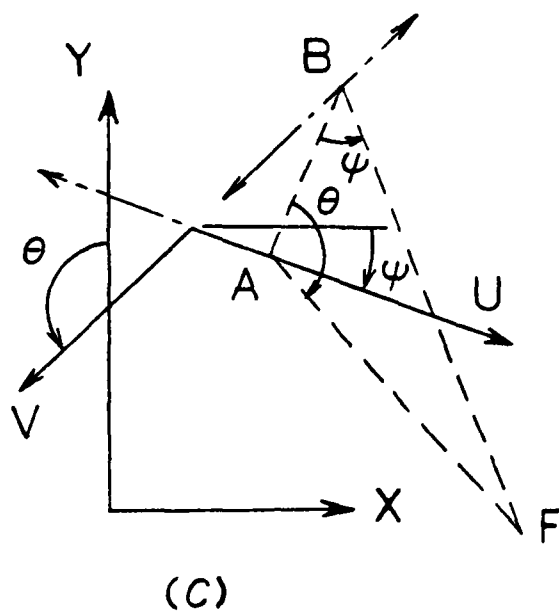
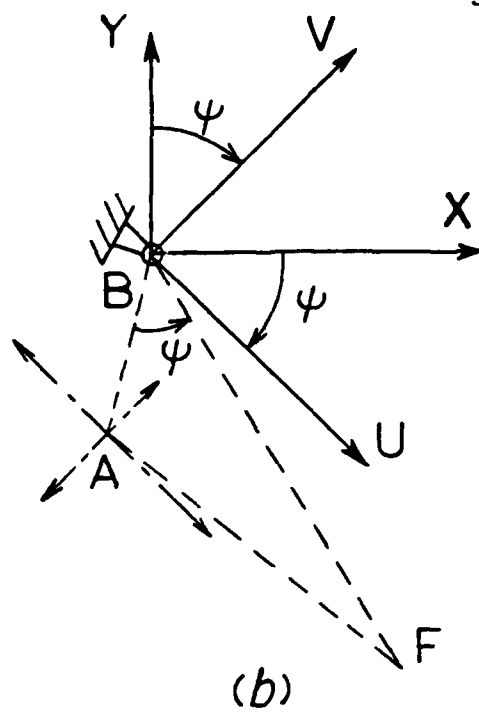
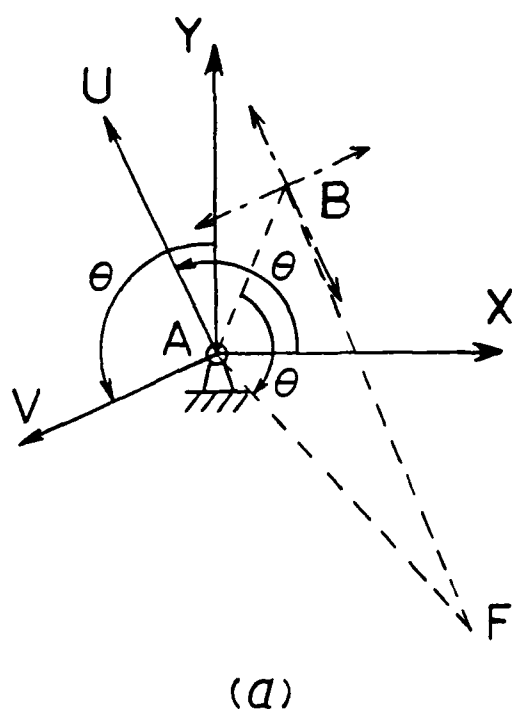


Figure 6.5: Principal axes and actuator arrangements of 2D pantographs.

In Case 4 (see Figure 6.5d), B generates X-movement of F and A generates Y-movement of F. By the argument given above, U is at angle $-\theta$ from the positive X-axis through B, and V is at angle $-\psi$ from positive Y-axis through A.

6.2.2.3 Singularities of 2D Pantographs

A geometrically singular position occurs when any three points defining a dyad in a pantograph are colinear. Figure 6.6 shows an example of a singular position where points A,C,B, points B,D,F, and points A,E,F are in colinear lines. When a pantograph is moved close to a singular position, it will either be stopped at the singular position or lose the motion characteristic after it passes the singular position. Also, motion in the neighborhood of a singular position creates high load in the link members. Therefore, elimination of singularities for a pantograph is necessary. Two angles, $\angle CAE$ and $\angle ACB$ are used to detect the singularities for a planar pantograph. When any of these angles becomes either 0° or 180° , a singular position is indicated.

6.2.3 Three Dimensional (3D) Pantographs

6.2.3.1 Basic Theorems

In Figure 6.7, ABF is the equivalent triangle of a planar pantograph. Therefore, points A, B and F define the principal plane. X-Y is a reference coordinate system in the principal plane. The Z-axis completes the three dimensional coordinate system according

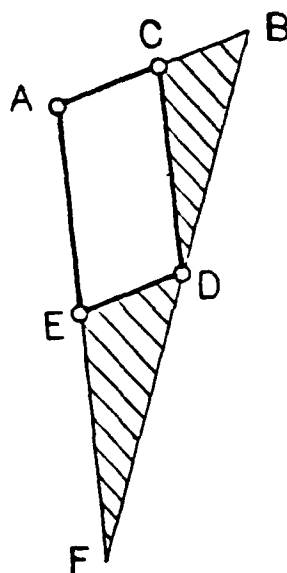


Figure 6.6: An example of a 2D singular position.

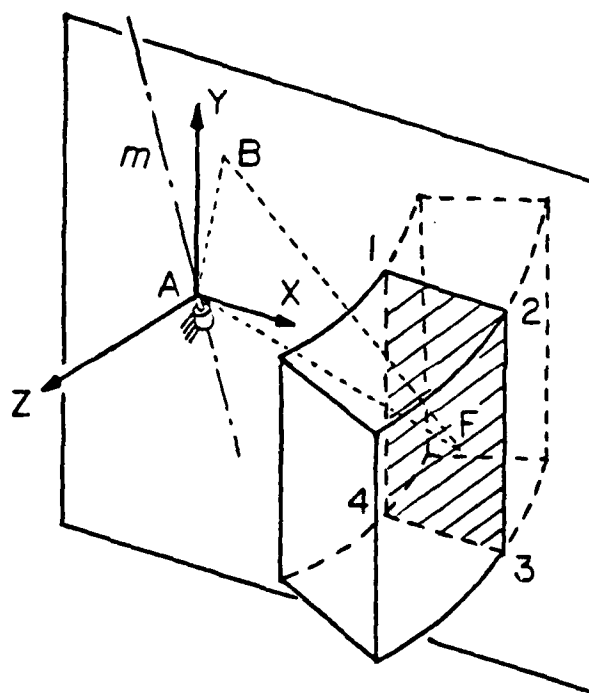


Figure 6.7: A 3D work space of pantographs.

to the right hand rule. Let 1234 be the planar work space of the following point F. If the reference point A is mounted on a pivot with plane axis m , which plane axis m is not parallel to the Z-axis, the planar work space can be extended into three dimensions by rotating the principal plane about plane axis m . The guiding point B should also be mounted on a pivot with pivot axis in the same direction as m so that such a rotation could be possible.

However, most of the three dimensional motions generated in this way are not fully decoupled. In fact, pantographs, except simple pantographs are all in this category. Rather than prove such a statement, an example is given below to show that a decoupled motion is impossible for these kinds of pantographs.

Figure 6.8a shows the equivalent triangle of a pantograph with a 90° skew angle. X-Y-Z is the reference coordinate system and X-Y is in the initial position of the principal plane. Point A is mounted on a pivot with plane axis m and m is in the principal plane. Assume a fully decoupled three dimensional motion can be generated by this pantograph. If B is moved in a straight line in the Z direction, F should follow along a straight line in the negative Z direction. After movement the equivalent triangle becomes $AB'F'$. According to Theorem 1 and the concept of the equivalent triangle, $\triangle AB'F'$ should be similar to $\triangle ABF$. That is, $\angle B'AF'$ should be 90° . However, $\angle B'AF'$ is not 90° . This can be understood by cutting two orthogonal planes with a third plane (see Figure 6.8b). The angles of the edges in the cutting plane change when the orientation of the cutting plane

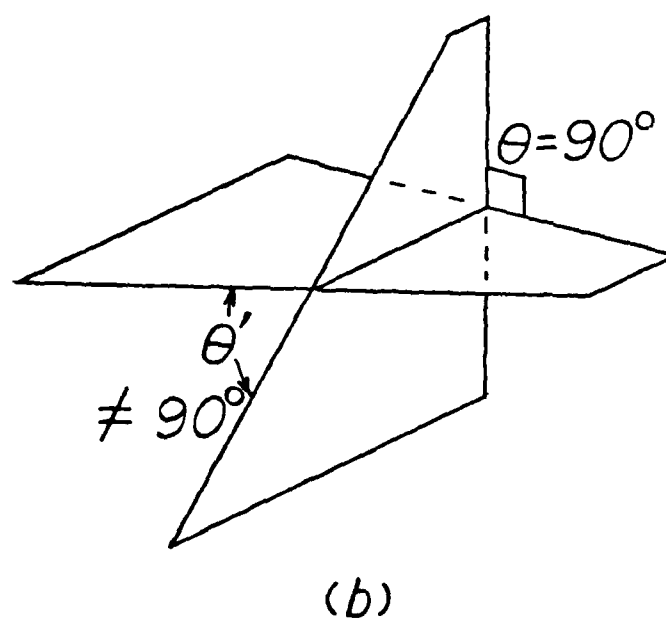
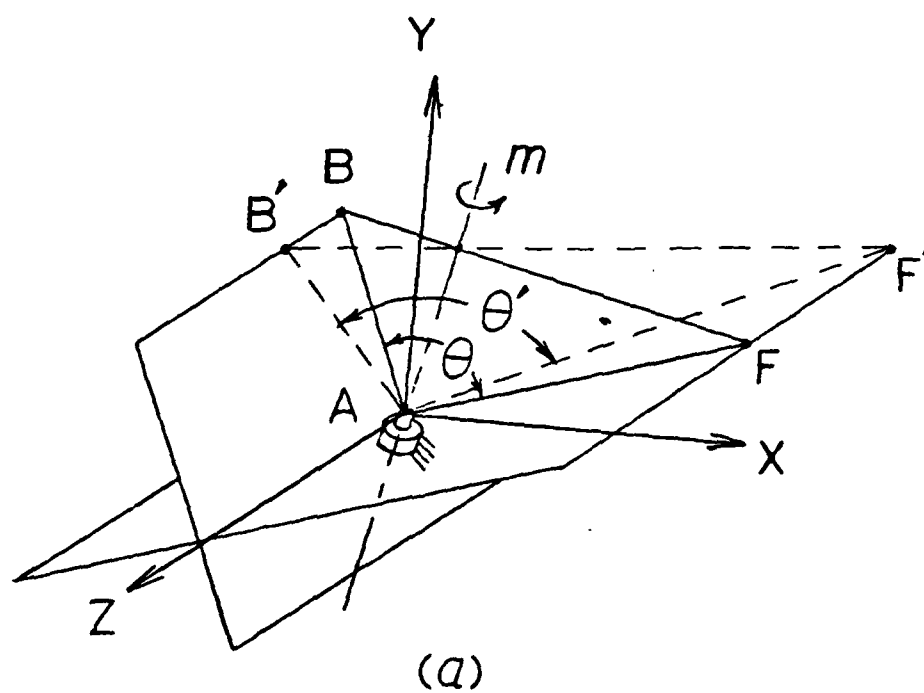


Figure 6.8: The impossibility of a 3D fully decoupled skew pantograph.

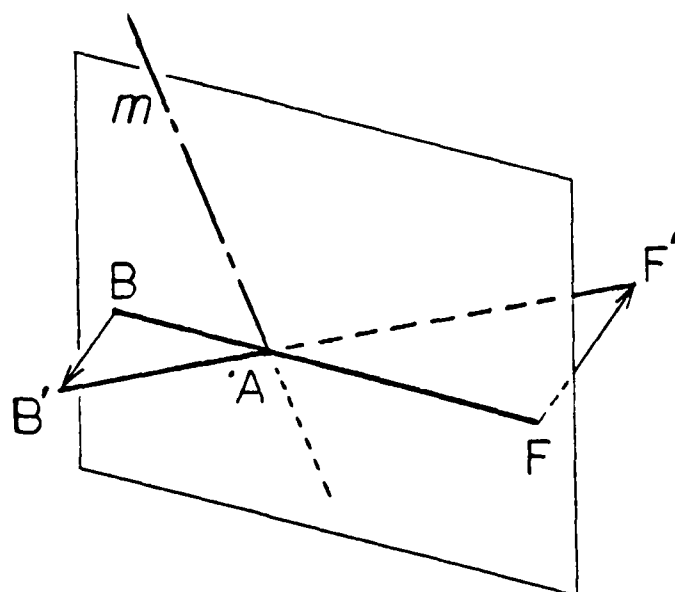
changes. Only when the third plane is perpendicular to either of these two planes, does the cut produce a 90° edge angle.

The same feature can be observed when m is not in the principal plane and when the skew angle is not 90° . This means the motion in the Z -direction is not decoupled. However, a fully decoupled motion can be generated by simple pantographs and is shown in the following theorems.

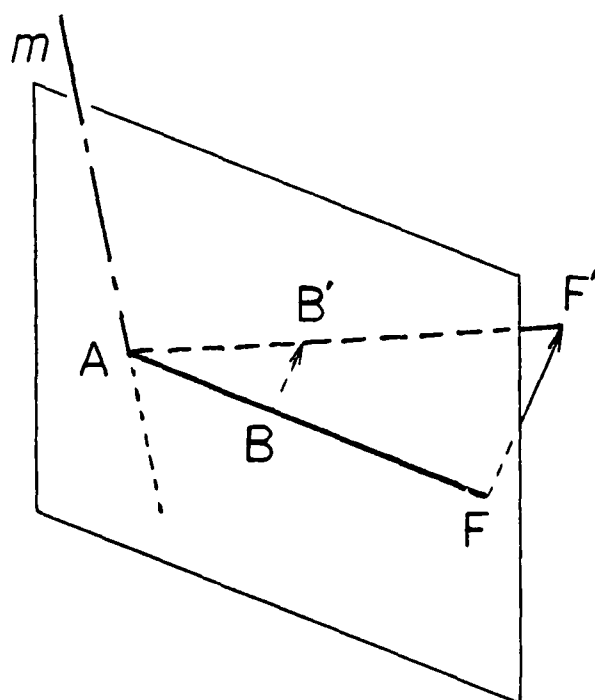
Theorem 3: In a simple pantograph, the reference point A is mounted on a plane axis which is not perpendicular to the principal plane. If any three dimensional curve is traced by point B , a similar three dimensional curve will be traced by point F . The curve will be magnified by the ratio R and rotate through its skew angle (either 0° or 180°). Where

$$R = \frac{AF}{AB} \quad (6.4)$$

Proof: Since the skew angle is either 0° or 180° , the equivalent triangle becomes an extendable bar (see Figure 6.9). From Theorem 1, AF/AB is constant during a planar motion. The same relationship must hold in three dimensional motion since the pantograph always remains in its principal plane. Figure 6.9a shows the simple pantograph with a 180° skew angle. $B'AF'$ is the pantograph after movement. Since AF/AB is constant in all positions, $AF'/AB' = AF/AB = R$. Therefore BB' is parallel to FF' and FF'/BB' is equal to R . Since B' and F' are opposite to BF , the motion is rotated through 180° . Figure 6.9b shows the simple pantograph with 0° skew angle. Since B' and F' are



(a)



(b)

Figure 6.9: 3D simple pantograph.

on the same side to BF, the motion is rotated through 0° . Therefore, the motion of F is rotated from the input motion by the skew angle for both simple pantographs.

Theorem 4: In a simple pantograph, the reference point B is mounted on a plane axis which is not perpendicular to the principal plane. If any three dimensional curve is traced by point A, a similar three dimensional curve will be traced by point F. The curve will be magnified by the ratio R' and rotate through an angle equal to $180^\circ - \theta$. where

$$R' = 1 + R \quad (6.5)$$

Proof: Since the planar relationship holds in all positions during the motion, the magnification ratio is obtained by substituting $\theta = 0^\circ$ and 180° into Theorem 2, which results in $1 + R$. The rest of the proof is very similar to that of Theorem 3. For a simple pantograph with a 0° skew angle, B is between A and F. The motion is thus rotated by 180° . For a simple pantograph with a 180° skew angle, A is between B and F. The motion has 0° degree rotation. Therefore, a $180^\circ - \theta$ rotation angle satisfies both cases.

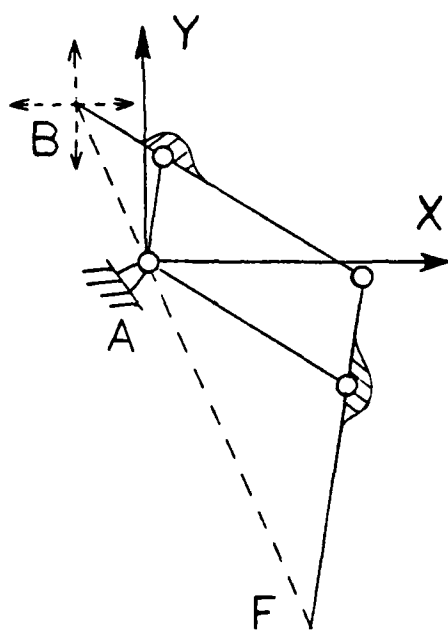
6.2.3.2 Principal Axes and Actuator Arrangements for 3D Pantographs

Since there are four possible actuator arrangements for a planar pantograph and either point A or point B can be connected to the third actuator, eight possible types of actuator arrangements result for a 3D pantograph. For each type of actuator arrangement a set of principal

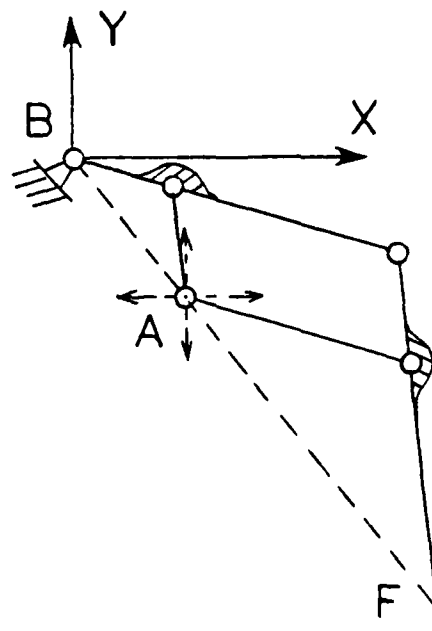
axes can be defined as in the following: Let the X and Y axes be in the principal plane and let the Z-axis complete the coordinate frame by the right hand rule. Since the X-Y axes are in the principal plane, two principal axes can be defined according to the rules for principal axes of 2D pantographs. The third principal axis is parallel to the Z-axis. By mounting three linear actuators on the principal axes, a fully decoupled motion can be generated.

6.2.3.3 Singularities of 3D Simple Pantographs

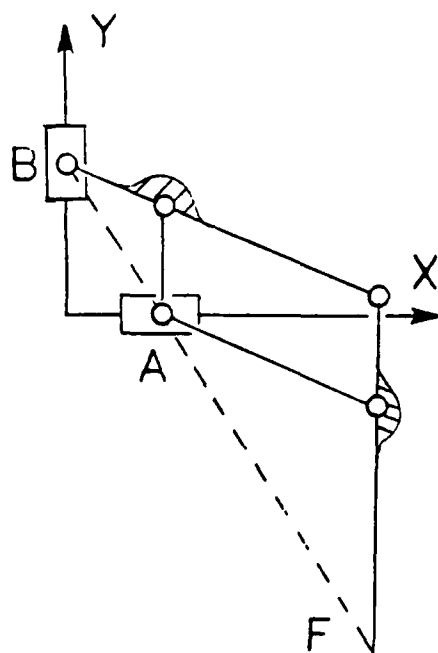
In addition to the planar singularities which were previously discussed, another singular position exists for 3D pantographs. Due to the requirements of 3D motion, both points A and B should freely rotate about a pair of parallel plane axes which are not perpendicular to the principal plane. When these two plane axes become colinear, the pantograph can freely rotate about this axis and is not under control. During such a rotation, the following point stays still for a 3D simple pantograph while it moves around the colinear plane axes for a 3D skew pantograph. This singular position is called the 3D singularity in order to differentiate it from the planar singularities. However, the 3D singular position does not create either non-linear motion or high load in contrast to the planar singularities. The uncontrolled rotation at the 3D singular position can be eliminated by adding a simple device which restrains the pantograph from free rotation.



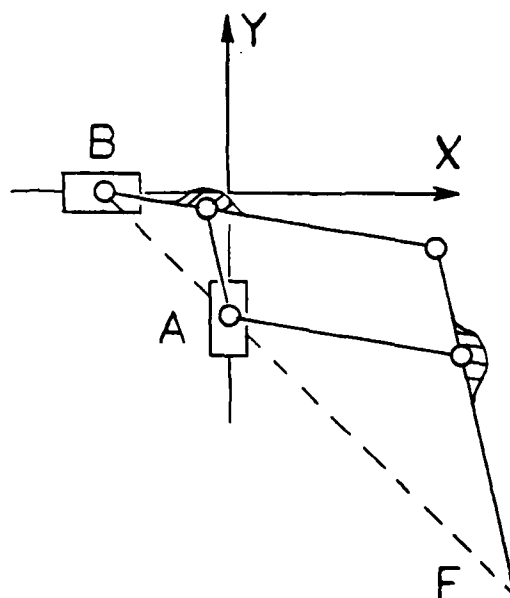
(a)



(b)



(c)



(d)

Figure 6.10: Analytical study of the work space for a 2D simple pantograph.

6.3 Design of a Pantograph Leg

6.3.1 Design Specifications

The design specifications of the pantograph leg were defined according to the mobility requirements and are given below:

- Stroke pitch: 5 feet.
- Leg strokes:
 - * Longitudinal stroke: 6 feet.
 - * Vertical stroke: 4 feet.
 - * Lateral Stroke: 4 feet.
- Loads: The vehicle weight was estimated to be 5,000 pounds at this time. The maximum loads at the foot are:
 - * Vertical load: 2500 pounds.
 - * Horizontal load: 1287 pounds.
 - * Lateral load: 855 pounds
- Leg size:
 - * Leg height: 7 feet.
 - * Leg width: Provide no interference between legs.
 - * Leg thickness: As thin as possible; about 2 feet.
- Leg weight: 300 pounds per leg.

6.3.2 Design Procedure

In order to have a decoupled motion of the foot point, the guiding point(s) of the pantograph should have linear motion. Although the guiding point(s) can be actuated by a linkage which

generates straight line motion, this arrangement will add complication to the leg mechanism. Also, the load distribution of the actuator in one step becomes non-linear. If possible, the device which generates the input motion to the guiding point(s) should be a linear actuator(s). Since a linear actuator can not bear large lateral load when it is extended, a guideway system should be included in the mechanism in order to take the lateral load. The guideway should be heavy duty because of the heavy load conditions of the ASV legs.

If a three dimensional pantograph is selected as the leg mechanism, one of the guiding points must have two degree-of-freedom input motion. A multi-step guideway system is needed for this guiding point. A preliminary design of such a multi-step guideway system showed that the system would be bulky and heavy. The concept of a three dimensional pantograph leg was eventually given up due to this difficulty.

A two dimensional pantograph was found to be adequate for the leg mechanism. No multi-step guideway system is needed if the two degree-of-freedom input motion is separately actuated on two guiding points. A preliminary design of the guideway system showed that a light weight system is possible if the sliding joints are sandwiched by two parallel guideways. Hence, a two dimensional pantograph leg mounted into a strong frame (see Figure 3.15) seemed to appropriate for the ASV leg. The frame is rotated about a longitudinal axis by the lateral actuator for leg abduction and adduction.

Thus, the two dimensional pantograph was chosen for detailed leg design. The design procedure was similar to that of the four-bar

leg design which was shown in Figure 5.14. The walking envelopes of different 2D pantographs were studied with the help of the computer program named PANTO. PANTO is an interactive program with graphical capability. After information such as the magnification ratio, the skew angle, the ratio of upper link to lower link, the actuator arrangement, the knee angle at mid-position and the leg height was entered, a pantograph leg was generated and displayed on the screen. The program then requested that the motion limits of the joints be entered. The walking envelope based on these constraints was then generated. In general, the following motion constraints were assumed:

1. None of the angles between links can be greater than 160° .
2. None of the angles between links can be less than 20° .
3. The knee joint can not be lower than the foot.
4. The foot can not be higher than the maximum height defined by the stroke of the lifting actuator.

Another capability of this program is the calculation of the bearing loads according to the load conditions of the foot.

The magnification factor of the pantograph was selected based on the compactness requirements and the results of stress analysis. A greater magnification factor results in a smaller actuating stroke and shorter actuators. However, the actuating load and the load taken by links as well as by the guideway system becomes greater too. At the initial stage of design, the minimum load condition was selected because of the possible difficulty in the design of the guideway system and the leg structure. Hence, the magnification factor was selected according to the maximum stroke length which can be mounted

in the limited space. A magnification factor of 4 was selected.

The walking envelopes were then optimized by various methods which will be described below. A few pantographs which generated satisfactory walking envelopes were then selected for further design. The interference problem between the links, the actuating systems, the frame and adjacent legs was studied. The bearing loads based on the vertical foot load condition were then calculated by the program. Finally, the stress analysis of the leg links when the foot is subjected to lateral load was studied by finite element methods. In the design procedure, a new pantograph was selected if any design criterion was not met.

6.3.2.1 Skew Angles and Actuator Arrangements

Pantograph legs with skew angles from 90° to 180° , and both T type actuator arrangements and inverted T type actuator arrangements were investigated. Figures 6.11 and 6.12 show some of the results. The dotted lines indicate the available foot path. From the results, it was found that the greater the skew angle is, the larger the area of the envelope cross section. Using an overlay of a 6 by 4 feet rectangle, an optimum walking envelope on the dotted line area can be identified. As may be seen, one corner of the rectangle is truncated because of rotary joint motion limits. In order to increase obstacle crossing ability, the size of this truncation should be minimized. The boundaries of the envelope can be shown to be segments of ellipses. The analytical form of the envelope will be discussed later.

Pantographs with 180° skew angle were selected for further design due to their large walking envelopes.

Another feature is the difference of walking envelope between T type and inverted T type actuator arrangement. The T type pantograph has slightly better envelopes as is shown in Figure 6.11 and 6.12, but this arrangement raises mechanical design problems. Since the two guiding joints and the upper link of the leg are sandwiched between two mounting plates (see front view of Figure 6.14), and the upper link of the T type leg sweeps one edge of the plates during the motion, only the other edge can be used to connect the two plates together. This type of leg frame structure was considered to be too weak. Therefore, inverted T type legs were selected for further optimization.

6.3.2.2 Offset of Walking Envelope

In Chapter 5, the overall walking volume was designed so that the rear legs were mounted reversed relative to the front legs. The reversing of the rear legs brings the offset of the center of stride from the vertical slide axis into consideration. Since the stroke pitch of the front and the middle pairs of legs and of the middle and the rear pairs of legs must be the same for a symmetric walking gait, the mounting space between the middle and the rear legs would become smaller because of the offset. This may reduce the required body length of the vehicle. However, since more space between the legs is needed for the mounting of the drive components, the offset should be minimized.

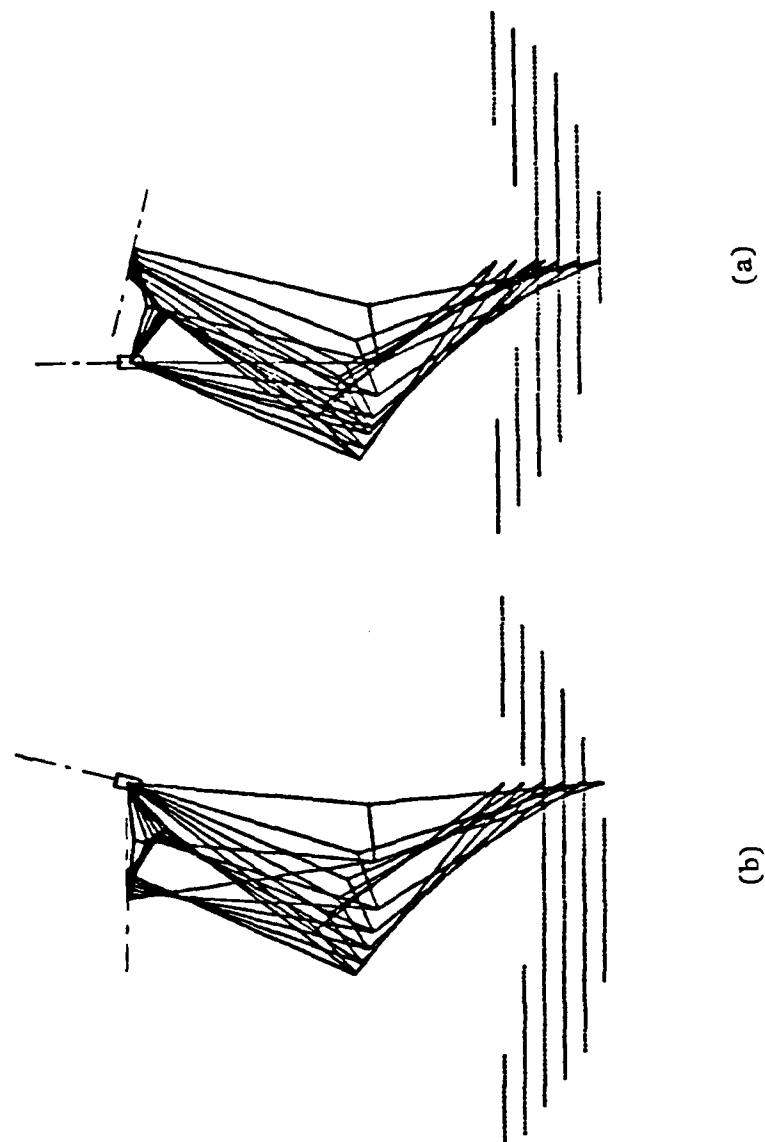


Figure 6.11: Walking envelopes of pantograph leg with 90° skew angle and (a) T type or (b) inverse T type actuator arrangement.

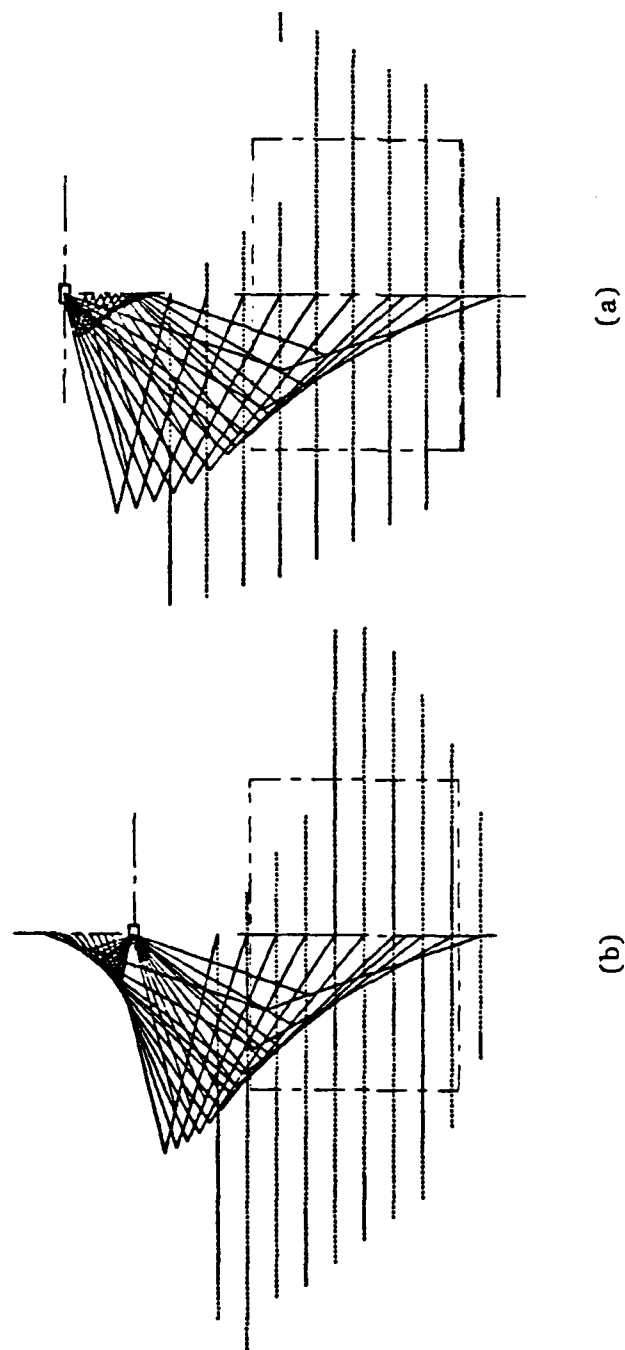


Figure 6.12: Walking envelopes of pantograph leg with 180° skew angle and (a) T type or (b) inverse T type actuator arrangement.

6.3.2.3 Ratio of Upper Link to Lower Link

The last step of optimization was to vary the ratio of the upper link to the lower link of the leg. The results showed that the smaller the ratio is, the better the walking envelope is. However, the distance of the two top joints can not be too small because of physical constraints. The results showed that ratios between 0.65 and 0.75 give very good walking envelopes and good structural geometries. A ratio of 0.7 was selected for further design. Figure 6.13 shows a comparison of the leg with ratio 0.7 to the leg with a unity ratio. After the leg geometry was properly designed, the overall geometry of the ASV was designed and is shown in Figure 6.14. The rear legs are reversed on the basis of the results of the mobility study.

6.3.3 Bearing Loads, Interference Study and Stress Analysis

The bearing loads at different foot positions were also calculated by the program. The results showed that the forces are of similar magnitude under the assumed joint limit positions, and they tend to very high values for some foot positions which go beyond the motion limits.

Interference between links, frame and actuating systems can be avoided by careful design. Figure 6.15 shows a design proposed by the engineers in the ASV project. Two pairs of actuators are mounted outside the frame for the two degree-of-freedom motion. These actuators are specially designed so that the oil is fed through the rods instead of into ports in the barrels. The reasons for this

ASV LEGS

RATIO a/b : — 0.7
 - - - 1.0

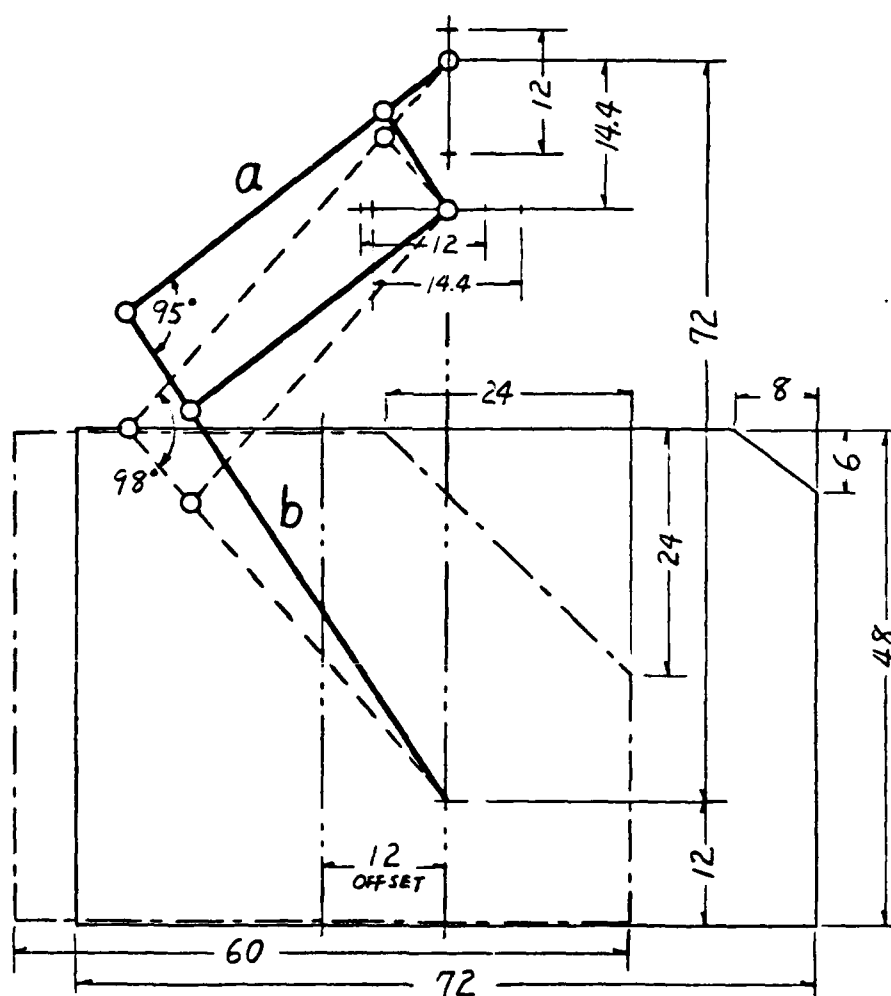


Figure 6.13: Comparison of walking envelopes of two pantograph legs.

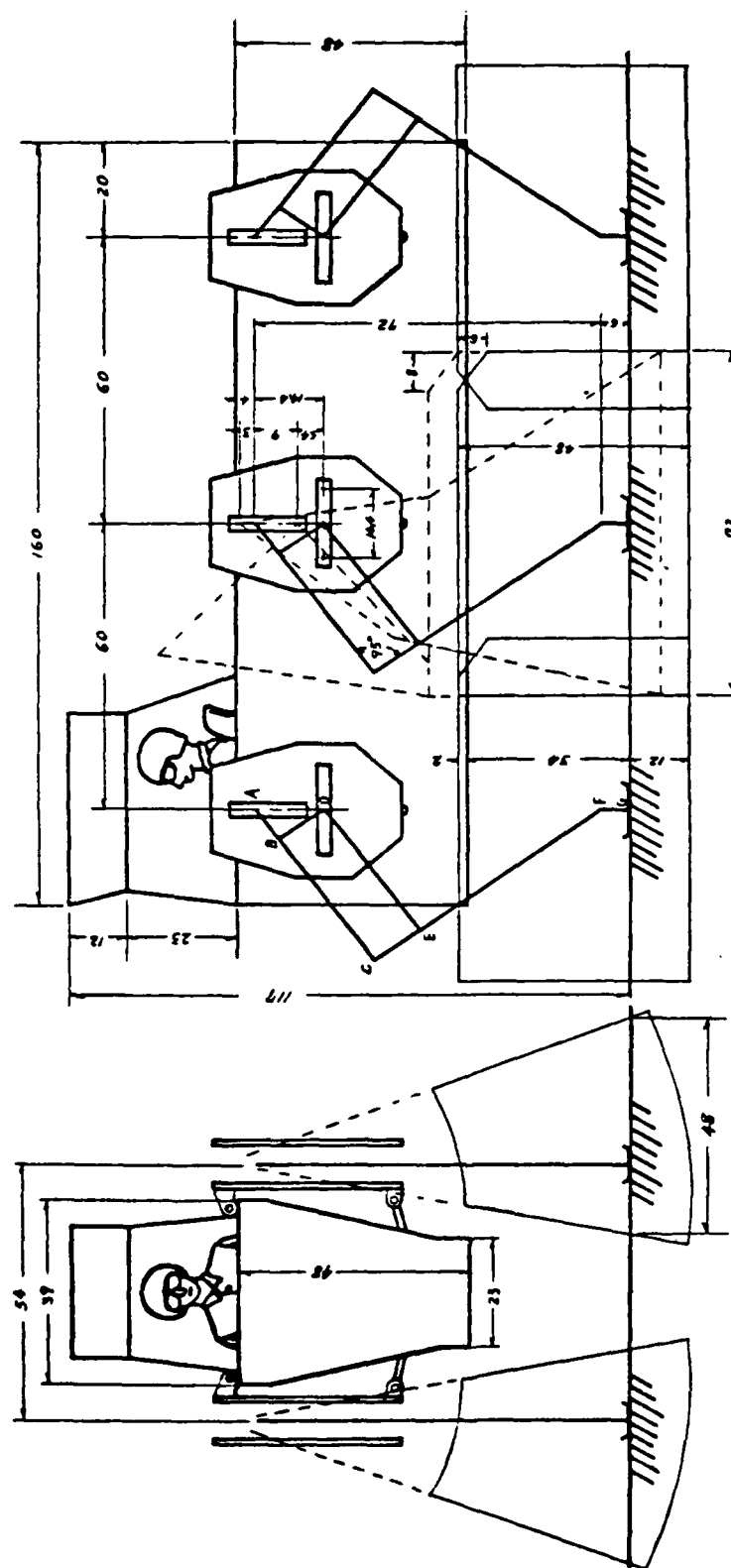


Figure 6.14: Overall walking volume of the ASV with simple pantograph legs.

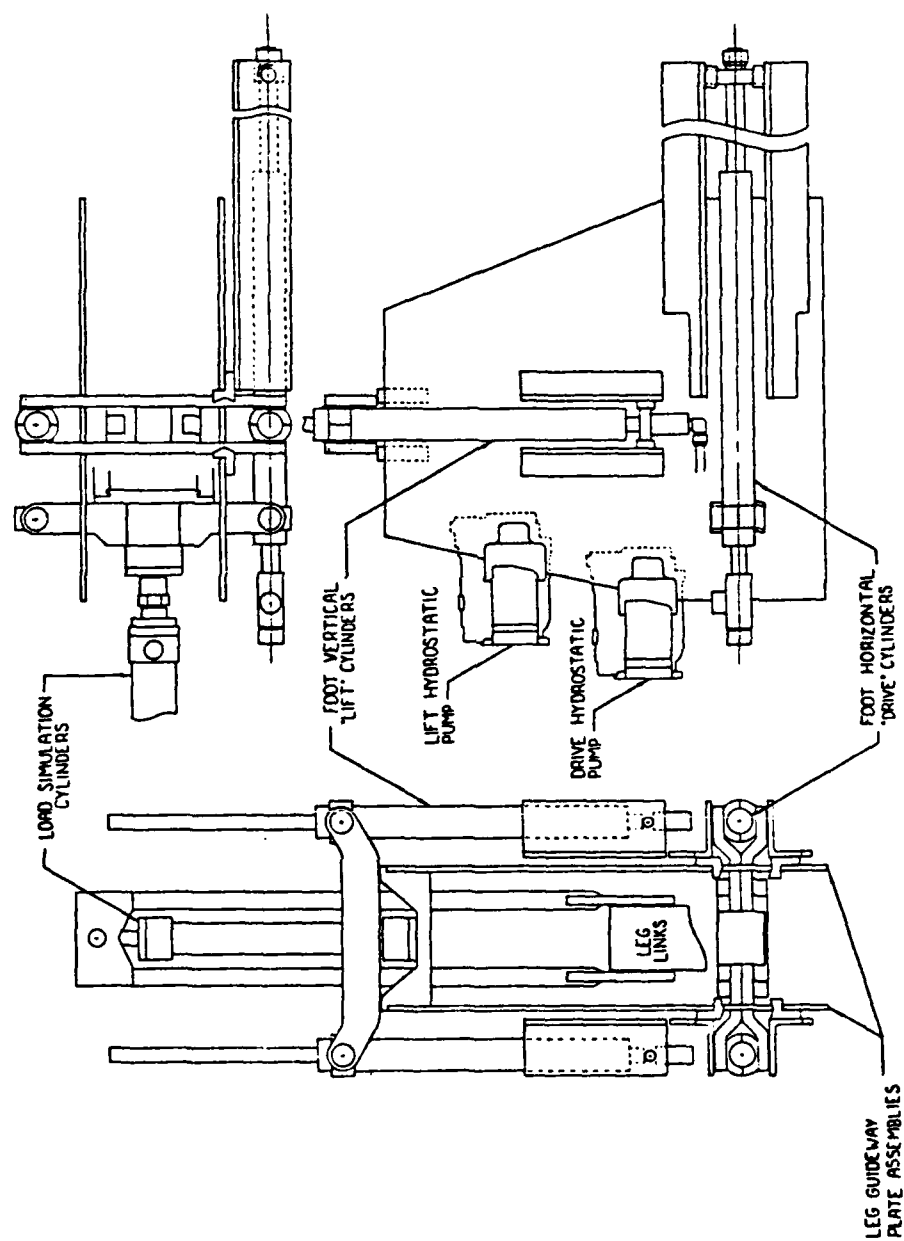


Figure 6.15: A design of the leg driving system.

design are not only reduction of mounting space, but also for the dynamic characteristics required by a hydrostatic driving system.

The interference between adjacent legs was studied by graphical methods. In Figure 6.14, the middle leg at its extreme positions is drawn in dashed lines. The space required for the link motion is mainly from the vertical slide axis to a distance equal to the upper link length ahead of it. If the driving components of the front leg are mounted outside this region, the interference is eliminated. The whole space between the middle and the rear legs can be used for the mounting of the driving components of these two legs.

The stress analysis of the leg under lateral load conditions was studied by finite element methods. Models of space beam elements were created according to five foot positions (four on the corners of the envelope and the normal position). The approach to this analysis is very similar to that used for the four-bar leg. The results were reviewed by the design engineers in the ASV projects. A leg geometry with ratio of 0.7 as shown in Figure 6.13 was found acceptable in all areas of the design specifications.

6.4 Analytical Study of the Walking Envelope of a Planar Pantograph Leg

The walking envelope of a pantograph leg is generally related to some physical motion limits, the singular positions, the strokes of the linear actuators and the actuator arrangements. The physical motion limits can be the results of interference between links, actuators, slides and the structure. Since interference can be avoided by careful design, it is not considered in this analysis.

As it was discussed in Section 6.2.2.3, singular positions created non-linear foot motion and high loads in link members. Hence, elimination of these positions is the first objective of this analysis. The strokes of linear actuators are sized according to the required walking envelope. The actuator arrangement will change the shape of the walking envelope. This arrangement should be designed giving due consideration to the problems of interference, load distribution, and ease of construction. The following is an analytical study of the walking envelope of planar pantograph leg:

6.4.1 Formulation of Equations of Motion Limits

The four motion constraints, or the motion limits, given in Section 6.3.2 can be described by four mathematical equations. By plotting these equations together, the walking envelope is obtained.

6.4.1.1 Equations of Motion Limits 1 and 2

The equations for the simple pantograph are derived first, then the general case of the skew pantograph is considered. If the angles between the links of a pantograph are kept constant, the whole mechanism will act as a rigid body on a double slide, that is, as an elliptic trammel mechanism [59]. Figures 6.10a through 6.10d show the four cases of actuator arrangements of a simple pantograph.

Referring to Figure 6.10a, let $p = AF$, $q = BF$. For case 1, the position of following point F can be defined as:

$$X_f = p \cdot \cos \beta \quad (6.6)$$

$$Y_f = p \cdot \sin \beta$$

Squaring both sides of the equations and adding gives

$$X_f^2 + Y_f^2 = p^2 \quad (6.7)$$

This is an equation of a circle with radius AF and center at (0,0).

For Case 2, referring to Figure 6.9b, a similar derivation gives

$$X_f^2 + Y_f^2 = q^2 \quad (6.8)$$

where

$$q = p + AB = ((R + 1)/R) \cdot p \quad (6.9)$$

Again, this is an equation of a circle.

For Case 3, referring to Figure 6.10c, the position of F can be defined as:

$$X_f = q \cdot \cos \beta \quad (6.10)$$

$$Y_f = p \cdot \sin \beta$$

Squaring both sides of the equations and adding gives

$$\frac{X_f^2}{q^2} + \frac{Y_f^2}{p^2} = 1 \quad (6.11)$$

Since $q \neq p$, this is an equation of an ellipse.

For case 4, referring to Figure 6.10d, the following point F can be defined as:

$$X_f = p \cdot \cos \beta \quad (6.12)$$

$$Y_f = q \cdot \sin \beta$$

This gives

$$\frac{X_f^2}{p^2} + \frac{Y_f^2}{q^2} = 1 \quad (6.13)$$

This is an ellipse which is identical in shape to the ellipse of Equation (6.11) but rotated through 90° .

The equations for motion limits 1 and 2 are obtained by substituting the following two values of p respectively into Equations (6.7), (6.8), (6.11) or (6.13) according to the actuator arrangement.

$$p_{\max} = [AE^2 + EF^2 - 2AE \cdot EF \cdot \cos (160^\circ)]^{1/2} \quad (6.14)$$

$$p_{\min} = [AE^2 + EF^2 - 2AE \cdot EF \cdot \cos (20^\circ)]^{1/2} \quad (6.15)$$

For skew pantographs other than simple pantographs, similar results are obtained. For Case 1, the equation is the same as equation (6.7). For Case 2, the equation is the same as equation (6.8). However, the value BF becomes

$$q = (1 + R^2 - 2 \cdot R \cdot \cos \phi)^{1/2} \cdot (p/R) \quad (6.16)$$

The value of ϕ is 160° and 20° for motion limits 1 and 2, respectively.

For Cases 3 and 4, the derivation of the equations is more complicated. Figure 6.16 shows a skew pantograph with a Case 3 actuator arrangement. The following point F is defined by:

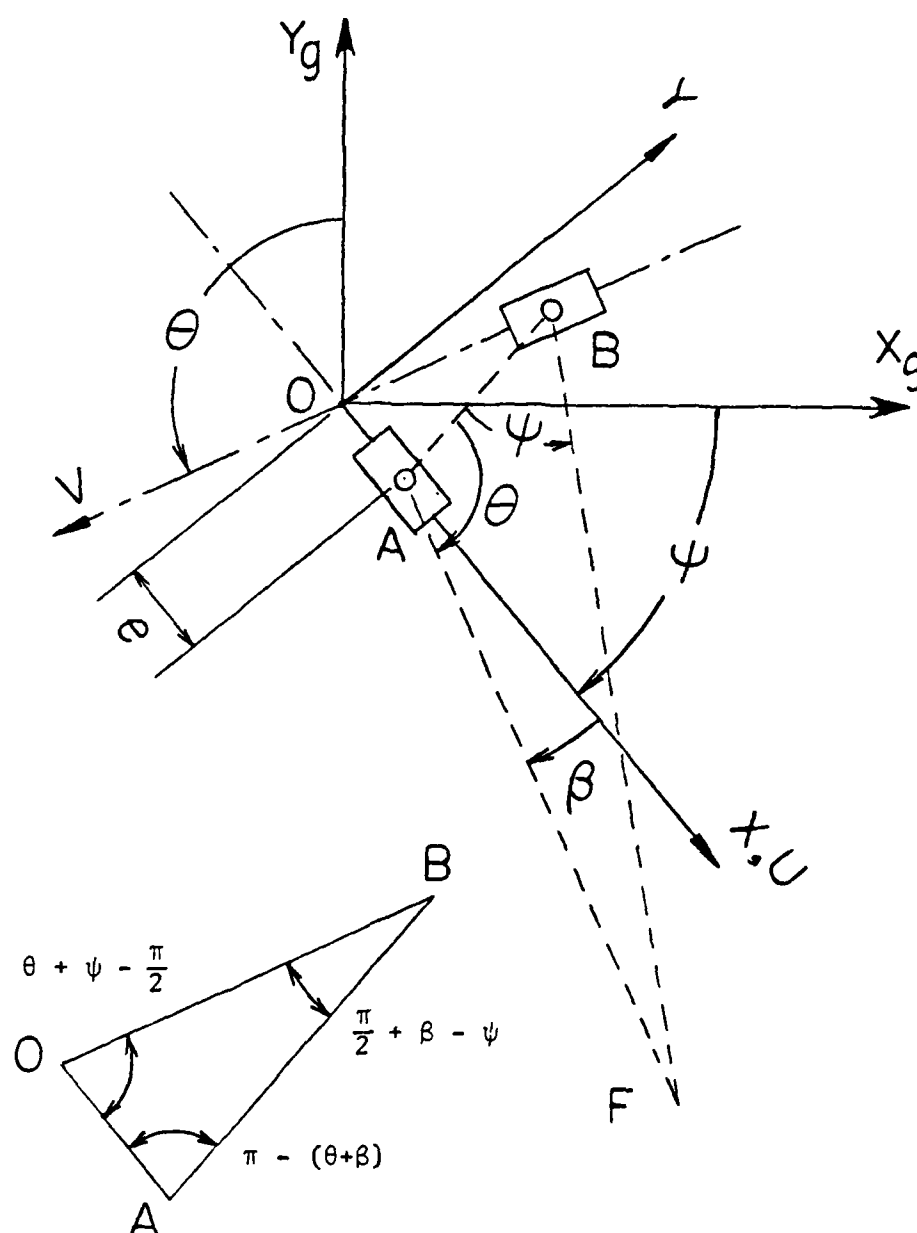


Figure 6.16: Analytical study of motion limit 1 and 2 of a skew pantograph leg with case 3 actuator arrangement.

$$\begin{aligned}
 X_f &= e + p \cdot \cos \beta \\
 Y_f &= p \cdot \sin \beta
 \end{aligned}
 \tag{6.17}$$

The law of sines applied to triangle OAB gives:

$$OA/\sin (\angle OBA) = AB/\sin (\angle AOB))$$

Substituting the values of angles gives

$$e/\sin (\pi/2 + \beta - \psi) = AB/\sin (\theta + \psi - \pi/2)$$

which gives

$$\begin{aligned}
 e &= [\cos (\beta - \psi) \cdot p]/[\cos (\theta + \psi) \cdot R] \\
 &= [(-\cos \beta \cdot \cos \psi - \sin \beta \cdot \sin \psi) \cdot p]/[R \cdot \cos (\theta + \psi)]
 \end{aligned}$$

Therefore equation (6.17) becomes:

$$\begin{aligned}
 [X_f + \frac{\sin \psi \cdot p}{R \cdot \cos (\theta + \psi)} \cdot \sin \beta] &= [p - \frac{\cos \psi \cdot p}{R \cdot \cos (\theta + \psi)}] \cdot \cos \beta \\
 Y_f &= p \cdot \sin \beta
 \end{aligned}
 \tag{6.18}$$

Eliminating β on the right side and letting $\sin \beta = Y_f/p$, the equation of the locus becomes:

$$a \cdot X_f^2 + 2h \cdot X_f \cdot Y_f + b \cdot Y_f^2 + c = 0 \tag{6.19}$$

where

$$a = 1/\{p^2 \cdot [1 - \cos \psi / (R \cdot \cos (\theta + \psi))]\}^2$$

$$h = a \cdot d$$

$$b = a \cdot d^2 + 1/(p^2)$$

$$c = -1$$

$$d = \sin \psi / [R \cdot \cos (\theta + \psi)]$$

This is the equation of a conic. Recall that the characteristic equation D specifies the sub-type of the conic:

$$D = \begin{vmatrix} a & h \\ h & b \end{vmatrix} \quad (6.20)$$

where $D > 0$ for an ellipse

$D = 0$ for a parabola

$D < 0$ for a hyperbola

Substituting the values of a , b and h into equation of D gives

$$D = a/(p^2) > 0 \quad (6.21)$$

Therefore, this is an equation of an ellipse. The principal axis of the ellipse intersects the X axis at angle α , where

$$\alpha = (1/2) \tan^{-1} [2h/(a - b)] \quad (6.22)$$

The equation of Case 4 can be derived in a similar way.

Referring to Figure 6.17, the following point F is defined by:

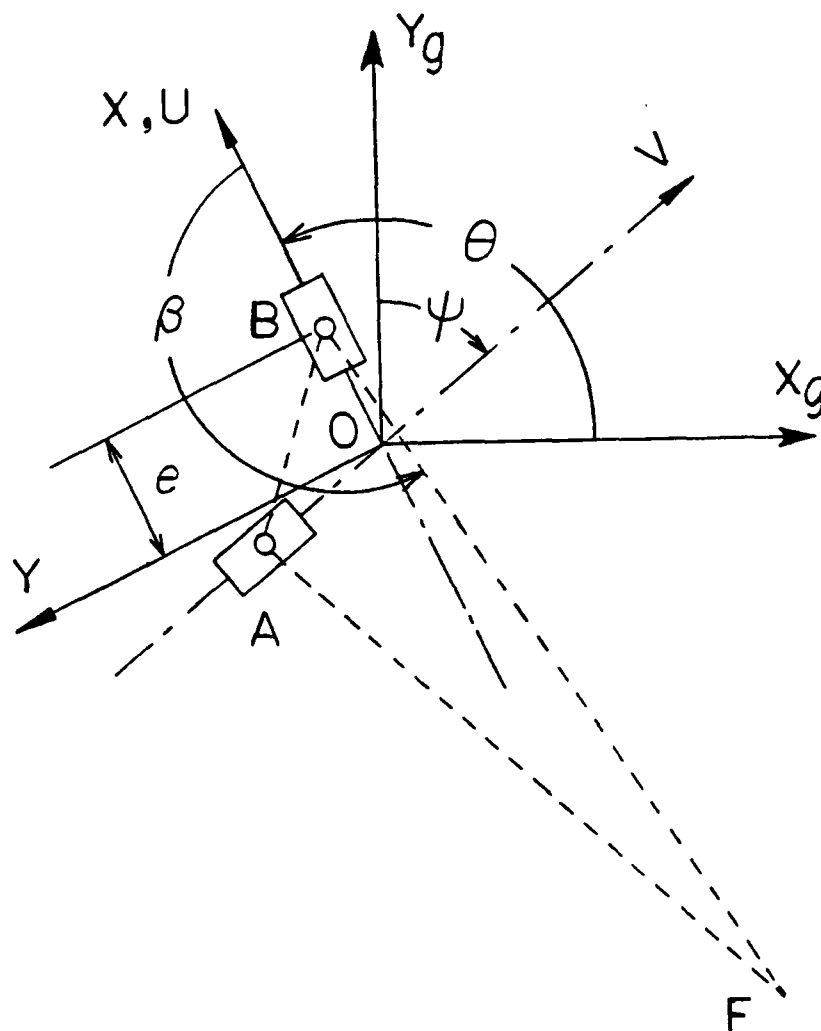


Figure 6.17: Analytical study of motion limit 1 and 2 of a skew pantograph leg with case 4 actuator arrangement.

$$\begin{aligned} X_f &= e + q \cdot \cos \beta \\ Y_f &= q \cdot \sin \beta \end{aligned} \quad (6.23)$$

The resulting equation becomes

$$a' \cdot X_f^2 + 2h' \cdot X_f \cdot Y_f + b' \cdot Y_f^2 + c' = 0 \quad (6.24)$$

where

$$a' = 1/\{p^2 \cdot [R'/R + \cos \psi / (R \cdot \cos (\theta + \psi))]\}^2\}$$

$$h' = a' \cdot d'$$

$$b' = a' \cdot d'^2 + 1/[(R'/R) \cdot p]^2$$

$$c' = -1$$

$$d' = \sin \psi / [R' \cdot \cos (\theta + \psi)]$$

The principal axis of this ellipse intersects the X-axis with an angle α' , where

$$\alpha' = (1/2)\tan^{-1}[2h'/(a' - b')] \quad (6.25)$$

6.4.1.2 Equation of Motion Limit 3

Figure 6.18 shows a skew pantograph at the position of motion limit 3 in which points D and F are on the same level. The position of point F relative to the ground coordinate system can be defined as

$$X_f = CD \cdot \cos \phi - DF \cdot \cos \psi + OC \quad (6.26)$$

$$Y_f = CD \cdot \sin \phi - DF \cdot \sin \psi \quad (6.27)$$

The relationship between the angles of the triangle OBC is shown at the bottom of the figure. Applying the law of sines gives

$$\begin{aligned} OC &= \frac{\sin (\pi/2 + \phi - \psi)}{\sin (\theta + \psi - \pi/2)} \cdot BC \\ &= \frac{-\cos \phi \cdot \cos \psi - \sin \phi \cdot \sin \psi}{R \cdot \cos (\theta + \psi)} \cdot CD \end{aligned} \quad (6.28)$$

Substitution of Equation (6.28) into Equation (6.26) and movement of all terms to the left side except $\cos \phi$, also, movement of all terms of Equation (6.27) to the left side except $\sin \phi$, followed by elimination by squaring followed by an addition of these two resultant equations, and finally substitution of the following equation into the remained equation gives an equation of conic.

$$\sin \phi = \frac{Y_f + DF \cdot \sin \psi}{CD} \quad (6.29)$$

Further manipulation of the resulted equation of conic leads to the following equation:

$$a \cdot X_f^2 + 2h \cdot X_f \cdot Y_f + b \cdot Y_f^2 + 2g \cdot X_f + 2f \cdot Y_f + C = 0 \quad (6.30)$$

where

$$a = 1/[CD^2 \cdot [1 - \cos \phi / (R \cdot \cos (\theta + \psi))]^2]$$

$$h = a \cdot d$$

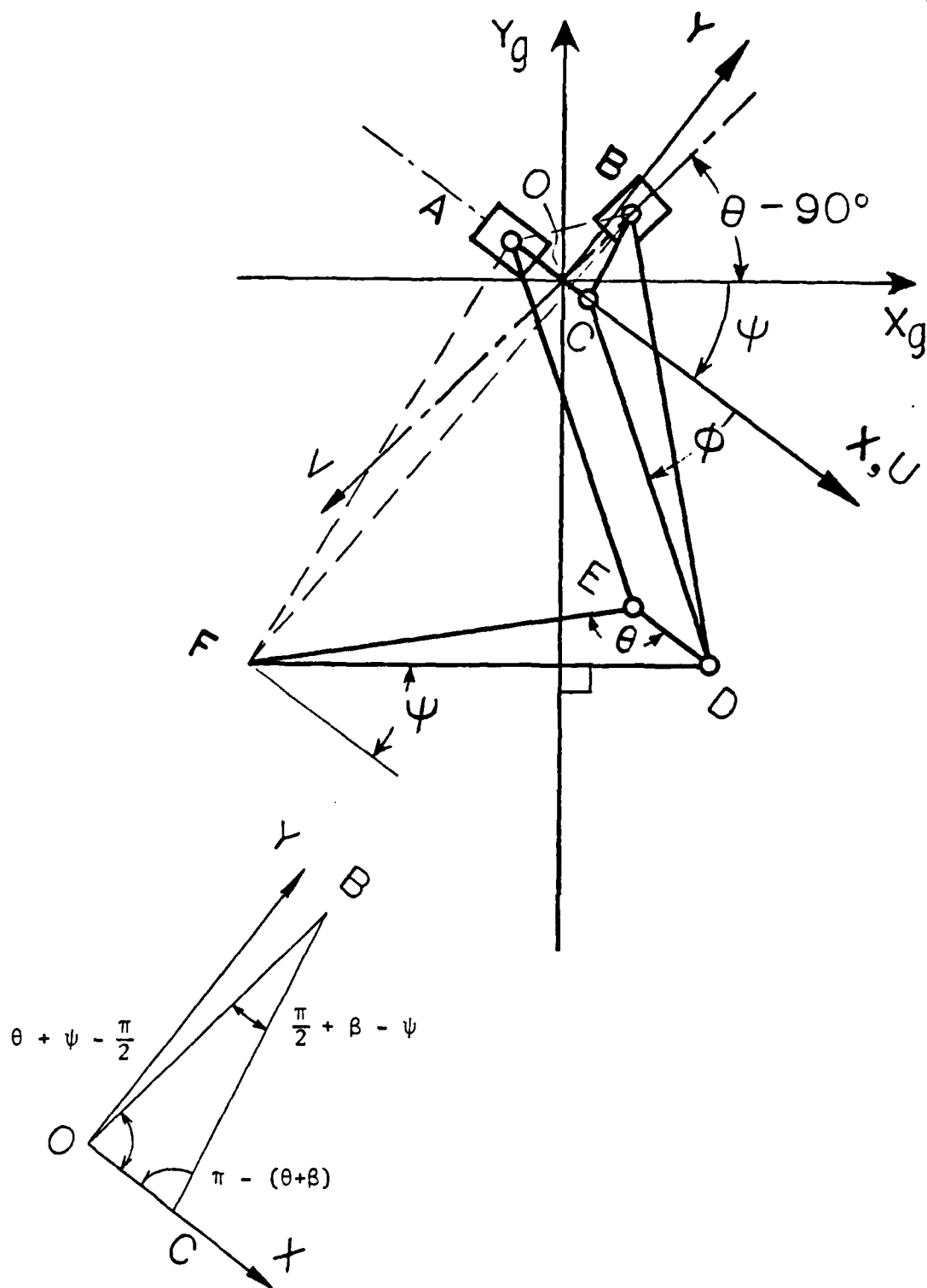


Figure 6.18: A skew pantograph leg at position of motion limit 3.

$$b = a \cdot d^2 + 1/(CD^2)$$

$$g = a \cdot i$$

$$f = e \cdot [a \cdot d^2 + 1/(CD^2)] + a \cdot i \cdot d$$

$$c = e^2 \cdot [a \cdot d^2 + 1/(CD^2)] + 2a \cdot i \cdot d \cdot e + a \cdot i^2 - 1$$

$$d = \sin \psi / [R \cdot \cos (\theta + \psi)]$$

$$e = DF \cdot \sin \psi$$

$$i = DF \cdot \cos \psi$$

Applying Equation (6.20) gives $D = a/(CD^2) > 0$. Therefore, this is an equation of an ellipse. The angle α between the principal axis of the ellipse and the X axis is

$$\alpha = (1/2)\tan^{-1}[2h/(a - b)] \quad (6.31)$$

6.4.1.3 Equation of Motion Limit 4

For any skew pantograph, since the two linear actuators are on the principal axes U-V, let the strokes of these two actuators be bounded by

$$\begin{aligned} U_1 &\leq U \leq U_2 \\ V_1 &\leq V \leq V_2 \end{aligned} \quad (6.32)$$

If the reference coordinate system X-Y has its origin at the intersection of the two principal axes, the accessible region of point F

can be defined according to each case.

For Case 1

$$\begin{aligned} R \cdot U_1 &\leq X_f \leq R \cdot U_2 \\ R \cdot V_1 &\leq Y_f \leq R \cdot V_2 \end{aligned} \quad (6.33)$$

For Case 2

$$\begin{aligned} (R + 1) \cdot U_1 &\leq X_f \leq (R + 1) \cdot U_2 \\ (R + 1) \cdot V_1 &\leq Y_f \leq (R + 1) \cdot V_2 \end{aligned} \quad (6.34)$$

For Case 3

$$\begin{aligned} R \cdot U_1 &\leq X_f \leq R \cdot U_2 \\ (R + 1) \cdot V_1 &\leq Y_f \leq (R + 1) \cdot V_2 \end{aligned} \quad (6.35)$$

For Case 4

$$\begin{aligned} (R + 1) \cdot U_1 &\leq X_f \leq (R + 1) \cdot U_2 \\ R \cdot V_1 &\leq Y_f \leq R \cdot V_2 \end{aligned} \quad (6.36)$$

The regions defined by these equations are either squares or rectangles.

For a given planar skew pantograph with a specified actuator arrangement, the corresponding equations of motion limits 1, 2, 3 and 4 can be established by substituting the parameters of the pantograph into the derived equations. By plotting these four equations together, four areas which are permitted by the corresponding motion limit are identified. The intersection of these four areas is the walking

envelope. Figure 6.19 shows an example of a walking envelope obtained by this method. A few pantograph leg geometries were selected to find their walking envelopes using this method. The results are consistent with the walking envelopes obtained through computer program PANTO.

6.4.2 Optimization of Walking Envelope

The way to optimize the walking envelope by analytical methods is to construct the walking envelopes of pantograph leg geometries with different skew angles, actuator arrangements, ratios of upper link length to lower link length ... etc. The optimal walking envelope can be selected according to the requirements. However, if the relationship of the shapes of the ellipses to each parameter is understood, the optimization will be easier. The following discussion demonstrates a simple relationship between the ellipses of motion limit 1 and the skew angle of a given pantograph leg. Other relationships can be found by similar approach to that presented.

For any given skew pantograph, a reference coordinate system is chosen so that the X-actuator, which generates X-movement of the X_g-Y_g coordinates, is in line with the X-axis. Since skew angles greater than 180° usually cause interference problems between the links, only skew angles between 0° and 180° are studied here. If the principal parallelogram remains the same, the variation of the skew angle only changes the length of BF of the equivalent triangle while keeping AB and AF the same.

For Case 1, the work space does not change at all. For case 2, the accessible region defined by motion limit 1 changes because the

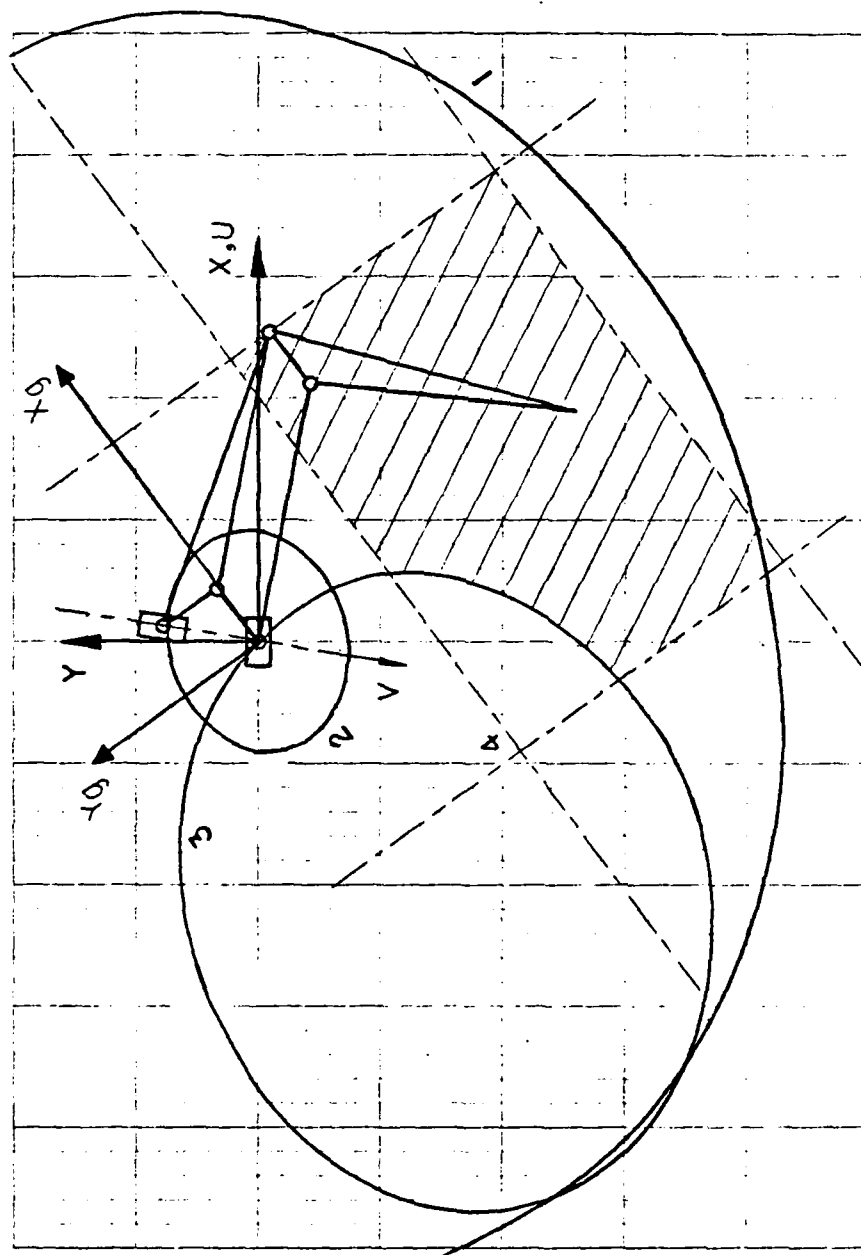


Figure 6.19: An example of the walking envelope obtained by analytical method.

radius BF of the circles changes. The difference is easy to understand. For Case 3, the influence is more hidden. Equations (6.19) and (6.22) give the equation of the ellipse and the direction of its principal axis. However, the angle α in equation (6.22) may be either the direction of the long axis or that of the short axis. A coordinate transformation through angle α should be calculated and compare the coefficients of X'^2 and Y'^2 . If the coefficient of X'^2 is greater than that of Y'^2 , the angle α should be replaced by $90^\circ + \alpha$. By rotating the reference coordinates through the new angle α , the equation of the ellipse in the new coordinate frame $X'-Y'$ is simplified into the standard form of an ellipse

$$\frac{X'^2}{A^2} + \frac{Y'^2}{B^2} = 1 \quad (6.37)$$

where $A > B$. $2A$ is the length of the long axis and $2B$ is the length of the short axis of the ellipse. The values of A and B are the inverses of the two roots of the following equation respectively.

$$Z^2 - (a + b) \cdot Z + D = 0 \quad (6.38)$$

where a and b are defined in equation (6.19) and D is defined in equation (6.20). By knowing A , B and the rotation angle α , the ellipse can be plotted easily. By plotting the ellipses of different skew angles, the affect of the skew angle on the work space can be seen. Figure 6.20 shows ellipses for pantographs of different skew angles with $AB = 0.8$, $R = 4$ and principal angle $\phi = 160^\circ$. As the skew

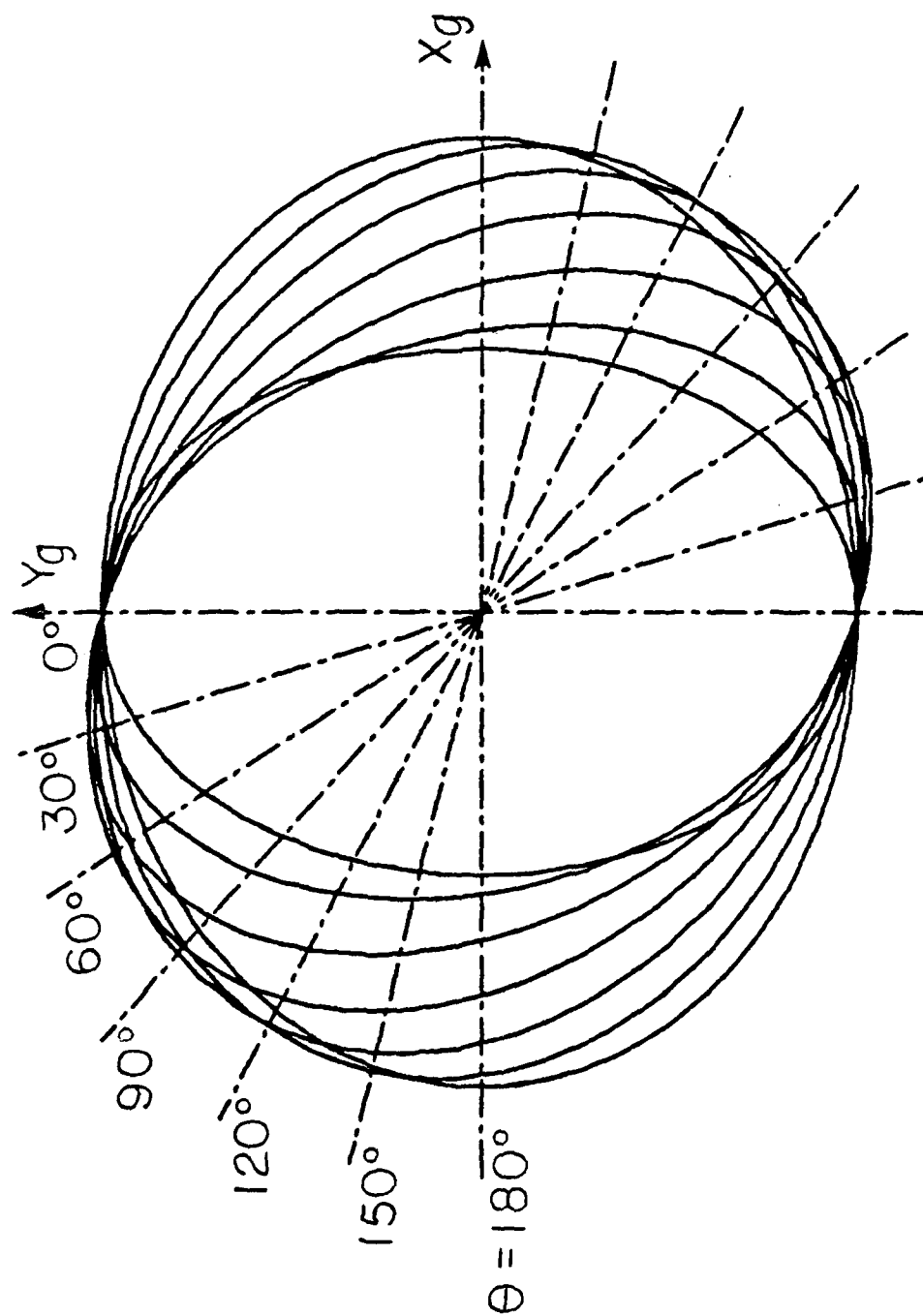


Figure 6.20: Ellipses of motion limit 1 with different skew angles, $\phi = 160^\circ$, $R = 4$, $AB = 0.8$, case 3 actuator arrangement.

angle increases from 0° to 180° the size of the ellipse increases, i.e., both elliptic axes increase, and the angle between the long axis and the corresponding X-direction decreases from 90° to 0° . Since the X-axis of the reference frame also rotates through an angle $-\psi$ from the X-axis relative to X_g-Y_g , the direction of the long axis relative to X_g-Y_g becomes $\alpha - \psi$. Thus it rotates from -90° to 0° as θ increases.

Another feature observed is that the difference between the two elliptic axes changes as θ changes. It starts with a value $2AB$ when θ is 0° and increases to a maximum at $\theta = 90^\circ$, then decreases to its initial value $2AB$ at $\theta = 180^\circ$. This means that the shape of the ellipse becomes sharper when θ is closer to 90° . The parameters of the ellipses of motion limit 1 with different skew angles are tabulated in Table 6.1.

Table 6.1

Characteristics of ellipses of motion limit 1 with case 3 actuator arrangement, $AB = 0.8$, $R = 4$ and $\phi = 160^\circ$.

θ	α	$\alpha - \psi$	2A	2B	2A - 2B
0	90.00	-90.00	6.40	4.80	1.60
30	67.94	-72.99	6.60	4.98	1.62
45	58.15	-67.43	6.81	5.17	1.64
60	49.40	-56.70	7.05	5.40	1.65
90	34.53	-42.43	7.47	5.82	1.65
120	22.02	-27.09	7.77	6.14	6.63
135	16.27	-20.18	7.88	6.26	1.62
150	10.75	-13.38	7.94	6.33	1.61
180	0.00	0.00	8.00	6.40	1.60

For the case 4 actuator arrangements, by applying equations (6.24) and (6.25) a similar result is obtained. As the skew angle increases from 0° to 180° the size of ellipse increases and the direction of the long axis relative to X_g-Y_g rotates from 0° to 90° .

The relationships of the shapes of ellipses corresponding to other motion limits to each optimization factor can be established in a similar way. The understanding of these relationships would save much time in optimizing a pantograph leg. These relationships can be easily extended to optimize the work space of a pantograph manipulator.

6.5 Comparison of the Seven-Bar and the Pantograph Leg

The advantages and disadvantages of the two leg geometries can be summarized as follows:

Seven-Bar Leg

Advantages:

1. The mechanism is connected by rotary joints only. This makes the mechanical design easier and the mechanism more reliable.

Disadvantages:

1. It requires longer total mechanism to produce desired walking envelope.
2. It only generates an approximate straight line foot path when only the drive actuator is used.
3. It is likely to have less energy efficiency because a linear motion is converted to a rotary motion, then is converted back to a linear motion.

Pantograph Leg

Advantages:

1. The leg geometry is more compact.
2. It generates an exact straight line.
3. It is likely to have better energy efficiency due to decoupled foot motion and exact straight line motion.
4. The actuators can be placed high on the leg minimizing rotating inertia.
5. It has a simpler coordination control algorithm due to decoupled motion and linear relationship between input and output motions.

Disadvantages:

1. The two linear actuating systems are hard to design and may have mechanical reliability problems.

Both the seven-bar leg and the pantograph leg have the potential to be suitable legs for the ASV. The only difficulty in designing a pantograph leg was the design of the heavy duty linear actuating systems. This difficulty was eventually removed by a design engineer in the ASV project. Hence, the pantograph leg was selected because of the many advantages stated above. The detailed design of mechanical parts of the leg can be found in reference [62].

Figure 6.21 shows a pantograph leg mounted on a frame. The ratio of the upper link to the lower link of this leg is unity, as indicated by the dashed lines in Figure 6.13, because the final leg geometry was not available at the time of construction of this leg. The shank is cranked to avoid possible interference between the leg and obstacles in front of the leg. A passive hydraulic ankle is also installed to keep the foot parallel to the body. This leg has been operating in the laboratory and the performance is satisfactory.

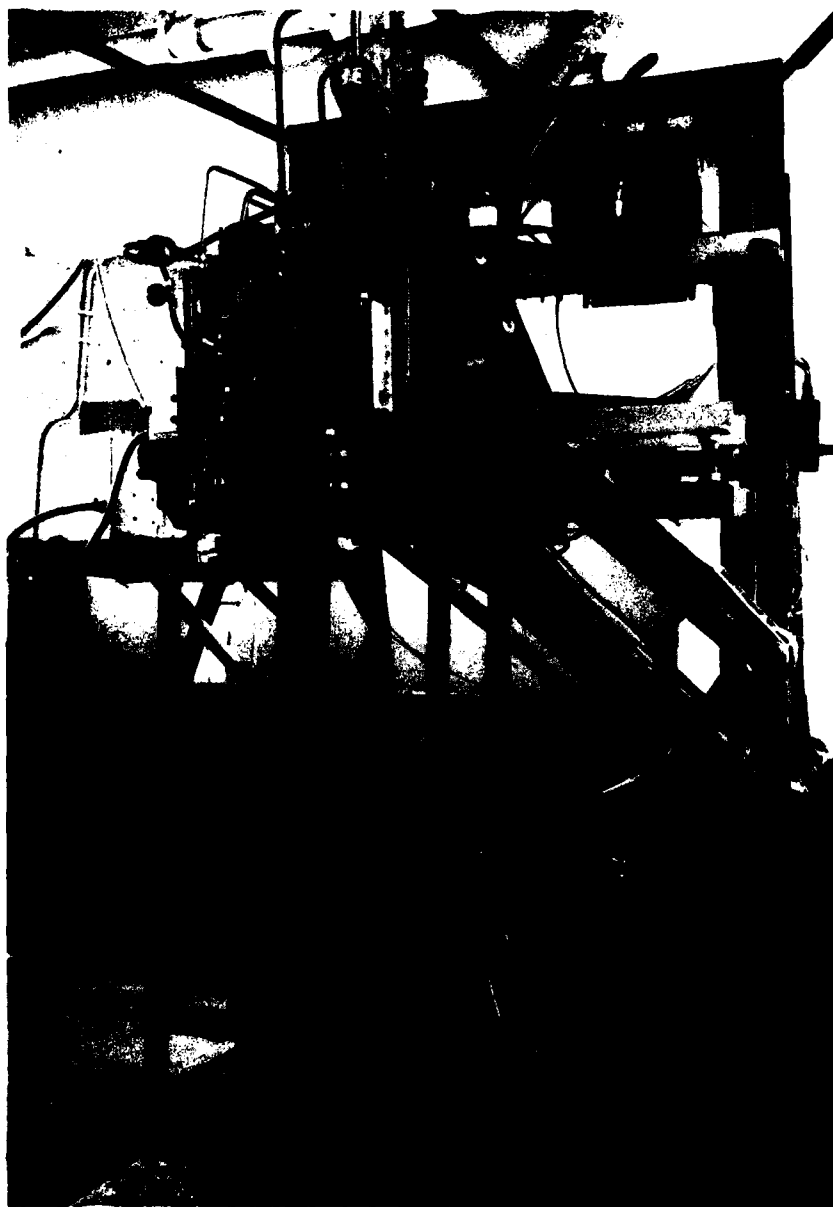


Figure 6.21: The breadboard leg.

6.6 Summary

In this chapter, a leg geometry based on a two dimensional pantograph mechanism was designed. A theoretical derivation of the basic theorems and equations relating to two and three dimensional pantographs was given. The motion characteristics of pantographs were then discussed. A leg geometry was designed by computer-aided graphical methods. The walking envelope of this leg geometry was optimized by varying the skew angle, using different actuator arrangements, adjusting the offset of the walking envelope, and changing the ratio of the upper link length to that of the lower link. By virtue this design, a pantograph leg which meets all the design specifications for the leg of the ASV was obtained. An analytical study of the work spaces of two dimensional pantographs was also given. The results of this analytical study confirmed the leg geometry designed by graphical methods. Finally, a comparison of pantograph legs to seven-bar legs was given, and the pantograph leg was selected to be the leg of the ASV-84.

Chapter 7

ANKLE DESIGN

7.1 Introduction

Leg linkages which generate satisfactory walking volumes were designed in Chapters 5 and 6. In those designs, a foot with rounded sole rigidly attached to the shank was assumed. Since the foot reference point was chosen to coincide with the center of the circular foot profile, the leg height was not altered by the rolling of the foot on the ground. Hence, the design of the leg linkage and the foot design could be carried out separately. However, the foot does strongly affect the leg performance and should be considered conceptually in the leg design.

Some walking machines built in the past used a rigid foot design. The G.E. Quadruped was one example of this type of foot design [10]. The shape of the foot used in the G.E. Quadruped was similar to a human foot. Since the vehicle's motion did not depend on a foot effective point which generates a straight line segment, the major function of its foot was mainly to provide firm support at all angles of foot contact. Other previously built walking machines have been equipped with feet which have ankle joints. The PV II was of this type [21].

The PV II used a parallel wire system to maintain foot attitude during walking.

A complete foot design should include a sole design and an ankle design. For each type of soil condition, a special sole should be designed, and different soles should be mounted interchangeably on the foot according to the soil condition. A complete sole design is complicated because soil mechanics should be involved in the design. Hence, it is not the intention in this chapter to cover the details of sole design. At this stage, a sole which provides sufficient traction and proper contact pressure and enables the vehicle to walk on hard surfaces should be adequate.

The ankle design has a strong affect on the leg performance. Hence, in the design of the leg linkage it is necessary to conceptualize the possible ankle systems which may be used on the vehicle. In Section 7.2, a comparison between a rigid foot and a foot with an ankle joint is made to show the importance of an ankle joint. In Section 7.3, a few conceptual designs of active ankle joints are introduced. In Section 7.4, two types of passive ankle systems, the parallel linkage system and the hydraulic master-slave ankle system, are introduced.

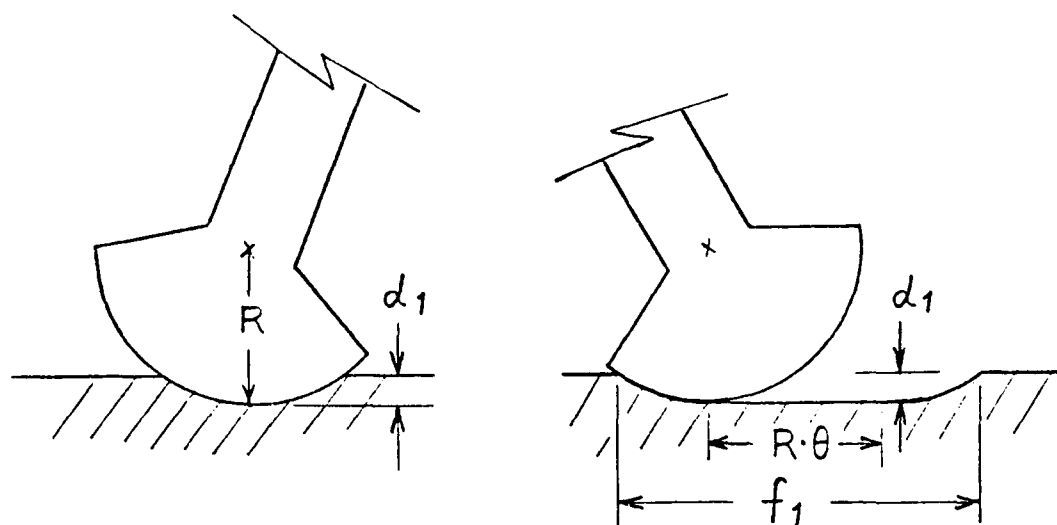
7.2 Rigid Foot and Foot with an Ankle Joint.

The rigid foot is simple in structure and was used on many walking machines built in the past. Since the angle of the shank relative to the ground changes continually during walking, the

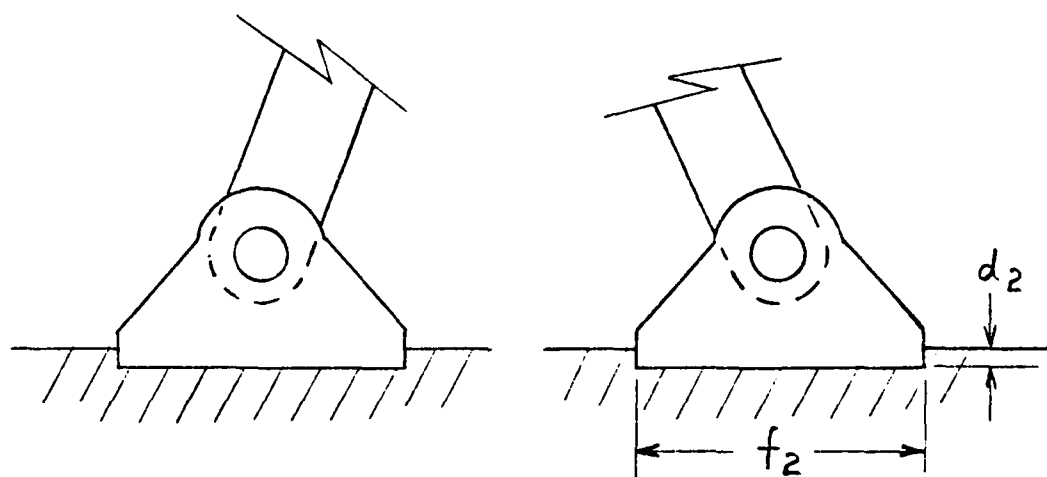
foot is rolling on the ground surface during the support phase. This change of shank angle is about 30° for the four-bar leg and the seven-bar leg (for 4.5 foot stroke), and it is about 60° for the pantograph leg (for 6 foot stroke and at normal walking height). Since the foot reference point used in the leg design coincides with the center of the foot profile, this rolling action does not alter the height of the foot reference point. However, if no slip occurs between the foot and the ground, the rolling action moves the foot reference point horizontally during walking. Let the change of shank angle in one step be θ and the radius of the foot profile be R , then the horizontal movement of the foot point is $R \cdot \theta$.

The rolling of the foot degrades the leg performance due to the following three deficiencies: The first deficiency is that the support of the foot is not firm. The vehicle usually depends on the sensors on the foot to detect whether the soil condition is suitable for weight bearing or not. If the contact area on which the foot is first placed is suitable, but the contact area moves into a weak soil area due to the foot rolling, the leg may lose its support and cause the vehicle to fall.

The second deficiency is that the horizontal movement of the foot reference point does not take place at constant speed due to the varying angular speed of the shank. This horizontal movement will alter the foot velocity relative to the body and make coordination among the legs difficult. If this difference in speed among legs which are on the ground is not compensated for by proper control,



(a)



(b)

Figure 7.1: Soil deformation of a rigid round foot and a flat foot with an ankle joint.

either slip of the feet or twisting of the body will occur and degrade vehicle stability and efficiency.

The third deficiency is that a rolling rounded foot will waste more energy in deforming the soil than a flat foot with an ankle joint will do. This can be seen by referring to Figure 7.1. If both feet have the same projected area and foot width, the maximum depth of deformation d_1 of a round foot is greater than that of a flat foot (d_2) due to its smaller contact area. After the rigid round foot is rolled through a step, the area of maximum deformation d_1 is lengthened by a distance of $R \cdot \theta$ provided no slip occurs. Hence, the total deformed length f_1 is longer than f_2 . It is reasonable to assume that the resisting force of the soil increases along with the depth of deformation. Since most of the area of the footprint made by the round foot is deeper than the footprint made by a flat foot, more work is required for the rigid round foot in soil deformation.

A proper design of a foot with an ankle joint can eliminate all three deficiencies mentioned above. One type of ankle joint which is found in walking machines built in the past is a ball or gimbal free joint. This type of ankle is in use on the OSU Hexapod [61]. Although this kind of ankle joint solves the problems mentioned above, it raises two other problems on some occasions: When the leg movement is fast, the dynamic foot displacement would cause the foot to be in a rotated position when it is placed, resulting in a stumble. Hence, the foot attitude in transfer phase should be kept unchanged

during leg motion. The second problem is that a small area as shown in Figure 7.2, which may be crucial in obstacle crossing, can not be selected for foot bearing if any free ankle joint is used. Hence, an ankle joint which can bear certain amount of torque and maintain constant foot attitude in support phase should be used. In general, there are two kinds of ankle systems which may be used to keep the foot attitude unchanged during walking: One is an active ankle system and the other is a passive ankle system.

7.3 Active Ankle System

An active ankle system has an actuator acting on the foot through a crank or mechanism. Figure 7.3 shows two conceptual designs for an active ankle system. In order to keep the foot attitude, the actuator has to be operating continuously during walking.

The advantage of an active ankle joint is that the additional degree of freedom increases the vehicle's mobility. However, an active ankle system was not considered for use on the ASV for the following two reasons: One is that the additional degree of freedom complicates the leg control which is originally complicated enough. The second reason is that to continue actuation during walking consumes significant energy and degrades vehicle efficiency.

7.4 Passive Ankle System

A passive ankle system would keep the foot attitude unchanged during walking without adding complexity to the leg control. Usually,

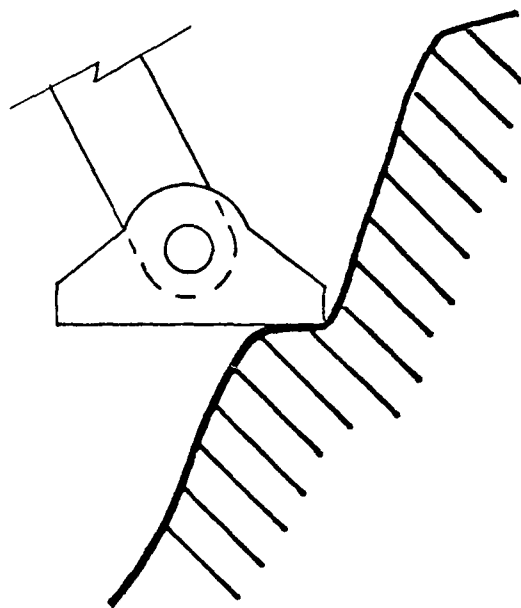
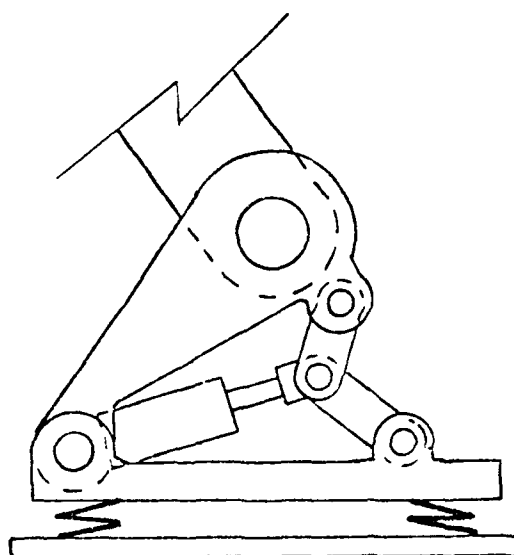
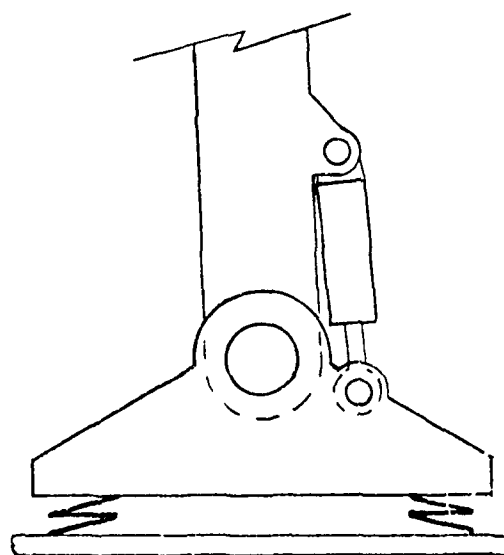


Figure 7.2: A weak support of a foot with a free ankle joint.



(a)



(b)

Figure 7.3: Two conceptual designs of active ankle system.

AD-A159 147

AN EXPERIMENTAL STUDY OF AN ULTRA-MOBILE VEHICLE FOR
OFF-ROAD TRANSPORTAT. (U) OHIO STATE UNIV RESEARCH
FOUNDATION COLUMBUS R B MCGHEE ET AL. MAY 85

5/5

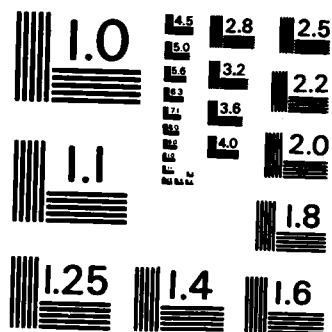
UNCLASSIFIED

MDA903-82-K-0058

F/G 13/6

NL

									END				
									FILED				
									DTIC				



MICROCOPY RESOLUTION TEST CHART
NATIONAL BUREAU OF STANDARDS-1963-A

the normal foot attitude is chosen to be the same as the body attitude. Two simple passive ankle systems are presented below: A parallel linkage system and a hydraulic master-slave system.

7.4.1 Parallel Linkage System

Figure 7.4a shows a double parallel linkage. The attitude of the middle coupler and the end coupler are kept the same as the base in all positions which the end coupler can reach. Figure 7.4b shows a modification of the double parallel linkage, which is the well known mechanism used in drafting machines. The four connecting cranks are replaced by machine elements which are rigid in the longitudinal direction yet flexible in the lateral direction. During motion, these flexible elements deflect on the round surfaces of the base and the two couplers without a slip. This modified linkage increases the reaching area of the end coupler. If the base is fixed to the body of the vehicle, and the middle and the end couplers are attached to the knee joint and the ankle joint, respectively, the foot attitude is kept parallel to the body at all times. If more joints exist between the ankle joint and the base, the same function can be achieved by adding one middle coupler to each middle joint. This type of ankle system has been applied on the PV II [21], in which a set of parallel linkages which maintains the foot attitude unchanged in both longitudinal and lateral direction is used.

The advantage of the passive ankle system is that it is potentially highly efficient. Figure 7.5 shows a pantograph leg with

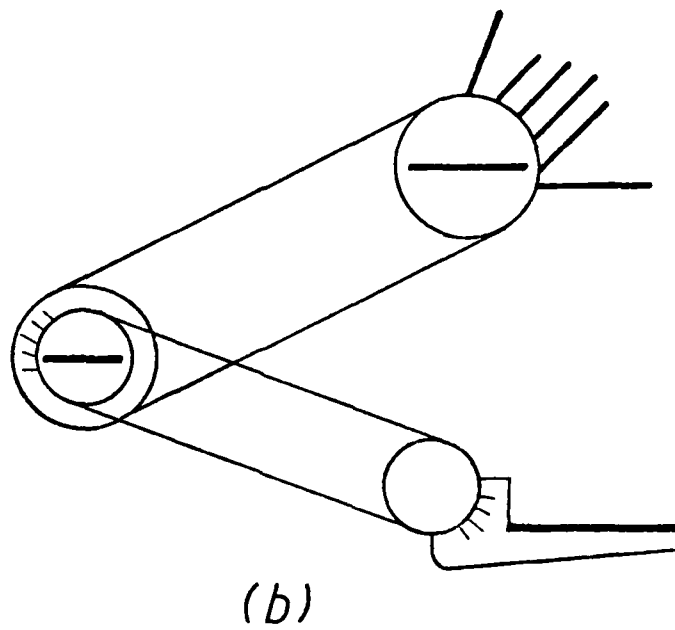
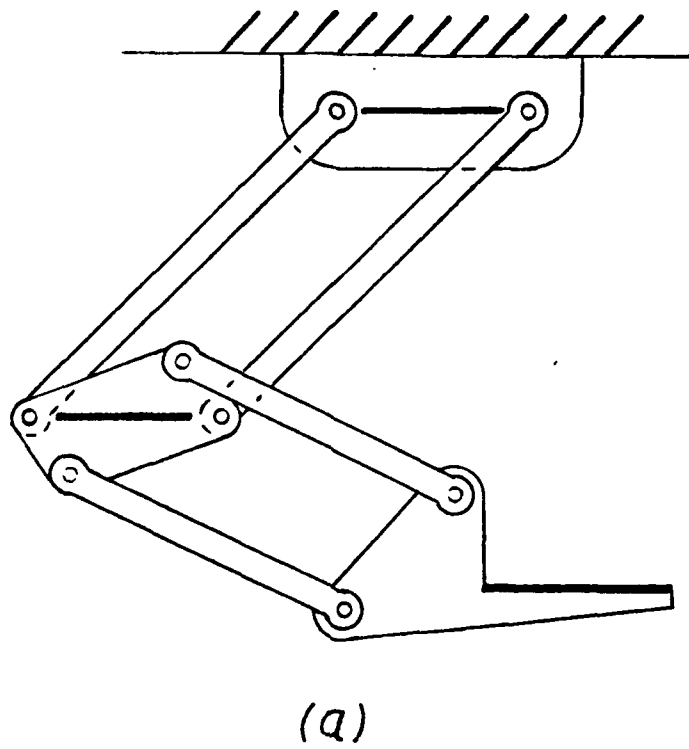


Figure 7.4: Two sets of double parallel linkages.

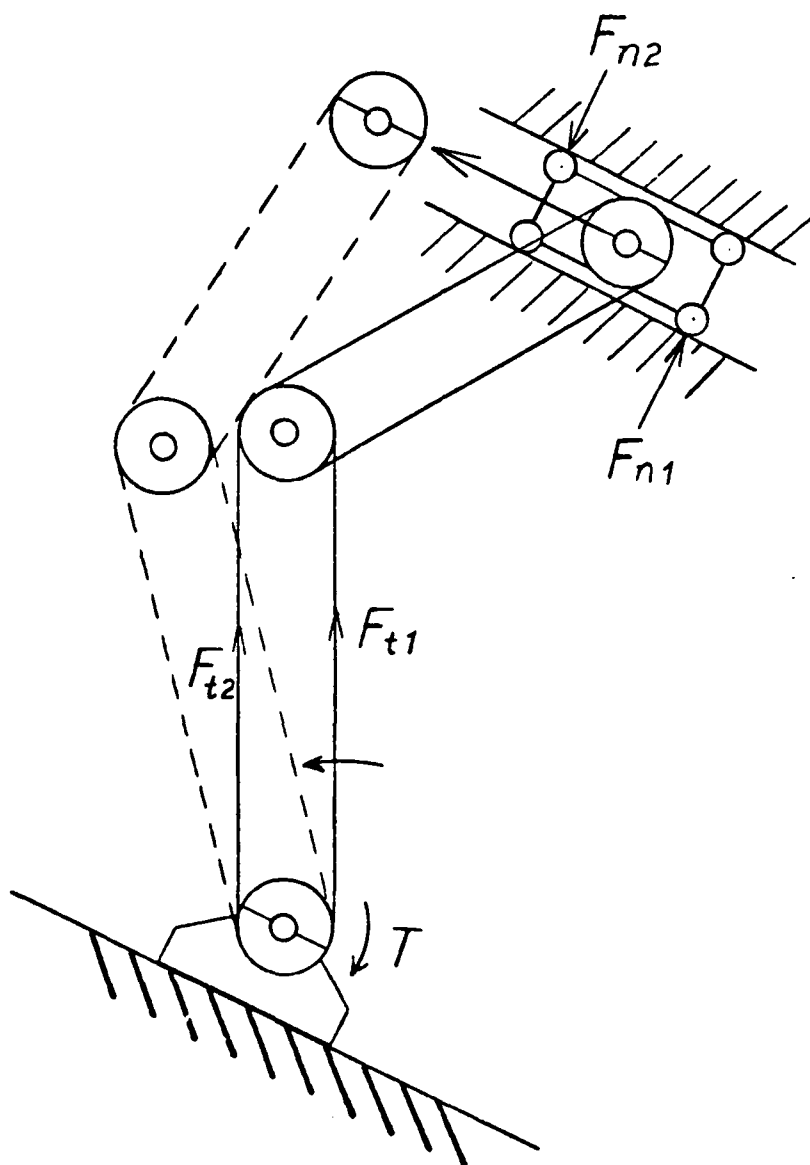


Figure 7.5: A parallel linkage passive ankle system.

a parallel linkage ankle system. The pantograph leg is only partially shown. Due to the heavy duty of the ankle for the ASV, roller chains and gears are suggested to connect the foot, the knee joint and the base, which is the sliding block. If there is any torque taken by the foot, this torque is taken by the guide ways through the roller chains. Since the reaction force F_{n1} and F_{n2} is normal to the sliding motion, and the tension in roller chains is normal to the motion of the chains, no work is required in maintaining the foot attitude provided no friction exists in the system. If the system is properly lubricated, a high energy efficiency of the ankle system can reasonably be expected.

Since the ground under each foot is not always parallel to the body attitude, a certain degree of rotary compliance of the foot is necessary in order to assure a large contact area for weight bearing and to reduce the torque taken by the ankle. This compliance may be obtained by adding linear springs in the roller chains or rotary springs on any joint, in addition to the compliance of the roller chains. The stiffness of these springs depends on the minimum torque requirement maintained at the ankle. Stopping blocks which constrain the ankle from excessive rotation and provide greater torque at the ankle should also be included in the system. This would provide a strong tip support at occasions such as that shown in Figure 7.2. These stopping blocks should limit the angle of foot rotation to a desirable range.

7.4.2 Hydraulic Master-Slave Ankle System

7.4.2.1 Rotary Actuator System

A hydraulic master-slave system can also be used to maintain the foot attitude. If the angular displacement of a crank relative to the body is always the same as the angular displacement of the foot relative to the shank throughout a step, a constant foot attitude can be maintained by a master-slave system, which is composed of a pair of identical rotary actuators. In a pantograph leg, since the foot attitude should be constant relative to the sliding block, both the shortest link and the shank have the same angular displacement relative to the sliding block and to the foot, respectively. Thus, a master-slave ankle system can be applied and is described as follows:

Referring to Figure 7.6, one rotary actuator is mounted to connect the sliding block and the shortest link of the pantograph leg so that the angular displacement of the rotary actuator is the angular displacement of the link relative to the sliding block. The second rotary actuator is mounted to connect the foot and the shank so that the angular displacement of the rotary actuator is the angular displacement of the shank relative to the foot. These two actuators are connected together to form a closed hydraulic loop. During walking, the first actuator, which is the master actuator, is actuated by the leg motion and the oil trapped in it is forced into the second actuator, which is the slave actuator, and actuates it through the same angle. Hence, the foot attitude is maintained constant throughout one step.

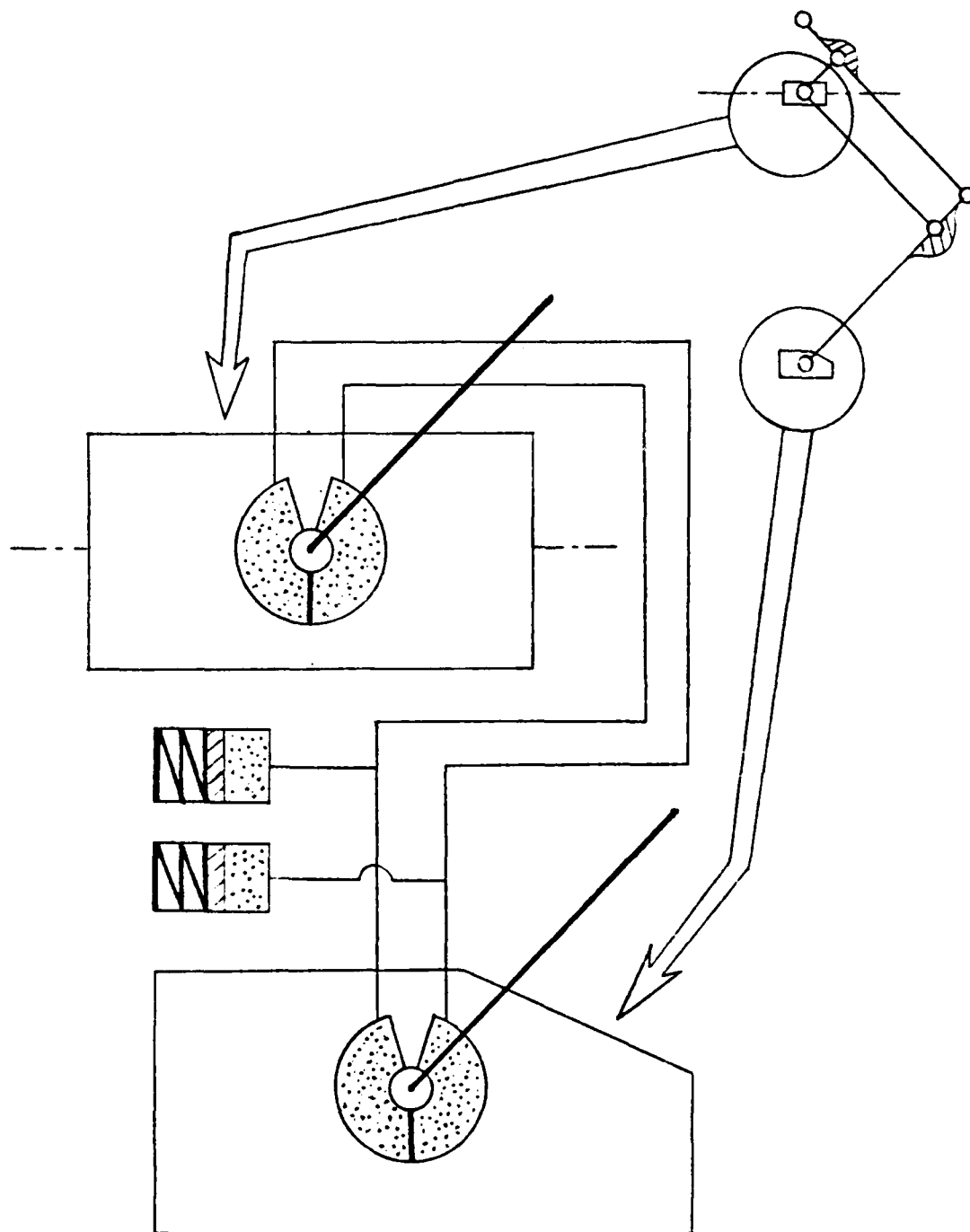


Figure 7.6: Hydraulic master-slave ankle system made by rotary actuators.

Accumulators should be connected to both ends of the actuators in order to provide the ankle with some rotary compliance.

Compared to the parallel linkage system, the advantage of this system is that the connecting pipe lines between the two rotary actuators can be adapted to any available space found in the leg. The disadvantage of this system is that regular commercial rotary actuators are too heavy, and special light weight designs are too expensive. The friction loss in machine elements of the parallel linkage system becomes the friction loss in hydraulic pipe lines of the master-slave ankle system. Hence, the energy efficiencies of both systems are expected to be comparable.

In order to remove the disadvantages of rotary actuators, linear actuators may be used instead. The following are four alternative configurations of hydraulic master-slave ankle systems of this type.

7.4.2.2 Some Alternatives

Figure 7.7 shows the angular displacement of the shank relative to the foot of the pantograph leg in one step (6 foot stroke). This angular displacement is 100° when the foot is fully lifted and is 50° when the foot is fully extended. The total angular displacement needed for the entire walking envelope is 115° . Hence, it is possible to replace the two rotary actuators by a pair of identical linear actuators.

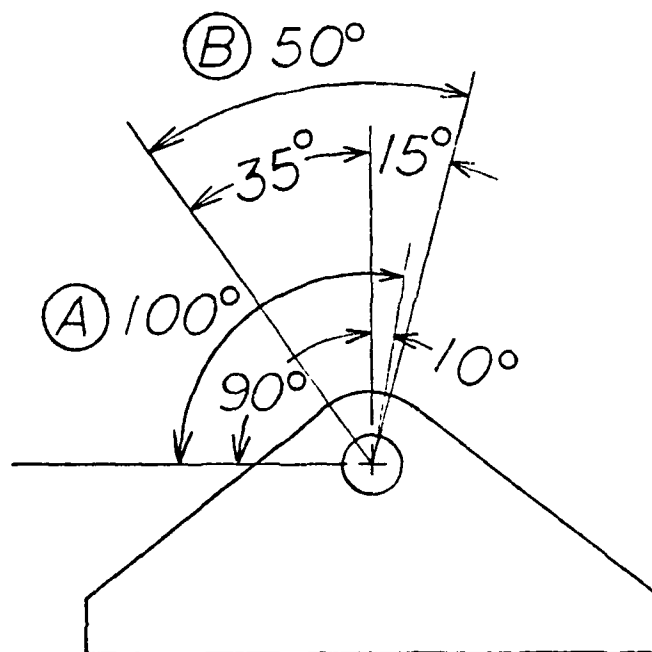


Figure 7.7: Angular displacement of the shank relative to the foot of the pantograph leg in one step.

There are four arrangements of linear actuators which can generate the desired ankle movement. The first employs double-ended actuators while the rest use single-ended actuators. Figure 7.8 shows the mounting of two double-ended actuators. The two actuators are mounted so that $\triangle OAB$ is identical to $\triangle O'A'B'$. A direct crossed connection of these two actuators forms a hydraulic closed loop. Due to the same cross-sectional area on both sides of the piston, the length of these two linear actuators is kept the same during walking and the foot

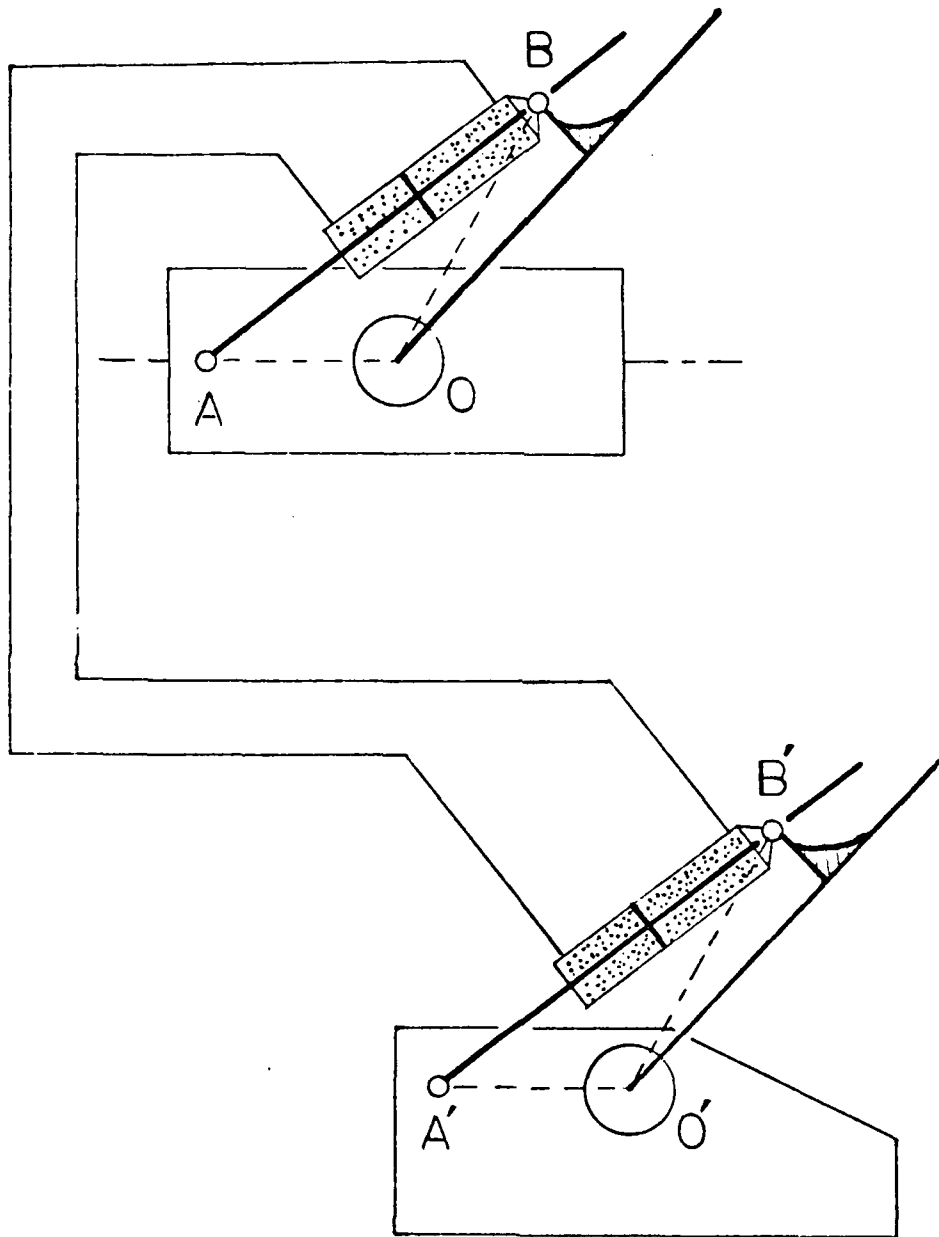


Figure 7.8: Hydraulic master-slave ankle system composed of two double-ended actuators.

attitude is maintained.

The two double-ended actuators can be replaced by two single-ended actuators with the configuration as shown in Figure 7.9. If the master actuator (the upper one) is lengthened by a distance, the slave actuator (the lower one) is shortened by the same distance. The distance between A' and B' is lengthened by the same distance (notice that the cylinder, not the rod, of the slave actuator is hinged to the shank). In a similar manner, if the master actuator is shortened by a distance, the distance between A' and B' is also shortened by the same distance. Hence, the length AB and A'B' is kept the same at all times. Thus, the foot attitude is maintained.

Figure 7.10 shows the third arrangement of the ankle system. Again, the two double-ended actuators of the first arrangement are replaced by two single-ended actuators, and the special mechanism of the slave actuator in the second arrangement is replaced by two dummy actuators. One dummy actuator is added to each pipe line between the two actuators. Since sides of the same cross-sectional area are connected together, any displacement in one actuator will cause the same displacement in the connected actuator in the reverse direction. Hence, any displacement in the master cylinder will cause the same displacement in the slave cylinder in the same direction. That is, the master and slave actuators have the same length all the time.

The fourth arrangement is shown in Figure 7.11. The sides of the same cross area are connected together to form a hydraulic closed loop. Hence, the sum of the displacement of these two actuators is zero at

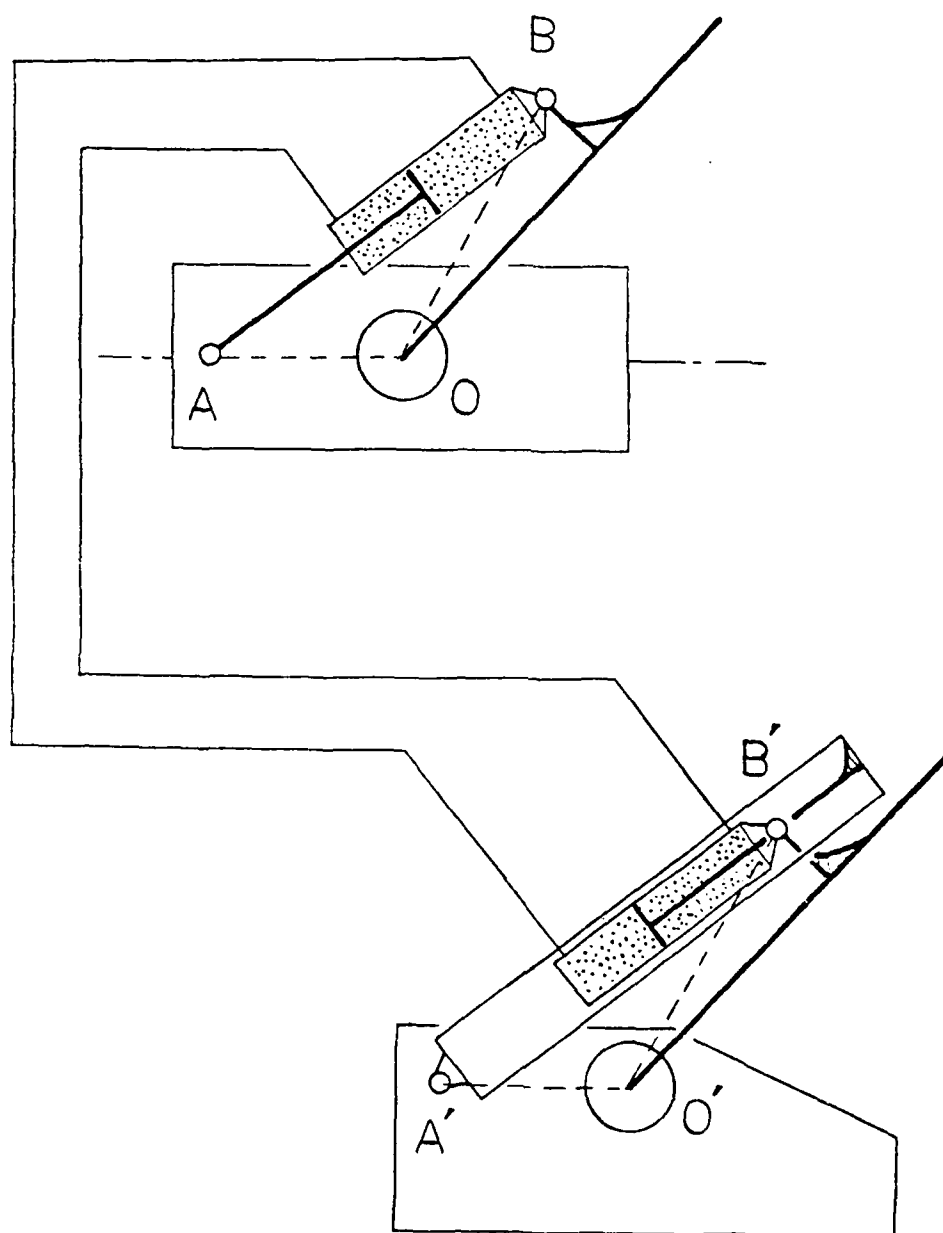


Figure 7.9: Hydraulic master-slave ankle system composed of two single-ended actuators and special mechanism.

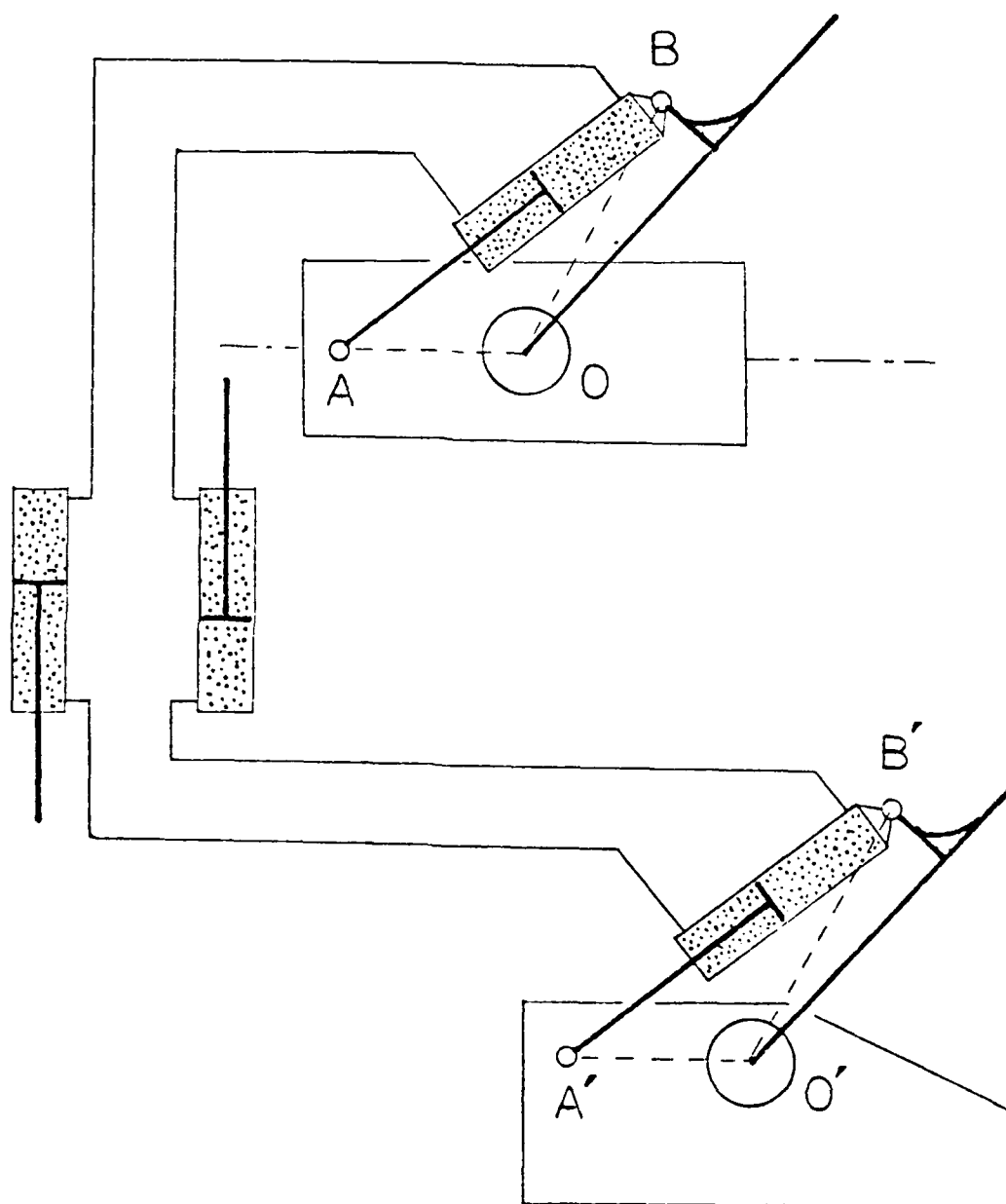


Figure 7.10: Hydraulic master-slave ankle system composed of two single-ended actuators and two dummy actuators.

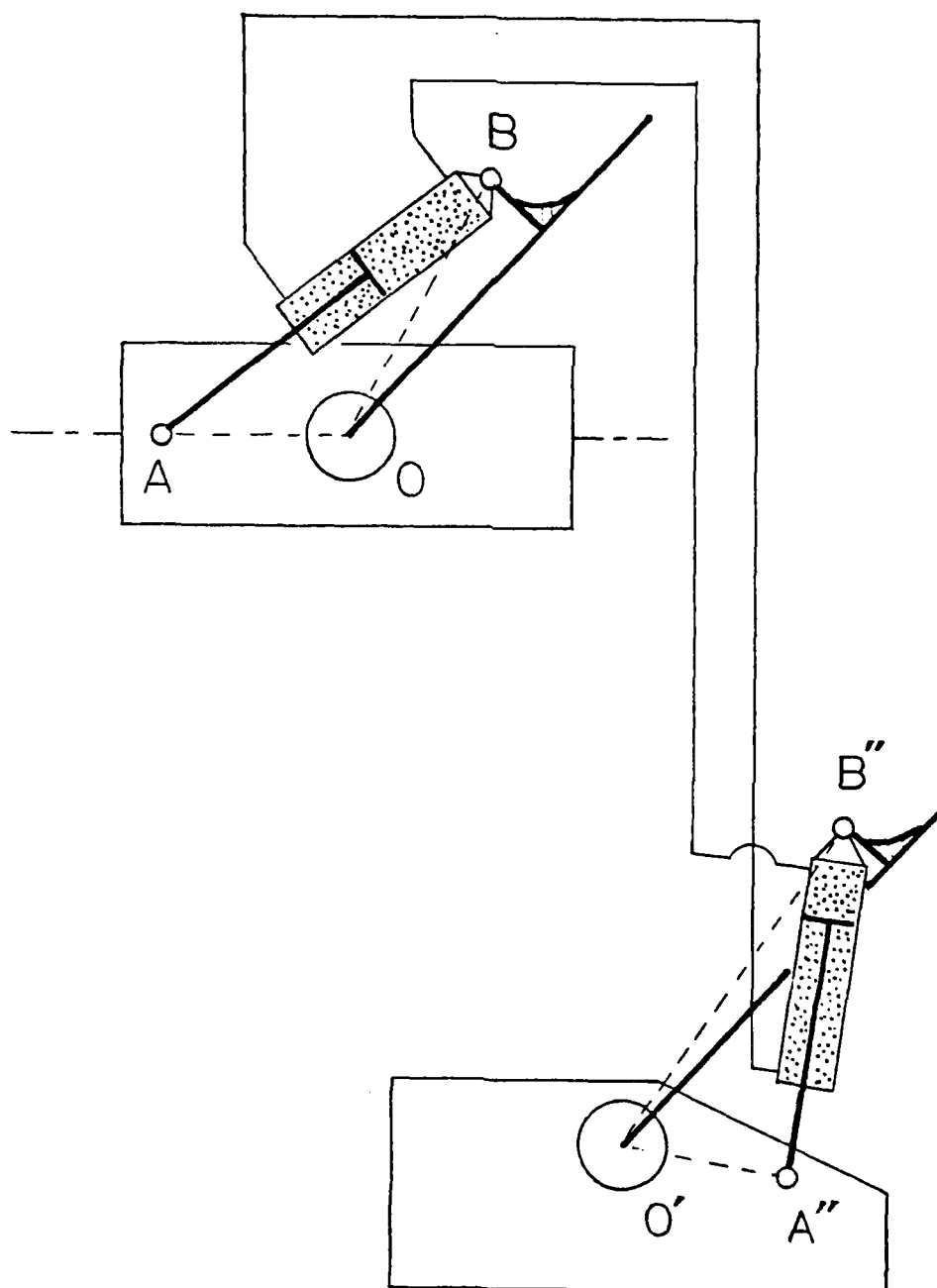


Figure 7.11: Hydraulic master-slave ankle system composed of two single-ended actuators.

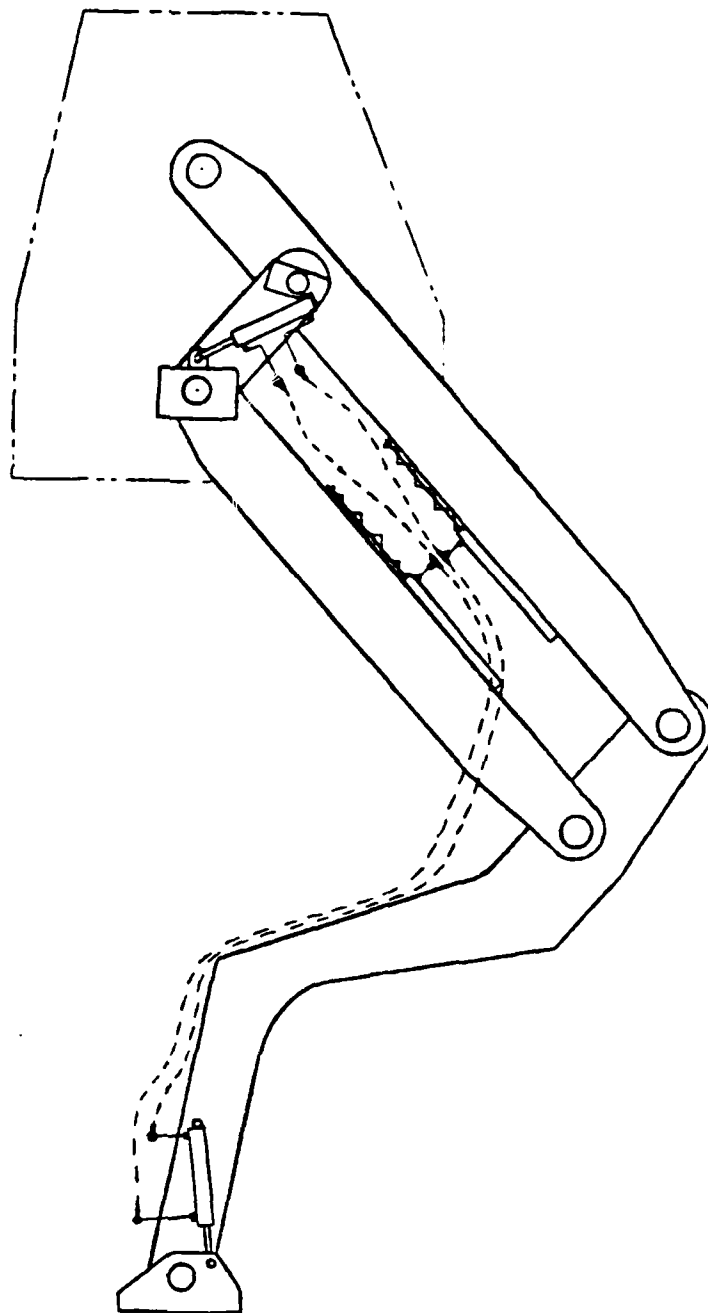


Figure 7.12: A schematic configuration of the master-slave passive ankle system used in the ASV breadboard leg.

all times. By proper selection of the positions of A'' and B'', the foot attitude can be maintained to within a small error. A computer program was developed to select the mounting positions of both actuators, and a difference of less than 3° in foot attitude relative to the body attitude throughout the entire walking envelope was achieved.

Since single-ended actuators require less space, and since the fourth arrangement has simpler structure and less weight, it was selected for the breadboard leg of the ASV-84. Figure 7.12 shows a schematic configuration of a pantograph leg equipped with a master-slave passive ankle system of this type. The two longer cylinders between the two joint actuators serve as accumulators which replenish the oil leakage and provide the necessary rotary compliance at the ankle. The two linear springs on these two accumulators are for adjustment of the ankle stiffness.

7.5 Summary

In this chapter, leg performance with a rigid round foot and with a foot with an ankle joint was compared. The design of a foot with an ankle joint was found to be better in three areas: better support, no effect on the horizontal foot speed, and less energy waste in deforming soil. An active ankle system was found to be too complicated in leg control and not economic in energy efficiency.

In addition to the active ankle system, two types of passive ankle systems were introduced: The first was the parallel linkage passive ankle. This system was expected to be energy efficient because

the only work required in actuation was to overcome the friction loss. A relatively large pathway for the roller chains between the foot and the base, which is the sliding block, was required. The second was the hydraulic master-slave passive ankle system. Both rotary and linear actuators were suitable for such a system. Four kinds of linear actuator arrangement were introduced. The advantages of the hydraulic master-slave system were a simple structure and a flexible pathway for the hydraulic pipe lines. Methods which provide foot rotary compliance for both passive systems were also introduced.

Chapter 8

CONCLUSION

8.1 Research Summarization and Evaluation

The research described in this dissertation is part of the ASV project. The main objective was the design of the leg geometry and the overall geometry of the ASV. In order to establish the proper background for the design of an energy efficient and compact leg, analyses of walking gaits and mobility were developed. The leg geometry was then designed according to the results of these analyses.

8.1.1 Gait Analysis

In the area of gait analysis, a simple analytical approach using the concept of leg local phase to calculate the stability margin of periodic gaits was developed. In the past, the stability margin was most often calculated by numerical methods, graphical methods, or complicated mathematics such as non-linear programming methods [27]. None of these methods are as efficient as the analytical approach. This approach has not only greatly enlarged the scope of the study of gaits, it has also initiated the understanding of the relationship between the stability of periodic gaits and leg walking volumes.

In addition to the analytical approach, the graphical method of stationary gait patterns was established by the author. It was found that this method is very efficient in calculating the stability margin of one certain gait and provides a good geometric understanding of it. Several important facts relating to periodic gaits were discovered with the help of the stationary gait pattern method.

The following are some important achievements in the study of periodic gaits: One valuable development was the formulation of the longitudinal stability margin of $2n$ -legged wave gait. In the past, only the longitudinal stability margin of the four-legged wave gait under the constraint that the stroke is not larger than the stroke pitch could be calculated by a simple equation. Calculation of longitudinal stability margins of other wave gaits depended on numerical computation. The developed formula not only cover the normal case of using equal stroke and stroke pitch, but also the case of using strokes not equal to stroke pitches. Hence, combinations of stroke and stroke pitch for different duty factors to attain an optimum stability of a wave gait can be found. In a similar way, the equation describing the effect on the longitudinal stability margin of shifting the center of the stroke was derived. With these equations, strategies useful in improving the stability of walking on a slope were established. The analytical approach was also used to formulate the equations of the longitudinal stability margin of other periodic gaits: the equal phase gait, the backward wave gait and the backward equal phase gait.

The discovery of the continuous FTL gait is also noteworthy. This gait provides the vehicle with a means of walking in rough terrain at reasonably high speed. Many useful strategies to avoid forbidden regions in rough terrain walking were also developed. The development of the continuous FTL gait also provides a good foundation for the study of statically unstable gaits. In addition to the continuous FTL gait, a general approach to the discontinuous FTL gait was developed. This general approach improves the mobility of the FTL gait developed in reference [36].

In the area of mobility study, large obstacle gaits (LOG's) for the crossing over of three terrain feature types were developed. A general approach which determines the maximum crossing ability over each terrain feature type was established. This approach uses the concept of the three phases of complete obstacle crossing, and the concept of the foot range and the foot conditions in each phase. This approach can also be applied to any other well defined terrain feature. As a result of this development, vehicle mobility was determined according to a set of specified walking volumes, and the motion characteristics in different types of obstacle crossing were understood. Thus, the overall walking volumes which provide the vehicle the required mobility were designed, and obstacle crossing using a fully automated LOG can be expected in the near future.

8.1.2 Leg Design

The design of the leg geometry was based on the studies of leg efficiency and gaits. The designs of four-bar and seven-bar legs

resulted in simple leg linkages which were potentially highly efficient. The seven-bar leg was a leg with only revolute joints. In both designs, linkage synthesis using computer graphics was applied extensively. Several techniques for the optimization of leg linkages were developed. These techniques can be applied directly to any synthesis of a four-bar linkage which generates a straight line segment. Neither design was selected for the ASV because of compactness problems and mechanical design problems.

The design of a pantograph leg depended at the beginning on a trial and error method based on computer-aided graphical programs. This design resulted in a leg geometry which satisfied all specifications. Later, an analytical approach to the study of both two dimensional and three dimensional pantographs was developed. This development included theorems relating basic motion features, singularities, principal axes and the derivation of equations which describe different motion limits. The analytical study is valuable because it makes the design of a pantograph leg more efficient. These results can be directly applied to the design of robot manipulators based on pantographs. The breadboard pantograph leg built according to the design developed here has exhibited satisfactory performance during extensive laboratory testing.

8.2 Research Extension

The design technology of walking machines is still in its infancy. Numerous areas need to be studied further. Only the areas which are directly related to the present work are discussed.

8.2.1 Gait Analysis

Several areas of gait study could be immediately extended on the basis of the work presented in this dissertation. These are:

- A development of discontinuous FTL gaits which is based on the backward periodic gaits.
- An implementation of the discontinuous FTL gait described in the general approach of discontinuous FTL gait.
- An implementation of the continuous FTL gait with different strategies of avoiding forbidden regions.
- A study and implementation of dexterous periodic gaits, especially the dexterous wave gait.
- A study of statically unstable gaits based on the development of the continuous FTL gait.
- An implementation of LOG's for the three terrain feature types.
- A study of LOG's for other terrain features and for an obstacle of combined terrain features.
- A study of the relationship of the mobility of four-legged walking machines to overall walking volumes.

8.2.2 Leg Design

In the area of leg design, further optimization of leg geometry is expected after a field test of the ASV. A full size seven-bar leg could be built in order to compare it to the pantograph leg.

The foot-ankle system strongly affects the leg performance. The design of the sole is needed immediately in order to enhance the vehicle mobility in different soil conditions. This design should include the mechanism for sole mounting. A passive master-slave

ankle system based on rotary actuators should be designed due to its better compactness and mechanical strength.

Since the trend of future walking machine design is expected to be toward lighter weight and fewer legs (the next generation of the ASV may have only four legs), the leg design could be very different. Under a light weight constraint, the design of the leg geometry is allowed more freedom, and a larger magnification factor of the pantograph leg should be considered. Also, the guideway system of the pantograph leg might be replaced by a simple linkage which generates straight line motion. Many existing straight line linkages, such as the Watt's linkage and the Peaucellier inversor linkage [57], should be evaluated for this purpose.

If the vehicle has only four legs, statically unstable gaits will necessarily be the major gaits. Hence, the leg should provide for fast movement and strong thrust. Due to the requirement of fast movement, dynamic effects should be carefully studied and included in the design of the leg geometry, and very light link members made using special materials should be considered.

Appendix A.

A GRAPHICAL METHOD TO FORMULATE THE GAIT STABILITY MARGIN OF 2N-LEGGED WAVE GAIT

The formula of the gait stability margin of a four-legged wave gait was derived by McGhee and Frank in reference [27]. This formula was stated as

$$S^* = \beta - 3/4 \quad \text{for } R \leq P \quad \text{and} \quad 3/4 < \beta < 1 \quad (\text{A.1})$$

The gait stability margins of wave gaits with leg numbers other than four mainly depended on numerical computation. This inconvenience was removed by an analytical approach which was shown in Chapter 3. Through this analytical approach, a formula of the gait stability margin for the general case of a 2n-legged wave gait was established. In this appendix, a graphical approach which results in the same formula is introduced. The formula of a six-legged wave gait is developed first. The same approach is then extended to cover an eight-legged wave gait. Finally, a formula for the general case of 2n-legged wave gait is developed.

The gait diagrams of six-legged wave gaits with duty factors equal to 1/2, 2/3, 3/4, 5/6 and 11/12 were shown in Figure 3.11. According to each gait diagram, a stationary gait pattern is drawn

to calculate the longitudinal gait stability margin, S . S is then normalized to the effective body length, $(n - 1) \cdot p$, to be S'_p , where

$$S'_p = S / [(n - 1) \cdot P] = S_p / (n - 1) \quad (\text{A.2})$$

In order to simplify the derivation, let $P = R = 1$. S'_p is then normalized to the stride λ to be

$$S'_\lambda = S'_p / \lambda = S'_p \cdot \beta \quad (\text{A.3})$$

Hence,

$$S'_\lambda = S / [(n - 1) \cdot \lambda] = S^* / (n - 1) \quad (\text{A.4})$$

According to Equation (A.1), the stability margin for $\beta = 1$ is taken by setting the extreme value of S^* equal to $1/4$ for a four-legged wave gait. Then according to Sun's dissertation [30], the increase of the gait stability margin S_p by adding one pair of legs is equal to 0.5 (when $P = R = 1$). Since $S_p = S^*$ at $\beta = 1$, the extreme value for the gait stability margin of $2n$ -legged wave gait at $\beta = 1$ should be

$$S^* = 1/4 + (n-2)/2 \quad (\text{A.5})$$

Dividing this extreme value by the effective body length $(n-1) \cdot P$, where $P = 1$, gives

$$S'_p = [1/4 + (n - 2)/2] / (n - 1) \quad (\text{A.6})$$

The dimensionless gait stability margins obtained from the stationary gait pattern method and Equation (A.6) are tabulated in Table A.1.

Table A.1
Stability margins of six-legged wave gait

β	1/2	2/3	3/4	5/6	11/12	1
S'_p	0	3/16	1/4	3/10	15/44	3/8
S'_λ	0	1/8	3/16	1/4	5/16	3/8

Since a simple term which is similar to $\beta - 3/4$ in equation (A.1) is expected to appear in the formula of the six-legged wave gait, different terms are calculated for investigation and are tabulated in Table A.2.

Table A.2
Different combinations of terms

duty factor, β						
term	1/2	2/3	3/4	5/6	11/12	1
$1 - \beta$	1/2	1/3	1/4	1/6	1/12	0
$1/\beta - 1$	1	1/2	1/3	1/5	1/11	0
$\beta - 1/2$	0	1/6	1/4	1/3	5/12	1/2

Comparing Table A.2 to Table A.1, $\beta - 1/2$ increases as β increases, which is the same as S'_{λ} in Table A.1, while the other two sets of values decrease as β increases. Hence, $\beta - 1/2$ is more likely to appear in the final formula of six-legged wave gait. By carefully examining the relationship between the values of S'_{λ} and $\beta - 1/2$, a factor of $3/4$ is found to convert all the values of $\beta - 1/2$ to the values of S'_{λ} . Thus, the following equation satisfies the values of S'_{λ} in Table A.1.

$$S'_{\lambda} = (\beta - 1/2) \cdot 3/4 \quad (A.7)$$

From Equation (A.4),

$$S^* = S'_{\lambda} \cdot (n - 1) = (\beta - 1/2) \cdot 3/2 \quad (A.8)$$

In order to verify this formula, program HSM2 is used to calculate the dimensionless gait stability margin S^* of the six-legged wave gait. The results show the values generated by equation (A.8) are exactly the same as the values generated by program HSM2.

A similar derivation of a formula for S^* of an eight-legged wave gait was also carried out. Table A.3 shows the values of S'_p and S'_{λ} obtained from stationary gait pattern methods. A set of values for $\beta - 3/8$ is also tabulated in Table A.3. This number $3/8$ is selected by examining Equations (A.1) and (A.8) and by trial and error.

By examining the last two rows of Table A.3, a factor of $2/3$ is found to convert all the values of $\beta - 3/8$ to the values of S'_{λ} . Thus, the following equation can be used to generate the value of S'_{λ} for the eight-legged wave gait in Table A.3.

Table A.3

Gait stability margins of eight-legged wave gaits

	Duty factor, β						
	3/8	1/2	2/3	3/4	5/6	11/12	1
S'_p	0	1/6	7/24	1/3	11/30	13/33	5/12
S'_λ	0	1/12	7/36	1/4	11/36	13/36	5/12
$\beta - 3/8$	0	1/8	7/24	3/8	11/24	13/24	5/8

$$S'_\lambda = (\beta - 3/8) \cdot 2/3 \quad (A.9)$$

Then

$$S^* = (\beta - 3/8) \cdot 2 \quad (A.10)$$

By carefully examining Equations (A.1), (A.8) and (A.10), the equation of S^* is a multiplication of two terms. The first term is β minus a constant, and the second term is a constant (which is 1 for Equation (A.1)). According to Sun [30], S^* is zero at $\beta = 3/(2n)$ for a $2n$ -legged wave gait. Since the second term is a constant, the first term has to be zero at $\beta = 3/(2n)$. Let $(\beta - 3/(2n))$ be the first term to satisfy this condition. The general form of S^* should be

$$S^* = (\beta - 3/(2n)) \cdot \text{FACTOR} \quad (A.11)$$

Since the extreme value at $\beta = 1$ can be obtained from Equation (A.5), the value of FACTOR can be found by equating (A.11) to (A.5) to be

$$\text{FACTOR} = n/2 \quad (\text{A.12})$$

Therefore, a general formula for the gait stability margin of a 2n-legged wave gait becomes

$$S^* = [\beta - 3/(2n)] \cdot n/2 \quad (\text{A.13})$$

or

$$S^* = (n/2) \cdot \beta - 3/4 \quad (\text{A.14})$$

This general formula does satisfy all the values of S^* obtained by graphical methods. It also satisfies the condition stated by Sun in reference [30], that any addition of a pair of legs will increase the gait stability margin S_p by 0.5. A more complete verification of this formula can be done by extending program HSM2 to 2n-legged wave gaits and comparing the resulting values.

After the development of the analytical approach given in Chapter 3 was completed, Equation (A.14) was compared to Equation (3.19) in Chapter 3 by setting $P = R = 1$. The two equations are exactly the same.

Appendix B

EFFECTS ON GAIT STABILITY MARGINS OF VARYING THE STROKE OBTAINED BY THE STATIONARY GAIT PATTERN METHOD

In a manner similar to the formulation of the equation of gait stability margin of wave gait in Appendix A, the effects on gait stability margins of varying the stroke can be established by either an analytical approach or a graphical approach. The analytical approach was shown in Chapter 3. The graphical approach is shown in the following by examples.

Figure B.1 shows the stationary gait pattern of a quadruped wave gait with $\beta = 5/6$. Since it is a symmetric gait, only support patterns for the first half cycle need to be shown. The support patterns which determine the front minimal SL and rear minimal SL are at times 2 and 1, respectively. Due to the symmetric feature of the gait, only one of these two support patterns need to be studied. The support pattern at time 2 is chosen for this study.

If there is any change in stroke length (the centers of the strokes are kept the same), the positions of the lift of leg 2 and of the placement of leg 4 will be separated. The footprints at time 2' in Figure B.1 show the case of $R > P$. These two new positions define two front boundaries. One (the dashed line) determines the front SL

$$\beta = 5/6$$

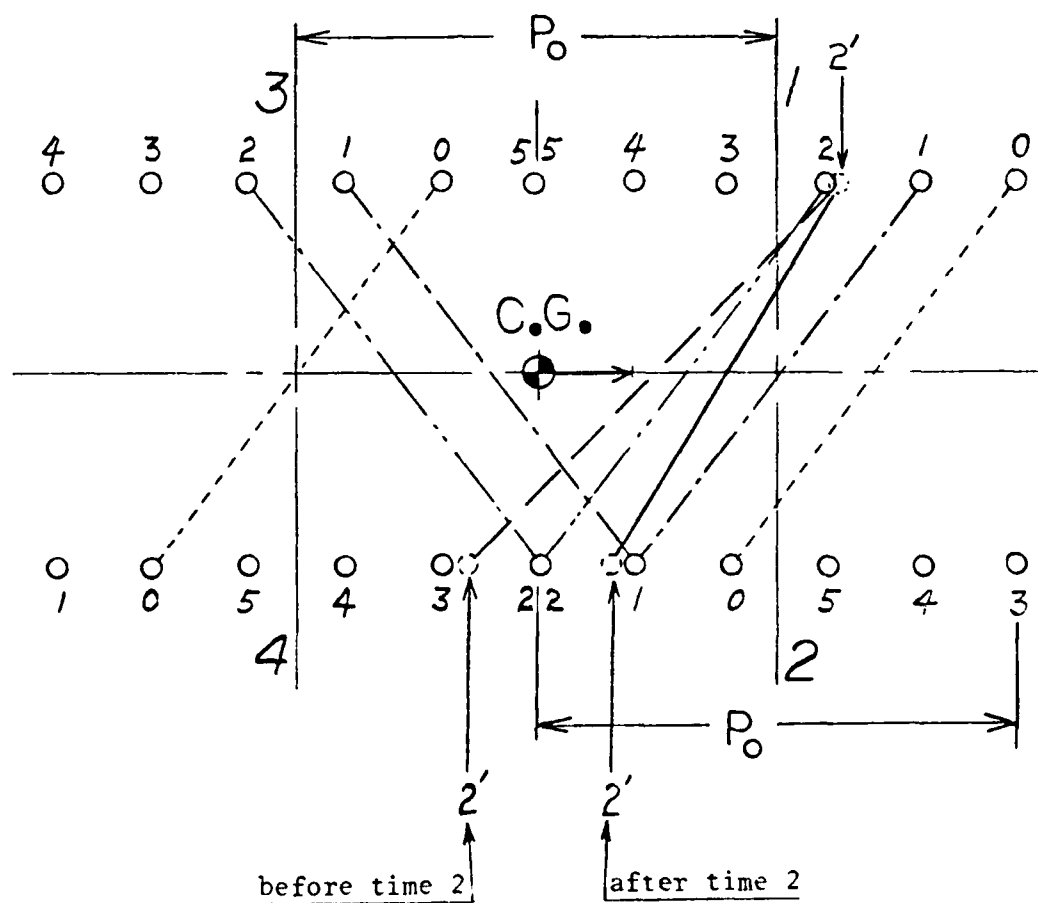
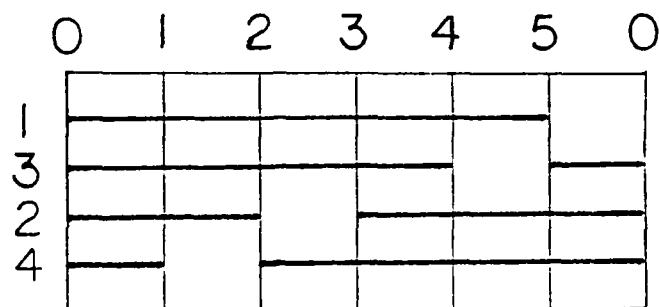


Figure B.1: Gait diagram and stationary gait pattern of a four-legged wave gait with $\beta = 5/6$.

before time 2 and the other (the solid line) determines the front SL after time 2.

Let m be the ratio of stroke R relative to stroke pitch P , where P is kept the same and $P = P_0$. Therefore,

$$m = R/P = R/P_0 \quad (B.1)$$

where m can be greater or less than 1. In Figure B.1, one full stroke is divided into five increments. The foot position of leg 1 at time 2 is at $P_0/2 + m \cdot P_0/10$.

After time 2, the front boundary is the solid boundary defined by legs 1 and 4. The position of leg 4 is at $-P_0/2 + m \cdot P_0/2$. During the same support pattern, the position of center of gravity proceeds from 0 to $m \cdot P_0/5$. Since $P_0 = 5$, the front SL can be calculated as

$$SL_1 = \frac{5/2 + m/2 - 5/2 + 5m/2}{2} - m = m/2 \quad (B.2)$$

Before time 2, the front boundary is the dashed boundary defined by legs 1 and 2. The foot position of leg 2 at time 2 is at $P_0/2 - m \cdot P_0/2$. Since the front boundary changes (to the solid boundary) immediately after time 2, the distance that the center of gravity proceeds is zero. The front SL can be calculated as

$$SL_2 = \frac{5/2 + m/2 + 5/2 - 5m/2}{2} = 5/2 - m \quad (B.3)$$

The shorter distance of SL_1 or SL_2 is the gait stability margin of the

wave gait with stroke $m \cdot P_o$. From Equation (B.3) by setting $SL_2 = 0$, the maximum value of m is $5/2$. This means the maximum stroke for a statically stable wave gait with $\beta = 5/6$ is $5P_o/2$. Equations (B.2) and (B.3) can be normalized to the stroke pitch P_o , which is equal to 5, to be

$$S_{p1} = m/10 \quad (B.4)$$

$$S_{p2} = 1/2 - m/5 \quad (B.5)$$

The shorter of these two is the normalized gait stability margin S_p .

Applying the same technique to a wave gait with $\beta = 3/4$ and $\beta = 11/12$, the resulting equations are shown as below:

$$\beta = 3/4 \quad S_{p1} = 0 \quad (B.6)$$

$$S_{p2} = 1/2 - m/6 \quad (B.7)$$

$$\beta = 11/12 \quad S_{p1} = 2m/11 \quad (B.8)$$

$$S_{p2} = 1/2 - 5m/22 \quad (B.9)$$

Equations (B.4) through (B.9) are plotted in Figure 3.14.

The same technique is applied to the hexapod wave gait with duty factors of $1/2$, $2/3$, $3/4$, $5/6$ and $11/12$ respectively. After being normalized to the stroke, the resulting equations are obtained as:

$$\beta = 1/2 \quad S_{p1} = 1/2 - m/2 \quad (B.10)$$

$$S_{p2} = 1 \quad (B.11)$$

$$\beta = 2/3, \quad S_{p1} = 1/2 - m/8 \quad (B.12)$$

$$S_{p2} = 1 - m/8 \quad (B.13)$$

$$\beta = 3/4, \quad S_{p1} = 1/2 \quad (B.14)$$

$$S_{p2} = 1 - m/6 \quad (B.15)$$

$$\beta = 5/6, \quad S_{p1} = 1/2 + m/10 \quad (B.16)$$

$$S_{p2} = 1 - m/5 \quad (B.17)$$

$$\beta = 11/12, \quad S_{p1} = 1/2 + 2m/11 \quad (B.18)$$

$$S_{p2} = 1 - 5m/22 \quad (B.19)$$

For each set of equations, the smaller is the normalized gait stability margin S_p . These equations are plotted as in Figure 3.14.

Appendix C

STRESS ANALYSIS OF FOUR-BAR LEG BY FINITE ELEMENT METHODS

When the four-bar leg designed in Chapter 5 is abducted or adducted, the load distribution in different nodes becomes too complicated to be calculated by analytical methods. A finite element method, SUPERB, is used for this calculation and is shown in the following. The leg position is chosen at the moment when the foot is being placed (see Figure C.1). The positions of the nodes are then calculated. Notice that the reference coordinate system is attached to the plate on which the leg is mounted. The type of element selected is the space beam element. The cross section area of each beam is a hollow circle with a 3 inch outside diameter and a .25 inch thickness. The material of the beam element is Aluminum. The physical properties of the beam are selected and calculated as follows:

Modulus of Elasticity:

$$\text{Tension: } E = 10,000,000 \text{ psi}$$

$$\text{Shear: } G = 4,000,000 \text{ psi}$$

Density:

$$\nu = 0.1 \text{ lb/in}^3$$

Cross section area:

$$A = \frac{\pi}{4} (d_o^2 - d_i^2) = 2.1598 \text{ in}^2$$

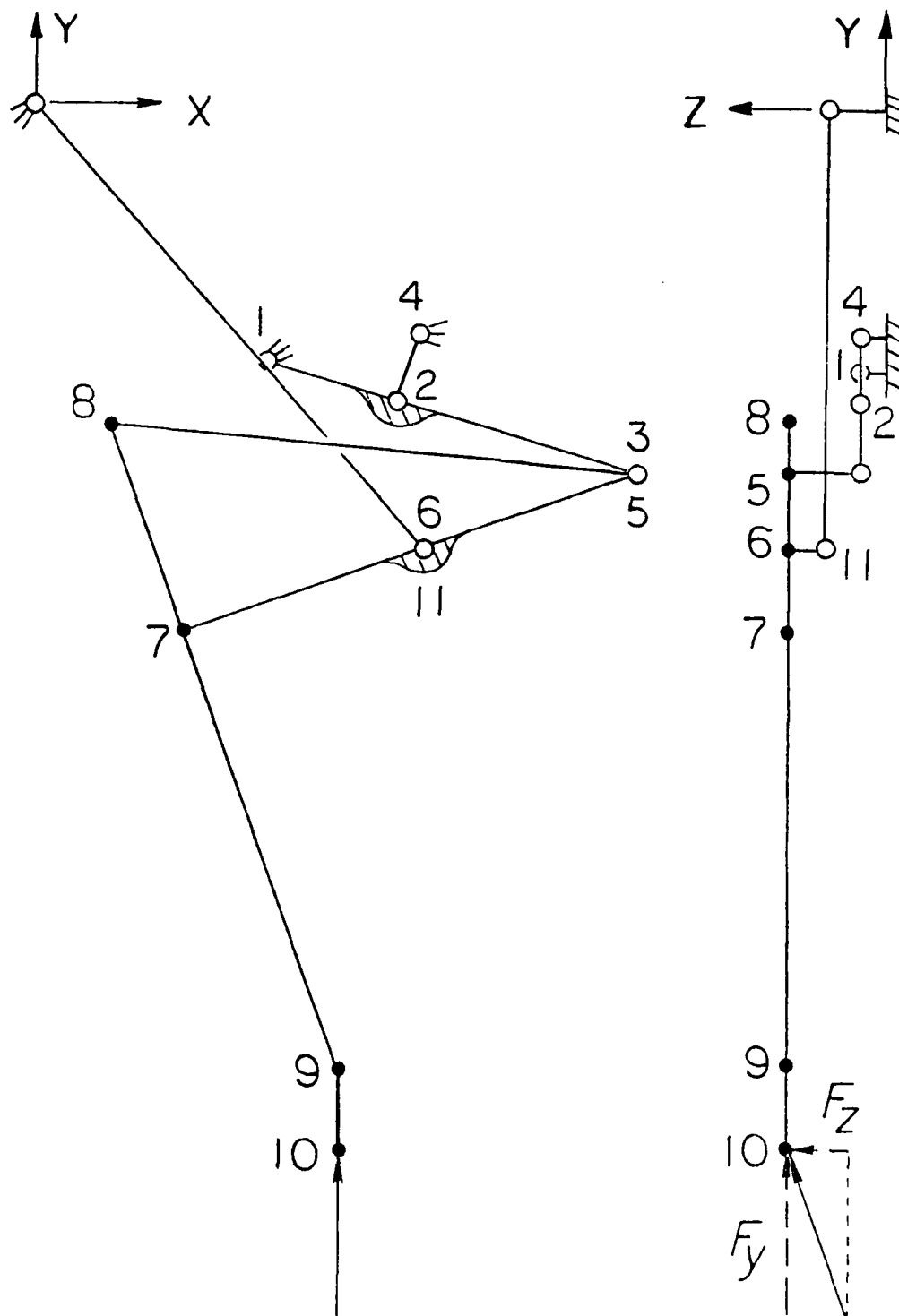


Figure C.1: A finite element model of the four-bar leg with space beam elements.

Area moment of inertia:

$$I_y = I_z = \frac{\pi}{64} (d_o^4 - d_i^4) = 2.0586 \text{ in}^4$$

Torsional constant: From page 292 of reference [63],

$$K = \frac{\pi}{2} (r_o^4 - r_i^4) = 4.1172 \text{ in}^4$$

Effective radius: From page 292 of reference [63],

$$S_{s,\max} = \frac{2T \cdot r_o}{\pi \cdot (r_o^4 - r_i^4)}$$

Hence,

$$R_{\text{eff}} = \frac{K \cdot S_{s,\max}}{T} = r_o = 1.5 \text{ in}$$

Shear area ratio: The shear area ratio is given by

$$a_y = \frac{A}{I_z^2} \int \frac{(\bar{a} \cdot \bar{y})^2}{b} dy$$

where

I_z = moment of inertia about z axis

\bar{a} = area above the y coordinate

\bar{y} = centroid of the area above the y coordinate

b = net width of cross section at y coordinate.

A program named SECPGM¹ is used to calculate the area shear ratio of the beam element. This gives

$$a_y = a_z = 1.4908$$

These properties are entered into an input data file for SUPERB and is shown in Table C.1. This input data file is then submitted to be processed by SUPERB. Some of the results of SUPERB are shown in Tables C.2 through C.5. These results are used as a design reference in the mechanical design of the leg. A plot of the deflected leg under the load condition can also be obtained.

¹ SECPGM is one of the programs in the package called GOCAD, which stands for Graphics Oriented Computer Aided Design. GOCAD is developed at the Department of Mechanical Engineering of the Ohio State University.

Table C.1

The input data file of the four-bar leg for SUPERB

FOUR-BAR LEG #203-2-3, TOUCH DOWN POSITION, SIDE LOAD
ANALYSIS

5	0	1					
ETABLE							
	1	5	1				
MTABLE							
	1	10.E6	4.E6		0.100		
PTABLE							
	1	2.1598	2.0586	2.0586	1.4908	1.4908	4.1172
*2		6					
*3							
*4		1.5	1.5	1.5			
	2	2.1598	2.0586	2.0586	1.4908	1.4908	4.1172
*2							
*3		6					
*4		1.5	1.5	1.5			
	3	2.1598	2.0586	2.0586	1.4908	1.4908	4.1172
*2		6					
*3		6					
*4		1.5	1.5	1.5			
	4	2.1598	2.0586	2.0586	1.4908	1.4908	4.1172
*2							
*3							
*4		1.5	1.5	1.5			
NODES							
	1	16.308	-18.264	0.000			
	2	25.680	-21.000	0.000			
	3	43.104	-25.944	0.000			
	4	27.000	-16.200	0.000			
	5	43.104	-25.944	6.000			
	6	27.348	-31.248	6.000			
	7	10.680	-37.200	6.000			
	8	5.280	-22.800	6.000			
	9	21.660	-67.776	6.000			
	10	21.660	-73.776	6.000			
	11	27.348	-31.248	3.000			
	12	0.000	0.000	3.000			

Table C.1 (continued)

ELEMENTS							
1	1	1	1	2			
1	2	1	2	3			
1	3	1	4	2			
1	4	1	3	5			
1	4	1	5	6			
1	4	1	6	7			
1	4	1	5	8			
1	4	1	8	7			
1	4	1	7	9			
1	4	1	9	10			
1	4	1	11	6			
1	3	1	12	11			
SUPPORTS							
	1		7				
	4		7				
	12		7				
LOADING							
ACCELS							
	0.0		0.0	0.0	0.0	0.939	0.342
FORCES							
	10		2	1409.			
	10		3	513.			
GEOMETRY							
1	1						
2	2						
3	3						
POST							
1					2		
OUTPUT							
1	12	1	1	12	1		
*1	1	1	1	1	1	1	1

Table C.2

The displacements of nodes

*** DISPLACEMENT SOLUTION *** UNIT : INCH

NODE	UX	UY	UZ	ROTX	ROTY	ROTZ
1	0.00000E+00	0.00000E+00	0.00000E+00	0.00000E+00	0.00000E+00	0.00000E+00
2	5.96844E-04	2.51541E-05	7.37526E-03	-3.11385E-03	-3.47489E-05	8.95849E-04
3	1.34985E-02	4.16830E-02	1.87667E-02	-2.11026E-02	7.11936E-03	2.66763E-03
4	0.00000E+00	0.00000E+00	0.00000E+00	0.00000E+00	0.00000E+00	0.00000E+00
5	6.50903E-02	1.81491E-01	1.89024E-02	-2.55456E-02	9.27033E-03	2.66763E-03
6	7.91637E-02	1.43017E-01	3.46387E-01	-3.25014E-02	1.09876E-02	5.71984E-04
7	7.83187E-02	1.47002E-01	7.63890E-01	-4.55907E-02	9.18468E-03	2.20207E-03
8	6.12246E-02	1.40441E-01	1.95376E-01	-3.99777E-02	7.42537E-03	6.11238E-04
9	3.95670E-01	2.63078E-01	2.41820E+00	-6.29318E-02	5.13692E-03	1.43801E-02
10	4.81951E-01	2.63469E-01	2.79812E+00	-6.33803E-02	5.13692E-03	1.43801E-02
11	4.81063E-02	4.70238E-02	3.46385E-01	-3.08862E-02	1.02475E-02	5.71984E-04
12	0.00000E+00	0.00000E+00	0.00000E+00	0.00000E+00	0.00000E+00	0.00000E+00

***** MAXIMUM DISPLACEMENTS *****

NODE	10	10	10	6	9
VALUE	4.81951E-01	2.63469E-01	2.79812E+00	-6.33803E-02	1.43801E-02

Table C.3

The end forces for beams

END FORCES FOR BEAMS AND SIMILAR ELASTIC ELEMENTS
(MEMBER COORDINATE DIRECTIONS)

ELEM	NODE	<i>lb.</i>			<i>in-lb</i>		
		FORCE-X	FORCE-Y	FORCE-Z	MOMENT-X	MOMENT-Y	MOMENT-Z
1	1	-1252.	511.4	-541.2	5026.	4553.	0.0000E+00
1	2	1252.	-509.5	541.9	-5026.	734.1	4983.
2	2	-1241.	-273.4	-486.9	1.7511E+04	2172.	-4983.
2	3	1240.	276.9	488.2	-1.7511E+04	6659.	-2.6073E-14
3	4	791.3	-0.1339	55.44	-2842.	1.2240E+04	0.0000E+00
3	2	-792.3	-0.1339	-55.07	2842.	-1.2515E+04	0.0000E+00
4	3	-488.2	72.12	1269.	0.0000E+00	-1.1186E+04	-1.5029E+04
4	5	488.6	-70.90	-1269.	0.0000E+00	3574.	1.5458E+04
5	5	1381.	-654.8	-649.2	-5988.	1.0163E+04	-2840.
5	6	-1382.	651.7	650.5	5988.	640.1	-8021.
6	6	663.8	1119.	-665.5	-1.2034E+04	9038.	8021.
6	7	-665.1	-1123.	666.8	1.2034E+04	2752.	1.1823E+04
7	5	-256.9	88.30	160.6	-6174.	-4675.	2840.
7	8	257.5	-95.97	-157.8	6174.	-1366.	657.3
8	6	196.9	191.8	157.8	3875.	4998.	-657.3
8	7	-199.8	-190.7	-156.6	-3875.	-7416.	3599.
9	7	1319.	-473.6	-510.2	1040.	1.9508E+04	-1.5421E+04
9	9	-1325.	475.8	512.6	-1040.	-2896.	6.4332E-12
10	9	1408.	3.6380E-12	-512.6	0.0000E+00	3077.	2.4556E-11
10	10	-1409.	-3.6380E-12	513.0	0.0000E+00	-4.8563E-11	1.2733E-11
11	11	-14.81	-1454.	-1269.	-5.6843E-14	-3176.	-1.3264E+04
11	6	15.03	1454.	1269.	5.6843E-14	6981.	8902.
12	12	1923.	2.773	-11.74	1.1126E+04	8441.	0.0000E+00
12	11	-1929.	2.773	14.81	-1.1126E+04	-7890.	0.0000E+00

Table C.4

The generalized forces transmitted to element
nodes in nodal coordinate directions

FOUR-BAR LEG #203-2-3, TOUCH DOWN POSITION, SIDE LOAD

LOADING CASE 1 (SEQUENCE 1)

GENERALIZED FORCES TRANSMITTED TO ELEMENT NODES IN LOCAL NODAL COORDINATE DIRECTIONS
(GEN. FORCES) = (ELEM. STIF. MATRIX) X (ELEM. DISP.) - (EQUIV. ELEM. NODAL FORCES)

ELEM	NODE	FORCE-X	FORCE-Y	FORCE-Z	MOMENT-X	MOMENT-Y	MOMENT-Z
1	1	-1059.	841.8	-541.2	6100.	2963.	0.0000E+00
1	2	1059.	-839.8	541.9	-4619.	2113.	4983.
2	2	-1269.	75.79	-486.9	1.7439E+04	-2691.	-4983.
2	3	1269.	-72.12	488.2	-1.5029E+04	1.1186E+04	-2.6073E-14
3	4	-210.0	-763.0	55.44	1.2555E+04	-504.9	0.0000E+00
3	2	210.0	764.0	-55.07	-1.2821E+04	577.9	0.0000E+00
4	3	-1269.	72.12	-488.2	1.5029E+04	-1.1186E+04	0.0000E+00
4	5	1269.	-70.90	488.6	-1.5458E+04	3574.	0.0000E+00
5	5	-1517.	180.2	-649.2	8917.	-7722.	-2840.
5	6	1517.	-176.8	650.5	-5471.	-2517.	-8021.
6	6	-248.7	-1278.	-665.5	1.4373E+04	-4465.	8021.
6	7	248.7	1281.	666.8	-1.0408E+04	-6639.	1.1823E+04
7	5	248.7	-109.3	160.6	6540.	4148.	2840.
7	8	-248.7	117.0	-157.8	-6040.	1873.	657.3
8	8	248.7	-117.0	157.8	6040.	-1873.	-657.3
8	7	-248.7	120.1	-156.6	-8304.	1024.	3599.
9	7	-2.3590E-12	-1401.	-510.2	1.8712E+04	5615.	-1.5421E+04
9	9	2.3590E-12	1408.	512.6	-3077.	-2.1560E-12	6.4332E-12
10	9	3.6380E-12	-1408.	-512.6	3077.	0.0000E+00	2.4556E-11
10	10	-3.6380E-12	1409.	513.0	-4.8563E-11	0.0000E+00	1.2733E-11
11	11	1269.	-1454.	-14.81	1.3264E+04	-3176.	-5.6843E-14
11	6	-1269.	1454.	15.03	-8902.	6981.	5.6843E-14
12	12	1269.	-1445.	-11.74	1.3679E+04	-2813.	0.0000E+00
12	11	-1269.	1454.	14.81	-1.3264E+04	3176.	0.0000E+00

Table C.5

The stress results for beam elements

FOUR-BAR LEG #203-2-3, TOUCH DOWN POSITION, SIDE LOAD

LOADING CASE 1 (SEQUENCE 1)

UNIT: PSI

STRESS RESULTS FOR BEAM ELEMENTS (STANDARD BEAM SIGN CONVENTION, TENSILE AXIAL FORCE = +)

ELEM	NODE	FX/A	FY/A	FZ/A	MX/SM	MY/SM	MZ/SM	MAX SX	MIN SX
1	1	5.7973E+02	2.3677E+02	-2.5059E+02	-1.8310E+03	3.3179E+03	0.0000E+00	3.8976E+03	-2.7381E+03
1	2	5.7948E+02	2.3589E+02	-2.5092E+02	-1.8310E+03	-5.3489E+02	3.6311E+03	4.7454E+03	-3.5865E+03
2	2	5.7464E+02	-1.2657E+02	-2.2542E+02	-6.3798E+03	1.5824E+03	3.6311E+03	5.7881E+03	-4.6388E+03
2	3	5.7417E+02	-1.2821E+02	-2.2604E+02	-6.3798E+03	-4.8517E+03	-1.8998E+14	5.4259E+03	-4.2776E+03
3	4	-3.6640E+02	-6.1974E-02	2.5667E+01	1.0355E+03	8.9186E+03	0.0000E+00	8.5522E+03	-9.2850E+03
3	2	-3.6685E+02	6.1974E-02	2.5497E+01	1.0355E+03	9.1190E+03	0.0000E+00	8.7521E+03	-9.4858E+03
4	3	2.2604E+02	3.3392E+01	5.8737E+02	0.0000E+00	-8.1505E+03	1.0951E+04	1.9327E+04	-1.8875E+04
4	5	2.2625E+02	3.2829E+01	5.8737E+02	0.0000E+00	-2.6043E+03	1.1263E+04	1.4094E+04	-1.3641E+04
5	5	-6.3919E+02	-3.0320E+02	-3.0060E+02	2.1815E+03	7.4056E+03	2.0690E+03	8.8354E+03	-1.0114E+04
5	6	-6.3969E+02	-3.0172E+02	-3.0116E+02	2.1815E+03	-4.6641E+02	-5.8442E+03	5.6709E+03	-6.9503E+03
6	6	-3.0736E+02	5.1832E+02	-3.0813E+02	4.3845E+03	6.5856E+03	-5.8442E+03	1.2122E+04	-1.2737E+04
6	7	-3.0792E+02	5.1988E+02	-3.0873E+02	4.3845E+03	-2.0052E+03	8.6145E+03	1.0312E+04	-1.0928E+04
7	5	1.1895E+02	4.0882E+01	7.4349E+01	2.2495E+03	-3.4066E+03	-2.0690E+03	5.5946E+03	-5.3567E+03
7	8	1.1925E+02	4.4434E+01	7.3051E+01	2.2495E+03	9.9548E+02	4.7896E+02	1.5937E+03	-1.3552E+03
8	8	-9.1144E+01	8.8807E+01	7.3051E+01	-1.4116E+03	3.6417E+03	4.7896E+02	4.0295E+03	-4.2118E+03
8	7	-9.2497E+01	8.8300E+01	7.2525E+01	-1.4116E+03	5.4033E+03	2.6222E+03	7.9330E+03	-8.1180E+03
9	7	-6.1059E+02	-2.1926E+02	-2.3621E+02	-3.7884E+02	1.4215E+04	1.1237E+04	2.4841E+04	-2.6062E+04
9	9	-6.1346E+02	-2.2030E+02	-2.3732E+02	-3.7884E+02	2.1099E+03	4.6875E+12	1.4964E+03	-2.7234E+03
10	9	-6.5181E+02	1.6844E-12	-2.3732E+02	0.0000E+00	2.2418E+03	-1.7893E-11	1.5900E+03	-2.8936E+03
10	10	-6.5238E+02	1.6844E-12	-2.3752E+02	0.0000E+00	3.5386E-11	9.2779E-12	-6.5238E+02	-6.5238E+02
11	11	6.8578E+00	-6.7308E+02	-5.8737E+02	2.0709E-14	-2.3140E+03	9.6652E+03	1.1986E+04	-1.1972E+04
11	6	6.9604E+00	-6.7336E+02	-5.8737E+02	2.0709E-14	-5.0871E+03	6.4868E+03	1.1581E+04	-1.1567E+04
12	12	-8.9039E+02	1.2840E+00	-5.4377E+00	-4.0533E+03	6.1509E+03	0.0000E+00	5.2605E+03	-7.0413E+03
12	11	-8.9333E+02	-1.2840E+00	-6.8578E+00	-4.0533E+03	5.7491E+03	0.0000E+00	4.8558E+03	-6.6424E+03

REFERENCES

- [1] Bekker, M.G., Off-The-Road Locomotion, University of Michigan Press, Ann Arbor, Michigan, 1960, pp. 8.
- [2] Bekker, M.G., Introduction to Terrain Vehicle System, University of Michigan Press, Ann Arbor, Michigan, 1969.
- [3] Anon., Logistical Vehicle Off-Road Mobility, Project TCCO 62-5, U.S. Army Transportation Combat Developments Agency, Fort Eustis, Va., February, 1967.
- [4] Shigley, J.E., The Mechanics of Walking Vehicles, Land Locomotion Laboratory Report No. LL-71, U.S. Army Tank-Automotive Command, Warren, Michigan, September, 1960.
- [5] McKenney, J.D., "Investigation for a Walking Device for High Efficiency Lunar Locomotion," Paper 2016-61, American Rocket Society, Space Flight to the Nation, New York, October 1961.
- [6] Baldwin, W.C., Miller, J.V., Multi-Legged Walker, Final Report, Space General Corporation, El Monte, California, January 30, 1966.
- [7] McGhee, R.B., "Finite State Control of Quadruped Locomotion," Proceedings of Second International Symposium on External Control of Human Extremities, Dubrovnik, Yugoslavia, August 1966.
- [8] Frank, A.A., Automatic Control Systems for Legged Locomotion, USCEE Report No. 273, University of South California, Los Angeles, California, May 1968.
- [9] Liston, R.A., Mosher, R.S., "A Versatile Walking Truck," Proceedings of 1968 Transportation Engineering Conference, ASME-NYAS, Washington, D.C., October 1968.
- [10] Mosher, R.S., "Test and Evaluation of a Versatile Walking Truck," Proceedings of Off-Road Mobility Research Symposium, International Society for Terrain Vehicle Systems, Washington, D.C., June 1968, pp. 359-379.
- [11] Cox, W., "Big Muskie," News in Engineering, Ohio State University, January 1970, pp. 25-27.

- [12] Vukobratovic, M., Ciric, V., Hristic, D., Stepanenko, J., "Contribution to the Study of Anthropomorphic Robots," Paper 18.1, Proceedings of V IFAC World Congress, Paris, June 1972.
- [13] Mocci, U., Petternella, N., Salinari, S., Experiments with Six Legged Walking Machines with Fixed Gait, Report 2-12, Institute of Automation, Rome University, Rome, Italy, June 1972.
- [14] Kato, I., and Tsuiki, H., "Hydraulically Powered Biped Walking Machine with a High Carrying Capacity," Proceedings of Fourth International Symposium on External Control of Human Extremities, Dubrovnik, Yugoslavia, August 1972.
- [15] Schneider, A.Y., Gurfinkel, E.V., Kanaev, E.M., and Ostapchuk, V.G., A System for Controlling the Extremities of an Artificial Walking Apparatus, Report No. 5, General and Molecular Physics Series, Physio-Technical Institute, Moscow, USSR, 1974 (in Russian)
- [16] Okhotsimski, D.E., Gurfinkel, V.S., Devyanin, E.A., Platonov, A.K., "Integrated Walking Robot Development," Machine Intelligence, 9, (Eds. J.E. Hayes, D. Michie, L.J. Mikulich), 1977.
- [17] Okhotsimski, D.E., "Motion Control System Development for a Mobile Robot," Automatic Control in Space: Proceedings of the 8th IFAC Symposium, Oxford, England, July 2-6, 1979.
- [18] Buckett, J.R., Design of an On-Board Electronic Joint System for a Hexapod Vehicle, M.S. thesis, The Ohio State University, Columbus, Ohio, March, 1977.
- [19] Briggs, R.L., Real-Time Digital Control of an Electrically Powered Vehicle Leg Using Vector Force Feedback, M.S. thesis, The Ohio State University, Columbus, Ohio, March 1977.
- [20] Pugh, D.R., An Autopilot for a Terrain-Adaptive Hexapod Vehicle, M.S. thesis, The Ohio State University, Columbus, Ohio September 1982.
- [21] Hirose, S., Umetani, Y., "The Basic Motion Regulation System for a Quadruped Walking Machine," ASME Paper 80-DET-34, September 1980.
- [22] Muybridge, E., Animals in Motion, New Dover Edition, Dover Publications, Inc., New York, 1957 (first published in 1899).
- [23] Muybridge, E., The Human Figure in Motion, Dover Publications, Inc., New York, 1955 (first published in 1901).

- [24] Tomovic, R., and Karplus, W.J., "Land Locomotion Simulation and Control," Proceedings Third International Analogue Computation Meeting, Opatija, Yugoslavia, September 1961, pp. 385-390.
- [25] Hildebrand, M., "Symmetrical Gaits of Horses," Science, Vol. 150, November 1967, pp. 701-708.
- [26] McGhee, R.B., "Some Finite State Aspects of Legged Locomotion," Mathematical Biosciences, Vol. 2, No. 1/2, February 1968, pp. 67-84.
- [27] McGhee, R.B. and Frank, A.A., "On the Stability Properties of Quadruped Creeping Gaits," Math. Biosciences, Vol. 3, 1968, pp. 331-351.
- [28] McGhee, R.B., and Jain, A.K., "Some Properties of Regularly Realizable Gait Matrices," Mathematical Biosciences, Vol. 13, No. 1/2, February 1972, pp. 179-193.
- [29] Bessenov, A.P., and Umnov, N.V., "The Analysis of Gaits in Six-Legged Vehicles According to Their Static Stability," Proceedings of Symposium on Theory and Practice of Robots and Manipulators, Udine, Italy, 1973.
- [30] Sun, S.S., A Theoretical Study of Gaits for Legged Locomotion System, Ph.D. Dissertation, The Ohio State University, Columbus, Ohio, March 1974.
- [31] McGhee, R.B., "Vehicular Legged Locomotion," To appear in Advances in Automation and Robotics, Ed. by G.N. Saridis, Jai Press, Inc., 1983.
- [32] Sindall, J.N., "The Wave Mode of Walking Locomotion," Journal of Terranmechanics, Vol. 1, 1964, pp. 54-73.
- [33] Wilson, D.M., "Insect Walking," Annual Review of Entomology, Vol. 11, 1966, pp. 103-121.
- [34] Wilson, D.M., "Stepping Patterns in Tarantula Spiders," Journal of Experimental Biology, Vol. 47, 1967, pp. 133-151.
- [35] Okhotsimski, D.E., and Platonov, A.K., "Control Algorithm of the Walking Climbing Over Obstacles," Proceeding of the Third International Joint Conference on Artificial Intelligence, Stanford, California, 1973.
- [36] Tsai, S.J., An Experimental Study of a Binocular Vision System for Rough Terrain Locomotion of a Hexapod Walking Robot, Ph.D. Dissertation, The Ohio State University, Columbus, Ohio, 1983.

- [37] McGhee, R.B., Orin, D.R., Pugh, D.R., and Patterson, M.R., "A Hierarchically-Structured System for Computer Control of a Hexapod Walking Machine," Proceeding of 5th IFTOMM Symposium on Robots and Manipulator Systems, Udine, Italy, June, 1984.
- [38] Klein, C.A., and Patterson, M.R., "Computer Coordination of Limb Motion for Locomotion of a Multiple-Armed Robot for Space Assembly," IEEE Trans. on Systems, Man, and Cybernetics, Vol. SMC-12, No. 6, December, 1982, pp. 913-919.
- [39] Patterson, M.R., Reidly, J.J., and Brownstein, B.J., Guidance and Actuation Techniques for an Adaptively Controlled Vehicle, Final Technical Report, Battelle Columbus Laboratories, Columbus, Ohio, 43201, March 1983.
- [40] McGhee, R.B., and Iswandhi, G.I., "Adaptive Locomotion of a Multilegged Robot Over Rough Terrain," IEEE Trans. on Systems, Man, and Cybernetics, Vol. SMC-9, No. 4, April 1979, pp. 176-182.
- [41] Ozguner, F., Tsai, S.J., and McGhee, R.B., "An Approach to the Use of Terrain Preview Information in Rough-Terrain Locomotion by a Hexapod Walking Machine," International Journal of Robotics Research, Vol. 3, No. 2, April 1984.
- [42] Doebelin, E.O., System Modeling and Response: Theoretical and Experimental Approaches, John Wiley & Son Inc., 1980, pp. 529.
- [43] Chao, C.S., Real-Time Multiprocessor Control of a Hexapod Vehicle, Ph.D. dissertation, The Ohio State University, Columbus, Ohio, August 1979.
- [44] Waldron, K.J., and Kinzel, G.L., "The Relationship Between Actuator Geometry and Mechanical Efficiency in Robots," Proceedings of 4th CISM-IFTOMM Symposium on Theory and Practice of Robots and Manipulators, Warsaw, Poland, September 8-12, 1981, pp. 366-374.
- [45] Gabrielli, G., and Von Karman, T.H., "What Price Speed," Mechanical Engineering, Vol. 72, No. 10, 1950, pp. 775-781.
- [46] Vidosic, J.P., Tesar, D., and Johnson, H.L., Theoretical Analysis of Four-Bar Mechanisms, Final Report, NSF Grant GP-2748, Georgia Institute of Technology, Engineering Experiment Station, Atlanta, 1966.
- [47] Vohnout, V.J., Mechanical Design of an Energy Efficient Robotic Leg for Use on a Multi-Legged Walking Vehicle, M.S. thesis, The Ohio State University, Columbus, Ohio, Spring 1982.

- [48] Brown, T.F. Jr., Dynamic Study of a Four-Bar Linkage Walking Machine Leg, M.S. thesis, The Ohio State University, Columbus, Ohio, Summer 1982.
- [49] Elftman, H., "Skeletal and Muscular Systems: Structure and Function," Medical Physics, 1944.
- [50] Raibert, M.H., and Sutherland, I.E., "Machines That Walk," Scientific American, Vol. 248, No. 2, January 1983, pp. 44-53.
- [51] Russell, M., "Odex 1: The First Functionoid," Robotics Age, Vol. 5, No. 5, 1983, pp. 12-18.
- [52] Waldron, K.J., Song, S.M., Wang, S.L., and Vohnout, V.J., "Mechanical and Geometric Design of the Adaptive Suspension Vehicle," Proceedings of Symposium on Theory and Practice of Robots and Manipulators, Udine, Italy, June, 1984.
- [53] Wang, S.L., The Study of a Hexapod Walking Vehicle's Maneuverability Over Level Ground and Obstacles and its Computer Simulation, M.S. thesis, The Ohio State University, Columbus, Ohio, August 1983.
- [54] Pearson, K.G., Report on Cinematographic Analysis of Animal Walking, final report on contract RF 714250-01, University of Alberta, Edmonton, Alberta, Canada.
- [55] Beyer, R., The Kinematic Synthesis of Mechanisms, Translated by H. Kuenzel, McGraw Hill, 1963.
- [56] Sylvester, "On the Plagiograph...", Nature, Vol. XII, 1875, pp. 168.
- [57] Kempe, A.B., How to Draw a Straight Line, Macmillan, London, 1877, (Also Published in Hobson, E.W. et al, Squaring the Circle and Other Monographs, Chelsea, New York, 1953).
- [58] Raibert, M.H., et al, Dynamically Stable Legged Locomotion, Progress Report: October 1982 - October 1983, Leg Laboratory, The Robotics Institution and Department of Computer Science, Carnegie-Mellon University, Pittsburgh, Pennsylvania, December 1983.
- [59] Roth, B., "On the Multiple Generation of Coupler-Curves," ASME paper 64-Mech-3, October 1964.
- [60] Kessiss, J.J., Rambaut, J.P., Penne, J., "Walking Robot Multi-Level Architecture and Implementation," Proceedings of 4th CISM-IFTOMM Symposium on Theory and Practice of Robot and Manipulators, Warsaw, Poland, September 8-12, 1981, pp. 297-304.

- [61] McGhee, R.B. and Waldron, K.J., An Experimental Study of an Ultra-Mobile Vehicle for Off-Road Transportation, Semi-Annual Report for Period April 1, 1983 to September 30, 1983, Ohio State University Research Foundation, May 1984.
- [62] Vohnout, V.J., Alexander, K.J. and Kinzel, G.L., "The Structural Design of the Legs for a Walking Vehicle," Proceedings of 8th Applied Mechanisms Conference, St. Louis, September 1983, pp. 501-508.
- [63] Roark, R.J. and Young, W.C., Formulas for Stress and Strain, 5th edition, McGraw-Hill Inc., 1975.

END

FILMED

10-85

DTIC